

University of Dundee

DOCTOR OF PHILOSOPHY

The characterisation of ion channels in human spermatozoa by whole cell patch clamp electrophysiology

Mansell, Steven A.

Award date:
2013

Awarding institution:
University of Dundee

[Link to publication](#)

General rights

Copyright and moral rights for the publications made accessible in the public portal are retained by the authors and/or other copyright owners and it is a condition of accessing publications that users recognise and abide by the legal requirements associated with these rights.

- Users may download and print one copy of any publication from the public portal for the purpose of private study or research.
- You may not further distribute the material or use it for any profit-making activity or commercial gain
- You may freely distribute the URL identifying the publication in the public portal

Take down policy

If you believe that this document breaches copyright please contact us providing details, and we will remove access to the work immediately and investigate your claim.

Download date: 17. Feb. 2017

DOCTOR OF PHILOSOPHY

The characterisation of ion channels in
human spermatozoa by whole cell patch
clamp electrophysiology

Steven A. Mansell

2013

University of Dundee

Conditions for Use and Duplication

Copyright of this work belongs to the author unless otherwise identified in the body of the thesis. It is permitted to use and duplicate this work only for personal and non-commercial research, study or criticism/review. You must obtain prior written consent from the author for any other use. Any quotation from this thesis must be acknowledged using the normal academic conventions. It is not permitted to supply the whole or part of this thesis to any other person or to post the same on any website or other online location without the prior written consent of the author. Contact the Discovery team (discovery@dundee.ac.uk) with any queries about the use or acknowledgement of this work.

The Characterisation of Ion Channels in Human Spermatozoa by Whole Cell Patch Clamp Electrophysiology

Steven A. Mansell

A dissertation submitted in fulfilment of the requirements for the
degree of Doctor of Philosophy

Division of Cardiovascular & Diabetes Medicine

University of Dundee

July 2013

Declaration

I hereby declare that I, Steven Antony Mansell, am the sole author of this thesis. The work, of which this thesis is a record, and was carried out by myself, and all references cited have been consulted by myself. None of the work contained within this thesis has been previously accepted for a higher degree.

Signature of Candidate

Steven Antony Mansell BSc.

Supervisor Statement

I certify that Steven Antony Mansell has fulfilled the conditions of ordinance 39 and of the relevant regulations, such that he is qualified to submit this thesis in application for the higher degree of Doctor of Philosophy.

Signatures of Supervisors

Professor Christopher L.R. Barratt

Dr Stuart M. Wilson

Dedicated to my Gogo

Acknowledgements

Firstly I would like to thank my supervisors Professor Christopher Barratt and Professor Stuart Wilson for giving me the opportunity to conduct my research at the University of Dundee. You have both been a great inspiration and guidance to me throughout my PhD. I would like to thank you both for believing in me even when I said I wanted to patch clamp human sperm! I would also like to thank everyone in the assisted conception unit for their support throughout my studies both financially and emotionally. I would also like to thank the Infertility Research Trust for providing some funding so I could carry out my work.

Particular thanks goes to Michael Gallacher for his help in teaching me the dark art of electrophysiology. Your enthusiasm and advice has been most greatly appreciated over these last 2 years. Most importantly I would like to thank Professor Polina Lishko and Professor Yuriy Kirichok for allowing me to visit their lab at the University of California, San Francisco, and teaching me how to patch clamp human sperm. Without their help this thesis would not have been possible.

I would obviously like to thank my parents, Neville and Marian Mansell, for their support over the course of my postgraduate studies. Without their support I would not have been able to pursue this 'adventure'. Special thanks goes to my Gogo (Catherine O'Neill) who I've always been able to turn to and to whom this thesis is dedicated.

Lastly I would like to thank my partner Dr Daniel Smith, for all his support and for always making me laugh when times were tough. Uhuh Aye!

Table of Contents

Declaration.....	ii
Supervisor Statement	iii
Acknowledgements.....	v
Table of Contents.....	vi
List of Figures.....	ix
List of Abbreviations	xi
Summary.....	xiv

Chapter 1 – Introduction

1.1. Male Infertility.....	2
1.2. Diagnosis: Semen Analysis.....	3
1.3. Treatment Options and Trends.....	4
1.4. Ion Channels as Therapeutic Targets.....	5
1.5. Ion Channel Screening.....	6
1.6. Diagnosis of Sperm Dysfunction by Functional Assays.....	8
1.7. Mechanics of Sperm Motility	10
1.8. Hyperactivation.....	12
1.9. Capacitation	13
1.10. Sperm electrophysiology- development of method.....	14
1.11. Human Sperm Patch Clamp recordings - The current approach	17
1.12. Limitation of Sperm Electrophysiology.....	18
1.13. Ion channels in sperm and their role in male fertility	19
1.13.1. Cation Channel of Sperm (<i>CatSper</i>)	19
1.13.2. Voltage-gated proton channel: <i>Hv1</i>	23
1.13.3. Potassium Channel of Sperm (<i>KSper/Slo3</i>).....	28
1.13.4. ATP-Gated <i>P2X2</i> Channel	30
1.13.5. Calcium Activated Chloride Channel (<i>TMEM16A/ Ano 1</i>).....	31
1.14. Overall Aim	34

Chapter 2 – Materials and Methods

2.1. Donors.....	36
2.2. Collection of semen sample and delivery to the laboratory.....	36
2.3. Sperm Preparation.....	37
2.4. Motility Assessment	37
2.5. Ca ²⁺ Measurements.....	39
2.6. Pharmacology	41
2.7. Electrophysiology	43
2.7.1. Patch clamping somatic cells	43
2.8. Experimental Design.....	44
2.9. Basic Electrophysiological principles of patch clamping.....	46
2.9.1. Liquid Junction potentials	46
2.10. Series resistance	47

2.11. Equilibrium Potential	49
2.12. The Goldman, Hodgkin, Katz Equation	49
2.13. Recording protocol	50
2.14. Statistics	52

Chapter 3 - Native Currents in Human Spermatozoa

3.1. Introduction.....	54
3.2. Aim	54
3.3. Results.....	55
3.3.1. <i>Native Current in Motile Human Spermatozoa</i>	55
3.3.2. <i>Outward current is carried by K⁺</i>	57
3.3.3. <i>Intracellular [pH]_i and K⁺ current</i>	58
3.3.4. <i>Pharmacology of K⁺ Current</i>	59
3.3.5. <i>Current Clamp: K⁺ Channel blockers and membrane potential</i>	62
3.3.6. <i>Biophysical Properties of the K⁺ current</i>	64
3.3.7. <i>Channel Ionic Selectivity</i>	66
3.3.8. <i>Pharmacology of the small Na⁺ Current</i>	68
3.3.9. <i>Mathematically Modelled Current and Resting Membrane Potential</i>	70
3.4. Discussion	72
3.4.1. <i>pH and K⁺ Current in Human Sperm</i>	73
3.4.2. <i>Pharmacology of K⁺ channel</i>	74
3.4.3. <i>Biophysical properties of human sperm K⁺ conductance</i>	75
3.4.4. <i>What is the underlying channel responsible for the K⁺ conductance in human sperm?</i>	76
3.5 Conclusion	77

Chapter 4 – CatSper and the K⁺ Current

4.1. Introduction.....	79
4.2. Aim	80
4.3. Results.....	81
4.3.1. <i>Classic CatSper Current</i>	81
4.3.2. <i>CatSper current and K⁺ Channel blockers</i>	83
4.3.3. <i>CatSper Channel Inhibitors and K⁺ Current</i>	84
4.3.4. <i>NNC55-0396 depolarises Membrane Potential and Blocks Small outward Na⁺ Current.</i>	87
4.3.5. <i>Effect of K⁺ Channel blockers on Progesterone induced Ca²⁺ Influx</i>	89
4.3.6. <i>Quinidine – K⁺ Current</i>	91
4.3.7. <i>Clofilium – K⁺ Current</i>	92
4.3.8. <i>Quinidine and Clofilium induced block of CatSper</i>	94
4.4. Discussion	96
4.4.1. <i>CatSper and progesterone induced Ca²⁺ signalling</i>	97
4.4.2. <i>K⁺ and CatSper current: One or two channels?</i>	98
4.5. Conclusion	99

Chapter 5 – Progesterone and the Tail Current

5.1. Introduction.....	102
5.2. Aim	103
5.3. Results.....	104
5.3.1. <i>Effects of Progesterone on K⁺ Current Over Time</i>	104
5.3.2. <i>Peak Progesterone response (I_{Peak})</i>	106
5.3.3. <i>The transient progesterone induced response (I_{Tran})</i>	108
5.3.4. <i>Progesterone sensitive tail current</i>	110
5.3.5. <i>I_{Tail} Ionic Conductance</i>	111
5.3.6. <i>Progesterone induced Ca²⁺ permeable tail current in human sperm</i>	113
5.3.7. <i>Biophysical properties of the open channel</i>	115
5.3.8. <i>Time course of open channel inactivation</i>	117
5.3.9. <i>Na⁺ and NMDG⁺ permeability of the open channel</i>	118
5.3.10. <i>Ionic permeability of the I_{Steady State}</i>	120
5.3.11. <i>Biophysical properties of the tail current</i>	122
5.4. Tail current pharmacology	125
5.4.1. <i>Clofilium</i>	125
5.4.2. <i>4-AP</i>	127
5.4.3. <i>Quinidine</i>	129
5.4.4. <i>Progesterone</i>	131
5.4.5. <i>Effect of clofilium, 4-AP, quinidine and progesterone on the biophysical properties of the channel.</i>	133
5.4.6. <i>Effects of clofilium, 4-AP, Quinidine and Progesterone on Sperm Motility and Hyperactivation.</i>	136
5.5. Discussion	138
5.5.1. <i>Progesterone response</i>	138
5.5.2. <i>Ionic permeability of the tail current</i>	139
5.5.3. <i>Biophysical Properties of the Tail Current</i>	141
5.5.4. <i>Pharmacology of the Tail current</i>	142
5.5.5. <i>Hyperactivation and the Tail Current</i>	143
5.6. Conclusion	144

Chapter 6 - General Discussion and Future Work

6.1. Aim of thesis.....	147
6.2. Key findings.....	147
6.2.1. <i>K⁺ efflux through CatSper</i>	151
6.3. Conclusions and Future Work	153
References	155
Appendix/ Publications	169

List of Figures

Chapter 1

Figure 1.1:	Cross section of sperm flagella	11
--------------------	---------------------------------------	----

Chapter 2

Figure 2.1:	Kinetic parameters of a human sperm cell as assessed by computer aided sperm analysis (CASA).	39
Figure 2.2:	A) Human sperm cells at 90x magnification (60x water immersion objective plus in built 1.5x optic). Arrows indicate cytoplasmic droplet and site of seal formation.	44
Figure 2.3:	Electrical circuit of human sperm cell.....	48

Chapter 3

Figure 3.1:	Native membrane current in motile human spermatozoa.....	56
Figure 3.2:	Outward current carried by K^+ efflux upon depolarisation of the membrane potential.	57
Figure 3.3:	Intracellular pH and K^+ current.....	59
Figure 3.4:	The effects of 3mM quinidine on the outward K^+ current	61
Figure 3.5:	Whole cell current clamp	63
Figure 3.6:	Biophysical properties of K^+ Current.....	65
Figure 3.7:	Ionic selectivity of the voltage-induced current.....	67
Figure 3.8:	Pharmacology of small outward Na^+ current	69
Figure 3.9:	Predicted membrane current and resting V_m	72

Chapter 4

Figure 4.1:	Confirmation of progesterone activated CatSper currents	82
Figure 4.2:	The effect of K^+ current blockers on the DVF CatSper current in human spermatozoa.....	83
Figure 4.3:	Effects of CatSper inhibitors on the physiological K^+ current.....	86
Figure 4.4:	Effects of specific CatSper inhibitor NNC55-0396 on resting V_m and small outward Na^+ current.....	88
Figure 4.5:	The effects of bupivacaine and clofilium on the progesterone induced Ca^{2+} influx in human sperm after 4 hours of capacitation.....	90
Figure 4.6:	Quinidine induced block of K^+ current	92
Figure 4.7:	Clofilium induced block of K^+ current.....	93
Figure 4.8:	Quinidine- and clofilium –induced block of CatSper.....	95

Chapter 5

Figure 5.1:	Effect of 500nM progesterone on the physiological K^+ current.	105
Figure 5.2:	Progesterone and I_{tail}	107
Figure 5.3:	Progesterone and I_{Trans}	109
Figure 5.4:	Confirmation of the progesterone induced tail current.	110
Figure 5.5:	Ionic conductance of the tail current.	112
Figure 5.6:	Progesterone enhances the Ca^{2+} permeable tail current.	114
Figure 5.7:	Biophysical properties of the open channel.	116
Figure 5.8:	Voltage dependence of inactivation.	117
Figure 5.9:	Na^+ and NMDG $^+$ permeability of the open channel.....	119
Figure 5.10:	Ionic selectivity of I_{out}	121
Figure 5.11:	The biophysical properties of I_{Tail}	123
Figure 5.12:	Activation and deactivation of I_{Tail}	124
Figure 5.13:	Effects of 50 μ M clofilium on the tail current.....	126
Figure 5.14:	Effects of 2mM 4-AP on the tail current.....	128
Figure 5.15:	Effects of 0.3mM quinidine on the tail current.	130
Figure 5.16:	Effects of 500nM progesterone on the tail current.....	132
Figure 5.17:	Effects of clofilium, 4-AP, quinidine and progesterone on the biophysical properties of the tail current.....	134
Figure 5.18:	Pharmacological affect on the time course of tail current inactivation	135
Figure 5.19:	Effects of clofilium, quinidine, 4-AP and progesterone on motility..	137

List of Abbreviations

4-AP	4-Aminopyridine
ALH	Lateral Head Amplitude
ART	Assisted reproductive technologies
ATP	Adenosine Triphosphate
BCF	Cilia Beat Frequency
CaCC	Calcium activated chloride channel
CASA	Computer Assisted Sperm Analysis
CatSper	Cation Channel of Sperm
C_m	Membrane Capacitance
CsMeSO ₃	Caesium methansulphonate
DIC	Differential interference contrast
E_{Cl^-}	Equilibrium potential for chloride
EDTA	Ethylenediaminetetraacetic Acid
EGTA	Ethylene Glycol-bis- <i>N,N,N',N'</i> -tetraacetic Acid
E_K^+	Equilibrium Potential for Potassium
E_{Na^+}	Equilibrium Potential for Sodium
E_{rev}	Reversal Potential
FBS	Foetal Bovine Serum
$G_{Ca^{2+}}$	Ca ²⁺ Conductance
GHK	Goldman Hodgkins Katz Equation
G_K^+	K ⁺ Conductance
G_m	Membrane Conductance
G_{Na^+}	Na ⁺ Conductance
HEPES	4-(2-hydroxyethyl)-1-piperazineethanesulfonic Acid

HFEA	Human Fertilisation and Embryology Authority
HS	Control bath solution
HS-CAP	Capacitating solution
HTF	Synthetic Human Tubal Fluid
H _v 1	Voltage gated proton channel
ICSI	Intracytoplasmic sperm injection
I _{Instant}	Instantaneous Current
I _K ⁺	Potassium Current
I _{K_{res}}	Residual K ⁺ Current
I _{Na} ⁺	Sodium Current
I _{Out}	Outward Current
I _{steady State}	Steady State Current
I _{Tail}	Tail Current
I _{Total}	Total Current
I _{trans}	Transient Current
IVF	<i>In vitro</i> fertilisation
KSper	K ⁺ Current of Sperm
LIN	Linearity
MES	2-(<i>N</i> -morpholino)ethanesulfonic acid
n _c	Number of Cells
N _D	Number of Donors
NMDG ⁺	<i>N</i> -Methyl-D-Glucammonium
NMDGCl	<i>N</i> -Methyl-D-Glucammonium Chloride
NMDGOH	<i>N</i> -Methyl-D-Glucammonium hydroxide
R _a	Access Resistance

R_m	Membrane Resistance
STR	Straightness
VAP	Average Path Velocity
VCL	Curvilinear Path Velocity
V_{Hold}	Holding potential
V_m	Membrane Potential
VSL	Straight Line Velocity
V_{Test}	Test potential
WHO	World Health Organisation
$\Psi_{\text{Ca}^{2+}}$	Driving force for calcium
Ψ_{K^+}	Driving force for potassium
Ψ_{Na^+}	Driving force for sodium

Summary

For fertilisation to occur, sperm have to undergo both induction as well as the modification of motility as they ascend the female reproductive tract. Role specific ion channels, that allow the sperm cell to migrate towards and penetrate the outer vestments of the oocyte, govern these changes in motility. Electrophysiological recordings of murine sperm have identified a number of ion channels important for fertility. These include Slo3, the dominant K^+ channel responsible for the regulation of membrane potential, and CatSper a Ca^{2+} channel important for hyperactive motility. In contrast, there is no electrophysiological data on the ion channels that govern sperm function in humans under physiological conditions. The work documented in this thesis identifies, for the first time, the native ion channels in human sperm using whole cell electrophysiology under quasi-physiological conditions.

Electrophysiological recordings from capacitated human sperm show an outwardly rectifying hyperpolarising K^+ current under conditions that maintained physiological Na^+ , K^+ and Cl^- gradients. Detailed analysis of this current showed that it was weakly pH sensitive, weakly voltage activated and poorly K^+ selective with a relative G_{K^+}/G_{Na^+} of ~ 7 . Furthermore, inhibition of this current with putative K^+ channel blockers quinidine, bupivacaine and clofilium caused a depolarisation of the resting membrane potential indicating the importance of this current in the regulation of membrane potential in human sperm.

Pharmacological assessment of the physiological current showed that the current was sensitive to both putative K^+ channel blockers as well as the CatSper specific blocker NNC 55-0396. Assessment of the outward CatSper current under divalent free

conditions showed that CatSper displayed the same pharmacological profile as the outward K^+ . This suggested that the K^+ current and CatSper current were flowing through the same population of channels. Furthermore, fluorometric analysis of the progesterone induced Ca^{2+} influx showed that application of K^+ channel antagonists, clofilium and bupivacaine, abolished this effect. This prompted further investigation into the presence of one or two channels underlying this current.

Progesterone, a potent agonist of CatSper, was therefore used to further assess if the K^+ current and CatSper currents flowed through the same population of ion channels. This data showed that progesterone had no effect on the outward K^+ current, however progesterone did cause a large increase in the tail current that developed over a 30 second period. Detailed investigation of the tail current showed that this current was less permeable to K^+ and Na^+ but had a high degree of Ca^{2+} permeability. As well as this the tail current had a different pharmacological profile and biophysical properties compared to the outward current. Furthermore, the tail current appeared to have a role in hyperactive motility as compounds that enhanced the tail current (quinidine, 4-AP and progesterone) increased basal hyperactivation. In contrast clofilium, a compound that abolished the tail current, significantly inhibited basal hyperactivation. Based on the differences in ionic permeability, biophysical properties and pharmacological profiles it would suggest the presence of two separate channels. These include: 1) the outwardly rectifying poorly selective K^+ current, involved in the regulation of V_m and 2) the progesterone sensitive, Ca^{2+} permeable CatSper current potentially involved in the regulation of basal hyperactivation.

Chapter 1 - Introduction

1.1. Male Infertility

The Human Fertilisation and Embryology Authority (HFEA) and the National Institute for Clinical Excellence (NICE), define infertility as the inability of a couple to conceive after 1 year of unprotected sexual intercourse. Infertility is recognised as a public health problem by the World Health Organisation (WHO) with infertility consumer groups, such as International consumer support for infertility or iCSI, suggesting that having a child is a basic human right. This is based on the UN Declaration of Human Rights, Article 16.1, stating: “Men and women of full ages, without any limitation due to race, nationality or religion, have the right to marry and to found a family.” None-the-less it provides an insight into how fertility is perceived to the international community. Internationally, infertility affects roughly 9% of the global population with 56% of these couples needing medical treatment (Hull et al. 1985; Boivin et al. 2007). In the UK, excluding regional variation, roughly 1 in 7 will experience infertility issues at some point in their reproductive life; this equates to roughly 3.5 million people of reproductive age (NICE 2013; HFEA 2010a). Furthermore, studies assessing semen parameters to characterise subfertility (concentration $< 20 \times 10^6/\text{ml}$) in the Danish population, showed that roughly 18% of 18-20 year olds could be classed as sub-fertile based on sperm concentration (Andersen et al. 2000). This is considerably higher than other prevalent diseases such as diabetes (~5% of the global population, Diabetes UK 2011, Wild et al. 2004). Thus, infertility is a major global problem. Although the causes of infertility can be multifactorial, e.g. affecting both male and female partners, epidemiological studies have suggested that the single most common cause of couples seeking infertility treatment is due to sperm dysfunction (~30%, HFEA 2010) (abnormal sperm function) (Hull et al. 1985). The classification of sperm dysfunction can be further

sub-divided into a number of categories based on abnormalities in concentration (Oligozoo-, Azoo-), motility (Asthenozoo-), morphology (Teratozoo-) or a combination (Oligoasthenozoo-, Oligoteratozoo-, Oligoteratoasthenozoo-, Teratoasthenozoo- spermia). A large retrospective study by Curi *et al.*, in 2003 showed that of the 1081 semen samples analysed approximately 81% had asthenozoospermia, of which 18% had asthenozoospermia as the sole phenotypic pathology and 63% had asthenozoospermia in combination with either oligo and/or teratozoospermia (Curi et al. 2003). However, to date the causes of sperm dysfunction still remain largely unknown.

1.2. Diagnosis: Semen Analysis

Diagnostic assessment of sperm dysfunction is currently assessed using descriptive semen analysis, where a concentration of $\leq 15 \times 10^6$ cell/ml, total motility of $\leq 40\%$, progressive motility $\leq 32\%$ and morphology of $\leq 4\%$ is classed as abnormal (WHO 2010). However, descriptive semen analysis is a poor method of diagnosing male infertility and is only considered useful in cases where the concentration of motile sperm is exceptionally low, e.g. $< 5 \times 10^6$ /ml (Macleod & Gold 1951; Hargreave & Elton 1983; Tomlinson et al. 1999; Guzick et al. 2001; Lefievre et al. 2007). This is due to an overlap by as much as 60% between the semen parameters of men with proven fertility and men with male factor infertility (Nallella et al. 2006). As a result there is not a clear demarcation between populations of fertile and infertile men (Macleod & Gold 1951; Nallella et al. 2006; Bartoov et al. 1993; Barratt et al. 1995), making the finite diagnosis of infertility very difficult.

1.3. Treatment Options and Trends

At present the only treatment for sperm dysfunction is Assisted Reproductive Technologies (ART). Depending on the severity of sperm dysfunction there are two main options: (1) *In Vitro* Fertilisation (IVF), where the sperm and the oocyte are brought into close proximity (mild sperm dysfunction) or (2) Intracytoplasmic Sperm Injection (ICSI). ICSI is most commonly used to treat men with severe male factor infertility where the concentration and/or motility are severely affected and involves directly injecting a single spermatozoon into an oocyte. In 2009 ICSI accounted for ~50% of all fresh cycles in the UK reflecting the prevalence of male factor infertility in the UK (HFEA 2010b). Globally, the use of ART has risen steadily per annum and now it is estimated that over 4 million children have been born through the use of ART (Biggers 2012). A recent study by Ferraretti *et al* in 2012 showed that 0.8 - 4.9% of children are born using ART across Europe with an overall proportion of children born *via* ART of 1.5% (Ferraretti *et al.* 2012). Although the usage of infertility treatment has risen over the last decade, a major determinate of couples seeking fertility treatment is affordability (Farley Ordovensky Staniec & Webb 2007; Connolly *et al.* 2010). In Scotland, couples can get access to up to 2 funded cycles of ART on the National Health Service (NHS) provided they meet new guidelines for referral to one of the four IVF centres in Scotland (Aberdeen, Dundee, Edinburgh and Glasgow). These include criteria based on factors that have been show to negatively impact fertility such as; increased female age, obesity (BMI > 30 kg/m²), smoking, and drug and alcohol abuse (National Infertility Group Report 2013). In cases where couples do not meet these criteria, the cost of a single fresh ART cycle can be as much as 20% of an individual's annual disposable income (Chambers *et al.* 2009), in

an age of austerity this simply places fertility treatment out of reach for certain couples. Consequently there is a real demand for cheaper, less invasive treatments to improve the chances of conceiving naturally. As sperm dysfunction is a major cause of couples seeking fertility treatment, it provides an attractive target for *in vivo* fertility enhancement.

1.4. Ion Channels as Therapeutic Targets

Ion channels are transmembrane proteins expressed in every cell that allow hydrated ions to move between the extracellular and intracellular environments. The ion channel family is closely involved in all aspects of cell physiology as well as being critical for many of the biological processes in living organisms such as muscle contractility, cell proliferation, cell migration, blood pressure regulation and sensory perception. Mutation or disruption of ion channels, known as ‘channel pathologies’, can often be the cause of many diseases such as cystic fibrosis (mutation of the cystic fibrosis transmembrane conductance regulator). At present there are more than 60 such channel pathologies resulting in conditions such as epilepsy, kidney failure, blindness and a number of cardiological disorders (Ashcroft 2006; Wickenden et al. 2012). Based on the key functional roles of ion channels in human physiology, distinct membrane location and tissue specific expression, ion channels provide an attractive target for therapeutic treatment of a number of conditions. This is evident by the large number of drugs that have been developed to treat specific diseases that are a manifestation of channel pathology (Ashcroft 2006). However there is no known drug to enhance sperm function.

1.5. Ion Channel Screening

In order to develop therapeutic agents for channel pathologies compounds are screened to identify 'hit' compounds for further investigation. Traditionally high throughput screening (HTS) technologies are utilised for this process. These commonly manifest as ion influx or fluorescence based assays. For ion flux methods, the flux of a radioactive isotope tracer ion (i.e. ^{45}Ca) is measured during channel activation. In fluorescent based assays, movement of ions through ion channel activation results in alterations in fluorescence from ion sensitive or membrane potential sensitive dyes. Fluorescent-based assays are traditionally the method of choice for assessing ion channels in human sperm, with calcium sensitive dyes the most frequently used. Although fluorescent-based methods are well suited to high throughput screening they do have a number of limitations that may impact the identification of ion channel modulators. For example many of these fluorescent-based assays rely on a variety of additional compounds in order to optimise the effectiveness of the assay. These include the addition of surfactants to prevent dye clumping, fluorescent quenching agents, addition of ionophores and other compounds that may have secondary effects on other endogenous channels or potentially toxic effects. As a consequence the data may indicate erroneous activity of ion channels using this method (Wickenden et al. 2012). Thus it is essential to undertake secondary screening in order to confirm hit compounds identified in the primary fluorescent-based screen. This is usually undertaken using whole cell patch clamp electrophysiology, the gold standard method for definitive ion channel screening. However this method is notoriously slow and labour intensive, as a result this negatively affects the likelihood of identifying promising drugs for further development. Furthermore, it should also be noted that until 2006 whole cell

electrophysiology was thought to be impossible on human sperm. The ideal method for drug screening is high throughput automated patch clamp, which could enhance the screening throughput and provide definitive identification of potential compound hits for further development (Wickenden et al. 2012). Unfortunately due the difficulty of patching human sperm current automated patch clamp systems cannot be implemented.

Although mainstream medicine has embraced ion channel modulators as a treatment for channel related pathologies, reproductive medicine has been left to apply more invasive/rudimentary methods for the treatment of male infertility. One possible explanation is due to the limited good quality and conclusive data on what ion channels are present in human spermatozoa. This is unsurprising considering direct assessment of ion channels in human sperm by whole cell electrophysiological methods was only achieved for the first time less than three years ago (Lishko et al. 2010). Consequently, financial investment by biopharmaceutical industries has been virtually non-existent and as a result there has been no drive to stimulate scientific interest in developing new pharmaceutical based treatments for male infertility. In order to advance the current state of ART knowledge in this area, good quality direct assessment of ion channels in human sperm by electrophysiology will have to be carried out. This will not only aid in the characterisation of human sperm ion channels but will also assess how disruption of these channels may lead to male infertility and aid the development of pharmaceutical modulators of ion channel function. Although somewhat obvious, the first critical step for successful development of ion channel modulators is target validation. In human sperm there is very little direct evidence for what ion channels are present and how they contribute to the fertilising capacity.

Therefore, the better the methods for characterisation and understanding of the ion channels in human sperm and their involvement in sperm function/dysfunction, the better we can identify potential drug candidates for screening. The main purpose of this thesis is to provide further information on the identification and functional role of ion channels in human sperm.

1.6. Diagnosis of Sperm Dysfunction by Functional Assays

In addition to basic semen analysis, sperm functional testing has been shown to provide additional and complimentary information for the diagnosis of male factor sperm pathologies (Aitken 2006; Oehninger et al. 2000; Aitken 2010). The basic principle behind sperm functional testing (SFT), is to evaluate the functional capability of sperm using bioassays that mimic biological obstacles the cell would encounter *in vivo*. These are usually designed around the capability of sperm to progress through viscous environments (representative of the cervical mucus) or the ability for sperm to interact with the oocyte (Hemi-zona assays) (Aitken 2006; Lefievre et al. 2007; Barratt et al. 2011; Franken & Oehninger 2012). In an ideal clinical setting the use of sperm functional test/s (SFT) should allow for the diagnosis of a specific sperm dysfunction, which would provide a predictive tool for potential fertilisation success and if poor, aid in decisions around the appropriate treatment path. Whilst some SFTs have shown to have relatively good predictive values for fertilisation outcomes, i.e. hyperactivation (Alasmari et al. 2013), many of these tests are hindered by the lack of standardized methodologies as well as the subjective nature of the assessment. These make SFTs completely reliant on the quality and experience of the practitioner. Secondly, although SFTs provide additional information for the diagnosis of male factor infertility (a broad term in itself), they do

not provide direct and conclusive information for the root cause of that particular pathology. As a consequence diagnosis is usually vague. Furthermore, in cases of severe male factor infertility functional testing is diagnostically inept as the treatment option will most typically be ICSI, which removes all functional requirements of the cell. Rather than using vague and crude methods of diagnosis, direct and objective assessments as to the underlying causes of sperm dysfunction may provide better and patient tailored, treatment options for men with male infertility.

One such example is the manifestation of sperm dysfunction through defects in Ca^{2+} signalling. Ca^{2+} is one of the major ions that contribute a number of key physiological processes required for fertilisation such as hyperactivation and acrosome reaction. In mammalian sperm there are at least two main sources of Ca^{2+} within the cells: influx of Ca^{2+} from the external environment through CatSper channels (See section 1.13.1) and intracellular stores located in the neck/midpiece region. Several studies have shown that the measurement of hyperactivation is a useful tool for the fertilisation potential of human sperm (Sukcharoen et al. 1995; Munire et al. 2004; Alasmari et al. 2013). Defects in hyperactivation and motility in mouse have been shown to be a result of ion channel knock-out studies (Quill et al. 2003; Ho et al. 2009; Jin et al. 2007; Carlson et al. 2005; Santi et al. 2010; Zeng et al. 2011). Therefore, direct assessment of ion channels in mammalian sperm, as well as the intra- and extracellular factors that regulate their function, may improve the ability to accurately diagnose the cause of certain male factor pathological phenotypes. As well as this, develop therapeutic agents for treatment without the need for invasive treatment options such as ICSI.

1.7. Mechanics of Sperm Motility

Motility is an important functional characteristic of sperm as it allows the cells to migrate towards the oocyte, therefore, defects in motility will result in infertility. Central to sperm motility is the axoneme, which stretches down the full length of the flagellum. The axoneme consists of microtubules arranged in a 9 + 2 arrangement (nine evenly spaced outer doublets with a single pair of microtubules, see Figure 1.1) which are supported by the outer dense fibres (De Jounge & Barratt 2006; Turner 2003). Projecting from microtubule **A** to the adjacent microtubule **B** are the dynein arms that facilitate active sliding of the microtubules. Each microtubule doublet are connected to each other by nexin links with radial spokes extending towards the central pair of doublets in a helical fashion (Smtih & Yang 2004). Attached to each **A** tubule are the inner and outer dynein arms that project towards the adjacent **B** tubules. These dynein arms form the basis of active motility in human sperm. Therefore defects in these structures can results in infertility. One such example is dyskinetic cilia syndrome which is congenital absence of the dynein arms in humans and has been associated with asthenozoospermia (Wilton et al. 1985). Based on bovine and bacterial studies, initiation of movement by the dynein arms is dependent on activation of dynein ATPase in a calcium and pH dependent manor (Gibbons & Rowe 1965; Carr et al. 1985). Activation of dynein ATPase results in the phosphorylation of the dynein arms causing them to interact with the adjacent **B** tubule and produce a sliding downward stroke the manifests as a bend in the flagella.

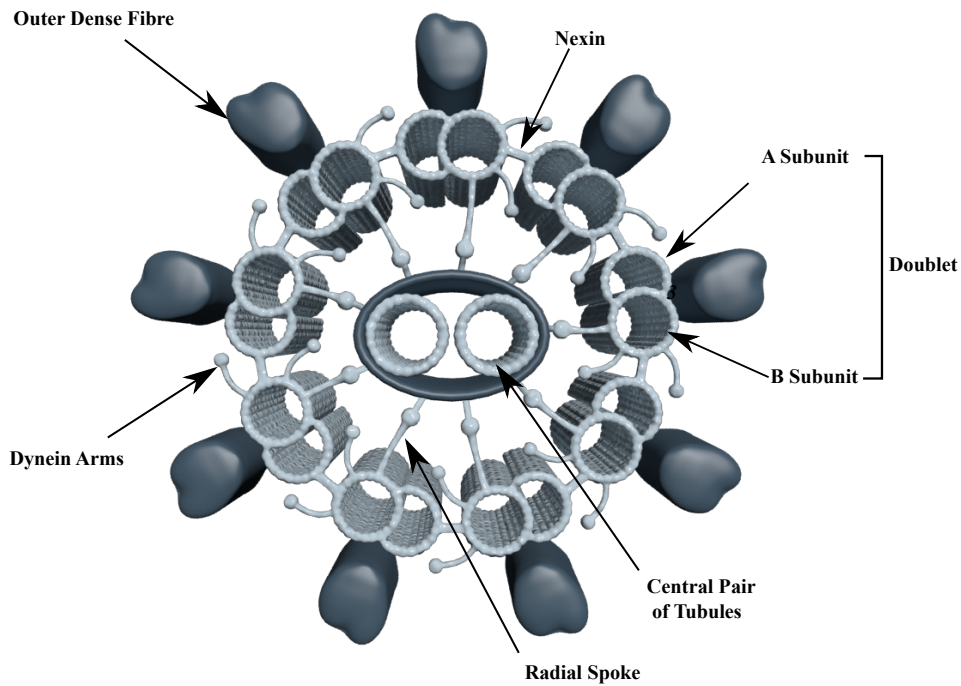


Figure 1.1: Cross section of sperm flagella adapted from Turner et al (Turner 2003)

Animal studies have shown that mammalian spermatozoa are kept in a quiescent state in the epididymis by low extracellular pH of ~ 6.8 rendering the cytoplasm acidic. This directly acts on the axoneme dynein in conjunction with high cauda epididymal fluid viscosity (Carr et al. 1985), inhibitory proteins such as semenogelin (Mitra et al. 2010; Yoshida et al. 2003) and increased K^+ and low Na^+ concentrations (Cooper 2011) to render the cell immotile. Upon ejaculation spermatozoa become motile for the first time due to constituents in the seminal plasma that promote the induction of motility, notably increased pH, HCO_3^- and Ca^{2+} . Failure to respond to changes in $[pH]_o$ or facilitate Ca^{2+} influx, can result in abnormalities in motility.

1.8. Hyperactivation

Hyperactivation is a Ca^{2+} -dependent and erratic form of motility that, based on studies in rodent spermatozoa, occurs in the upper portions of the female reproductive tract (Katz & Yanagimachi 1980; Suarez et al. 1983; Suárez & Osman 1987; Shalgi & Phillips 1988; Chang & Suarez 2012). Hyperactivation is characterised by an asymmetrical increase in the bend of the flagella. In non-viscous media hyperactivated sperm have been documented swimming in star-spin, figure-of-eight and helical patterns (Ho & Suarez 2001; Su et al. 2012).

First observed in 1970 by Yanagimachi in hamster spermatozoa, hyperactivation is thought to have a number of physiological roles that aid the cell during their progression toward the oocyte. Largely based on animal studies, due to the ethical constraints of human research, hyperactivation has been shown to be important for the ability of spermatozoa to migrate through the viscous environment of the oviduct, detach from the epithelial lining and penetrate the outer vestments of the oocyte (Suarez 2008; Suarez & Dai 1992; Ho & Suarez 2001). The induction of hyperactivation is dependent on external and internal sources of Ca^{2+} as removal of Ca^{2+} from the external environment by chelating agents prevent the induction of hyperactivation in mouse sperm (Marquez et al. 2007). The strict relationship between hyperactivation and Ca^{2+} (Bedu-Addo et al. 2008; Marquez & Suarez 2007; Quill et al. 2003; Ho et al. 2002; Ho & Suarez 2001; Ren, et al. 2001) means that cell must be able to modulate the internal concentration of Ca^{2+} in a efficient and time dependent manor in response to its external environment. As previously mentioned increase in intracellular calcium has two origins, (1) influx of Ca^{2+} from the extracellular environment through CatSper (**C**ation channel of **S**perm) channels located on the

principle piece and (2) Ca^{2+} release from the internal stores (Costello et al. 2009). It is therefore unsurprising that CatSper knock out murine sperm that are unable to hyperactivate, also: fail to progress passed the oviductal sperm reservoir *in vivo* (Ho et al. 2009); fail to penetrate artificial mucus (Quill et al. 2003); and fail to penetrate the outer vestments of the oocyte (Ren et al. 2001; Quill et al. 2003). Although the data in mouse shows a strong role for CatSper in the induction of hyperactivation, it does not mean that men with low basal hyperactivation are necessarily CatSper deficient. Electrophysiological studies from murine and human sperm have shown that CatSper is activated by increased $[\text{pH}]_i$ (governed by Hv1 in humans, see section 1.13.2) and depolarisation of the membrane potential (regulated by K^+ channels, see section 1.13.3). Therefore, the inability to hyperactive may be due to defects in other channels that indirectly affect CatSper activity rather than a defect within the CatSper channel itself. Evidence for this comes from murine knock out studies investigating Slo3 (dominate K^+ channel in mouse sperm). These studies demonstrated that Slo3^{-/-} murine sperm showed a similar pathological phenotype to CatSper^{-/-} even though CatSper was unaffected in these cells (Santi et al. 2010; Zeng et al. 2011). This potentially multifactorial cause resulting in a single pathological phenotype further highlights the poor diagnostic value of functional testing.

1.9. Capacitation

Freshly ejaculated spermatozoa are unable to fertilise an oocyte, instead they have to undergo an ill-defined process of maturation known as capacitation (Austin 1951; Chang 1951). The ability for a sperm cell to become capacitated cannot be contributed to a single event, but is an amalgamation of molecular, chemical and physical changes that result in the cell being able to reach, penetrate and fertilise an

oocyte. As it occurs post ejaculation, capacitation is often described as time-dependent process where sperm are required to spend a period of time within the female reproductive tract. *In vitro* capacitation can also be achieved by removal of the cells from seminal plasma and incubating for 2-4 hours in media supplemented with HCO_3^- and albumin (cholesterol acceptor) (Flesch et al. 2001)

In 1951 Austin and Chang independently identified that sperm had to reside within the female reproductive tract for a period of time before fertilisation could occur (Austin 1951; Chang 1951). This was based on studies that showed rabbit sperm injected directly into the oviduct were unable to fertilise oocytes. A number of key molecular events have been documented in association with the progression of capacitation. These include, the reorganisation and increased fluidity of the plasma membrane, aided by the removal of non-covalently attached glycoproteins, cholesterol and other sterols such as desmosterol (Lishko et al. 2012; De Jonge 2005); ionic fluxes resulting in changes in sperm membrane potential in mouse (Chávez et al. 2013) and human sperm (Brewis et al. 2000); and bicarbonate dependent increased protein tyrosine phosphorylation (Battistone et al. 2013). These changes cause induction of hyperactive motility and finally acrosome reaction which is thought to be a marker for the completion of capacitation (Zeng, 1995; Darszon et al. 2011; Visconti et al. 1995; Visconti et al. 1999; Flesch et al. 2001; de Vries 2003) of which ion channels play a significant role (See section 1.13) (Visconti et al. 2002).

1.10. Sperm electrophysiology- development of method

In 1981 Hamill *et al.*, revealed a cutting edge method for the direct assessment of plasma membrane ion channels (Hamill et al 1981). The method involved pulling a

portion of the plasma membrane into the opening of glass electrodes to form a tight seal, also called a giga ohm seal. This allowed direct assessment of ionic currents over the entirety of the cell (Whole cell configuration) or by assessing electrical activity of single channels (cell attached and inside-out configuration). Patch clamping provided three distinct advantages over other indirect methods of assessing ion channels i.e. ion sensitive dyes. Such benefits included: direct assessment of ion channel activity; superior time resolution of $< 1\text{ms}$; and control of both intracellular and extracellular environments. These advantages paved the way for the biophysical characterisation of ion channels in somatic cells and vastly improved our understanding of how ion channels contribute to normal cell physiology.

With ion channels playing an equally crucial role in sperm physiology, the technique naturally leant itself to being applied to spermatozoa in the mid 1980's. Despite the successes in somatic cells, early attempts with spermatozoa were unsuccessful due to the inability to form a seal between the recording electrode and the plasma membrane. This issue was thought to occur as a result of the native properties of the sperm and the plasma membrane, notably the size of the cell and composition of the plasma membrane (Kirichok & Lishko 2011).

In 1987 Guerrero et al did report the first formation of a tight seal between the head of the sperm and the recording electrode in sea urchin. However, this proved to be inefficient and successful seal formation was still extremely difficult to achieve, as reflected in the very low probability of seal formation (Guerrero et al. 1987). Later groups reported that two methods improved the likelihood of tight seal formation. These included positioning the electrode perpendicular to the sperm head and

swelling the cells by incubation in hypotonic solution (Espinosa et al. 1998; Gorelik et al. 2002; Gu et al. 2004; Jiménez-González et al. 2007; Babcock et al. 1992; Sánchez et al. 2001). Although tight seals could be achieved using these methods, the seal was not stable enough to gain whole cell access. Thus, early work only assessed single ion channel activity either by cell attached or inside-out configurations. Secondly, hypotonic induced swelling of the cell was thought to affect channel properties as well as inducing the release of hydrolytic enzymes that could lead to membrane destabilisation (Kirichok & Lishko 2011). Although sperm electrophysiology was still exceptionally difficult, these studies showed that tight seal formation between the electrode and sperm plasma membrane could occur and the reason for poor seal formation was not due to the plasma membrane composition.

Work by Yuriy Kirichok in the mid 2000's achieved a breakthrough in the evolution of sperm electrophysiology. Kirichok showed by electron micrographs of mouse spermatozoa that the issues around seal formation were due to the low cytoplasm to plasma membrane ratio, resulting in a tight association of the plasma membrane with the rigid underlying intracellular structures. This association arises in insufficient 'give' in the plasma membrane for a seal to occur and was the reason why swelling of the membrane was effective in improving seal formation as it 'loosened' this association. These studies also identified a structure, 1-3 μ m in diameter, known as the cytoplasmic droplet (CD) that was not attached to the underlying structures and could provide enough plasma membrane to form a tight seal. Application of traditional electrophysiological techniques targeted to this structure in mouse sperm showed that this was the only region where a successful seal formation and break-in could occur (Kirichok et al. 2006).

1.11. Human Sperm Patch Clamp recordings - The current approach

As in mouse, the human cytoplasmic droplet is the primary location for seal formation. Human sperm, unlike mouse or boar sperm, maintain their cytoplasmic droplet post ejaculation without affecting fertility (Cooper et al. 2011). Another difference between humans and other mammalian species is that the cytoplasmic droplet does not migrate down the flagella and is retained in a region just behind the head. At first glance the cytoplasmic droplet may appear inconspicuous owing to its relatively small size in comparison to mouse sperm, however, placement of a recording electrode in this region does result in seal formation (Lishko et al. 2010). After successful seal formation has occurred ($> 8G\Omega$), the area under the pipette is precisely ruptured to gain electrical access to the whole cell (whole cell configuration) as demonstrated by the fluorescent dyes placed in the pipette solution (Kirichok et al. 2006; Orta et al. 2012; Lishko et al. 2010). This is usually achieved by constant negative pressure in conjunction with the application of high voltage pulses (0.6-1V) (Kirichok & Lishko 2011; Lishko et al. 2013). It has been recently shown that whole cell electrical access can also be achieved by perforated patch, where a hole is created over the seal by a detergent placed in the pipette solution (Orta et al. 2012). After break-in, electrophysiological recordings are carried out in precisely the same way as somatic cells. Electrophysiological recordings are not exclusively confined to the entire cell. Treatment with trypsin and gentle trituration results in the fragmentation of the cell into either head plus mid piece or mid piece plus flagella without loss of membrane integrity (Kirichok et al. 2006). These fragments can be patch clamped in whole cell configuration to identify the subcellular locality of ion channels. This method was used to identify the localisation of CatSper (section

1.13.1) (Lishko et al. 2011), P2X2 (section 1.13.4) (Navarro et al. 2011), and K_{Sper} (section 1.13.3) (Navarro et al. 2007).

1.12. Limitation of Sperm Electrophysiology

Successful whole cell electrophysiology assumes that the entire cell is exposed to the same potential applied over the electrode. This is often dependent on the shape and size of the cell as well as the resistance over the opening of the electrode and ruptured patch, known as the access resistance (R_a). For example, the higher the R_a value, the higher the voltage drop resulting in poor voltage clamp control. In somatic cells R_a is relatively low ($< 10\text{M}\Omega$) however in sperm cell electrophysiology, R_a is usually considerably higher (30 - 100 $\text{M}\Omega$). Therefore, care must be taken when analysing electrophysiological recordings from spermatozoa and the voltage drop should be corrected post recording to obtain representative results (See materials and methods). Secondly, due to the length ($> 50\mu\text{m}$) and cross sectional cytoplasmic area ($< 1\mu\text{m}^2$), dialysis of the internal pipette solution to all areas of the sperm interior is relatively slow (~ 15 seconds)(Lishko et al. 2010; Orta et al. 2012). Therefore, data acquisition should be undertaken only after such time. For the same reason, there may be issues associated with spatial clamp (same voltage applied to all portions of the cell). However, based on low error in predicted reversal potentials from whole cell currents this does not appear to be a problem (Kirichok & Lishko 2011). In summary, in order to prevent experimental errors R_a should be as low as possible with the voltage drop corrected in the final results and data acquisition should only occur after a period of ~ 15 seconds to allow for complete dialysis of the internal contents.

1.13. Ion channels in sperm and their role in male fertility

1.13.1. Cation Channel of Sperm (*CatSper*)

Calcium is critical for normal sperm and somatic/germ-line cell physiology - increases in intracellular Ca^{2+} are responsible for changes in motility such as hyperactivation as well as the induction of the acrosome reaction. Early studies investigating the channel or channels responsible for rises in intracellular calcium believed voltage-gated Ca^{2+} channels were the principal Ca^{2+} channels in mature spermatozoa. This was based on studies indicating increased intracellular Ca^{2+} in response to high K^+ / high pH extracellular solutions with ion sensitive dyes, as well as electrophysiological recordings of rat and mouse spermatocytes, indicated clear voltage activated Ca^{2+} currents (Hagiwara & Kawa 1984; Arnoult et al. 1996; Wennemuth et al. 2000). Interestingly, mice deficient in $\text{Ca}_v2.2$, $\text{Ca}_v2.3$ and $\text{Ca}_v3.1$ remain fertile, thus introducing a major caveat to the role of Ca_v channels and their involvement in rises in intracellular Ca^{2+} (Saegusa et al. 2000; Beuckmann et al. 2003; Alnawaiseh et al. 2011; Björling et al. 2013) . From these studies it could be concluded that Ca_v channels are not essential for male fertility in mature spermatozoa. In 2001, a pivotal leap in the understanding of the role of ion channels in male fertility was achieved by the discovery of the Cation channel of sperm (*CatSper*). The cation channel of sperm or *CatSper* (later named *CatSper1*) was first characterised by Ren et al in 2001 where they described in *Nature*, a sperm specific ion channel as, ‘an unusual sperm cation channel’. Based on hydrophobicity plots Ren et al showed that the *CatSper* gene encodes a single six transmembrane spanning domain very similar in structure to voltage gated K^+ channels (K_v), cyclicnucleotide gated proteins (CNG) and transient receptor proteins (TRP). However, BLAST analysis reveals the pore

region showed homology with voltage gated Ca^{2+} channels suggesting CatSper was Ca^{2+} selective (Ren et al. 2001). Immunocytochemistry experiments indicated CatSper was exclusively expressed in the flagella of mouse sperm suggesting a role in motility. This was confirmed by the generation of CatSper knock out mice, with sperm from these animals demonstrating impaired motility and an inability to become hyperactive. As a result of these defects, the sperm were unable to penetrate the outer investments of the oocyte (zona pellucida) and these animals were completely infertile. Since then a further 6 CatSper subunits have been identified that make up the heteromeric CatSper channel. Structurally, the CatSper pore complex is comprised of four α subunits encoded by 4 different genes *CatSper1*, *CatSper2*, *CatSper3* and *CatSper4* making it the most complex ion channel ever discovered (Quill et al. 2001; Lobley et al. 2003; Qi et al. 2007). The 4 pore forming α subunits each possess a pair of negatively charged aspartic acid residues, allowing Ca^{2+} to selectively bind within the pore and confers Ca^{2+} selectivity (Chung et al. 2011). Three auxiliary subunits *CatSper β* , *CatSper γ* and *CatSper δ* are associated with this pore complex (Wang et al. 2009; Liu et al. 2007; Chung et al. 2011). Although biochemical studies have clearly shown *CatSper β* , *CatSper γ* and *CatSper δ* are directly associated with the α subunits (Chung et al. 2011; Wang et al. 2009; Ren et al. 2010; Liu et al. 2007), only *CatSper δ* has been shown to be essential for CatSper channel function as *CatSper δ ^{-/-}* mice are infertile (Chung et al. 2011). Furthermore, these studies have indicated that all subunits are required for the channel complex to be formed and functional (Carlson et al. 2005; Liu et al. 2007; Wang et al. 2009; Chung et al. 2011).

Direct assessment of CatSper in mouse spermatozoa was achieved in 2006 by whole cell electrophysiology (Kirichok et al. 2006). Recordings from wild type and

CatSper1 deficient mouse sperm revealed that CatSper was required for the Ca^{2+} selective current in mice, and knock-out studies of other CatSper subunits confirmed all subunits were required for CatSper to be functional (Jin et al. 2007; Chung et al. 2011). Electrophysiological recordings of flagellar fragments confirmed that the current originated from the flagella and was heavily gated by intracellular pH. Alkalisiation of intracellular pH from 6.0 to 7.0 results in a ~ 7 fold increase of the CatSper current. This pH sensitivity is thought to be linked to the large abundance of histidine on the *N*-terminus of CatSper1 (Ren et al. 2001), however, due to the inability to conduct mutagenic studies of CatSper, this is still to be elucidated. Mouse CatSper current or I_{CatSper} is very weakly voltage activated compared to other voltage gated channels - this is thought to be due to the unusual voltage sensing properties of the α pore forming unit (CatSper1-4). Ion channels that are strongly voltage gated contain positively charged amino acids (lysine/arginine) every third residue on the voltage-sensing domain (S1-S4), thus conferring the channel's sensitivity to voltage. However, CatSper is unusual, the number of charged residues on the S4 domain differs between the four α subunits. CatSper1 is the only subunit that follows convention, whereas CatSper 4, 2 and 3 have increasingly fewer charged residues in the particular domain (Qi et al. 2007; Navarro et al. 2008). This was confirmed by electrophysiological assessment of the Boltzmann constant (κ) that conveys the channel's sensitivity to voltage. Classical voltage gated channels have a relatively steep Boltzmann constant of ~ 4 , however, the Boltzmann constant of mouse CatSper is ~ 30 confirming this unusual property (Kirichok et al. 2006).

Human CatSper displays a number of similar features associated with mouse CatSper. Both are expressed exclusively on the flagella, weakly voltage dependent and

activated by intracellular alkalinisation. However, human CatSper does display a few unique features including a slightly increased voltage dependence of $\kappa = 20$ compared to $\kappa = 30$ in mouse (Kirichok et al. 2006; Lishko et al. 2011). Secondly, further analysis of the biophysical properties of the human CatSper channel revealed that the half maximal activation of the channel (V_{50}) was extremely depolarised (+85mV compared to +11mV in mouse). This large activation potential is very unusual and therefore questioned how CatSper would become activated under physiological conditions. Direct assessment of the human CatSper channel identified that progesterone, a major female hormone present in the female reproductive tract, strongly activated human CatSper and shifted the activation kinetics towards more typical physiological ranges (Lishko et al. 2011). Progesterone has been shown to robustly induce rapid increases in intracellular calcium (Blackmores et al. 1990; Thomas & Meizel 1989). Due to this rapid increase in Ca^{2+} and the inability for progesterone receptor inhibitor RU846 to inhibit this response, it was concluded that this robust effect was not *via* the classic nuclear progesterone receptor (Lösel & Wehling 2003; Luconi et al. 2004). As these recordings were carried out with no second messengers in the pipette solution, such as ATP or cAMP, it can be concluded that progesterone induced Ca^{2+} influx is independent of intracellular factors and the likely action of progesterone is thought to be by binding directly to the CatSper channel (Lishko et al. 2011; Strünker et al. 2011). As well as progesterone, CatSper is activated by a vast number of compounds, some of which are present in the female reproductive tract and seminal plasma such as prostaglandins (Lishko et al. 2011; Brenker et al. 2012). As a result, CatSper is classified as a polymodal channel (see Table 1).

Cases of human CatSper deficient men are unsurprisingly rare, which is most likely a result of ‘natural selection’ due to their infertile phenotype and inability to pass on the mutation to their offspring. Therefore, reported cases are usually within a single generation with one or more male siblings affected. To date, two cases of CatSper mutations in humans have been identified; one from an Iranian family (CatSper1 mutation) and another from a French family (CatSper 2 mutation). Semen analysis of these men showed that motility was severely affected as is the case with CatSper^{-/-} mice (Ren et al. 2001). In conjunction with this, sperm concentration and normal morphology were also severely affected with sperm exhibiting short, coiled flagella (Avidan et al. 2003; Avenarius et al. 2009). Men with the CatSper 1 deletion did not appear to have any other distinguishable phenotype. However, all three brothers with the CatSper 2 deletion were completely deaf (Avidan et al. 2003). Electrophysiological recording of one of the CatSper 2 deleted man revealed a complete absence of the CatSper current and an inability to respond to progesterone. This indicated the first direct evidence for a genetic link between CatSper mutation and physiological loss of function in humans (Smith et al. 2013). However, progesterone-induced Ca²⁺ imaging was not carried out in this study and it remains to be tested if the classical rise in intracellular Ca²⁺ is mediated solely *via* CatSper or in combination with other sources such as internal stores.

1.13.2. Voltage-gated proton channel: H_v1

Intracellular pH is a key regulator of many physiological processes in mammalian spermatozoa. Before 2010 the specific mechanism for proton efflux from the intracellular environment was speculative in nature due to a lack in direct methods of recording ion channels in sperm. In 1983 Babcock *et al* postulated that the mechanism

for proton efflux from bovine sperm was *via* a voltage-gated proton channel. Evidence for this was based on the use of pH sensitive dyes and membrane depolarisation with 120mM K^+ . This method demonstrated that cytosol of bovine sperm becomes alkaline with membrane depolarisation (Babcock et al. 1983). Later studies focused on the role of Na^+/H^+ exchangers (NHE) and Cl^-/HCO_3^- as potential mechanisms for intracellular alkalinisation in rat and mouse spermatozoa (Garcia & Meizel 1999; Woo et al. 2002; Zeng et al. 1996). Due to the increase in external Na^+ upon ejaculation and flagellar localisation, the NHE was proposed as an attractive mechanism for sperm alkalinisation. Indeed, $NHE^{-/-}$ mice were completely infertile due to impaired motility (Wang et al. 2003). However, the major caveat was that sperm from these animals also had extremely low expression of sACY. Motility could also be rescued by application of membrane permeable cAMP analogues suggesting that this may be the cause of the infertile phenotype (Wang et al. 2007).

With the advent of whole cell patching clamping, electrophysiological recordings of human sperm showed a large voltage activated outwardly rectifying H^+ current. This large H^+ current was aptly named HSper (H^+ channel of Sperm). HSper was shown to be highly H^+ selective, with strong outward conductance that was governed by H^+ gradients between the intracellular and extracellular environments as well as exhibiting an extreme sensitivity to Zn^{2+} (inhibition at nanomolar concentrations) (Lishko et al. 2010). Based on these unique biophysical properties, it was deduced that HSper closely resembled the voltage-gated channel H_v1 (Ramsey et al. 2006; Sasaki et al. 2006). The identification of H_v1 in human sperm was further confirmed by western blot analysis of H_v1 in native human sperm and transfected COS7 cells as well as by immunocytochemistry. Interestingly, immunostaining of H_v1 in human

sperm indicated that the channel was highly expressed in the flagella and this confirmed electrophysiological recordings indicating HSper originated from the flagella (Lishko et al. 2010).

Hv1 is comprised of a voltage sensing domain, which is structurally similar to that of voltage gated cation channels (Ramsey et al. 2006; Sasaki et al. 2006). The channel does not possess a pore domain as described by Ramsey et al., with the efflux of H⁺ thought to be *via* an internal water wire created by the voltage dependent movement of the voltage sensing S4 helix (Ramsey et al. 2006). The channel forms a functional dimer in the plasma membrane, although this dimer formation is not critical as remarkably each H_v1 subunit can function independently as a H_v1 channel (Tombola et al. 2008; Lee et al. 2008; Koch et al. 2008). Mutations in H_v1 appear to be extremely rare with only one case of a single substitution mutation being reported (Iovannisci et al. 2010). Iovannisci and colleagues only assessed the affect of this mutation in airway epithelial cells, as a result there is no data regarding the affect of this mutation on fertility.

In physiological terms, ejaculated spermatozoa are combined with the seminal plasma, which contains high concentrations of Zinc (~2mM) (Kirichok & Lishko 2011) and as such directly inhibits H_v1 function. It was been reported that as sperm progress through the female reproductive tract, divalent zinc is chelated by proteins in the oviductal fluid and therefore remains inhibited until the sperm cell reaches the fallopian tube (Lu et al. 2008; Kirichok & Lishko 2011). Electrophysiological data has shown that H_v1 is strongly potentiated by micromolar concentrations of anandamide, an endogenous cannabinoid found in male and female reproductive fluid

thought to interact directly with H_v1 (Lishko et al. 2010). The physiological relevance of this effect has been subjected to controversy as the physiological concentration of anandamide in the male and female reproductive tract are in the low nanomolar range (El-Talatini et al. 2009; Schuel et al. 2002; Decoursey 2013). However, it has been highlighted that the cumulus cells surrounding the oocyte synthesise anandamide (El-Talatini et al. 2009), therefore, in theory, sperm should be exposed to higher concentrations during penetration of the oocyte (Kirichok & Lishko 2011; Lishko et al. 2012). While this appears to be a logical explanation, to date no experimental evidence to confirm this hypothesis has been published.

In contrast to human sperm, mouse spermatozoa do not possess H_v1 . Therefore, the mechanism for H^+ efflux in mouse still remains uncertain, although, NHE still remains an attractive mechanism. Unfortunately as NHE is electroneutral (no overall net charge), traditional electrophysiological techniques cannot be implemented to investigate if NHE is the alkalising mechanism in mouse sperm. It does, however, highlight species-specific differences in ion channels that regulate fertility (Table 1).

Table 1: Ion channels assessed by electrophysiology in human and mouse sperm. Adapted from Lishko *et al.* 2012 (Lishko et al. 2012)

Channel/ Species Assessed	Gene	Ion selectivity	Subunit(s)/ Composition	Location	Role in Sperm Physiology, including sperm specificity	Endogenous Regulators	Knockout phenotype	Pharmacological antagonists and concentrations.	Pharmacological agonists and concentrations
CaSper (Human) (Mouse)	CatSper1 CatSper2 CatSper3 CatSper4 CatSperβ CatSperγ CatSperδ	Ca ²⁺	Stoichiometry unknown. Heteromeric: CatSper1-4 (pore), CatSperβ,γ,δ (auxiliary subunits)	Principle Piece	Ca ²⁺ influx resulting in hyperactivation. Sperm specific	Progesterone PGE1 (h), pH _i , egg coat proteins, albumin.	Infertile poor motility	NNC55-0396 (1-10μM) Mibefradil (30μM) MDL12330A (100μM)	PGE1 (500nM) Progesterone (500nM) Undecanal (50μM) Bourgeonal (50μM) Helional (100μM) Cyclamyl (10μM) 8-Br-cGMP (5mM) (-) Menthol (3mM)
KSper (Mouse)	Slo3	K ⁺	Probable Tetramer	Principle Piece	Regulation of membrane potential. Sperm specific	pH _i , PIP ₂ , LCR52	Infertility hairpin morphology poor motility	Quinine (500μM) Clofilium (50μM) EIPA (50μM) Mibefradil (5μM)	4-AP (4mM) NH ₄ Cl (1mM)
HV1 (Human) (Mouse)	Hvsn1	H ⁺	Probable homomeric dimer	Principle Piece	Removal of intracellular H ⁺ from flagellum, alkalises cytoplasm. Not sperm specific.	pH _i , V _m , removal of zinc, anandamide.	Not in mouse, Hv1 ^{-/-} are fertile	Not investigated	Oleic acid (100μM) Anandamide (>3μM)
IATP (Mouse)	P2rx2	Na ⁺ K ⁺ , Ca ²⁺	Probable homomeric	Midpiece	Widespread		P2rx2 ^{-/-} mice are fertile	Not investigated	ATP (100μM)
CaCC (Human)	<i>Ano1</i>	Cl ⁻	Probable tetramer	Unknown	Cl ⁻ efflux resulting in AR	Ca ²⁺	Ano1 ^{-/-} lethal at birth in mouse.	Not investigated	NFA (10μM) DIDS (20μM) TMEM16A _{inh} (10μM)

1.13.3. Potassium Channel of Sperm (*KSper/Slo3*)

As highlighted in sections 1.13.1 and 1.13.2 both H_v1 and CatSper rely on voltage, in various degrees, for channel gating. This membrane voltage is known as the membrane potential. In somatic cells the resting membrane potential is primarily set by voltage gated K^+ channels (Shieh et al. 2000) and this is also true for sperm cells. As well as regulation of membrane potential, studies have also indicated a potential role in volume regulation that prevents osmotic shock when sperm are deposited in the female reproductive tract (Barfield et al. 2006)

In 2007, Navarro *et al.*, reported a weakly voltage activated hyperpolarising K^+ current in mouse spermatozoa by whole cell electrophysiology for the first time. This current was initially named KSper (potassium channel of sperm) (Navarro et al. 2007). Examination of the KSper current using symmetrical K^+ based solutions showed that KSper possessed a number of similar features to CatSper. For example both were gated by intracellular pH, weakly voltage dependent and expressed in the flagella (based on recording from fractionated sperm). Pharmacological assessment of KSper showed it was sensitive to external application of barium, quinine, clofilium, EPIA and mibefradil. Based on this biophysical and pharmacological profile it was proposed that KSper could be a the sperm specific channel Slo3 (Navarro et al. 2007). However, in order to confirm this hypothesis, Slo3 knockout mice would need to be assessed.

Murine Slo3 knockouts were attained and as a result confirmed the identity of the KSper current as being the alkaline potentiate Slo3 channel (Santi et al. 2010; Zeng et

al. 2011). Sperm from these animals showed defects in motility, acrosome reaction and osmo-regulation as well as being completely infertile. As previously mentioned, capacitation results in alkalinisation of the cytoplasm, as Slo3 is potentiated by intracellular alkalinisation, mouse sperm membrane potential becomes hyperpolarised to $\sim -60\text{mV}$ during capacitation. However, in the Slo3^{-/-} mice this process did not occur: conversely membrane potential appeared to depolarise (Santi et al. 2010). Interestingly, the basal resting membrane potential of both wild type and Slo3^{-/-} sperm were identical in uncapacitated cells indicating the resting membrane under these conditions may not be set by Slo3. This hypothesis has yet to be assessed.

Expression of both murine and human Slo3 in *Xenopus* oocytes does show that the channel is weakly voltage sensitive as well as pH sensitive. There are, however, a few discrepancies between the endogenous mSlo3 and heterologously expressed mSlo3. Most notably is that heterologously expressed mSlo3 is inactive at $\text{pH}_i < 7$ and at potentials $< 0\text{mV}$ (Martínez-López et al. 2009; Zhang et al. 2006), while in contrast, currents can be recorded in mouse (Navarro et al. 2007; Santi et al. 2010; Zeng et al. 2011). It is therefore possible that Slo3 may require other subunits/mechanisms for normal function that are not expressed in heterologous systems. Evidence for this is provided by data on LRRC52 (leucine rich repeat containing protein no. 52), a protein found in high abundance in the testis and has been shown to alter the gating properties of Slo3 to that seen in endogenous systems (Yang et al. 2011). In conjunction with LRRC52 recent papers have also indicated the Slo3 gating is governed by intracellular factors such as cAMP (Martínez-López et al. 2009) and phosphatidylinositol 4,5-bisphosphate (PIP₂) (Tang et al. 2010).

Evidence for Slo3 in human sperm is still unclear. Slo3 mRNA has indeed been shown to be present in human testicular tissue but there is no evidence of the presence of Slo3 proteins in ejaculated human sperm (Schreiber et al. 1998). Heterologous expression of human Slo3 in *Xenopus* oocytes also indicated that human Slo3 is pH sensitive as well as requiring LRRC52 for normal function (Leonetti et al. 2012). However, unpublished data by Lishko and colleagues reported eluded that human KSper is pH insensitive (Lishko et al. 2012). The only evidence of KSper in humans comes from an electrophysiological based study of a CatSper 2 deficient man. The KSper current recorded in the normozoospermic group from this paper did show an outwardly rectifying hyperpolarising current similar to that described in mouse (Smith et al. 2013). This current was reduced in the CatSper 2 deficient man, although this was not further investigated. The paper by Smith et al., did not provide any evidence for the pH sensitivity of human KSper. Although the channel responsible for the human KSper still remains unidentified, the main hypothesis is that human KSper is likely to be a homolog of Slo3.

1.13.4. ATP-Gated P2X2 Channel

The ATP-gated P2X2 channel is a non-selective, Ca^{2+} permeable channel in mouse sperm. Discovered in 2011 by Navarro et al, P2X2 was activated by external application of ATP and therefore was referred to as I_{ATP} . Electrophysiological recordings of I_{ATP} showed the current was almost exclusively inwardly rectifying, originated from the head and mid piece, was potentiated by external Zn^{2+} and intracellular acidification. Based on these biophysical properties it was deduced that I_{ATP} resembled heterogeneously expressed P2X2 channels (Navarro et al. 2011).

Confirmation of P2X2 as the channel responsible for I_{ATP} was achieved by the absence of I_{ATP} in P2X2^{-/-} mouse sperm. Despite this knockout, P2X2^{-/-} mice had normal sperm concentration, motility, and morphology and were able to undergo acrosome reaction. Moreover, these mice were fertile. This therefore questioned the importance of this channel for male fertility. However, Navarro et al. showed that fertility in the P2X2^{-/-} mice decreased with frequent mating. From this the authors postulated that P2X2 provided an evolutionary advantage by supplying Ca^{2+} to the mitochondria and aided ATP production, improving overall sperm 'fitness' (Navarro et al. 2011). To date no such channel has been identified in human sperm.

1.13.5. Calcium Activated Chloride Channel (TMEM16A/Ano 1)

Chloride has been shown to be essential for capacitation. Studies of mouse sperm have shown that cells incubated in the absence of external Cl^- show defects in hyperactivation, tyrosine phosphorylation and the acrosome reaction. As a consequence, these sperm are unable to fertilise. Given these effects, it is interesting that general motility is not affected (Chen et al. 2009; Wertheimer et al. 2008). Chloride channels have also been shown to be present in human sperm and pharmacological inhibition of these channels results in a similar phenotype to that seen in mouse. However, inhibition of Cl^- channels in human sperm does not suppress tyrosine phosphorylation (Li et al. 2013). In somatic cells Cl^- channels in conjunction with K^+ channels are thought to be the principle ions that allow volume regulation to occur and protect the cell from osmotic stress (Fürst et al. 2002). This is important as spermatozoa experience dramatic changes in osmolarity as they ascend the female reproductive tract. Based on pharmacological studies it is thought that Cl^- channels

are also implemented in this function in human spermatozoa (Yeung et al. 2005). In particular, the calcium activated chloride channels (CaCC) are thought to be relevant to sperm function as niflumic acid (NFA) and 4,4'-diisothiocyanostilbene-2,2'-disulphonic acid (DIDS), inhibitors of CaCC's, have been shown to inhibit acrosome reaction in mouse sperm (Espinosa et al. 1998). As human sperm ascend the female reproductive tract it is thought that intracellular calcium is raised by increased CatSper activity. This in turn may help modulate CaCC's to prime the cell for the induction of acrosome reaction. However, before 2012 the direct assessment of CaCC's in human sperm had never been assessed and therefore direct confirmation of their role in sperm physiology remained unclear.

Orta and colleagues used perforated patch clamp to achieve direct assessment of a calcium dependent chloride conductance in human sperm in 2012. Unlike traditional sperm electrophysiological techniques (whole cell configuration via the cytoplasmic droplet), Orta and colleagues demonstrated that accurate recordings of the whole cell could be achieved by forming a seal over the head region that were comparable to traditional whole cell techniques. This breakthrough is thought to enable the electrophysiological recordings of spermatozoa from species that do not retain their cytoplasmic droplet post ejaculation e.g. sea urchin. However, the main premise of the paper was the direct electrophysiological recordings of chloride conductance in human sperm. Using this technique they demonstrated that human sperm possess a highly selective chloride conductance. This was identified by experiments where concentrations of external Cl^- were modified to cause a change in the reversal potential of Cl^- (E_{Cl^-}), which in turn was shown to accord well with the predicted E_{Cl^-} as calculated by the Nernst equation (Equation 2.9.3 materials and methods).

Furthermore, the channel showed strict dependence on intracellular concentration of Ca^{2+} (activation $\geq 250\text{nM}$) as well as voltage dependence. Based on these biophysical properties it was concluded the conductance resembled that of CaCC's and heterologously expressed TMEM16A or Ano1 (Suzuki et al. 2006). Further characterisation was achieved using pharmacological methods. These experiments showed the Ca^{2+} dependent Cl^- conductance was inhibited by DIDS, NFA as well as a TMEM16A specific inhibitor TMEM16A_{inh} at a similar concentration that resembled the pharmacological profile of native CaCC's and heterologously expressed TMEM16A (Hartzell et al. 2005; Caputo et al. 2008; Yang et al. 2008). As mentioned previously, inhibition of the chloride channel in human and mouse is correlated with the inability to undergo acrosome reaction (Espinosa & Darszon 1995; Li et al. 2013; Espinosa et al. 1998). Addition of NFA, DIDS and TMEM16A_{inh} also demonstrated a significant inhibition of rhZP3 induced acrosome (Orta et al. 2012). From this, it was hypothesised that the channel played a functional role in normal acrosomal exocytosis. Although Orta et al., were unable to accurately identify the locality of the channel using immunofluorescence or Western blot analysis, they did manage to detect a faint band at the relevant molecular mass suggesting the protein was present. It is evident that further work is required to determine the precise localisation and mechanism in which TMEM16A regulates physiological events such as the induction of acrosome reaction

1.14. Overall Aim and Hypothesis

The aim of this thesis is to record and characterise native currents from human spermatozoa under conditions that maintain physiological ionic concentrations of Na^+ , K^+ , Cl^- and Ca^{2+} . Furthermore, this thesis aims to assess how these ion channels contribute to normal sperm function. The main hypothesis is that human sperm ion channels are implicated in sperm motility and disruption of these channels results in sperm dysfunction.

Chapter 2 - Materials and Methods

2.1. Donors

Donors were recruited in accordance with the ethical approval from the Tayside Committee of Medical Research Ethics B (number 09/s1402/6) and written consent was provided from each donor in accordance with the Human Fertilisation and Embryology Authority (HFEA) 8th code of practice. Donors were aged between 19 and 50 years old with > 90% from the local student population with 13% (4/31) of this population having contributed to a pregnancy. Normozoospermic donors were identified by an initial semen analysis based on WHO 2010 criteria for sperm concentration (≥ 15 million/ml) and motility ($\geq 32\%$ progressive and $\geq 40\%$ total motility) (WHO, 2010). All donors were asked on recruitment to fill out a questionnaire regarding their lifestyle and background (see appendix). According to these questionnaires none of the donors had a sexually transmitted infection or known fertility issues that could affect the final results.

2.2. Collection of Semen Sample and Delivery to the Laboratory

Donors had clear instructions both written and verbally regarding the collection and delivery of semen samples. Samples were collected after 2 – 4 days of sexual abstinence but no longer than seven days. This was maintained throughout the course of the research to reduce semen variability. Samples were produced by masturbation on the donor's own premises into a sterile wide mouthed plastic container (lab supplied). Samples were delivered to the lab by the donor within an hour of production, these samples were kept warm by placing the collection pot in an inside jacket pocket. Donors were informed as to why this was important. For auditing purposes, the collection pots were labelled with the donor's ID number, date, time of

production and the period of abstinence. These details were double checked with the donor to ensure accuracy.

2.3. Sperm Preparation

Samples were placed in a 37 °C air incubator for 10-20 minutes to allow for liquefaction. Motile sperm were collected using the swim-up method into artificial human tubal fluid solution (HTF, Table 3). This was achieved by placing 1 ml of raw semen under 5 ml HTF in a 50 ml Falcon tube. Tubes containing semen and HTF were placed at a 45 degree angle to increase surface area in a 37 °C air incubator for 1 hour before collecting the top 3 ml of HTF containing the highly motile sperm. Care was taken to ensure semen was not drawn up into the pipette when harvesting the top 3 ml. The cells were transferred to a clean Falcon tube and allowed to settle and form a loose pellet for ~ 1 hour at room temperature (20-25 °C). The pellet was collected and placed in capacitating media (HS-CAP, equilibrated for 90 minutes in a 37 °C 5% CO₂ incubator prior to use, Table 3). Cells were then placed in a 37 °C 5% CO₂ incubator for 2 - 4 hours to capacitate. This method of preparation was used over density gradient centrifugation to prevent damage to the cytoplasmic droplet and rupture of the annulus.

2.4. Motility Assessment

Motility of human sperm cells in the presence and absence of putative K⁺ channel blockers were assessed using a Hamilton Thorn CEROS machine (version 12) equipped with an external microscope. Capacitated samples from normozoospermic donors were adjusted to 20-30 × 10⁶/ml before addition of the agonist/antagonist. To

ensure homogeneity, the cells and agonist/antagonist samples were lightly mixed by pipetting up and down, before placing 3 μl of sperm onto a pre-warmed MicroCell counting chambers (Vitrolife San Diego USA, 20 μm depth). Loaded chambers were placed on a heated stage attached to the Olympus CX41 microscope and left for ~ 2 minutes at 37°C prior to data acquisition. This was done to allow for sample 'drift' to cease. Approximately 800 cells were counted at random from each sample population using a CEROS negative phase contrast (10x objective, final magnification 100x). Sperm cell recognition and motility analysis was collected using CASA inbuilt settings of 60Hz; low and high size gates, 0.35 and 2.80, respectively; low and high intensity gates, 0.5 and 2 respectively; minimum number of data points, 13; non-motile head size, 6 pixels and non-motile head intensity, 160. To ensure error was reduced during collection, the CASA playback system was utilized. Throughout the data collection at least 90% of spermatozoa were identified per field of view. Sperm motion parameters assessment for individual spermatozoa included average path velocity (VAP), straight-line velocity (VSL), curvilinear velocity (VCL), beat cross frequency (BCF), amplitude of lateral head displacement (ALH, Figure 2.1), straightness (STR, defined as VSL/VAP) and linearity (LIN, defined as VSL/VCL) (Mortimer, 2000). General motility classification included: rapid cells ($\text{VAP} > 25 \mu\text{m/s}$); moderate ($\text{VAP} 5\text{-}25 \mu\text{m/s}$) and slow ($\text{VAP} < 5 \mu\text{m/s}$ and $\text{VSL} < 11 \mu\text{m/s}$). Progressive motility was classified as any cells with a $\text{VAP} > 25 \mu\text{m/s}$ and a straightness $> 80\%$. Hyperactivation was expressed as a percentage of total number of motile cells and classified using standard criteria: $\text{VCL} \geq 150 \mu\text{m/s}$, linearity $\leq 50\%$ and an $\text{ALH} \geq 7$ (Mortimer et al., 1998).

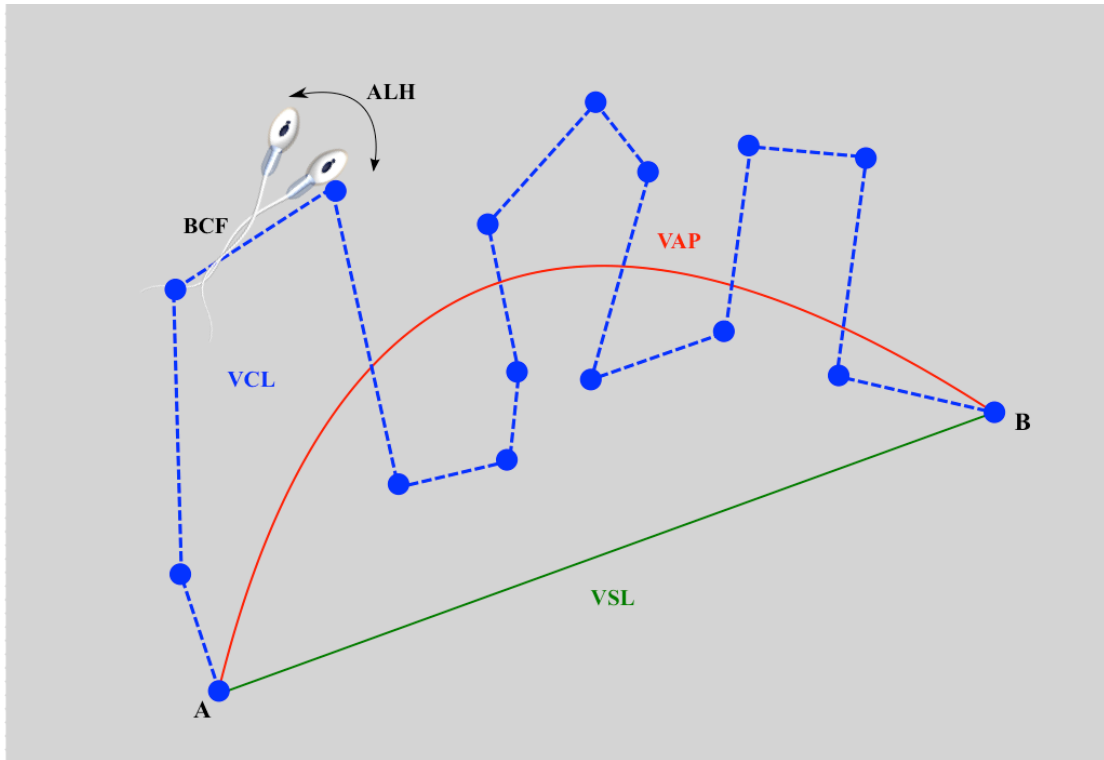


Figure 2.1: Kinetic parameters of a human sperm cell as assessed by computer aided sperm analysis (CASA). Adapted from WHO manual 2010 (WHO, 2010).

2.5. Ca^{2+} Measurements

Capacitated spermatozoa ($\sim 2 \times 10^6/\text{ml}$) were incubated with $1 \mu\text{M}$ Fura 2-AM for 45 minutes at 37°C in the dark. To maximize Fura-2AM loading, Pluronic F127, a non-ionic surfactant polyol, was added to the cell suspension at a concentration of 0.05% (v/v). After loading, cells were pelleted by centrifugation (10 minutes at $700 \times g$) and the sperm pellet transferred to 1 ml of fresh HS solution before repeating the washing process. The supernatant was removed being careful not to disturb the pellet and was subsequently re-suspended in $45 \mu\text{l}$ of HS or HS + inhibitor (see Table 4) before being placed in a 96 well plate ($50 \mu\text{l}/\text{well}$). Fluorescent measurements were recorded using FLUOstar Omega (BMG Labtech Offenburg Germany) by alternating the excitation wavelengths between 340 nm (Ca^{2+} bound Fura) and 380 nm (Ca^{2+} free Fura) and recording emissions at 510 nm . Progesterone

induced increase in $[Ca^{2+}]_i$ of control and treated samples were recorded by injections of 5 μ l progesterone (36 μ M Stock, final concentration 3.6 μ M) and the stimulus induced increase in the 340/380 nm ratio were calculated. Resting Ca^{2+} levels were recorded before injection of progesterone (20 data points at 5 seconds between points) and background fluorescence was calculated after quenching with 5 μ l $MnCl_2$ (100mM stock, final concentration 9mM) before being removed from each data point.

List of Solutions

Pipette Solutions

Table 2: List of intracellular pipette solutions used in this thesis.

Pipette Solutions composition	CatSper	Quasi-physiological $[K^+]_i = 114mM$	Cs^+ based $[K^+]_i = 0mM$	Na^+ Based $[K^+]_i = 0mM$	NMDG ⁺ Based solution	Low Na^+
NaCl (mM)	-	10	10	28	-	10
KCl (mM)	-	18	-	-	-	-
NMDGCl	-	-	-	-	28	18
Na-Gluconate (mM)	-	-	-	92	-	-
K-Gluconate (mM)	-	92	-	-	-	-
NMDG-Gluconate	-	-	-	-	92	92
$CsMeSO_3$ (mM)	130	-	-	-	-	-
$CsCl_2$ (mM)	-	-	18	-	-	-
$CsOH$ (mM)	-	-	92	-	-	-
EGTA (mM)	3	1	1	1	1	1
EDTA (mM)	2	-	-	-	-	-
$MgCl_2$ (mM)	-	0.5	0.5	0.5	0.5	0.5
$CaCl_2$ (mM)	-	0.6	0.6	0.6	0.6	0.6
HEPES (mM)	40	10	10	10	10	10
Tris HCl (mM)	1	-	-	-	-	-
pH	7.4	7.4	7.4	7.4	7.4	7.4
Adjusted with	$CsOH$	KOH	Gluconic Acid	$NaOH$	NMDGOH	NMDGOH
Osmolality (mOsmols)	~320	~250	~250	~250	~250	~250

Bath Solutions

Table 3: Composition of different bath solutions used in this thesis.

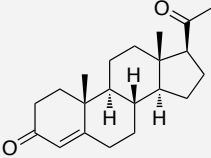
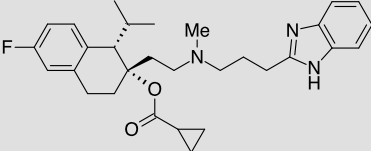
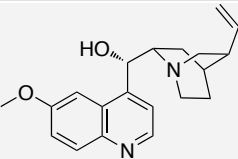
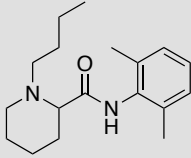
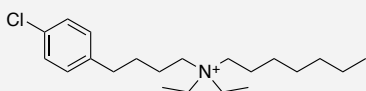
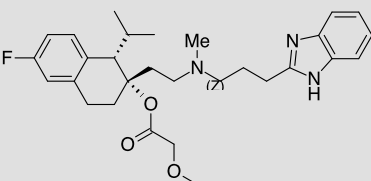
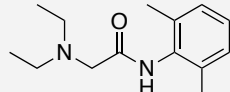
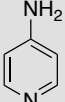
Bath Solution Components (mM)	HS	HS-CAP	HS-DVF	HTF	DVF	HKS	Low Na ⁺	2mM [Ca ²⁺] ₀	10mM [Ca ²⁺] ₀
NaCl	135	135	135	97.8	-	10	10	25	25
NMDGCl	-	-	-	-	-	-	125	112	96
KCl	5	5	5	4.69	-	130	5	3	3
CsMeSO ₄	-	-	-	-	130	-	-	-	-
MgCl ₂	-	-	-	-	-	-	-	-	-
MgSO ₄	1	1	-	0.2	-	1	1	1	1
CaCl ₂	2	2	-	2.04	-	2	2	2	10
HEPES	20	20	20	21	40	20	20	20	20
Glucose	5	5	5	2.78	-	5	5	5	5
Lactic acid	10	10	10	21.4	-	10	10	10	10
Na-pyruvate	1	1	1	0.33	-	1	1	1	1
EGTA	-	-	1	-	1	-	-	-	-
Mannitol	-	-	-	-	-	-	-	-	8
NaHCO ₃ (mM)	-	25	-	-	-	-	-	-	-
FBS (% v/v)	-	20	-	-	-	-	-	-	-
pH	7.4	7.4	7.4	7.4	7.4	7.4	7.4	7.4	7.4
Adjusted with	NaOH	NaOH	NaOH	NaOH	CsOH	KOH	NMDGOH	NMDGOH	NMDGOH
*Osmolality (mOsmols)	~320	~330	~320	~290	~320	~320	~320	~320	~320

*Osmolality was based of solutions by Lishko et al 2010, 2011 and fell within the physiological range of human semen (Cooper et al., 2005). Although at the upper limit of the physiological range, no detrimental effects on motility were observed under these conditions.

2.6. Pharmacology

In order to characterise and assess the biophysical properties of the channels discussed, a number of compounds were used in functional as well as electrophysiological experiments (Table 4). All pharmacological compounds were obtained from Sigma Aldrich, Dorset, UK unless otherwise stated.

Table 4: List of pharmacological compounds used for the characterization of ion channels in human spermatozoa

Compound	Function	Vehicle	Final Conc. (μM)	Reference
Progesterone 	CatSper channel agonist	Ethanol	0.5 - 3.6	(Lishko et al., 2011; Strünker et al., 2011)
NNC 55-0396 	CatSper Channel antagonist	H ₂ O	2	(Lishko et al., 2011; Strünker et al., 2011)
Quinidine 	Broad K ⁺ channel antagonist	HS media	300-3000	(Inglis et al., 2007)
Bupivacaine 	Local anaesthetic, sodium and potassium channel antagonist	HS media	3000	(Inglis et al., 2007)
Clofilium 	Kv11.1, Kv1.5, TASK5.1 and Slo3 K ⁺ channel antagonist	H ₂ O	50	(Navarro et al., 2007)
Mibefradil 	K ⁺ and CatSper Channel antagonist	H ₂ O	30	(Brenker et al., 2012; Navarro et al., 2007)
Lidocaine 	K ⁺ channel antagonist	DMSO	3000	(Inglis et al., 2007)
4-AP 	Non-selective Kv channel antagonist	H ₂ O	2000	(Navarro et al., 2007)

2.7. Electrophysiology

2.7.1. *Patch clamping somatic cells*

Patch clamping is a technique that records the electrical activity of ion channels over the surface of a cell membrane. Depending on the type of configuration used, this can either be recordings from multiple (whole cell configuration) or single (cell attached, outside-out excised patch, inside-out excised patch) ion channels. In this thesis whole cell patch clamping was the only method used and is described below.

Patch clamping begins by positioning a glass electrode filled with appropriate filling solutions into close proximity to the cell membrane. Next, light suction is applied causing the membrane to be pulled up into the electrode blocking the opening. This forms a tight seal between the cell membrane and the glass electrode, characterised by an increase in the electrical resistance between the cell and electrode to a value greater than 1 giga ohm ($G\Omega$). This is known as a $G\Omega$ seal and is an essential starting point for accurate electrical recordings. Next, in order to gain electrical access to the cell, the cell membrane needs to be precisely ruptured to cause a hole under the area of the electrode opening without disrupting the $G\Omega$ seal. Short, sharp suction pulses, sometimes in conjunction with voltage pulses, mechanically ruptures the membrane and a drop in the access resistance characterises successful break-in. Immediately after break-in the contents of the cells are replaced by the pipette solution in a process known as dialysis and as a consequence allows control of the intracellular conditions, therefore tailor-made pipette solutions can be designed to target specific ion channels. However, dialysis also removes all intracellular second messengers such as ATP and

other important intracellular compounds. As a result, care must be taken when making up appropriate intracellular solutions.

2.8. Experimental Design

After 2 - 4 hours capacitation $\sim 2 \times 10^4$ motile sperm cells were seeded out onto clean glass cover slips (World Precision Instruments, Inc USA, mini cover slips 5 mm diameter) in fresh HS solution and allowed to adhere for 5-10 minutes at room temperature (20-25 °C). Cover slips were placed in a rapid perfusion chamber (chamber volume = 50 μ l) mounted on an Olympus IX71 microscope equipped with differential interference contrast (DIC) and 60 \times water immersion objectives to clearly visualise the cytoplasmic droplet (Figure 2.2A).

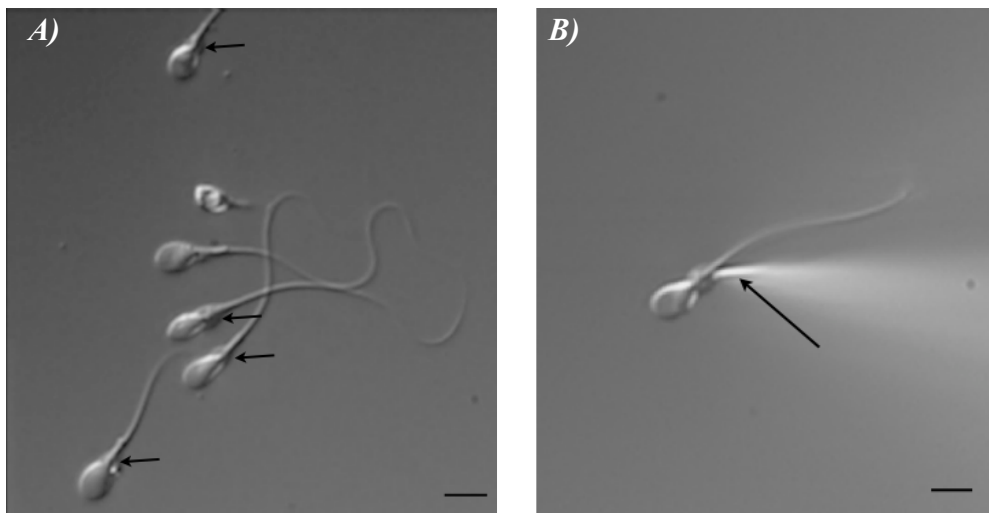


Figure 2.2: A) Human sperm cells at 90x magnification (60x water immersion objective plus in built 1.5x optic). Arrows indicate cytoplasmic droplet and site of seal formation. B) Human sperm attached to recording electrode and elevated off cover slip. Arrow indicating recording electrode attached *via* the cytoplasmic droplet. Scale bar represents 5 μ m.

Control of the external solution was achieved using a pinch valve perfusion system (Scientific Instruments ALA-VM8 scientific instruments, Inc. USA). Sperm cells with moderate sized cytoplasmic droplets as described by Lishko and colleagues (2011) were approached at a 45° angle with a borosilicate glass microelectrode pipette fire polished to 10-17 M Ω using a Narishige microforge (MF-83, Japan). Seals were formed by positioning the microelectrode close to the cytoplasmic droplet of the cell using a MP-225 micromanipulator (Sutter Instruments) and applying light suction. Once a stable G Ω seal had formed ($\geq 8\text{G}\Omega$) cells were lifted off the cover slip to prevent rupture of the seal by slight movement during the duration of the recording (Figure 2.2B). Whole cell electrical access was achieved by multiple 1 ms voltage pulses (499 - 644 mV) in conjunction with constant light suction. Successful break-in was determined by a fall in access resistance to a stable value of between 30-80 M Ω , however in experiments where NMDG⁺ was the main cation an acceptable access resistance was between 30 - 120 M Ω (Lishko et al., 2010). Seal formation and break-in success was subject to the donor used and minor adjustments in suction strength were used to improve the chance of a successful seal formation. On average successful seal formation was $\sim 80\%$ and successful break in was achieved in $\sim 50\%$ of cells. In these experiments cells with a membrane capacitance (C_m) between 0.5 - 1.2pF, membrane resistance (R_m) $> 2.5\text{G}\Omega$ and an access resistance (R_a) between 30 and 80M Ω were considered eligible for recording. On average these values were; $C_m = 0.94 \pm 0.01\text{ pF}$, $R_m = 9.87 \pm 0.52\text{ G}\Omega$ and $R_a = 62.63 \pm 0.72\text{ M}\Omega$, number of cells (n_C) = 487, number of donors (N_D) = 31 and accorded well with studies that have previously assessed ion channels in human sperm (Lishko et al., 2010, 2011; Orta et al., 2012).

2.9. Basic Electrophysiological principles of patch clamping

2.9.1. *Liquid Junction potentials*

An inevitable source of voltage error is introduced into any electrophysiological experiment by simply placing the pipette into the bath. This is due to a difference in ion concentration and mobility between the bath and pipette solutions. This therefore results in the movement of ions between the interface of the pipette opening and bath producing a voltage error. This error is known as the liquid junction potential and can be calculated (for a single solute) using the formula:

$$V = \frac{u - v}{u + v} \frac{RT}{F} \ln \left[\frac{c_1}{c_2} \right]$$

Where V is the voltage difference, u and v are the cation and anion mobilities for the desired solutions, R is the gas constant, T is the absolute temperature, F is Faraday's constant and c_1 and c_2 are the concentrations of the solute in the bath and pipette. However, calculation of the liquid junction potential in solutions that contain more than one solute is complicated. In order to calculate the junction potential of solutions with multiple solutes as used in this thesis, JPCal, a pre-installed program in the pClamp software (Barry, 1994) was utilised. In the experiments described here, the junction potential was 12 mV in HS solution using standard pipette solution and 4mV using NMDG⁺ based pipette solution. All results presented in this thesis have been corrected for this. In conjunction with this, a salt bridge containing 3 M KCl in 4% agar was used to ground the solutions to ensure negligible changes in liquid junction potential by changing bath solutions (Barry & Lynch, 1991)

2.10. Series resistance

The electrical activity of a cell can be modelled as an RC circuit due to the properties of the membrane to store charge (like a capacitor, C_m) and conduct charge (comparable to a resistor, R_m), which are connected in parallel (Figure 2.3B). However, transition to a whole cell configuration, as used in this thesis, introduces another resistance between the intracellular compartment and the opening of the pipette known as the access or series resistance (R_a , Figure 2.3C). As the access resistance is in series with the membrane resistance the voltage applied by the command voltage (V_c or V_{hold}) will be subjected to a voltage drop over R_m and R_a introducing a voltage error in the recording protocol.

In conventional whole patch clamping the R_a tends to be relatively low (<10 M Ω), however in sperm patch clamping this value is between 30-80 M Ω due to the size and shape of the pipettes and the cell. The voltage error for a R_a this size can be estimated using the formula below.

$$V_m = V_c - I_p R_a$$

Where V_m is the true voltage carried over the cell, V_c is the command voltage, I_p is the current recorded at V_c and R_a is the access resistance of the cell. Thus, a cell with a R_a of 80 M Ω , V_c of 80 mV that generates 40 pA (average peak current in thesis), would have a V_m of:

$$V_m = 8 \times 10^{-2} V - 4 \times 10^{-11} A \cdot 8 \times 10^7 \Omega$$

$$V_m = 8 \times 10^{-2} V - 0.0032$$

$$V_m = 76.8 mV$$

Therefore a R_a of 80 M Ω would result in a voltage drop of 3.2mV (4% decrease) in V_{hold} . Even the highest R_a would have a negligible effect on V_{hold} in the data presented in this thesis.

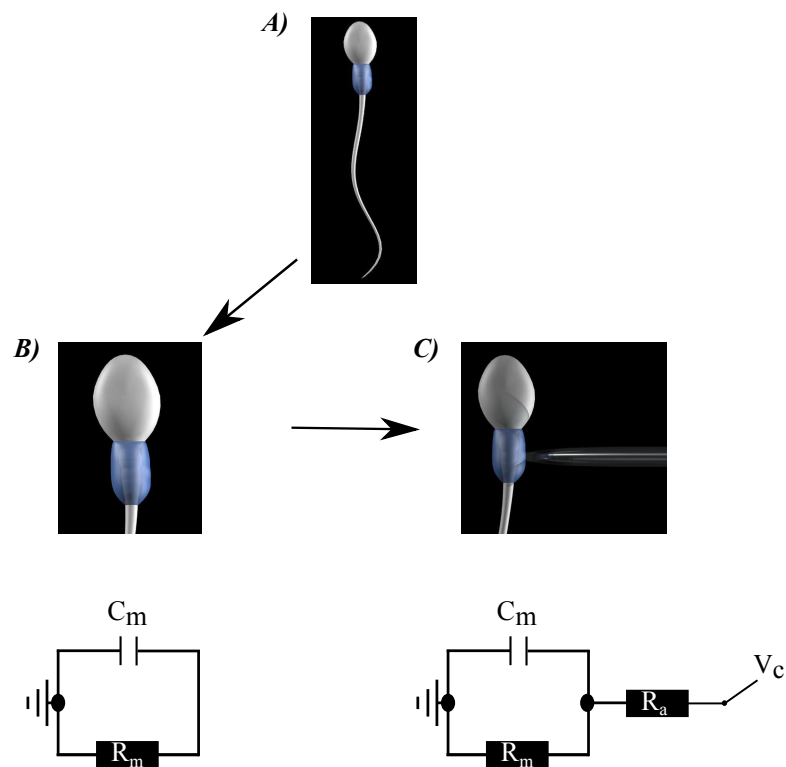


Figure 2.3: Electrical circuit of human sperm cell. A) Illustration of intact human spermatozoa with cytoplasmic droplet. B) Close up of intact human sperm with schematic illustrating the cell membrane as an RC circuit with membrane capacitance (C_m) and membrane resistance (R_m) in parallel C) Sperm cell in whole cell configuration with the introduction of access resistance (R_a) and command voltage (V_c).

2.11. Equilibrium Potential

Throughout this thesis equilibrium potentials were calculated using the Nernst equation given as:

$$E_S = 2.303 \frac{RT}{Z_s F} \log_{10} \frac{[S]_o}{[S]_i}$$

Where R is the gas constant ($8.31 \text{ J K}^{-1} \text{ mol}^{-1}$), T is the temperature in Kelvin (K), Z_s is the valency of the ion (S), F is the Faraday constant ($9.65 \times 10^4 \text{ C mol}^{-1}$) and $[S]_o$ and $[S]_i$ are the extracellular and intracellular ion concentrations, respectively. An example calculation of the equilibrium potential of K^+ under quasi-physiological conditions (physiological ionic concentrations of K^+ , Na^+ , Ca^{2+} and Cl^-), as described in this thesis, would be:

$$E_K = 2.303 \frac{(8.31 \text{ JK}^{-1} \text{ mol}^{-1})(296.16 \text{ K})}{1(9.65 \times 10^4 \text{ C mol}^{-1})} \log_{10} \frac{[5\text{mM}]_o}{[114\text{mM}]_i}$$

$$E_K = 58.5 \text{ mV} \log_{10} \frac{[5\text{mM}]_o}{[114\text{mM}]_i}$$

$$E_K = -79.5 \text{ mV}$$

2.12. The Goldman, Hodgkin, Katz Equation

Although a very powerful equation, one weakness of the Nernst equation is that it can only be used to predict the reversal potential of a single ionic species. As this thesis focuses on the electrophysiology of human spermatozoa under quasi-physiological

conditions the resting membrane potential may not be governed by a single ionic species but a combination of K^+ , Na^+ and Cl^- (major contributors to cellular resting membrane potential). Therefore, in order to predict the resting membrane potential under these conditions the Goldman, Hodgkin, Katz equation (GHK) was employed:

$$V_m = \frac{RT}{F} \ln \left(\frac{P_{K^+} [K^+]_o + P_{Na^+} [Na^+]_o + P_{Cl^-} [Cl^-]_i}{P_{K^+} [K^+]_i + P_{Na^+} [Na^+]_i + P_{Cl^-} [Cl^-]_o} \right)$$

Where V_m is the resting membrane potential, $P_{K,Na,Cl}$ are the relative membrane permeability for K^+ , Na^+ and Cl^- respectively, R is the gas constant ($8.31 \text{ JK}^{-1}\text{mol}^{-1}$), T is the temperature in Kelvin (K) and F is the Faraday constant ($9.65 \times 10^4 \text{ C mol}^{-1}$).

2.13. Recording Protocol

Membrane currents (I_m) were recorded from a single motile human spermatozoon held under voltage clamp in a whole cell configuration. In this thesis two types of recording protocols were used. The first was a ramp protocol where the holding potential (V_{hold}) was ramped up from -92 to +68 mV over a 250 ms or 5 second period at 1Hz (holding potential was either 0 or -92 mV). The second was a pulse protocol where the V_{hold} was jumped from the holding potential of -92 mV to a test potential over a 0.5 – 1 second period. In order to remove influence of passive membrane currents (or leak current) a leak subtracted pulse protocol was used. This was achieved by 2 sub-sweeps of -92 mV for 100 ms prior to the actual test pulse. As the leak current has a linear response, which follows Ohm's law ($V = IR$), the leak current

was calculated by the accumulated responses to the 2 sub-sweeps and digitally subtracted it from the total current generated to give the voltage-activated current.

In all ramp experiments the average of 10 consecutive sweeps were used to generate graphs showing the relationship between I_m and V_{hold} with downward deflections indicating depolarizing inward current and upward deflections indicating hyperpolarizing outward current. The reversal potential (E_{rev}) was inferred from the value of V_{hold} at which I_m was zero. Direct measurement of V_m was also assessed by whole cell current clamp in which data was sampled at 5 kHz and filtered at 3 kHz.

To ensure that variation in cell size did not influence the observed current, the magnitude of current in all cells were normalized to the C_m for that individual cell. Therefore, all data within this thesis are presented as pApF^{-1} .

Regression analyses of the $\Delta I_m / \Delta V_{hold}$ for depolarized potentials (14 to 66 mV) were used to calculate membrane conductance (G_m), where ΔI_m is the change in membrane current between 14 and 66mV and ΔV_{hold} is the change in voltage between 14 and 66mV. For pH sensitive K^+ currents, pipette solutions were adjust with KOH to a pH of 6.2, 6.4, 6.8, 7.4 or 8, buffered with 5mM 2-(*N*-morpholino)ethanesulfonic acid (MES) and 5mM 4-(2-hydroxyethyl)-1-piperazineethanesulfonic acid (HEPES). To ensure a consistent concentration of $[\text{Ca}^{2+}]_i$, additional CaCl_2 was added to the pipette solution as calculated by WebMAXC extended (final concentration 0.1 μM , physiological resting Ca^{2+} level in human sperm (Ho et al., 2002; Suarez, 2008). All recordings were collected using an Axopatch 200B amplifier (Molecular Devices, Sunnyvale, CA) and recorded using Clampex 10.1 (Molecular devices).

2.14. Statistics

All data are presented as a mean \pm s.e.m with n_C values denoting the number of individual cells assessed and N_D values denoting the number of donors used. Analyses of significant differences were assessed using Student's t-test (paired and unpaired) or analysis of variance (ANOVA), where appropriate. Hyperactivation data was arcsine transformed before testing for significance. A significant result was reported as a p value < 0.05

**Chapter 3 - Native Currents in Human
Spermatozoa**

3.1 Introduction

Ion channels are pivotal in spermatozoa physiology. Mammalian spermatozoa have to undergo a variety of physical, molecular and chemical modifications in order to fertilise an oocyte, known as capacitation. Key to these alterations is the ability to sense and react to changes in the extracellular milieu of the female reproductive tract through the movement of ions *via* ion channels.

To date there has been very little electrophysiological work carried out on ion channels in human sperm with only three channels characterised; CatSper (hormone sensitive Ca^{2+} channel), Hv1 (voltage gated proton channel) and a calcium activated chloride channel (Orta et al. 2012). This lack of information is primarily due to the infancy of this field of research and the difficulty of the technique. Furthermore, to date studies have assessed ionic currents under conditions that do not maintain physiological ionic gradients (quasi-physiological conditions) and therefore do not provide evidence for channel activity under physiological conditions.

3.2 Aim

The aim of this chapter was to record native currents from motile human sperm cells in quasi-physiological conditions under voltage clamp. Alterations in the external and internal ionic environments along with pharmacological methods will be used to identify and characterise native currents.

3.3 Results

3.3.1. *Native Current in Motile Human Spermatozoa*

The first task was to document the native current in human sperm, the following work documents this. Figure 3.1A shows noisy current from 10 consecutive depolarising ramps from -92mV to 68mV over a 250ms protocol from a single human spermatozoon under quasi-physiological conditions, which were subsequently averaged. Figure 3.1B shows the pooled current to voltage (I_m - V_m) relationship and reversal potential (E_{rev}), calculated by regression analysis, of motile human spermatozoa from 7 different donors perfused with 5mM $[K^+]_o$ (HS control conditions Figure 3.1B.i) and 130mM $[K^+]_o$ (HKS, Figure 3.1B.ii) bath solutions. In the presence of 5mM $[K^+]_o$ spermatozoa exhibited a strongly outwardly rectifying hyperpolarising current upon depolarisation of the membrane potential past -30 mV ranging from 25 – 45 pApF⁻¹ as shown in Figure 3.1B.i) ($n_C = 12$, $N_D = 7$). At hyperpolarised potentials, there was a very small inward current ranging from -0.8 to -5.1 pApF⁻¹ (Average = -2.1 ± 0.4 pApF⁻¹). Assessment of the membrane conductance at hyperpolarised (< -45 mV) *versus* depolarised potentials (> 14 mV) showed a 15.8 ± 3.0 fold greater membrane conductance at depolarised potentials compared to hyperpolarised potentials (562 ± 78 pSpF⁻¹ vs 43.7 ± 6.8 pSpF⁻¹ respectively, $p < 0.0001$). Furthermore, increasing external $[K^+]_o$ to 130mM (Na^+ substitution) caused a significant depolarising rightward shift in the reversal potential (E_{Rev}) from -35.0 ± 3.0 mV to -10.3 ± 8.4 mV (Figure 1.B.iii, $n_C = 11$, $N_D = 7$, $p < 0.004$). This set of data indicates the presence of a K^+ conductance (G_{K^+}) in motile human sperm cells.

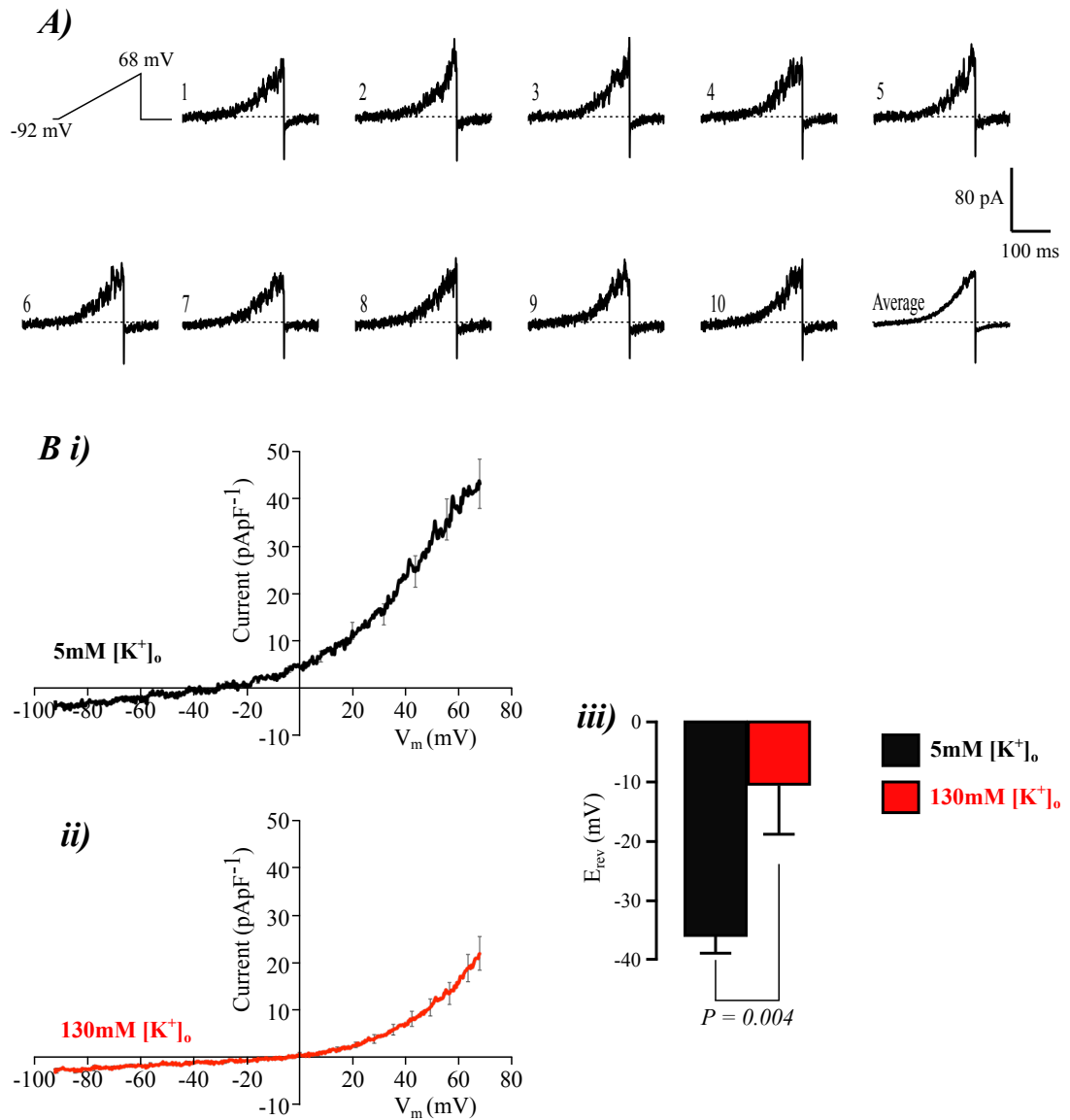


Figure 3.1: Native membrane current in motile human spermatozoa. (A) Native outwardly rectifying current of a single spermatozoon recorded in 5mM $[K^+]_o$ via a ramp protocol over 10 consecutive sweeps (V_m -92 to +68mV, $V_{hold} = -92$ mV, HS control conditions : $n_C = 12$ $N_D = 7$, $C_m = 0.78 \pm 0.05$ pF, $R_a = 68.3 \pm 3.5$ M Ω). (B) Currents recorded from spermatozoa in the presence of 5mM $[K^+]_o$ (i) and 130mM $[K^+]_o$ (Na^+ substitution). (iii) Reversal potential (E_{rev}) of human spermatozoa in 5mM $[K^+]_o$ and 130mM $[K^+]_o$. E_{rev} values were calculated by further analysis of the $I_m - V_m$ relationship (see methods). Data shown as average of ten consecutive sweeps and error bars indicate s.e.m. Significance was calculated using Student's paired t-test ($p < 0.05$).

3.3.2. Outward current is carried by K^+

Figure 3.2 shows the $I_m - V_m$ relationship from data investigating the role of $[K^+]_i$ on the outwardly rectifying current in repeat conditions to Figure 3.1B ($n_c = 8$, $N_D = 3$). This was achieved by ionic substitution of $[K^+]_i$ for $[Cs^+]_i$ (e.g. $[K^+]_i = 0\text{mM}$ see Table 2 materials methods, page 40).

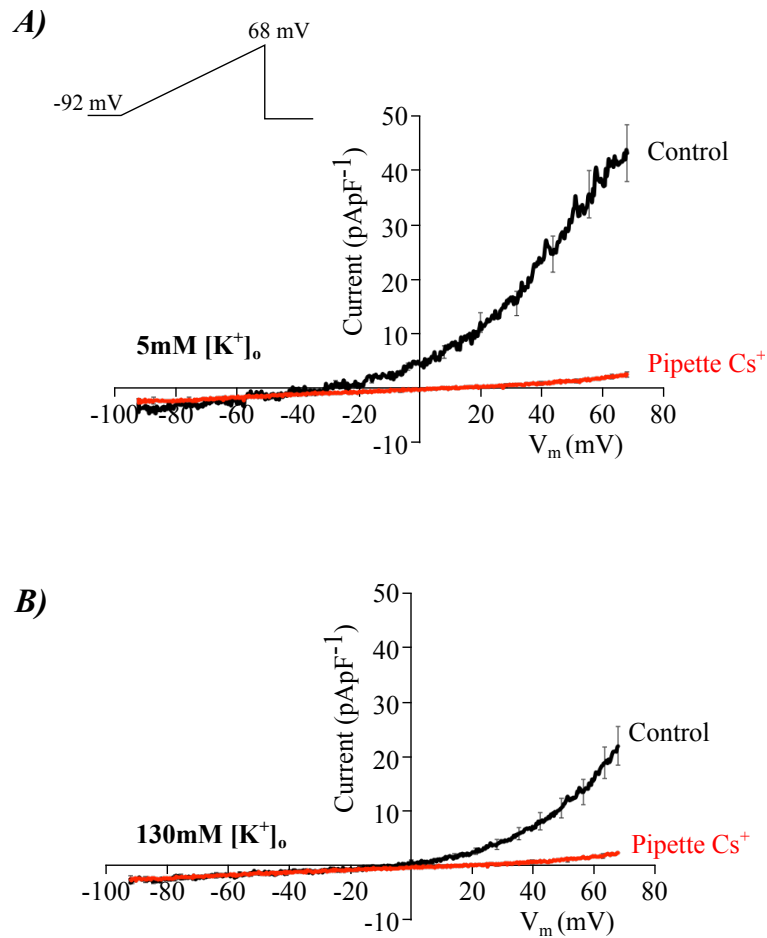


Figure 3.2: Outward current is carried by K^+ (A) Native currents recorded under identical conditions to Figure 3.1 *via* a ramp protocols over a 250ms period in the presence and absence of intracellular K^+ (Cs^+ substitution, V_m -92 to +68mV, $V_{hold} = -92\text{mV}$, $n_c = 8$, $N_D = 3$, $C_m = 0.96 \pm 0.04\text{pF}$, $R_a = 58.6 \pm 4.9\text{M}\Omega$). A shows the abolishment of the outward current when intracellular K^+ is removed from the pipette solutions (red trace) in control HS bath solution. (B) Shows the abolishment of the outward current when intracellular K^+ is removed from the pipette solutions in 130mM $[K^+]_o$ bath solution. Traces generated by averaging 10 consecutive sweeps with error bars indicating s.e.m.

This data shows that removal of $[K^+]_i$ consistently abolished the outward current in both 5mM (Figure 3.2A) and 130mM $[K^+]_o$ (Figure 3.2B) experimental bath conditions ($p < 0.001$, Student's paired T-test) and reduced G_m to 8.8 ± 2.0 % of the control value ($p < 0.001$). Increasing $[K^+]_o$ to 130mM with pipette Cs^+ had no effect on E_{rev} . Overall, this indicates the outward current is dominated by hyperpolarising K^+ efflux under these conditions.

3.3.3. Intracellular $[pH]_i$ and K^+ current

Data from Figures 3.1 & 3.2 implied that the outward current is carried by K^+ . In murine sperm the dominant K^+ current is carried by the pH sensitive Slo3 channel (Navarro et al. 2007). Therefore, subsequent experiments were aimed on assessing the pH sensitivity of the human K^+ current.

Figure 3.3 shows a set of data aimed to assess the pH sensitivity of the K^+ current in motile human sperm cells. These data showed that acidification of the intracellular environment from pH 7.4 to pH 6.2 caused a reduction in the max outward current from 36.1 ± 3.0 to 12.6 ± 2.2 pApF⁻¹, respectively. Further analysis of the slope from 14mV to 66mV showed a significant inhibition in the membrane conductance (G_m) of the channel at $[pH]_i < pH 6.8$ compared to the control Figure 3.3C (pH 6.4: $n_C = 7$, $N_D = 3$, $p = 0.03$, pH 6.2: $n_C = 5$, $N_D = 4$ $p = 0.02$). Alkalisiation of $[pH]_i$ to pH 8.0 had no significant effect on the G_m or average peak current of the channel compared to control Figure 3.3C (pH 8.0: $n_C = 4$, $N_D = 3$, $p = 0.3$). Further analysis of the I_m-V_m data showed no significant change in E_{rev} upon acidification of the intracellular environment, Figure 3.3B ($p = 0.150$, ANOVA/ Dunnet's post Hoc test). This data indicates that the outward current shows sensitivity to intracellular acidification. However, in contrast to previous

findings in murine sperm this acidification has no effect on the resting membrane potential of human sperm.

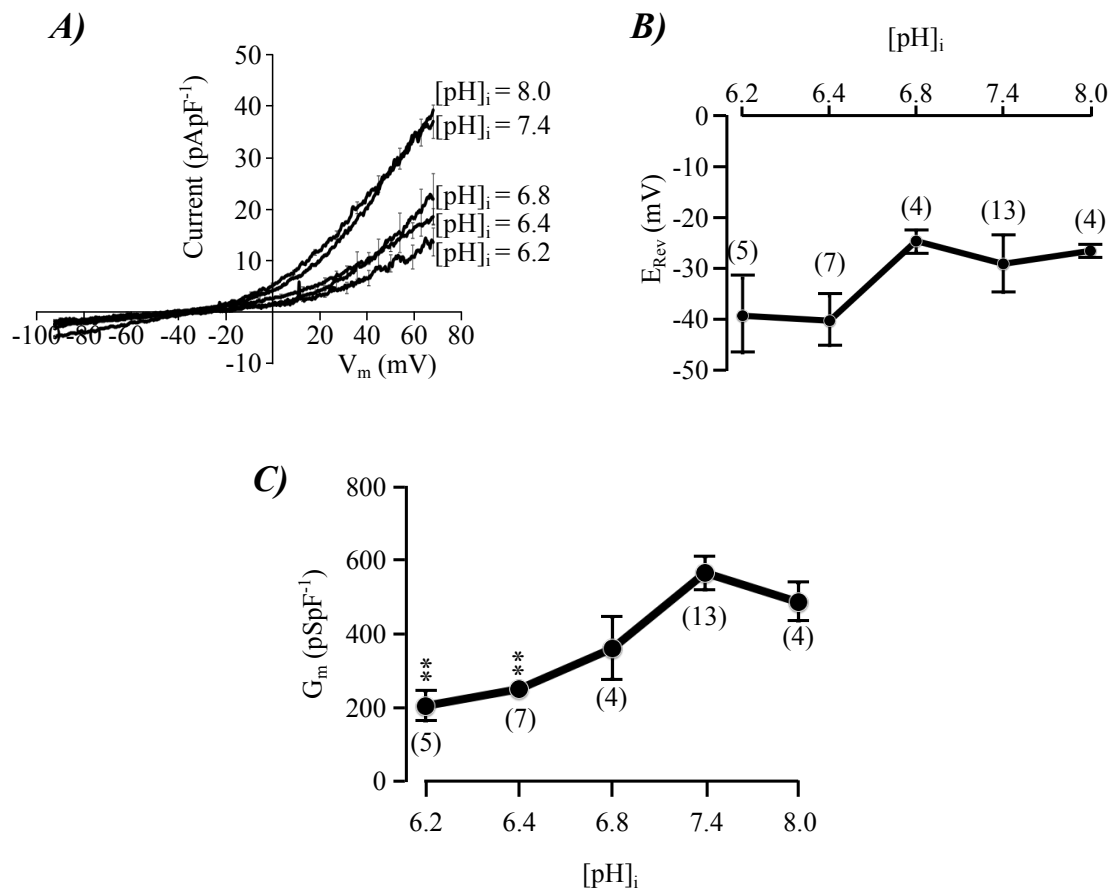


Figure 3.3: Intracellular pH and K⁺ current. (A) Plots showing the $I_m - V_m$ relationship of the K⁺ current in response to different intracellular pH environments ($C_m = 0.84 \pm 0.02$, $R_a = 65.3 \pm 2.1$ nC = 4 - 13, $N_D = 9$). (B) Analysis of membrane potential indicates no significant change in resting membrane potential upon acidification or alkalinisation of intracellular environments ($p > 0.05$, ANOVA). (C) Further analysis of the data was used to obtain the G_m of the outward K⁺ current under different intracellular pH environments indicating a reduction of G_m at $[pH]_i < 6.8$. All data are presented as mean \pm sem, ** denotes statistical significance compare to paired control (pH 7.4, $p < 0.05$).

3.3.4. Pharmacology of K⁺ Current

In order to characterise and identify the K⁺ current, pharmacological methods were used (See Table 4, Materials and methods, page 42). Figure 3.4A shows $I_m - V_m$ relationships of the K⁺ current before and after the addition of putative K⁺ channel blockers quinidine

(3mM) and bupivacaine (3mM). Currents were generated as described in Figure 3.1. Analysis of the outward current shows that quinidine caused a statistically significant inhibition (> 90%) of the outward current at depolarised potentials (control 31.34 ± 2.78 pApF⁻¹, 3mM quinidine 2.18 ± 0.55 pApF⁻¹, $n_c = 7$, $N_D = 4$ $p < 0.001$ Student's paired t-test). Figure 3.4B shows the $I_m - V_m$ relationship of cells recorded in control and 3mM bupivacaine recording conditions. This data shows that the outward K⁺ current is significantly inhibited by 3mM bupivacaine by 85.6 ± 1.6 % (control: 34.0 ± 4.4 pApF⁻¹, 3mM bupivacaine: 4.9 ± 0.7 pApF⁻¹, $n_c = 8$, $N_D = 4$, $p < 0.001$ Student's paired t-test). Both compounds caused a similar residual current observed in currents recorded with Cs⁺ pipette solution. In order to quantify the effect of a number of K⁺ blockers, the percentage inhibition of the G_m after the addition of each compound was assessed. Figure 3.4C shows percentage inhibition of G_m after the addition of 3mM quinidine, 3mM bupivacaine, 50 μ M clofilium, 3mM lidocaine and 2mM 4-AP. These data show that quinidine, bupivacaine and clofilium significantly inhibited the G_m by 93.0 ± 2.7 %, 86.1 ± 1.9 % and 73.7 ± 10.2 % respectively ($n_c = 3 - 12$, $N_D = 2 - 7$ $p < 0.001$). Lidocaine also showed a significant, albeit weaker, inhibition of G_m compared to quinidine and bupivacaine. Clofilium showed a 33.3 ± 6.9 % inhibition ($n_c = 7$, $N_D = 4$, $p = 0.04$ Student's paired t-test), in contrast, 2mM 4-AP showed no significant inhibition of the G_m (% inhibition: -8.8 ± 7.7 %, $n_c = 4$, $N_D = 4$, $p = 0.4$ Student's paired t-test). Further assessment of E_{rev} by regression analysis showed that quinidine and bupivacaine caused a significant rightward depolarising shift in E_{rev} ($p < 0.01$). Lidocaine and clofilium also showed slight depolarising of E_{rev} , however, this did not reach statistical significance. Notably, 4-AP had no effect on resting E_{rev} .

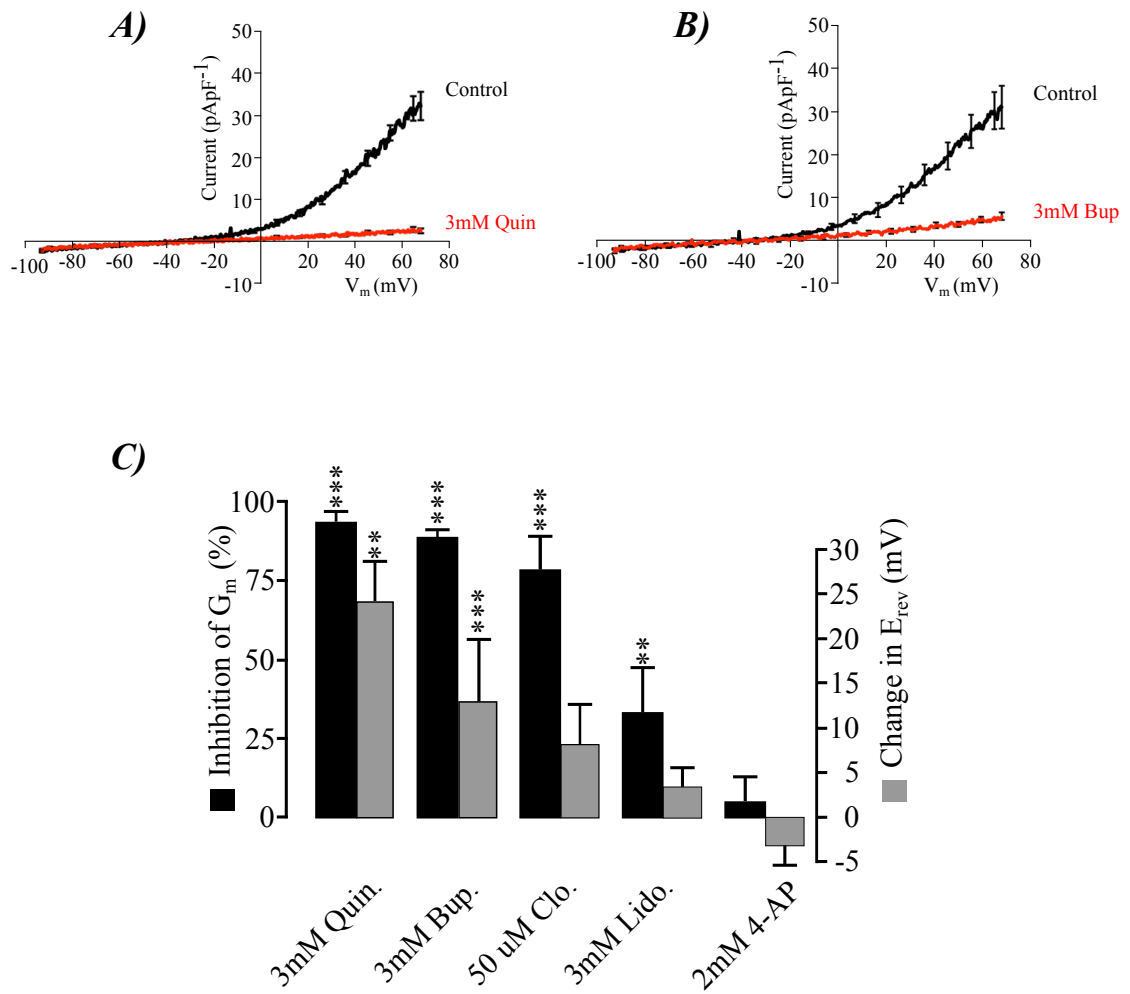


Figure 3.4: The effects of putative K⁺ blockers on the outward K⁺ current. (A and B) Native currents recorded under identical conditions to Figure 3.1 *via* ramp protocols over a 250ms period in the presence and absence of 3mM quinidine and bupivacaine (V_m -92 to +68mV, V_{hold} = -92mV, n_c = 7, N_D = 4, C_m = 0.92 ± 0.04 pF, R_a = 68.71 ± 3.60 MΩ). C) Analysis of % inhibition of G_m calculated by ΔI/ΔV between 14 - 66mV and E_{rev} after 10 - 20 second of treatment with putative K⁺ antagonists. Traces generated by averaging 10 consecutive sweeps with error bars indicating s.e.m. Asterisks denote statistical significance, (** < 0.01, *** < 0.001, Student's paired t-test).

3.3.5. Current Clamp: K^+ Channel blockers and membrane potential

Whole cell current clamp was used to directly assess the effect of K^+ channel blockers on the resting V_m of human sperm. Figure 3.5 shows a representative recording from a single motile human sperm in a period of control (HS bath solution, 20 seconds) and a period of treatment (HS bath solution plus compound, 50 seconds) with averaged data represented on the right of each trace. Direct assessment by whole cell current clamp confirmed that the resting membrane potential of capacitated human sperm was $\sim -30\text{mV}$ ($-29.8 \pm 1.4 \text{ mV}$, $n_c = 20$, $N_D = 6$). Furthermore, HKS ($\Delta V_m = 29 \pm 0.85$; $p < 0.0001$, $n_c = 3$); 0.3mM quinidine ($\Delta V_m = 447 \pm 3.2$; $p < 0.0001$, $n_c = 7$); 3mM bupivacaine ($\Delta V_m = 53.2 \pm 5.0$; $p < 0.0001$, $n_c = 5$) and 50 μM clofilium ($\Delta V_m = 27.1 \pm 0.6$; $p < 0.0001$, $n_c = 5$) all caused a depolarising shift in V_m . The application of 4-AP had no significant effect on resting V_m . This data indicates the importance of the K^+ current in the regulation of human sperm V_m .

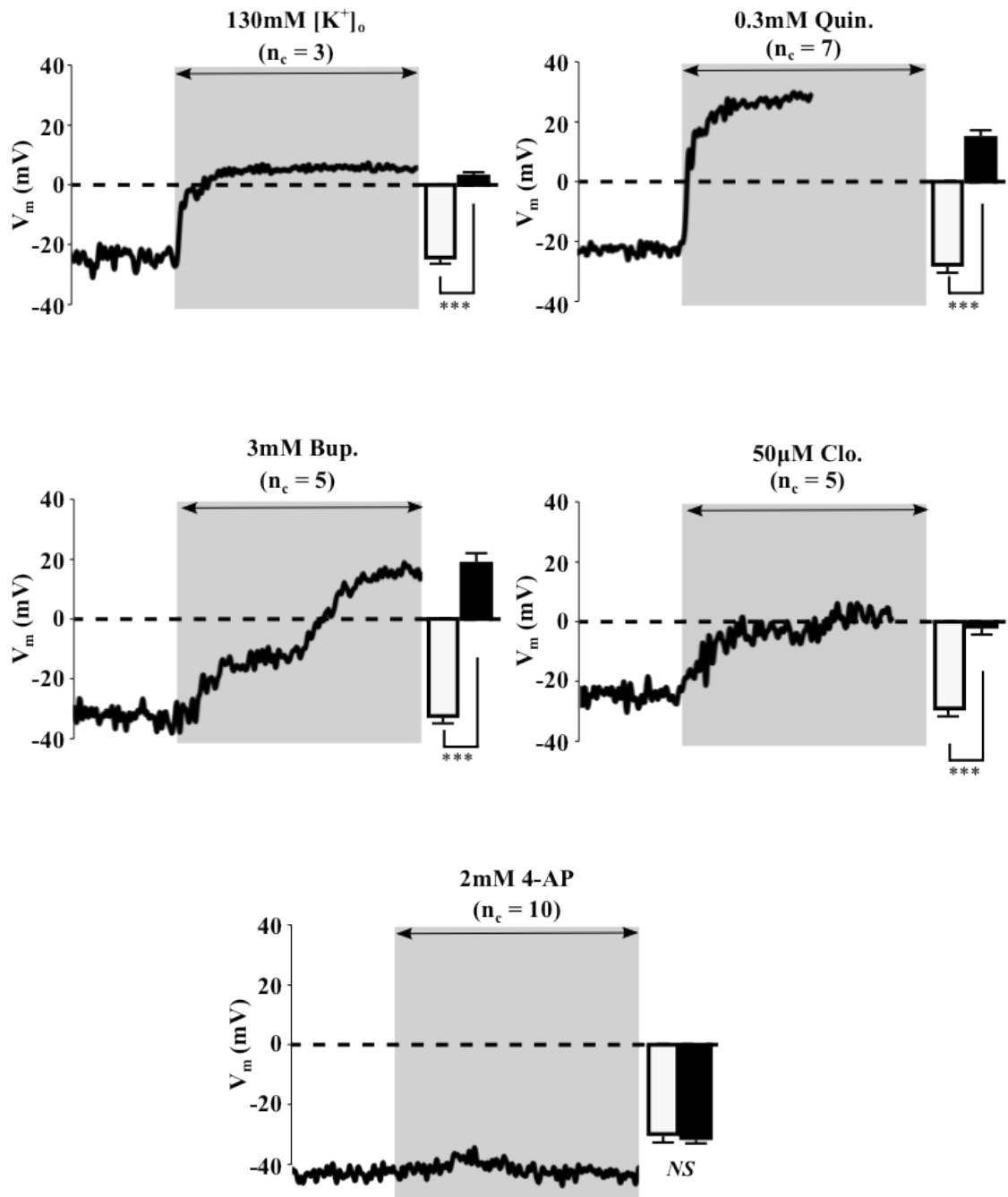


Figure 3.5: Whole cell current clamp data assessing the effects of K^+ channel blockers on the resting membrane potential of motile human spermatozoa with high K^+ as a control. Each graph represents a trace of the resting V_m from a single spermatozoon in a period of control conditions (20 seconds) and a period of treatment (50 seconds). Histograms on the right of each trace show the averaged resting V_m in control (white bars) and after treatment (black bars). Error bars indicate s.e.m. Significance $p < 0.05$, Student's paired t-test.

3.3.6. *Biophysical Properties of the K⁺ current*

Following on from the studies on the K⁺ current, the biophysical properties of this current were next studied. Figure 3.6 shows hyperpolarising K⁺ current recorded from motile human sperm at different test potentials using a leak-subtracted protocol to isolate the voltage induced current. Data collected showed that depolarisation of the membrane to potentials $\geq -52\text{mV}$ evoked outwardly rectifying hyperpolarizing current that developed over a 250ms period (Figure 3.6A). In order to measure the effects of depolarisation on membrane conductance, measurements of the steady state current (maximal activation) were collected. These data were then used to model the voltage-induced conductance of the membrane at different test potentials ($G_v = I/V$) shown in Figure 3.6B. Analysis of these data using the Boltzmann Equation showed that the half maximal activation (V_{50}) of the channel was $+ 25 \pm 2.3 \text{ mV}$ with a Boltzmann slope constant (κ) of $19.1 \pm 2.2 \text{ mV}^{-1}$ which describes the channel's sensitivity to voltage (Figure 3.6B). This data shows that the K⁺ current in human sperm is weakly voltage activated.

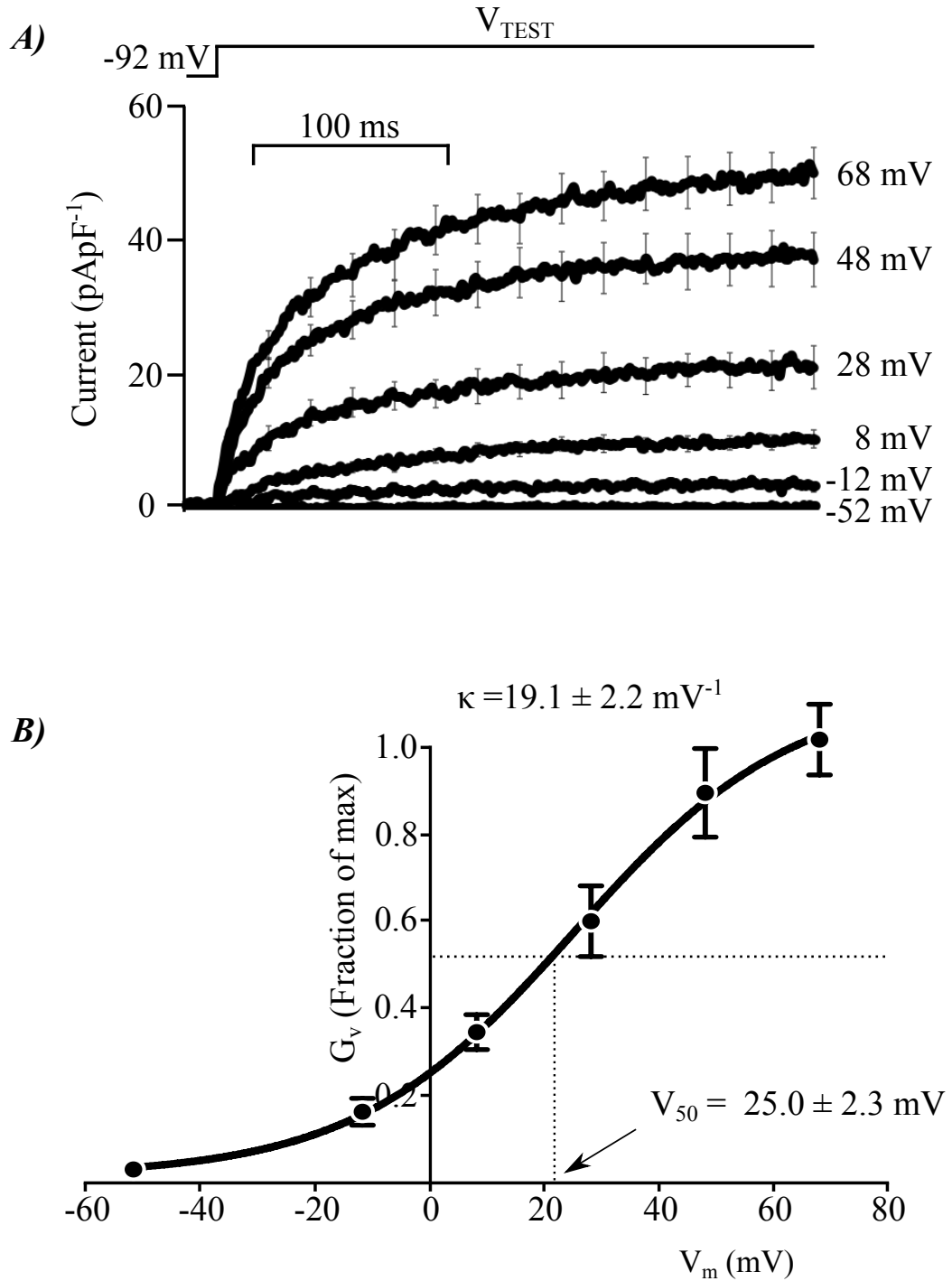


Figure 3.6: Biophysical properties of K⁺ Current. (A) Leak subtracted membrane currents ($n_c = 7-16$, $N_D > 2$) from human spermatozoa at different sustained test potentials (V_{test}) showing depolarising current evoked at potential ≥ -52 mV. (B) Membrane conductance was calculated from the final 50 ms of the steady state current using the equation $G_v = I/V$. These results were plotted against V_m and used in the analysis of the Boltzmann equation to calculate the half maximal activation (V_{50}) and Boltzmann constant (κ). Error bars denote s.e.m.

3.3.7. Channel Ionic Selectivity

The next set of experiments aimed to assess the channel's selectivity to K^+ evoked by step depolarisation to +68mV under quasi-physiological bath conditions. Figure 3.7Ai confirms the depolarisation induced K^+ current as well as showing currents recorded by replacing intracellular pipette K^+ with Na^+ . This showed that, although smaller than control, depolarisation evoked a ~ 2 pApF⁻¹ (2.76 ± 0.24 pApF⁻¹, $n_C = 38$) outward current under these conditions. Replacing intracellular K^+ and Na^+ with NMDG⁺, as shown in Figure 3.7B, completely abolished the depolarisation induced outward current (-0.32 ± 0.01 pApF⁻¹, $n_C = 9$). In all experiments intracellular and extracellular Cl⁻ was maintained at 29mM and 144mM respectively, therefore the outward current is not carried by Cl⁻. This data indicates the outward current is permeable to cations. As the V_m was depolarised to the Na^+ equilibrium potential (E_{Na^+}) the current must therefore be carried by K^+ under standard conditions. As a result voltage induced increase in K^+ conductance was calculated using the equation $G_K = I_m / \Delta\Psi_K$, where Ψ_K is the electrochemical driving force on K^+ (*i.e.* $V_m - E_K^+$). This protocol was also used on the small outward Na^+ current and the respective conductances are shown in Figure 3.7Aii. Analysis of this data showed that the channel had a ~ 7 times greater selectivity for K^+ over Na^+ (270.1 ± 28.21 vs 44 ± 3.78 pSpF⁻¹ $n_C = 18$ and 38 , respectively). Figure 3.7C shows the effect of removing extracellular Mg^{2+} and Ca^{2+} from the bath solution from cells recorded using K^+ and Na^+ based pipette solution. Upon removal of extracellular divalent cations, there was an increase in outward current. Further analysis of G_K^+ / G_{Na^+} indicated that under these conditions the relative permeability for K^+ vs Na^+ was ~ 1 as shown in Figure 3.7Cii. This therefore suggests the ionic selectivity of the channel is governed by divalent cations.

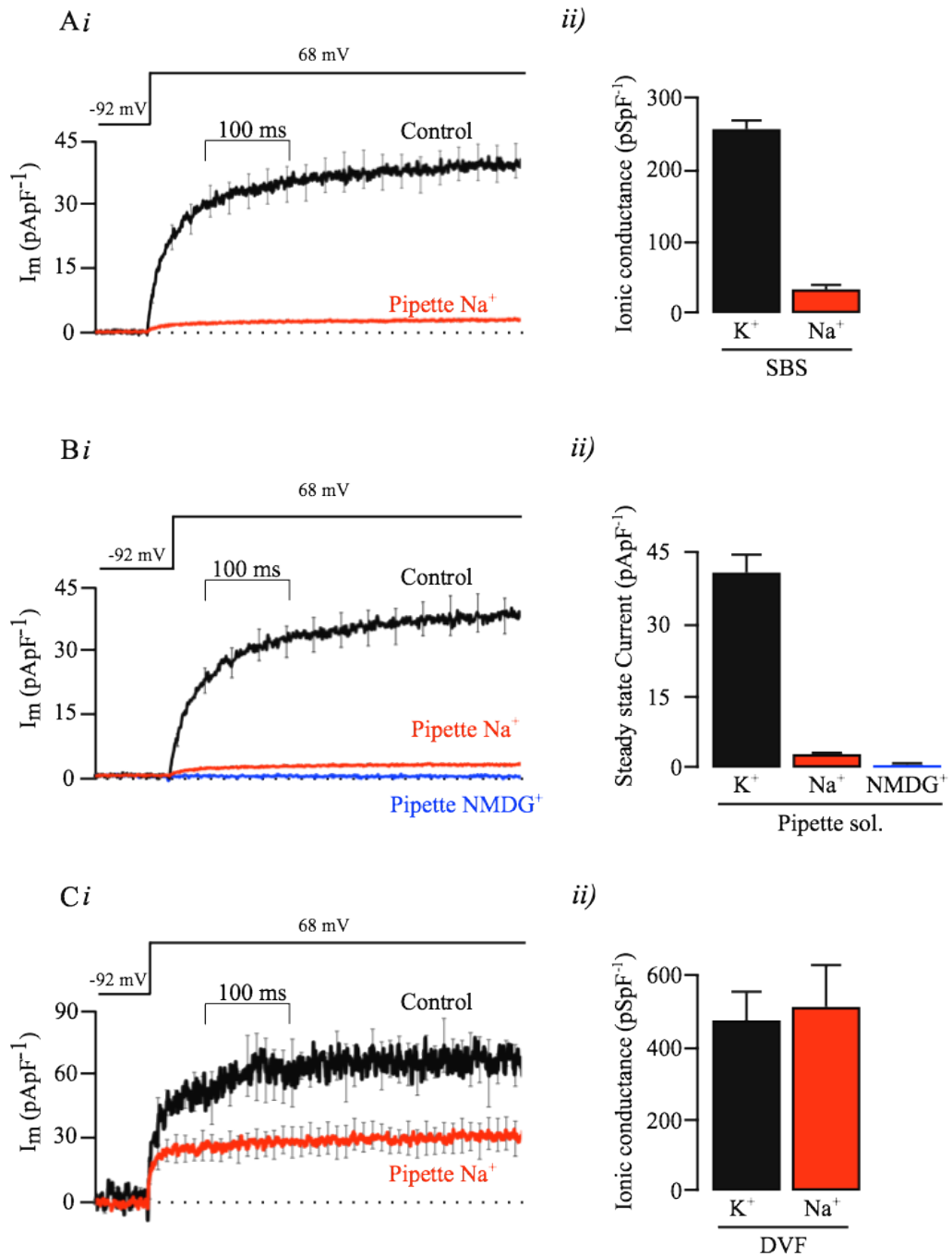


Figure 3.7 Ionic selectivity of the voltage-induced current: A) Voltage-induced outward current evoked by a single depolarising step to +68mV in human spermatozoa recorded using K⁺ based pipette solution (Black line, $N_C = 18$) and Na⁺ pipette solution (Red line, $[K^+]_i = 0\text{mM}$, $n_C = 38$). Aii) K⁺ and Na⁺ ionic conductance under quasi-physiological bath conditions quantified by analysis from data in Ai. B) Voltage induced outward current with NMDG⁺ based pipette solution (Blue line, $n_C = 9$) with steady state currents over the last 50ms presented in Bii. C) Currents evoked using identical voltage pulse protocol under divalent free bath conditions from cells in A that were stable enough (K⁺ based pipette solution $n_C = 3$; Na⁺ based pipette solution $n_C = 5$) to last over the period of bath exchange. Cii) K⁺ and Na⁺ ionic conductances under divalent free bath conditions quantified by analysis from data in Ci. All data presented at mean \pm s.e.m.

3.3.8. Pharmacology of the small Na^+ Current

In order to assess if the small outward Na^+ current had the same pharmacology as the K^+ current recorded under control conditions, the same K^+ channel blockers were used as in Figure 3.4. Figure 3.8 shows the effect of K^+ channel blockers quinidine, bupivacaine, clofilium and 4-AP on the small outward Na^+ current. Control data indicated that depolarisation induced a small outward current of 2-5 pApF^{-1} under these conditions. Application of putative channel blockers showed that 0.3mM quinidine (Figure 3.8A), 3mM bupivacaine (Figure 3.8B) and 50 μM clofilium (Figure 3.8C) all caused a significant block of > 80%. However, 4-AP was ineffective at inhibiting the outward current. This data indicates that the outward current recorded under control conditions and the current recorded under Na^+ rich pipette solution share the same pharmacology. Subsequently, the K^+ and Na^+ current must therefore flow *via* the same population of ion channels.

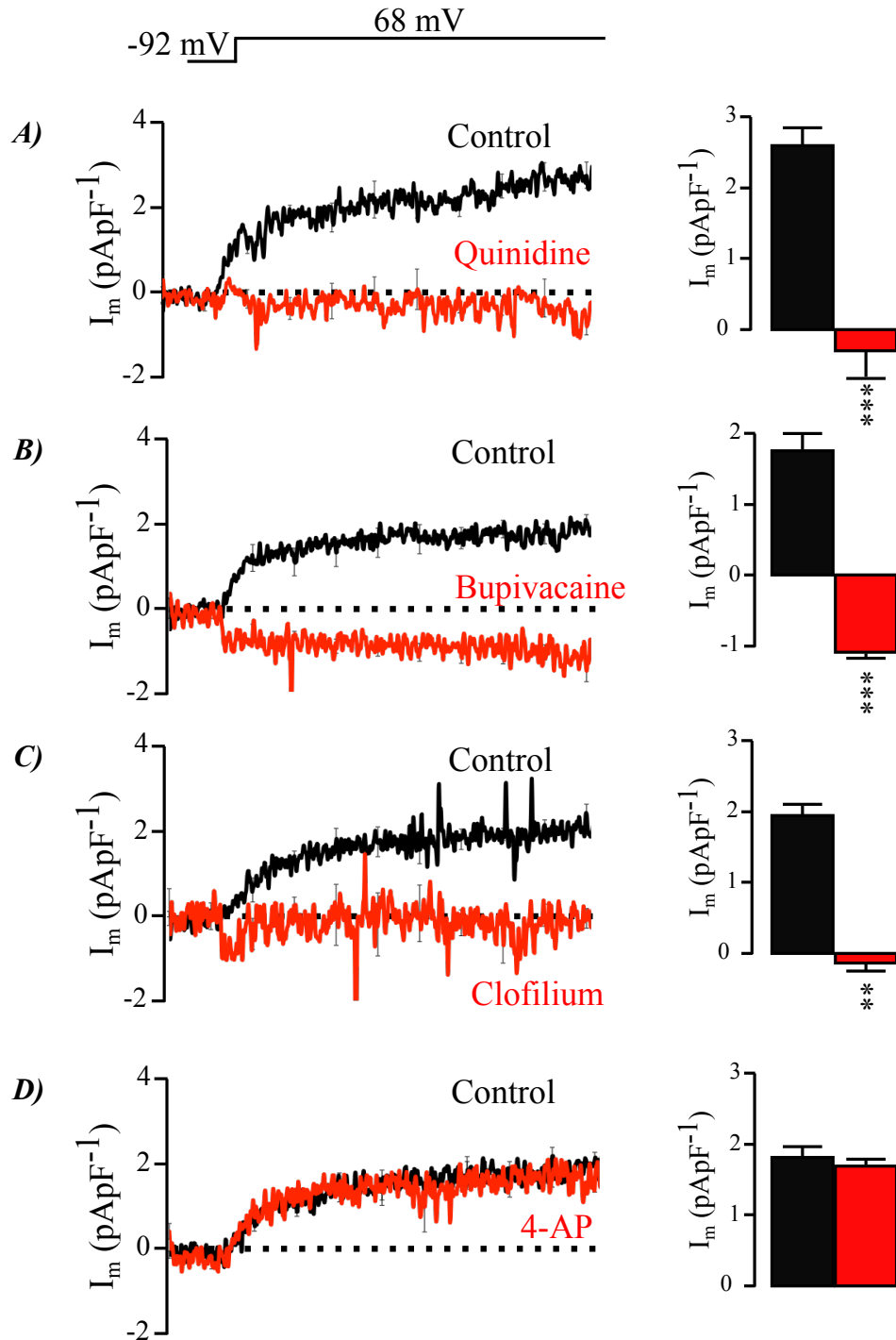


Figure 3.8 Pharmacology of small outward Na^+ current: Na^+ currents evoked by step depolarisation to $+68 \text{ mV}$ recorded using Na^+ rich pipette solutions. Panels on the left show current evoked by step depolarisation with panels on the right indicating mean current quantified over the last 300ms of the pulse. In each experiment currents were recorded in a period of control conditions (standard bath solution) and after 20-30 seconds exposure to 0.3mM quinidine (A, $n_C = 5$, $N_D = 2$), 3mM bupivacaine (B, $n_C = 6$, $N_D = 3$), 50 μM clofilium (C, $n_C = 5$, $N_D = 3$) and 2mM 4-AP (D, $n_C = 5$, $N_D = 3$). All data presented as mean \pm s.e.m; asterisks denote statistical significance (** $p < 0.02$, *** $p < 0.001$, Students paired t-test)

3.3.9. Mathematically Modelled Current and Resting Membrane Potential

The current described here displays relatively weak selectivity for K^+ as well as being weakly voltage activated. This was somewhat perplexing as traditional K^+ channels traditionally display strict K^+ selectivity and strong voltage dependence. Therefore mathematical models were used to predict the properties of a channel with similar biophysical characteristics as described in Figures 3.6-3.8. To achieve this, experimentally derived parameters for the Boltzmann equation, as indicated in Figure 3.6 ($V_{50} = 25.0 \pm 2.3\text{mV}$, $\kappa = 19.1 \pm 2.2 \text{ mV}^{-1}$), were used to calculate the fractional availability (A) of the membrane conductance at a series of holding potentials (mV). Data from Figure 3.6 also provided the relative G_{K^+} of the channel and the predicted K^+ current (I_{K^+}) was calculated by substituting these values into the equation, $I_{K^+} = \psi_{K^+} \cdot A \cdot G_{K^+}$, where ψ_{K^+} is the electrochemical driving force on K^+ ($V_m - E_{K^+}$), A is the fractional availability and G_{K^+} is the K^+ conductance of the membrane. I_{Na^+} was calculated in an identical fashion by experimentally derived data on G_{Na^+} as shown in Figure 3.6Aii. The results for this are presented in Figure 3.9Ai. This data was then subsequently used to calculate the predicted current by calculating I_{Total} ($I_{K^+} + I_{Na^+}$). This value was then added to the leak current, calculated as the residual current that could not be blocked by 0.3mM quinidine or 3mM bupivacaine (~5% of maximum current) and plotted against V_m (mV) as shown in Figure 3.9Aii. Recorded currents from 70 individual cells were then superimposed on top of the predicted current to provide a comparison. Figure 3.9Aii shows that the predicted and the recorded current are virtually identical indicating that current described in this chapter can be mathematically modelled and therefore providing further evidence that the current

observed in human spermatozoa flows through a poorly selective, weakly voltage activated cation channel.

Data collected from this set of experiments were also used to calculate the predicted resting membrane potential of a cell with the same biophysical properties as human spermatozoa. This was achieved by calculating the resting V_m using the Goldman Hodgkin Katz equation (See materials and methods, pages 49-50) using the concentrations of K^+ and Na^+ in standard bath and pipette solutions as well as the experimentally derived permeability of each ion. Figure 3.9Aiii shows the recorded resting membrane potential via whole cell current clamp from 34 human spermatozoa from 6 different donors (Black bar) and the predicted resting membrane potential calculated using the GHK equation (red bar). The recorded and predicted currents accorded well with each other (recorded; -31.0 ± 1.2 mV, predicted; -33.0 mV). This also showed that both K^+ and Na^+ contribute to the resting membrane potential in human sperm.

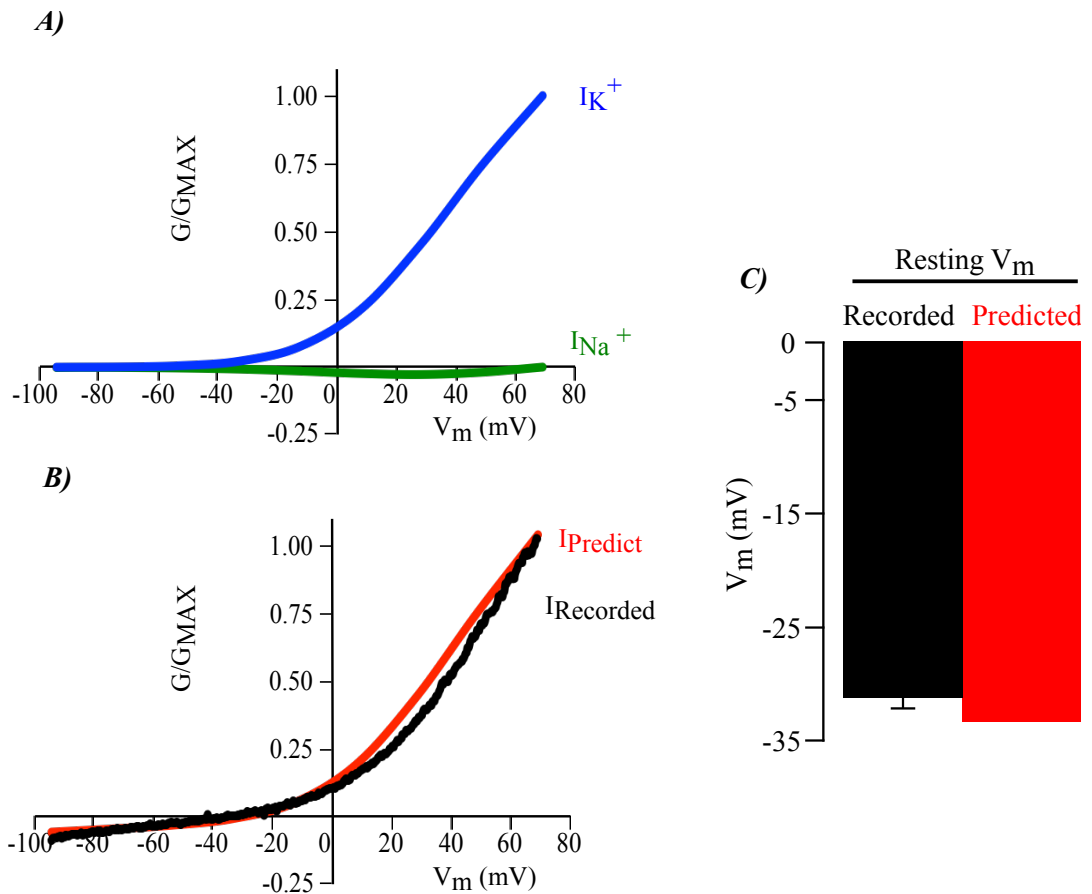


Figure 3.9: Predicted membrane current and resting membrane potential for human spermatozoa: A) Experimentally derived currents for K^+ (I_{K^+}) and Na^+ (I_{Na^+}) using the Boltzmann equation. B) Predicted current ($I_{Predicted}$) of a human spermatozoa with experimentally derived biophysical properties with recorded data from 70 pooled human spermatozoa ($I_{recorded}$). C) Predicted (Red bars) and actual (Black bars) resting membrane potential of a cell recorded in standard bath and pipette solution calculated using GHK equation. Error bars indicate s.e.m.

3.4 Discussion

The aim of this chapter was to record native currents from motile human spermatozoa under conditions that maintain physiological concentrations of Na^+ , K^+ and Cl^- . The data in this chapter shows that human spermatozoa possess a voltage-gated K^+ conductance that is important for the maintenance of V_m , indicated by depolarisation of V_m in high external K^+ bath conditions. In experiments where Cs^+ replaced intracellular K^+ , loss of outward current confirmed the hyperpolarising current was carried almost

exclusively by K^+ . The whole cell data presented in this chapter does however differ from work published recently by Orta and colleagues (Orta et al. 2012), who reported an $\sim 200\text{pA}$ inward current at hyperpolarised potentials. This is a marked difference to data presented here where there was only $\sim 5\text{pA}$ of inward current recorded at these potentials. Orta also reported the resting V_m of human sperm to be $\sim -12\text{mV}$ that is more depolarised in comparison to data recorded here ($\sim -30\text{mV}$). One explanation for this may be due to the concentration of Cl^- in the pipette and bath solutions. Pipette solutions used in this thesis was designed based on studies on human epithelial and colonic cells where it was shown that isotonic concentrations of Cl^- promote cell swelling resulting in “volume sensitive” Cl^- conductance (Worrell et al. 1989). In the present conditions, internal Cl^- was maintained at 29mM and the pipette solution was $\sim 80\text{ mOsmols}$ more hypotonic than the bath solution (see Table 2 materials and methods, page 40). In the Orta paper pipette Cl^- was isotonic to the bath solution (160mM) and could therefore result in cells swelling and a larger conductance. Secondly, Orta et al showed that human sperm possess Ca^{2+} sensitive anion channels that only showed substantial activation when $[\text{Ca}^{2+}]_i$ was raised above $0.25\mu\text{M}$. This differs greatly to our pipette solution where $[\text{Ca}^{2+}]_i$ was maintained at $0.1\mu\text{M}$, roughly the normal resting level of intracellular Ca^{2+} . These differences may help explain the discrepancies observed in the work presented here.

3.4.1. pH and K^+ Current in Human Sperm

One unexpected finding was that acidification of intracellular pH caused a significant inhibition of the outward portion of the current at depolarised potentials compared to control, however, E_{rev} was virtually unaffected. In murine sperm the dominant K^+ channel is *Slo3* (KCNMA3) a pH sensitive K^+ channel that promotes hyperpolarisation

of the membrane during murine sperm capacitation. Studies by Navarro et al. (Navarro et al. 2007) showed that acidification of the intracellular environment resulted in a reduction in the current generated at depolarised as well as hyperpolarised potentials resulting in depolarisation of the resting V_m . However, the data presented here indicates that although intracellular acidification can cause a significant decrease in membrane conductance, the residual current is sufficient to maintain resting V_m in human sperm. This indicates that human sperm K^+ current shows weak sensitivity to changes in intracellular pH and provides further evidence toward the difference between mouse and human spermatozoa.

3.4.2. Pharmacology of K^+ channel

Figure 3.2 confirmed that the outward current was carried by K^+ . Therefore the next stage was to use inhibitors of different K^+ channel subtypes to further characterise the outward current. Initial experiments focused on two K^+ channel blockers, quinidine and bupivacaine, at a concentration previously used in the laboratory to inhibit endogenous G_{K+} in H441 cells (3mM) (Inglis et al. 2007). After 10 - 20s exposure to both quinidine and bupivacaine, there was a > 90% inhibition of the outward current to levels observed in currents where intracellular K^+ was replaced with Cs^+ . Further assessment of other K^+ channel blockers on the conductance of the membrane showed that the K^+ current was sensitive to quinidine, bupivacaine (as previously mentioned), clofilium and to a lesser extent lidocaine whereas 4-AP was ineffective. Analysis of the reversal potential by regression analysis showed that quinidine, bupivacaine and clofilium all had a significant depolarising effect on the resting V_m where was lidocaine and 4-AP did not. In experiments where V_m was measured directly by whole cell current clamp the depolarising effects of quinidine, bupivacaine and clofilium were further confirmed,

these experiments also confirmed 4-AP was ineffective at altering resting V_m . These findings accord well with data from mouse where quinidine and clofilium caused an inhibition of the hyperpolarising Slo3 channel whereas 4-AP was ineffective (Navarro et al. 2007; Zeng et al. 2011; Santi et al. 2010). Although quinidine, bupivacaine and clofilium all cause depolarisation of V_m , the kinetics of onset were different. Quinidine was more rapid compared to clofilium and bupivacaine, interestingly bupivacaine consistently caused a biphasic response. Although the physiological basis of this phenomenon was not investigated further. Furthermore, quinidine caused a large depolarisation of V_m to potentials $> +10\text{mV}$. This suggests quinidine may be activating a depolarising current (see Chapter 5).

3.4.3. Biophysical properties of human sperm K^+ conductance

Experiments where V_m was stepped to a number of test potentials confirmed depolarisation evoked hyperpolarising current in human sperm. This compliments data in the literature that has shown the presence of voltage gated K^+ channels in human sperm that are important for motility and volume regulation (Barfield et al. 2006). However, analysis of data presented here showed that the half maximal activation ($V_{50} = 25 \pm 2.3\text{mV}$) and the channel's sensitivity to changes in voltage ($\kappa = 19.1 \pm 2.2 \text{mV}^{-1}$) differed remarkably to classic voltage gated K^+ channels. Traditionally, voltage gated K^+ channels are highly sensitive to changes in voltage and this is reflected by more hyperpolarised half maximal activation and steeper Boltzmann constant values ($\sim -20\text{mV}$ and $\sim 8\text{mV}^{-1}$ respectively) (Nguyen et al. 1994). Thus, the present data indicates that the human K^+ conductance shows very weak sensitivity to voltage. In comparison to other mammalian sperm channels, the K^+ conductance described here shows similar biophysical properties to the well characterised Cation

Channel of Sperm (CatSper) as well as mouse Slo3 which also displays weak voltage dependence (CatSper; $V_{50} = \sim 85\text{mV}$, $\kappa = \sim 20\text{mV}^{-1}$, Slo3 mouse; $V_{50} = \sim 77\text{mV}$, $\kappa = \sim 20\text{mV}^{-1}$) (Lishko et al. 2011; Santi et al. 2009). Another unusual feature of this conductance is the poor selectivity of K^+ vs Na^+ . In experiments where intracellular K^+ was replaced with Na^+ a small outward current of 2-5 pApF⁻¹ was observed, which was also blocked by quinidine, bupivacaine and clofilium but not 4-AP. The present data suggests that K^+ and Na^+ flow *via* the same channel with a relative permeability of ~ 7 . Mathematical modelling of predicted current and resting membrane potential accurately replicated a current from a cell with similar biophysical properties. This poor selectivity for K^+ vs. Na^+ is also characteristic of Slo3 channels as studies assessing K^+ selectivity in murine sperm have indicated murine Slo3 is also poorly K^+ selective (~ 10) (Santi et al. 2009).

3.4.4. What is the underlying channel responsible for the K^+ conductance in human sperm?

Based on the data collected in this chapter, the evidence would suggest that the K^+ conductance in human spermatozoa shows similar properties to that of the testis specific K^+ channel Slo3. However, although mRNA has been detected in human testicular tissue (Schreiber et al. 1998), Slo3 protein has not been identified on ejaculated human spermatozoa. As well as this, endogenous Slo3 in murine sperm is sensitive to quinidine, clofilium but insensitive to 4-AP and show weak dependence on voltage for activation with low K^+ selectivity. However, in studies where Slo3 knockout murine sperm were assessed a residual K^+ current was observed at depolarised potential, known as I_{Kres} (Zeng et al. 2011). The investigators concluded this residual current was flowing

through CatSper. This is surprising as CatSper is thought to be a hormone sensitive Ca^{2+} channel rather than a K^+ channel. However, the data in Figure 3.7C may provide some indication for the role of CatSper in the K^+ conductance observed here. It is widely accepted that removal of divalent cations from the bath solution promotes ionic flux through CatSper with a loss of channel selectivity. This accords well with data collected in Figure 3.7C where removal of $\text{Ca}^{2+}/\text{Mg}^{2+}$ from the bath resulted in an increase in hyperpolarising current and a loss of K^+ vs. Na^+ selectivity (~ 1).

3.5 Conclusion

The data presented in this chapter has shown human spermatozoa display a weakly voltage and pH sensitive K^+ conductance with poor K^+ selectivity involved in the regulation of resting V_m under conditions designed to maintain physiological concentrations of K^+ , Na^+ and Cl^- . However, the channel responsible for this conductance remains unclear with possible involvement of CatSper. Therefore the next chapter will assess if the K^+ current reported in this chapter can be distinguished from CatSper.

Chapter 4 - CatSper and the K^+ Current

4.1. Introduction

Catsper (**C**ation **C**hannel of **S**perm) is a pH dependent channel located exclusively in the principle piece of mouse and human spermatozoa flagella (Ren et al. 2001). The accepted primary function of this channel is to provide a gateway for Ca^{2+} influx into the cell upon stimulation from extracellular factors in the female reproductive tract (*e.g.* progesterone) leading to Ca^{2+} - dependent hyperactivated motility (Carlson et al. 2003). Without hyperactivated motility, human and mouse spermatozoa cannot traverse the female reproductive tract or penetrate the outer vestments (zona pellucida) of the oocyte, therefore CatSper is essential for fertility. Surprisingly, electrophysiological studies have shown CatSper and murine K^+ channel Slo3, have very similar properties *i.e.* both are pH dependent, weakly voltage activated (Navarro et al. 2007; Lishko et al. 2011) and located in the principle piece of the flagella. As well as this both Slo3/CatSper KO mice and CatSper deficient men present with defects in motility as well as infertility (Avenarius et al., 2009; Avidan et al., 2003; Jin et al., 2007; Zhang et al., 2007; Santi et al., 2010).

Chapter 3 demonstrated that human sperm possess a poorly selective hyperpolarising K^+ current important for the regulation of membrane potential. As previously mentioned, Slo3 is a pH sensitive K^+ channel which governs the regulation of membrane potential in murine sperm. Although Slo3 knock-out abolishes capacitation-associated hyperpolarisation of the sperm membrane, there is no difference in the resting membrane potential between wild type and knock out sperm under non-capacitating conditions (Santi et al. 2010). Furthermore, although sperm from these animals do not express Slo3, a hyperpolarising K^+ current can be recorded, known as I_{Kres} (Zeng et al. 2011). Zeng et al, proposed that this residual current was a result of K^+ efflux through

endogenous CatSper channels. CatSper has been shown to be freely permeable to monovalent cations when Ca^{2+} and Mg^{2+} are removed from the external environment. Indeed, the binding of Ca^{2+} to a site within the channel's pore confers the Ca^{2+} selectivity of the channel and removal of external Ca^{2+} allows the channel to become freely permeable to monovalent cations such as potassium (Lishko et al. 2011; Kirichok et al. 2006; Strünker et al. 2011). Under physiological levels of external Ca^{2+} CatSper has been suggested to show no measurable conductance for monovalent cations (Kirichok et al. 2006; Lishko et al. 2011; Smith et al. 2013; Strünker et al. 2011). One major caveat to this proposal is that all these studies assessed CatSper using Cs^+ as the only permeable cation that characteristically flows through CatSper in divalent free conditions. However, in the Zeng study, significant K^+ currents were recorded in the presence of 2mM external Ca^{2+} and therefore proposes that CatSper can allow K^+ efflux even in the presence of external Ca^{2+} at strongly depolarised potentials (Zeng et al. 2011). This suggests that CatSper could aid in the regulation of V_m in mouse sperm.

4.2. Aim

The aim of this chapter is to try to identify if CatSper or a separate K^+ channel carries the K^+ current recorded in Chapter 3. This will be achieved using pharmacological methods to assess the pharmacological profiles of each current.

4.3. Results

4.3.1. Classic CatSper Current

Figure 4.1 shows CatSper currents recorded under control (HS), divalent free (DVF, bath solution devoid of Ca^{2+} and Mg^{2+} where Cs^+ is the only permeable cation) and DVF + 500nM progesterone treated conditions (Lishko et al. 2011; Strünker et al. 2011). Figure 4.1A shows a representative trace of a single spermatozoon recorded by ramp protocol (-87 mV to 73 mV, $V_{\text{Hold}} = -7$ mV) over a 400 ms period (HS: blue line, DVF: black line and DVF + 500nm progesterone: red line). Figure 4.1B shows the I_m - V_m relationship calculated by further analysis of the individual recordings. This figure shows that under control conditions where Ca^{2+} and Mg^{2+} are present in the bath solution there is very little inward or outward current (-12.5 ± 6.4 vs. 10.3 ± 3.5 pApF $^{-1}$, respectively, blue line $n_c = 4$). Upon removal of all external divalents, where Cs^+ is the principle ionic carrier, a large Cs^+ current was observed (peak outward current: 169.3 ± 36.0 pApF $^{-1}$, peak inward current: -51.2 ± 18.0 pApF $^{-1}$, red line). Application of 500nM progesterone to the DVF bath solution caused a rapid (< 5 second) increase in the Cs^+ current as shown in Figure 4.1B (red line). This data is consistent with data published in the literature regarding the progesterone activated Cs^+ current through CatSper (Lishko et al. 2011). In subsequent experiments the Cs^+ current will be referred to as the CatSper current.

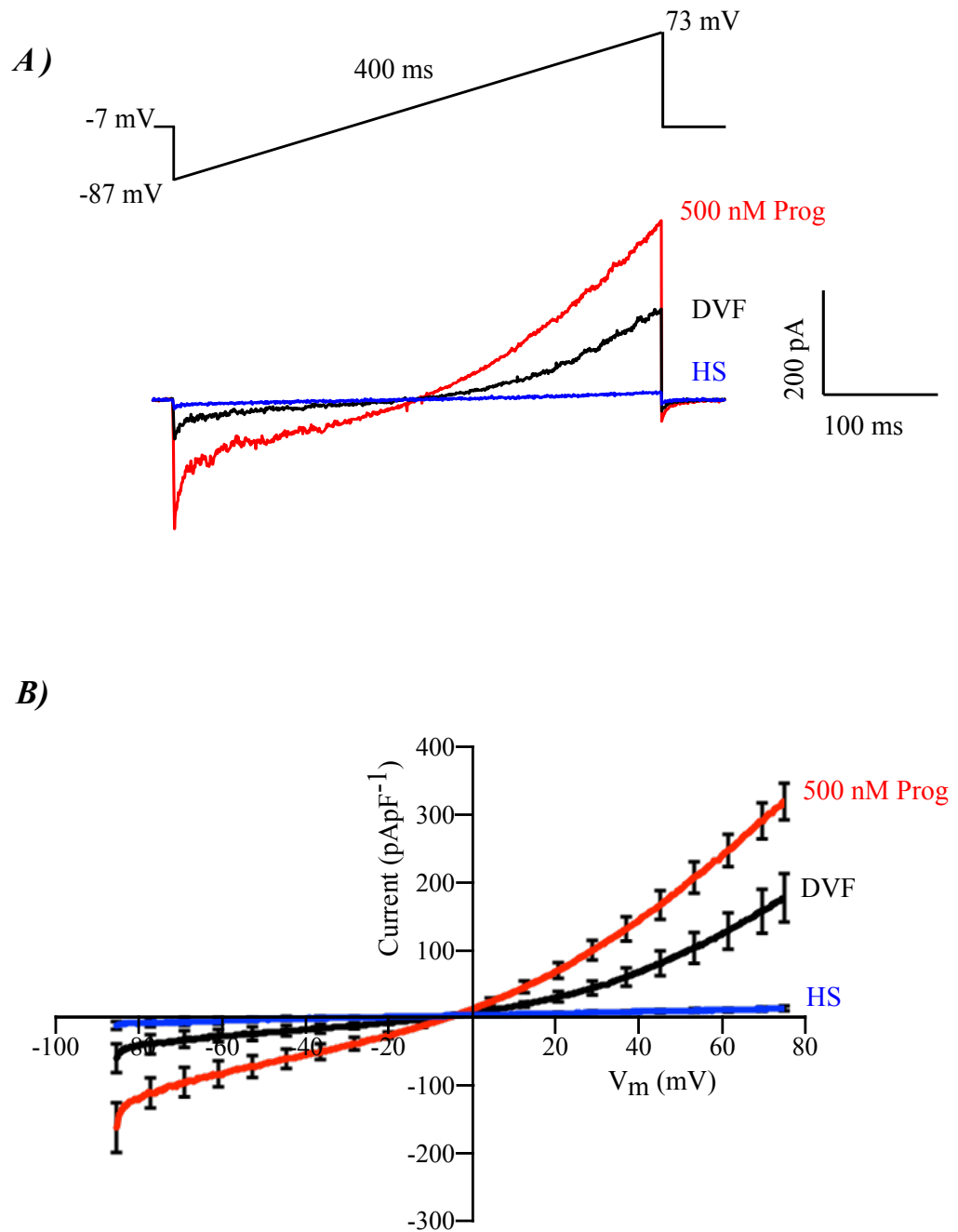


Figure 4.1: Confirmation of progesterone activated CatSper currents: Classic CatSper current recorded under control (HS, blue line), divalent free (DVF, black line) and in the presence of 500nM progesterone (red line). A) Shows the raw trace of a single human sperm cell recorded under the 3 conditions by a ramp protocol (-87 to 73mV over a 400 ms period with a holding potential of -7mV). B) Shows the current to voltage relationship of the CatSper current in motile human sperm cells under the 3 conditions ($n_C = 4$, $N_D = 4$, $C_m = 1.2 \pm 0.2$ pF, $R_a = 52.0 \pm 18.3$ M Ω , $R_m = 7.5 \pm 2$ G Ω)

4.3.2. *CatSper* current and K^+ Channel blockers

Figure 4.2 shows the effect of quinidine (3mM), bupivacaine (3mM), clofilium (50 μ M) and 4-AP (2mM) on *CatSper* currents recorded under conditions devoid of Ca^{2+} and Mg^{2+} and where Cs^+ was the principle cation. Switching from HS to DVF bath solution caused an increase in the *CatSper* current, characteristic of *CatSper* channels.

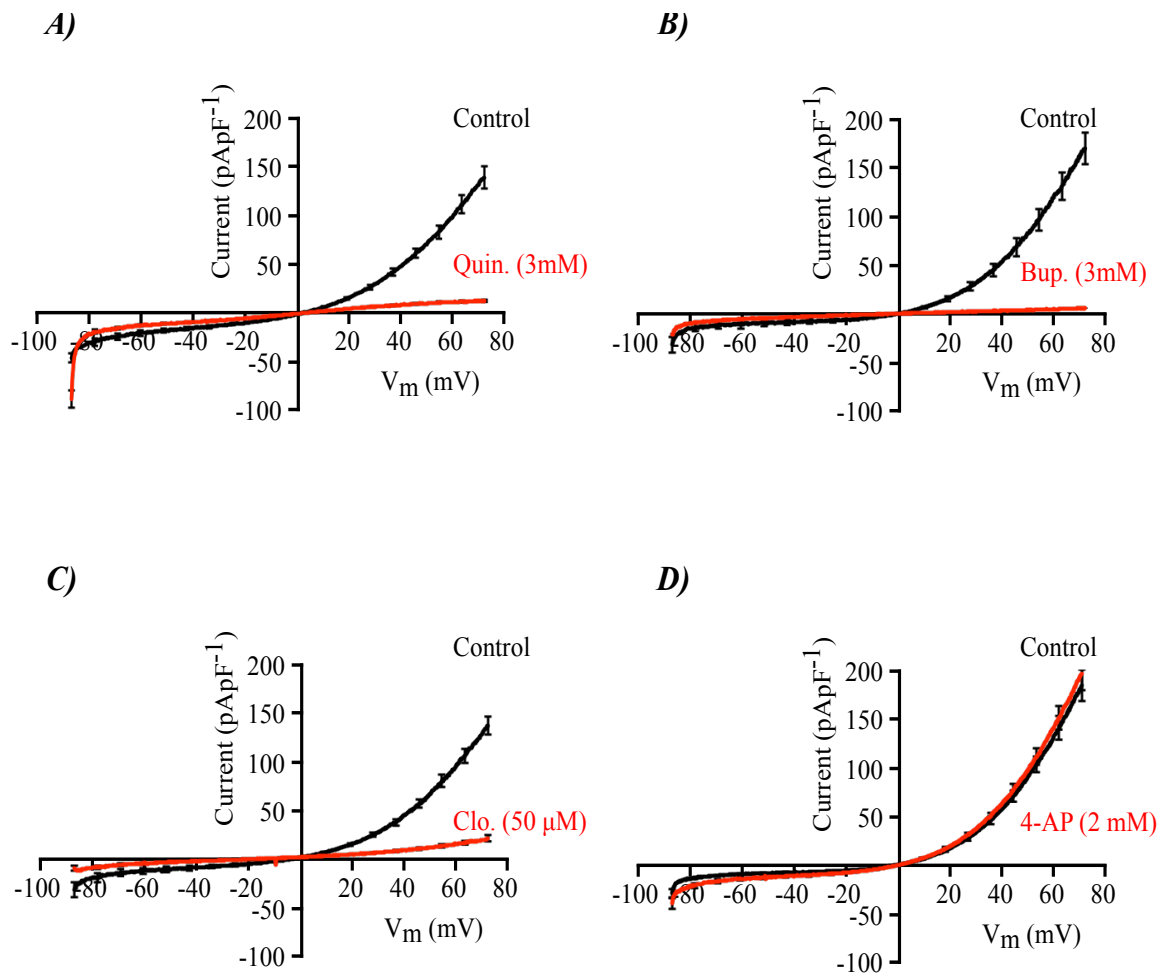


Figure 4.2: The effect of K^+ current blockers on the DVF *CatSper* current in human spermatozoa: Currents recorded using a ramp protocol (-87 to 73mV over a 1 second period with a holding potential of 0mV). Each panel shows relationship between I_m and V_m in control conditions devoid of divalent cations (DVF, black line) and after 20-30s exposure to 0.3mM quinidine (A, $n_c = 8$), 3mM bupivacaine (B, $n_c = 7$), 50 μ M clofilium (C, $n_c = 5$) and 2mM 4-AP (D, $n_c = 7$).

Perfusion of the chamber (20 - 30 seconds) with quinidine, bupivacaine or clofilium resulted in an inhibition of the outward current by $90.0 \pm 1.1\%$ ($p < 0.001$, Student's paired t-test), $96.2 \pm 0.2\%$ ($p < 0.001$, Student's paired t-test) and $85.6 \pm 2.6\%$ ($p < 0.001$, Student's paired t-test), respectively as indicated by the red traces (Figure 4.2A-C). 4-AP had no effect on the outward current as indicated in Figure 4.2D (% inhibition $-7.5 \pm 2.0\%$, $p > 0.05$, Student's paired t-test).

4.3.3. *CatSper Channel Inhibitors and K^+ Current*

Experiments designed to assess the effect of CatSper channel inhibitors, mibefradil ($30\mu\text{M}$) and NNC 55-0396 ($2\mu\text{M}$) (Strünker et al. 2011; Lishko et al. 2011), on the K^+ current as described in Figure 4.3. Currents were generated using an identical ramp protocol as describe in Chapter 3 (-92mV to $+68\text{mV}$ over a 250ms period, $V_{\text{hold}} = -92\text{mV}$). Figure 4.3 shows the effects of $30\mu\text{M}$ mibefradil and $2\mu\text{M}$ NNC55-0396 on the outwardly rectifying hyperpolarising current under conditions designed to maintain physiological ionic gradients assessed using a ramp protocol as described in Chapter 3. Control experiments confirmed that depolarisation induced outwardly rectifying hyperpolarising current as previously described. Perfusion of the chamber with $2\mu\text{M}$ NNC 55-0396 and $30\mu\text{M}$ mibefradil for 20 - 30 seconds caused a statistically significant inhibition of the outward current by $\sim 85\%$ (control: $32.4 \pm 3.4 \text{ pApF}^{-1}$, NNC 55-0396: $5.1 \pm 1.4 \text{ pApF}^{-1}$, $p < 0.0001$, Student's paired t-test) and 95% (control: $43.0 \pm 4.8 \text{ pApF}^{-1}$, mibefradil: $2.6 \pm 0.6 \text{ pApF}^{-1}$, $p < 0.0001$, Student's paired t-test) respectively, indicating the current's sensitivity to the two compounds (Figure 4.3A). Further analysis of the membrane conductance (G_m) as a percentage of the control between 14 and 66 mV (see Materials and Methods page 51) showed that $30\mu\text{M}$ mibefradil (control: $654.51 \pm 58.43 \text{ pSpF}^{-1}$, mibefradil:

$28.93 \pm 8.71 \text{ pSpF}^{-1}$, $p < 0.001$, Student's t-test) and $2 \mu\text{M}$ NNC 55-0396 (control: $470.20 \pm 30.50 \text{ pSpF}^{-1}$, NNC 55-0396: $74.51 \pm 16.43 \text{ pSpF}^{-1}$, $p < 0.001$, Student's t-test) significantly inhibited G_m . This was comparable to experiments where intracellular K^+ was replaced with Cs^+ as indicated by the dotted line (Figure 4.3B). Figures 4.3C and D show the effects of NNC 55-0396 and mibefradil on the reversal potential (E_{rev}) calculated by further analysis of data in Figure 4.3A. This demonstrated that NNC 55-0396 (Control: $-25.81 \pm 4.0 \text{ mV}$, NNC 55-0396: $-9.85 \pm 3.4 \text{ mV}$, $n_c = 6$, $N_D = 3$, $p = 0.008$) and mibefradil (Control: $-36.14 \pm 6.7 \text{ mV}$, mibefradil: $0.78 \pm 10.0 \text{ mV}$, $n_c = 6$, $N_D = 3$, $p = 0.006$) caused a statistically significant depolarisation of E_{rev} . These data suggest that the DVF CatSper current and physiological K^+ current share the same pharmacological profiles.

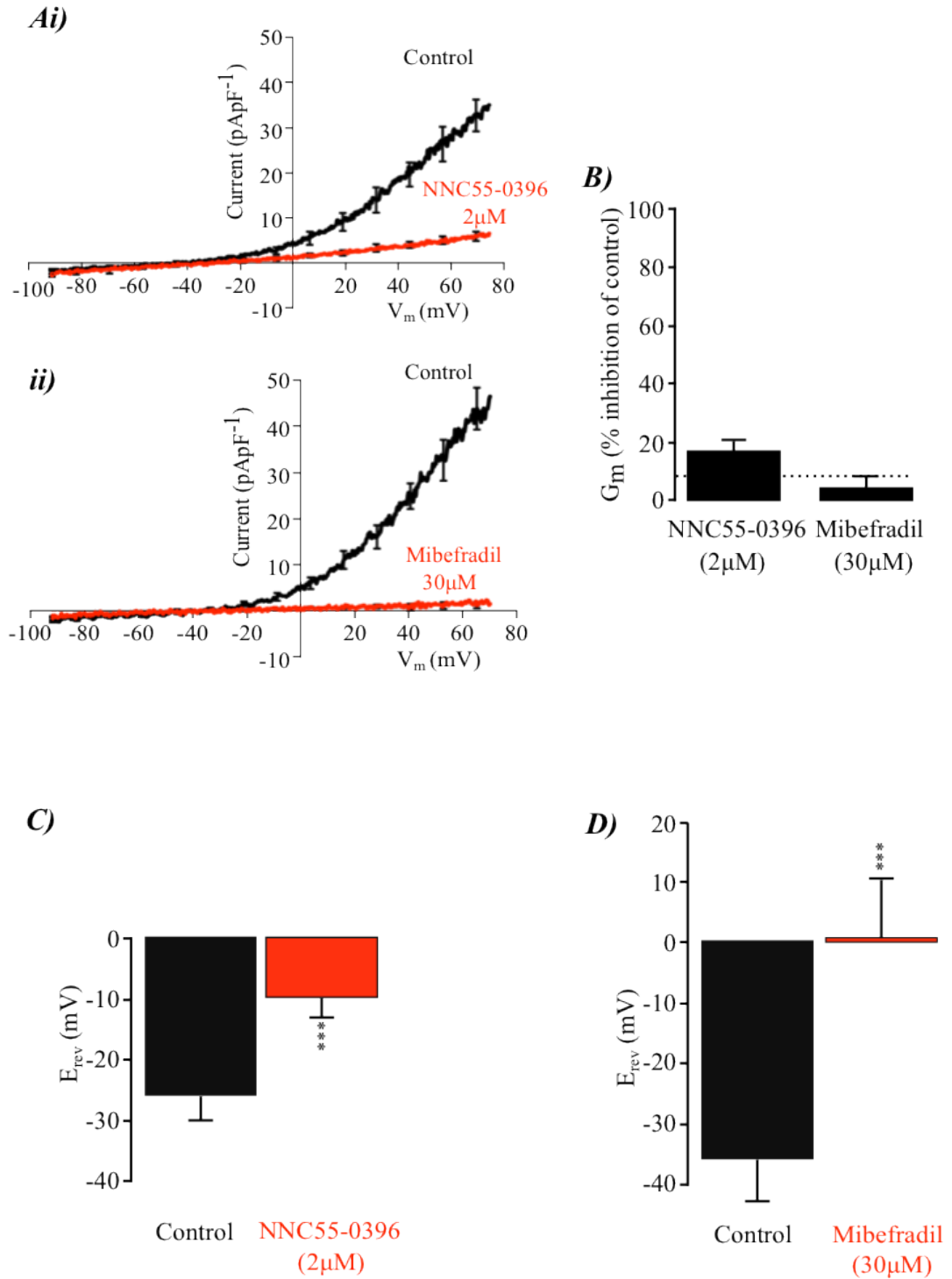


Figure 4.3: Effects of CatSper inhibitors on the physiological K⁺ current. (A) Relationship between I_m and V_m quantified under control conditions and after 20-30 s exposure to 2µM NNC55-0396 (Ai, n_c = 5) or 30µM mibefradil (Aii, n_c = 6). (B) Inhibition of G_m as a percentage of control generated by analysis of data in A, with dotted line indicating percentage G_m when pipette K⁺ is replaced with Cs⁺. (C&D) Assessment of resting V_m under control conditions and after 20-30 seconds exposure to NNC55-0396 or mibefradil with error bars indicating s.e.m and asterisks denoting p < 0.001, Student's paired t-test.

4.3.4. *NNC55-0396 depolarises Membrane Potential and Blocks Small outward Na⁺ Current.*

Figure 4.4A shows the effects of 2 μ M NNC55-0396 on the resting membrane potential of human sperm assessed by whole cell current clamp. On the left, a representative trace of the resting membrane potential recorded from a single spermatozoon in a period of control bath conditions (20 seconds) and during a period of 2 μ M NNC55-0396 perfusion (50 seconds). The bar chart on the right shows pooled data of 4 individual cells from 3 different donors. Under control conditions the resting membrane potential was confirmed to be ~ -30 mV. Application of 2 μ M NNC55-0396 caused a slow depolarisation of V_m from -34.65 ± 3.81 to 4.75 ± 1.65 mV over a 20 second period ($n_C = 4$, $N_D = 3$, $p < 0.001$, Student's paired t-test). Figure 4.4B, shows data from a single spermatozoon on the left with the average of 4 cells from 3 different donors on the right where the effect of 2 μ M NNC55-0396 was assessed on the small outward Na⁺ current as described in Chapter 3 (Figure 3.7A). Under control conditions depolarisation by a single step to 68mV caused outward current of 5.82 ± 0.58 pApF⁻¹. Perfusion of the bath with 2 μ M NNC55-0396 for 20-30 seconds caused a significant inhibition of the outward current by $\sim 84\%$ to 0.85 ± 0.26 pApF⁻¹ ($p < 0.001$, Student's paired t-test).

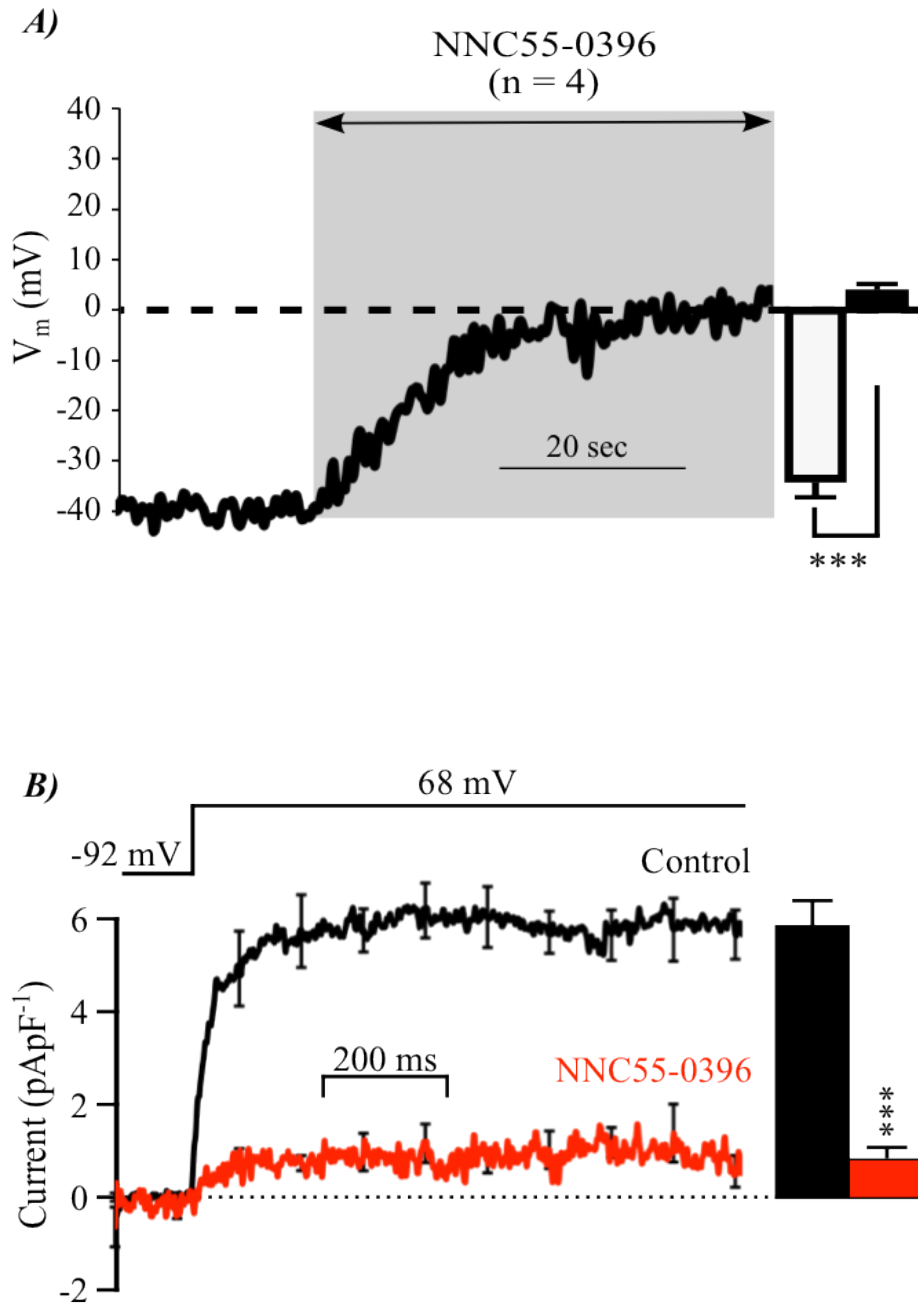


Figure 4.4: Effects of specific CatSper inhibitor NNC55-0396 on resting V_m and small outward Na^+ current. (A) Continuous recording of resting V_m by whole cell current clamp of a single spermatozoon in a period of control conditions (20 seconds) and during exposure to $2\mu\text{M}$ NNC55-0396 (50 seconds). Panel on the right shows pooled data of 4 cells from 3 different donors. (B) Panel on the left shows mean currents evoked by step depolarisation to 68mV that were recorded using Na^+ based pipette solution, whilst the right hand panels show pooled currents of 4 cells from 3 different donors quantified over the final 300 ms of the voltage pulse. Data was recorded during exposure to standard bath conditions (control) and after 20-30 seconds exposure to $2\mu\text{M}$ NNC55-0396. All data are presented as mean \pm s.e.m with asterisks denoting values that differed significantly from control ($p < 0.001$, Student's paired t-test)

4.3.5. *Effect of K⁺ Channel blockers on Progesterone induced Ca²⁺ Influx*

Figure 4.5 shows the effect of two K⁺ channel blockers, bupivacaine (3mM) and clofilium (50μM) on the progesterone induced Ca²⁺ influx measured by fluorometric dye Fura-2AM (See Materials and Methods, page 39). Assessment of the resting Ca²⁺ level prior to application of 3.6μM progesterone showed that resting levels of Ca²⁺ did not differ statistically in control and treated samples indicating clofilium and bupivacaine did not cause alterations in resting intracellular Ca²⁺.

The addition of 3.6μM progesterone showed that in the control population, addition of progesterone induced a transient increase in intracellular calcium, after which a secondary and sustained increase in [Ca²⁺]_i was observed (Figure 4.5 black lines). Pre-treatment of the cells with either 3mM bupivacaine or 50μM clofilium for 5 minutes completely abolished the fast transient phase observed in control conditions, however the secondary sustained phase was not affected (Δ sustained: Control 0.4 ± 0.1 vs. bupivacaine 0.3 ± 0.1 $p = 0.4$ ANOVA/ Bonferroni post Hoc, Control 0.3 ± 0.1 vs. clofilium 0.3 ± 0.1 $p = 0.8$, ANOVA/ Bonferroni post Hoc). Analysis of the change in peak ratio of the transient phase, calculated as the peak response ratio minus the basal level ratio, showed that bupivacaine and clofilium caused a reduction in Δ peak from 1.4 ± 0.2 to 0.3 ± 0.1 ($N_D=4$, $p = 0.002$ ANOVA/ Bonferroni post Hoc) and 1.7 ± 0.3 to 0.5 ± 0.1 ($N_D=4$, $p = 0.007$ ANOVA/ Bonferroni post Hoc), respectively.

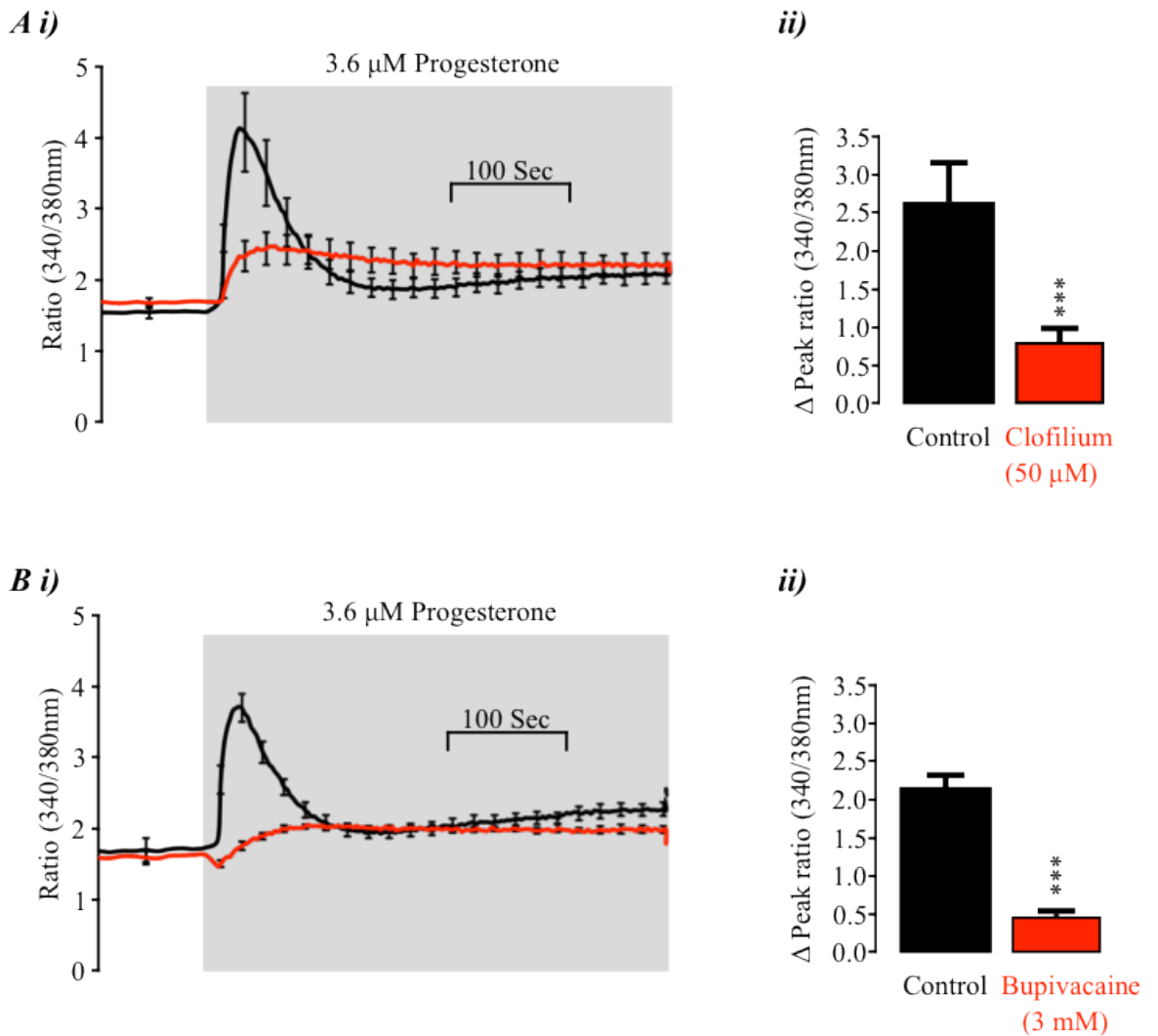


Figure 4.5: The effects of bupivacaine and clofilium on the progesterone induced Ca^{2+} influx in human sperm after 4 hours of capacitation. *Ai&Bi*) Panels on the left represent mean fluorimetric population responses to 3.6 μ M progesterone from 4 different donors under control conditions (black trace) or in the presence of 50 μ M clofilium (A) or 3mM bupivacaine (B), red traces. Grey boxes indicate exposure time to progesterone. All data was normalised for background fluorescence by addition of 9mM MnCl_2 . Changes in fluorescence was quantified from data in *Ai* and *Bi* and are represented at bar charts on the right. All data are represented as mean \pm s.e.m with asterisks denoting statistical significance compared to control ($p < 0.001$, ANOVA/ Bonferroni post Hoc).

4.3.6. Quinidine – K^+ Current

Detailed experiments designed to distinguish between the K^+ current and CatSper based on clofilium and quinidine reversibility as described by Zeng and colleagues (Zeng et al. 2011) are presented below.

Figure 4.6A shows voltage-induced K^+ currents evoked by depolarising ramps. Data in Chapter 3 showed that the voltage-induced current developed relatively slowly therefore the duration of the voltage ramp was increased from 250ms (Chapter 3) to 6 seconds to accommodate for this. Depolarisation evoked noisy outward currents (I_{Out}) and the current over the final few ms was quantified and this was $\sim 50\text{pApF}^{-1}$. Addition of 0.3mM quinidine caused a rapid inhibition of I_{Out} (5-10 seconds) to $\sim 5\%$ of control (Figure 4.6B). However, removal of quinidine from the bath solution showed that this inhibition was fully reversible, albeit relatively slow (~ 2 minutes). Figure 4.6C shows the I_m - V_m relationship constructed using data recorded under 3 different conditions: (i) under control conditions (Figure 4.6, black trace); (ii) at maximal inhibition (Figure 4.6, red trace) and (iii) 3 minutes after quinidine was removed from the bath (Figure 4.6, blue trace). Analysis of G_m between 14 and 66mV (Figure 4.6C) confirmed quinidine caused a $\sim 95\%$ inhibition of G_m and that this was fully reversible upon removal of quinidine from the bath solution (Figure 4.6D). Analysis of E_{rev} showed that quinidine significantly depolarised E_{rev} by $\sim 25\text{mV}$. Again, this was fully reversible upon removal of quinidine from the bath solution (Figure 4.6E).

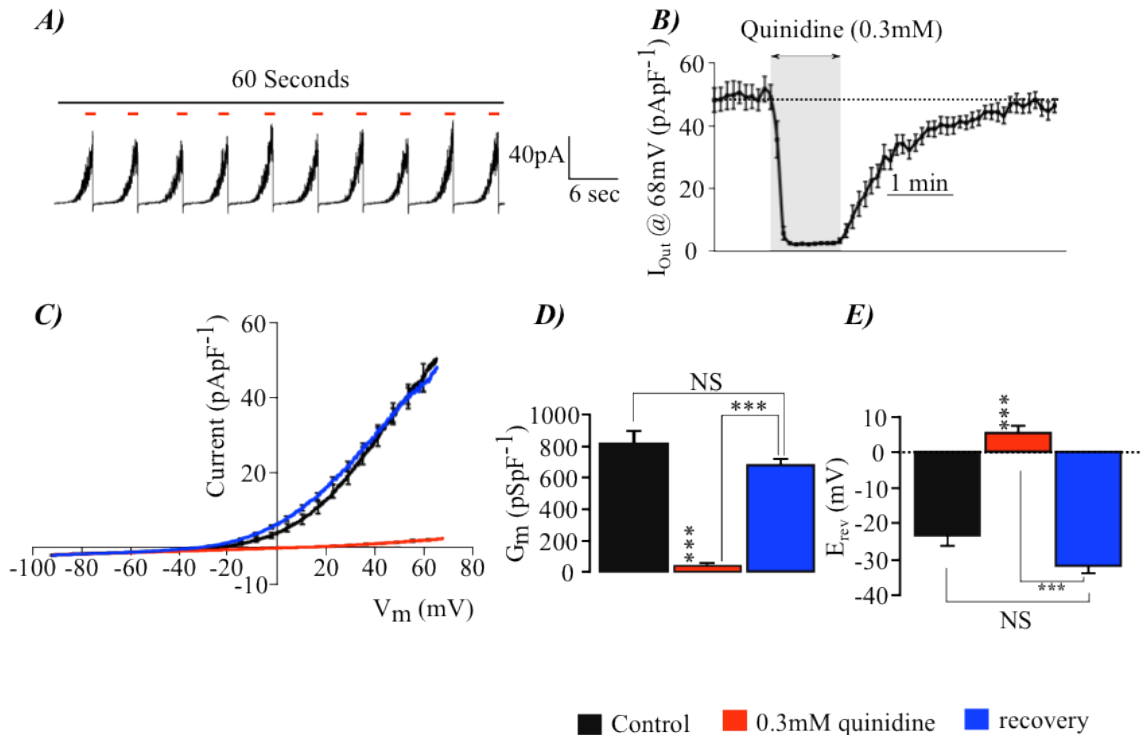


Figure 4.6: Quinidine induced block of K^+ current: A) Continuous recordings of membrane current evoked by a series of depolarising 6 second ramps with red bars indicating the period of which mean outward currents were quantified for further analysis. B) Time course showing the effects of 0.3mM quinidine upon I_{out} ($n_C = 9$, $N_D = 3$). C) I_m - V_m relationships constructed using data recorded under control conditions (black); at maximal inhibition with quinidine (red) and 3 minutes after quinidine was removed from the bath (blue). D) Values for membrane conductance (G_m) quantified under each condition. E) Values for the reversal potential (E_{rev}) quantified under each condition. All data presented as mean \pm s.e.m with asterisks denoting statistical significance (** $p < 0.001$, NS = not significant). All statistical tests were assessed by one-way ANOVA).

4.3.7. Clofilium – K^+ Current

Figure 4.7 shows data from experiments that used an identical protocol described in Figure 4.6 to explore the effect of 50 μ M clofilium on the K^+ current. Figure 4.7A shows that clofilium significantly inhibited I_{out} over a 1 minute period to $\sim 5\%$ of control. In contrast to quinidine (Figure 4.6), removal of clofilium from the bath solution showed that the block was irreversible. Figure 4.7B shows I_m - V_m relationships constructed using data recorded 3 different conditions: (i) under control conditions; (ii) at maximal

inhibition and (iii) 3 minutes after clofilium was removed from the bath. Analysis of G_m between 14 and 66mV from data in 7B confirmed clofilium caused a ~95% irreversible inhibition of G_m (Figure 4.7C). Analysis of E_{rev} showed that clofilium significantly depolarised E_{rev} by ~30mV. However this depolarisation was irreversible upon removal of clofilium from the bath solution (Figure 4.7D).

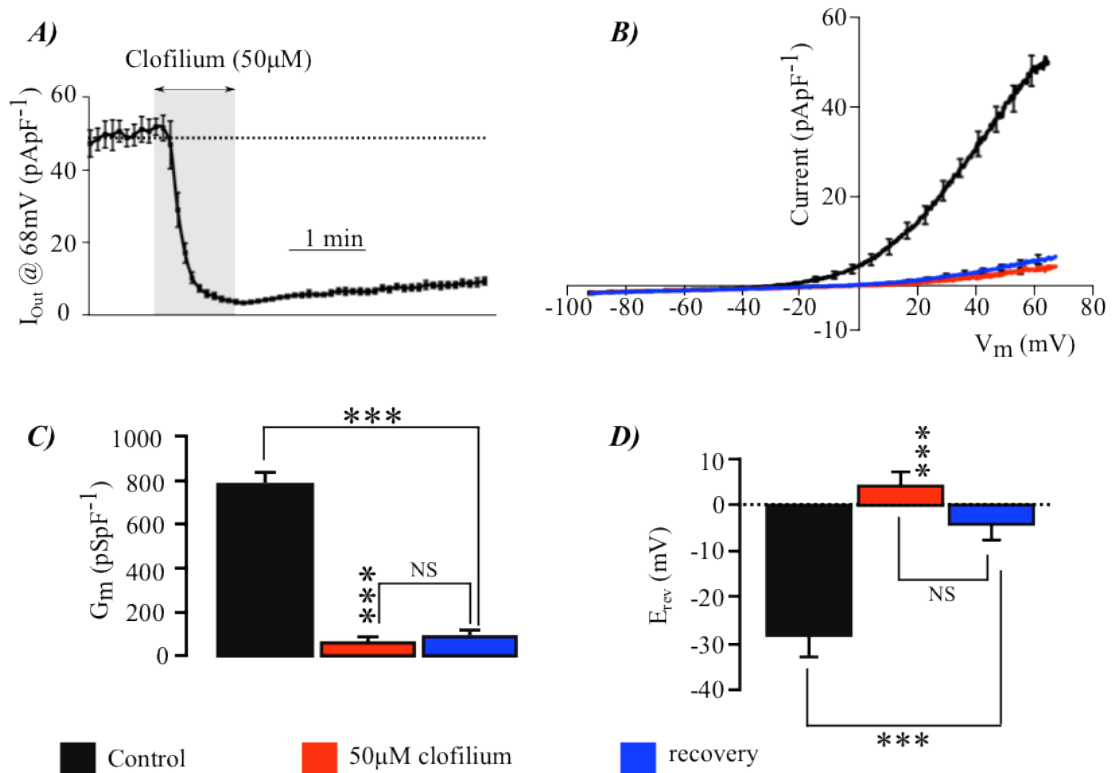


Figure 4.7: Clofilium induced block of K^+ current: A) Time course showing the effects of 50µM clofilium upon I_{out} ($n_c=6$, $N_D=3$). B) I_m - V_m relationships constructed using data recorded under control conditions (black); at maximal inhibition with clofilium (red) and 3 minutes after clofilium was removed from the bath (blue). C) Values for membrane conductance (G_m) quantified under each condition. D) Values for reversal potential (E_{rev}) quantified under each condition. All data presented as mean \pm s.e.m with asterisks denoting statistical significance (***) $p < 0.001$, NS = not significant). All statistical tests were assessed by one-way ANOVA).

4.3.8. Quinidine and Clofilium induced block of CatSper

Experiments examining the effect of 50 μ M clofilium and 0.3mM quinidine on the I_m - V_m relationship and G_m of currents recorded under DVF conditions designed to provide a read out of CatSper activity are presented in Figure 4.8. Removal of divalent cations Ca^{2+} and Mg^{2+} (DVF solution) from the extracellular solutions caused a large outwardly rectifying current of ~ 150 pApF $^{-1}$ typical of CatSper (149.38 ± 12.95 pApF $^{-1}$, $n_c = 10$, $N_D = 5$) (Lishko et al. 2011). Perfusion of the bath with DVF+ 50 μ M clofilium (Figure 4.8A) or 0.3mM quinidine (Figure 4.8D) for 60 seconds caused a $> 90\%$ inhibition of the DVF current and confirmed the inhibitory effect of the compounds as presented in Figure 4.2 (% inhibition: 50 μ M clofilium = $91.86 \pm 1.23\%$ $n_c = 5$, $N_D = 3$, $p < 0.001$, one-way ANOVA; 0.3mM quinidine = $90.96 \pm 1.58\%$ $n_c = 5$, $N_D = 3$, $p < 0.001$, one-way ANOVA). The time course of block showed similar inhibition kinetics to the K^+ current, as clofilium took ~ 1 minute to fully block CatSper, whereas the block caused by quinidine was rapid with full inhibition after ~ 10 seconds. Figures 8B and E shows the I_m - V_m relationships constructed using data recorded (i) under control conditions (black line); (ii) at maximal inhibition with either clofilium (red line, Figure 4.8B) or quinidine (red line, Figure 4.8E); and (iii) 3 minutes after the test compound was removed from the bath (blue line). Assessment of the G_m between 14 and 66mV also confirmed addition of clofilium (Figure 4.8C, control: 2.81 ± 0.31 nSpF $^{-1}$, clofilium: 0.19 ± 0.03 nSpF $^{-1}$, $p < 0.001$, one-way ANOVA) or quinidine (Figure 4.8F, control: 2.99 ± 0.49 nSpF $^{-1}$, quinidine: 0.15 ± 0.02 nSpF $^{-1}$, $p < 0.001$, one-way ANOVA) caused a statistically significant inhibition of the G_m . Removal of quinidine from the extracellular solution for 3 minutes caused complete recovery of the outward DVF current. However, removal of clofilium from the extracellular solution

over the same period only showed partial recovery of ~20%. Analysis of currents after removal of clofilium from the bath solution showed that these currents did not differ statistically from current recorded in the presence of the blocker. This indicates that clofilium irreversibly blocks CatSper DVF currents in human sperm.

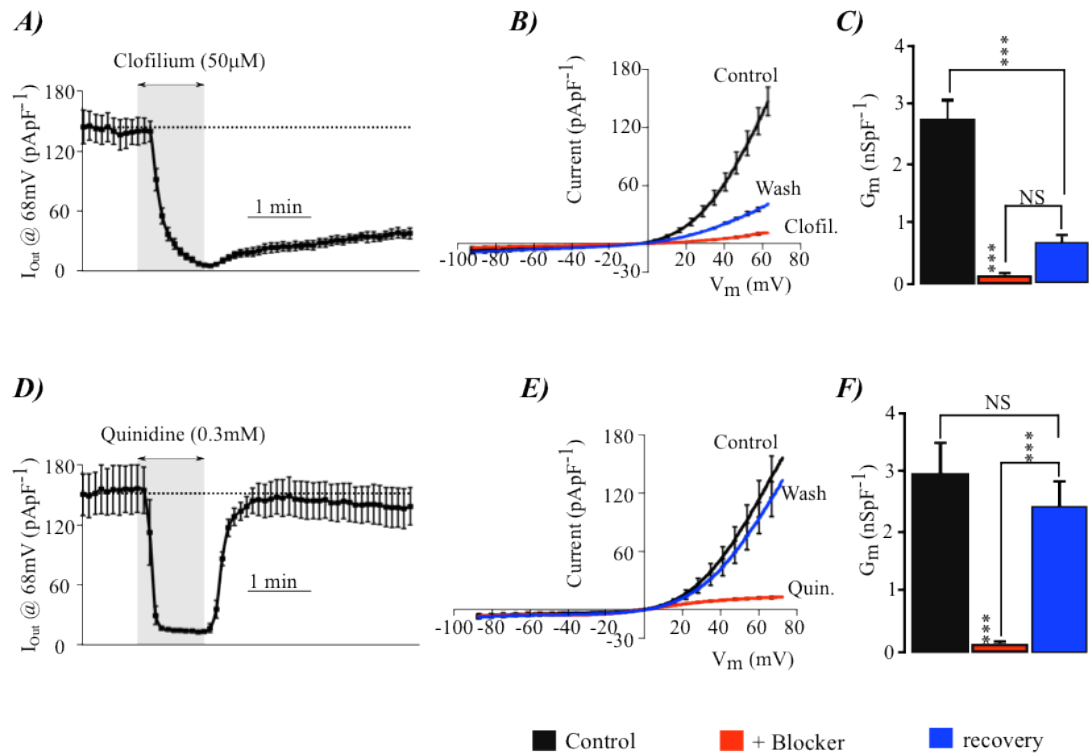


Figure 4.8: Quinidine- and clofilium –induced block of CatSper. Membrane currents were quantified using pipette and bath solutions devoid of divalent cations that contained Cs⁺ as the only permeable ion. A) Time course showing the effects of 50 μ M clofilium on the outward current (I_{out}) quantified using voltage ramp protocols described in Figure 6 ($n_c = 5$, $N_D = 3$). B) I_m - V_m relationships constructed using data recorded under control conditions (black); at maximal inhibition with clofilium (red) and 3 minutes after clofilium was removed from the bath (blue). C) Effects of 50 μ M clofilium on G_m . D) Time course showing the effects of 0.3 mM quinidine on I_{out} ($n_c = 5$, $N_D = 3$). E) I_m - V_m relationships constructed using data recorded under control conditions (black); at maximal inhibition with quinidine (red) and 3 minutes after quinidine was removed from the bath (blue). F) Effects of 0.3 mM quinidine on G_m . All data represented as mean \pm s.e.m with asterisks denoting statistical significance (***) $p < 0.001$, NS = not significant). All statistical tests were assessed using one-way ANOVA).

4.4. Discussion

The data presented in this chapter demonstrates that the classic divalent free outward CatSper current and the physiological K^+ current share the same pharmacology and, to our knowledge, this is the first time that this has been assessed in motile human spermatozoa. In the present study CatSper currents were recorded under conditions devoid of Ca^{2+} and Mg^{2+} and where Cs^+ was the principle cation to provide a read-out of CatSper activity. Furthermore, CatSper activity was confirmed by the addition of 500nM progesterone. Based on the data presented in Figure 4.1, our data accords well with other electrophysiological studies assessing the effect of progesterone on the DVF CatSper current (Lishko et al. 2011; Strünker et al. 2011; Brenker et al. 2012). Subsequent experiments sought to explore the effect of known K^+ channel inhibitors highlighted in Chapter 3 on the DVF CatSper current. It is clear from data presented in Figure 4.2 that the outward CatSper current is sensitive to quinidine, bupivacaine and clofilium but unaffected by 4-AP. This therefore suggested that the outward K^+ current assessed in Chapter 3 and the outward CatSper current show the same pharmacology and therefore may flow through the same population of channels. To further explore if the CatSper current and the K^+ current were the same, experiments were designed to assess the effect of known CatSper channel antagonists mibefradil and NNC 55-0396 on the K^+ current under physiological bath and pipette conditions. The inhibition of the physiological K^+ current with mibefradil and NNC 55-0396 provided further evidence that the CatSper current and K^+ current may flow *via* the same channel or channels. Furthermore, NNC 55-0396 was effective at depolarising resting membrane potential when assessed using whole cell current clamp confirming data presented in Chapter 3 on the role of the outward current in the regulation of membrane potential. Lastly,

NNC55-0396 was also effective at inhibiting the small Na^+ current induced by replacing $[\text{K}^+]_i$ with Na^+ confirming the current underlying the K^+ current and DVF CatSper current share identical pharmacology. Although mibefradil has been shown to inhibit certain K^+ channels (Chouabe et al. 1998; Gomora et al. 1999; Perchenet & Clement-Chomienne 2000; Navarro et al. 2007), NNC 55-0396, a proposed CatSper specific inhibitor, has no known action on K^+ channels. As a result, CatSper and the physiological K^+ current cannot be distinguished using pharmacological methods.

4.4.1. CatSper and progesterone induced Ca^{2+} signalling

Intracellular Ca^{2+} increases in response to progesterone are crucial for fertilising ability of human sperm. This is based on studies that have shown a correlation between poor Ca^{2+} responses to progesterone and fertilisation success in IVF patients (Alasmari et al. 2013; Krausz et al. 1996). It is therefore interesting to see that application of clofilium or bupivacaine completely abolishes the progesterone induced Ca^{2+} signal suggesting the channel could be important for fertility in humans. Furthermore, both clofilium and bupivacaine had very specific effects by only affecting the transient increase in Ca^{2+} that is thought to be rapid Ca^{2+} influx through CatSper (Nash et al. 2012). In contrast neither compound had an effect on resting Ca^{2+} levels, or the secondary increase in Ca^{2+} thought to be due to activation of intracellular stores. It is therefore tempting to postulate that clofilium and bupivacaine directly inhibit progesterone-activated Ca^{2+} entry. However, more detailed studies will need to be carried out in order to prove this hypothesis.

4.4.2. K^+ and CatSper current: One or two channels?

Electrophysiological studies on murine sperm have identified that CatSper and Slo3 are two distinct channels with different physiological roles (Kirichok et al. 2006; Navarro et al. 2007; Santi et al. 2010; Zeng et al. 2011). However, data presented here shows that in humans this distinction is unclear. Potassium channel antagonists as well as CatSper specific antagonist NNC55-0396 all cause inhibition of the K^+ current as well as the CatSper current resulting in the depolarisation of resting V_m and inhibition of the progesterone induced $[Ca^{2+}]_i$ influx. This suggests the channel underlying the K^+ current and the CatSper current are the same. Some evidence by Zeng et al in Slo3 knock out murine sperm has suggested CatSper can allow K^+ efflux even in the presence of extracellular Ca^{2+} . Zeng et al showed that although deletion of Slo3 caused a reduction in hyperpolarising outward K^+ current, a substantial residual hyperpolarising K^+ current could still be recorded. This current was subsequently called $I_{K_{res}}$ and was thought to be K^+ efflux through endogenous CatSper channels. This is surprising as electrophysiological studies of CatSper have shown that the channel is normally strictly Ca^{2+} selective, however, this is dependent on the binding of the Ca^{2+} ion within the pore region of the channel (Kirichok et al. 2006; Lishko et al. 2011). In contrast, removal of extracellular Ca^{2+} results in a loss of channel selectivity and as a result large non-selective cation currents can be recorded as observed in Chapter 3 Figure 3.7C. Zeng et al proposed that depolarisation of the membrane potential facilitates Ca^{2+} removal of the pore region allowing K^+ efflux and this was the current underlying $I_{K_{res}}$ in the Slo3^{-/-} mouse sperm. Zeng et al also proposed that in mouse spermatozoa Slo3 and $I_{K_{res}}$ currents could be distinguished based on their reversibility to clofilium block, as $I_{K_{res}}$ was completely reversible after 3 minutes wash out whereas Slo3 only showed partial recovery. This approach was replicated in this chapter to try and distinguish if

the K^+ and CatSper current were flowing through a single or two separate channels. Data presented here showed that in both the K^+ and CatSper currents, clofilium caused a slow block of the outward current, consistent with the theory that clofilium blocks the channel on the intracellular surface and therefore requires time to partition into the cell membrane (Castle 1991; Young et al. 1992). Removal of clofilium from the extracellular bath solution caused an irreversible block assessed after ~ 3 minutes wash. Some degree of recovery was observed in the CatSper current of ~ 20% after 3 minutes however this was not significant. The data presented here does not resemble that of the $Slo3^{-/-}$ studies, suggesting that the outward CatSper and K^+ currents cannot be accurately distinguished using pharmacological methods. This therefore suggests the K^+ and CatSper currents might flow via the same population of ion channels.

4.5. Conclusion

The data presented in this chapter shows that the K^+ current recorded under physiological levels of Ca^{2+} cannot be distinguished from CatSper based on pharmacology. This therefore implies that the K^+ currents recorded here flow through a similar channel rather than two distinct populations of K^+ channels. Further evidence for this hypothesis comes from a recent study by Smith *et al* where electrophysiological recordings from sperm of a naturally occurring CatSper 2 deleted patient were undertaken (Smith et al. 2013). Smith *et al* showed that this genetic mutation completely abolished the CatSper current recorded in divalent free conditions which was identical to studies of CatSper deleted murine sperm (Qi et al. 2007). However, this patient also showed a ~70% reduction of the hyperpolarising K^+ current (Smith et al. 2013). Another interesting observation from this study was that sperm from this individual did not show progesterone activated CatSper current therefore providing

evidence that progesterone acts on CatSper to allow Ca^{2+} influx in human sperm. Therefore, if the K^+ current and CatSper current were flowing through the same channel we would expect progesterone to enhance the K^+ current. The next chapter will aim to establish if the K^+ current and CatSper can be distinguished based on their sensitivity to progesterone.

Chapter 5 - Progesterone and the Tail Current

5.1. Introduction

Progesterone, a steroid hormone released by the cumulus cells that surround the oocyte, is a well-established and potent inducer of intracellular Ca^{2+} influx in human sperm (Publicover et al., 2007). Progesterone-induced increase in $[\text{Ca}^{2+}]_i$ is vital for a number of Ca^{2+} -dependent processes such as acrosome reaction (AR), and hyperactivation (Harper et al., 2003; Suarez et al., 2008a), that are both necessary for fertilisation. The ability to respond to progesterone has been shown to be a marker of fertilising capacity, as men with poor progesterone induced Ca^{2+} responses have impaired fertility (Alasmari, et al., 2013; Krausz et al., 1996). Fluorometric studies have shown that upon addition of progesterone human sperm show a rapid (seconds) elevation of intracellular Ca^{2+} that peaks within 1-minute post progesterone application. This rapid increase in $[\text{Ca}^{2+}]_i$ is mediated by Ca^{2+} entering the cells via the external environment as removal of $[\text{Ca}^{2+}]_o$ or addition of La^{3+} (a non selective Ca^{2+} channel inhibitor) abolished this effect (Blackmores et al., 1990; Foresta et al., 1993; Garcia & Meizel, 1996; Kirkman-Brown et al., 2000; Publicover et al., 2007). Furthermore, the action of progesterone is not *via* a classical progesterone receptor due to the ineffective action of RU486 (a progesterone receptor antagonist) on the progesterone-induced $[\text{Ca}^{2+}]_i$ influx (Yang et al., 1994). In addition to this, the rapid effect of progesterone is thought to be *via* a non-genomic pathway due to the inaccessibility of the DNA for transcription and lack of translational machinery in sperm (Luconi et al., 2004). In 2011, two independent groups identified that the progesterone induced Ca^{2+} influx was mediated by CatSper (Lishko et al., 2011; Strünker et al., 2011) using whole cell patch clamp electrophysiology. Results from the direct assessment of the CatSper channel showed that progesterone induced a large inward current, which was not altered when the cells were treated with RU496. Furthermore, the importance of CatSper in the progesterone induced Ca^{2+} entry has

been recently demonstrated by the direct assessment of CatSper in a CatSper2-deficient male by Smith et al (Smith et al., 2013). This study showed loss-of-function genetic evidence for the activation of CatSper by progesterone as sperm from this individual did not possess the classic progesterone activated CatSper current.

Results in chapter 4 demonstrated that the physiological K^+ current and outward divalent free (DVF) CatSper current could not be distinguished based on their pharmacological profiles. This therefore suggested that these two currents might flow via the same channel, providing a potentially novel role for CatSper in human sperm physiology.

As progesterone is a potent agonist of CatSper, it can be used as a tool to establish if the current underlying the K^+ conductance and the DVF CatSper current flow via the same population of ion channels.

5.2. Aim

The aim of this chapter is to use progesterone, a potent stimulator of CatSper, to assess if the physiological K^+ conductance and DVF CatSper current flow through the same population of ion channels.

5.3. Results

5.3.1. Effects of Progesterone on K^+ Current Over Time

Figure 5.1 shows the effects of 500nM progesterone on the physiological K^+ conductance, described in Chapter 3, over time. Imposing depolarising 5 second voltage ramps (-92 to 68mV, $V_{\text{hold}} = -92\text{mV}$) to spermatozoa under control bath conditions (HS solution) evoked outward current that accorded well with similar currents described in Chapter 3. To obtain a complete understanding if progesterone had an effect on this current, three areas of interest were assessed. These included the maximal outward current between 66-68mV (I_{out}), the tail current (the current mediated by channels open at the moment of repolarisation) evoked by repolarisation from 68 to -92mV (I_{Tail}), and the steady state current at -92mV ($I_{\text{Steady State}}$) as indicated in the top right hand panel of Figure 5.1A. Figure 5.1B shows the effect of 500nM progesterone and vehicle control (EtOH 0.001%) on I_{out} , I_{Tail} and $I_{\text{Steady State}}$ over a three-minute period. A total of 10 consecutive sweeps were recorded in HS bath solution (60 seconds), a period of treatment of either 500nM progesterone or vehicle control (EtOH 0.001%, 60 seconds), and after a period of wash (HS bath solution, 60 seconds). Each data point represents one complete run of the voltage ramp protocol with this data plotted against time. Prior to treatment both vehicle control and progesterone treated cells showed stable and comparable I_{out} , I_{Tail} and $I_{\text{Steady State}}$ currents. Analysis of these data showed that addition of the vehicle control had no observable effect on I_{out} , I_{Tail} or $I_{\text{Steady State}}$ during or after the treatment period. Conversely, application of 500nM progesterone showed a transient inhibition (I_{Tran}) of I_{out} that developed immediately after application of 500nM progesterone before returning to a basal level after 20 seconds (Figure 5.1B).

Furthermore progesterone caused a steady increase in both I_{tail} and $I_{Steady\ state}$ that developed immediately after application of progesterone reaching a peak response (I_{peak}) after 30 seconds (Figure 5.1B).

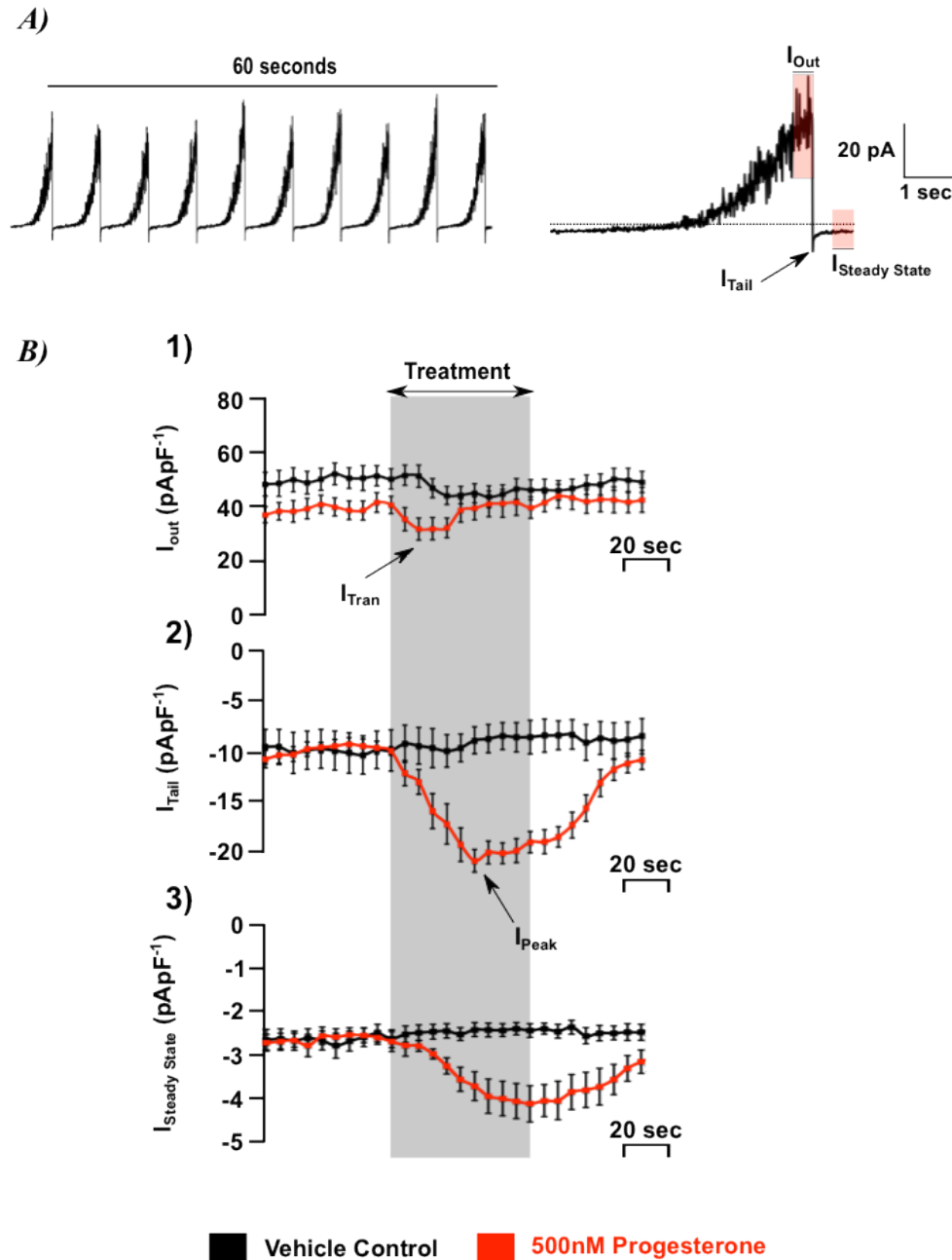


Figure 5.1: Effect of 500nM progesterone on the physiological K^+ current. A) Outwardly rectifying hyperpolarising current generated by 5 seconds voltage ramps with stimulation every 6 seconds. Figure on the right indicating the 3 areas of assessment. B) Analysis of data at each area of interest over time. Black lines indicate currents generated during treatment with vehicle control (0.001% EtOH). Red lines indicate currents generated from sperm treatment with 500nM progesterone. I_{tran} represents the transient inhibition of outward current with progesterone and I_{Peak} represents the peak response after application of 500nM progesterone. $n_C = 8 - 9$, $N_D = 3 - 4$ with values in B represented as mean \pm s.e.m.

5.3.2. Peak Progesterone response (I_{Peak})

Figure 5.2 shows the effect of vehicle control (0.001% EtOH) and 500nM progesterone treated cells on I_{out} , I_{tail} and $I_{steady\ State}$ at I_{peak} by further analysis of data in Figure 5.1B. Analysis of this data showed that application of 0.001% EtOH did not cause a significant effect on I_{out} , (Figure 5.2A: $p = 0.5$), I_{tail} (Figure 5.2C: $p = 0.8$) or $I_{steady\ State}$ (Figure 2E: $p = 0.7$, $n_c = 9$, $N_D = 3$, One-way ANOVA). Assessment of the progesterone treated cells at the same time points also showed that progesterone did not have a statistically significant affect on the I_{out} (Figure 5.2B, Control: 40.02 ± 3.19 pApF⁻¹, I_{Peak} : 36.31 ± 3.36 pApF⁻¹, recovery: 43.40 ± 4.0 pApF⁻¹, $n_c = 8$, $N_D = 3$, $p = 0.4$, One-way ANOVA). However, assessment of I_{Tail} and $I_{steady\ State}$ clearly demonstrated that progesterone caused a statistically significant increase in both I_{Tail} (Control = -10.03 ± 0.70 pApF⁻¹, 500nM progesterone = -20.23 ± 1.1 pApF⁻¹, $p < 0.001$, $n_c = 8$, $N_D = 3$, One-way ANOVA) and $I_{steady\ State}$ (Control = -2.65 ± 0.19 pApF⁻¹, 500nM progesterone = -3.44 ± 0.32 pApF⁻¹, $p = 0.03$, $n_c = 8$, $N_D = 3$, One-way ANOVA) following 30 seconds of treatment. Assessment of the I_{Tail} and $I_{steady\ State}$ after 40 seconds of progesterone removal from the bath showed that both currents were reversible and did not show statistical significance when compared to control. From the data presented here the dominant action of progesterone appears to be on the tail and steady state currents.

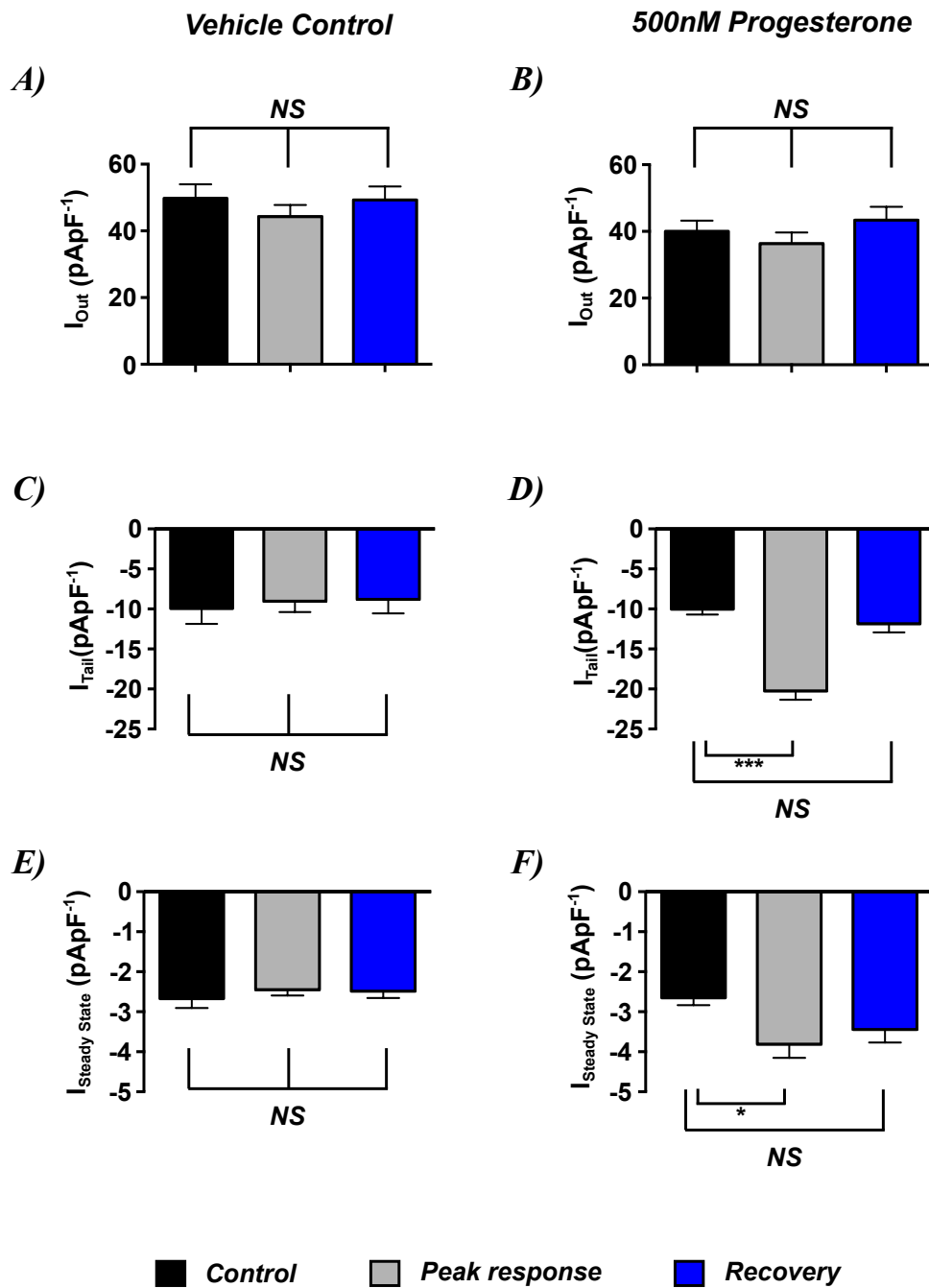


Figure 5.2: Further analysis of data from experiments that explored the effects on 500nM progesterone on I_{Out} , I_{Tail} and $I_{Steady State}$ under conditions that maintained physiological K^+ , Na^+ and Cl^- gradients. Data quantified prior to treatment (black bars), at peak tail current response (grey bars) and 40 seconds after treatment was removed from the bath (blue bars). Left hand panels show data quantified for I_{out} , I_{Tail} and $I_{Steady State}$ in the vehicle control treated group (A, C and E) with right hand panels showing similar data in the progesterone treated group (B, D and F). All data presented as mean \pm s.e.m with asterisks denoting statistical significance (* $p < 0.05$, *** $p < 0.001$, $n_c = 8$, $N_D = 3$, One-way ANOVA).

5.3.3. *The transient progesterone induced response (I_{Tran})*

Figure 5.3 shows data quantified by further analysis of results in Figure 5.1B exploring the transient (I_{Tran}) inhibition of I_{Out} by progesterone.

Figure 5.3A show the I_m-V_m relationship from spermatozoa in control conditions, at I_{Tran} and 40 seconds after removal of the treatment from the bath by further analysis of the pooled data in Figure 5.1A. This showed that under vehicle control conditions there was no observed effect on the I_m-V_m relationship at any of the time points analysed (Figure 5.3A). Analysis of the reversal potential (E_{rev}) and the membrane conductance (G_m) between 14 - 66mV calculated by linear regression showed that 0.001% EtOH had no effect on either of these parameters at all three time points ($p > 0.5$, One-way ANOVA). Assessment of the I_m-V_m relationship under 500nM progesterone treated conditions showed that application of progesterone caused a significant inhibition of the outward current from 41.33 ± 3.61 pApF⁻¹ to 27.81 ± 3.41 pApF⁻¹ ($p < 0.05$, One-way ANOVA). Further analysis of E_{rev} and G_m showed that 500nM progesterone had no effect on E_{rev} ($p = 0.8$, One-way ANOVA), however, there was a statistically significant inhibition of G_m at I_{Tran} with application of 500nM progesterone ($p < 0.05$, $n_c = 8$, $N_D = 3$, One-way ANOVA). Removal of progesterone from the bath showed that these effects were not persistent. This data shows that 500nM progesterone causes a transient inhibition of the outward current and G_m , however this effect does not alter the reversal potential of the cell.

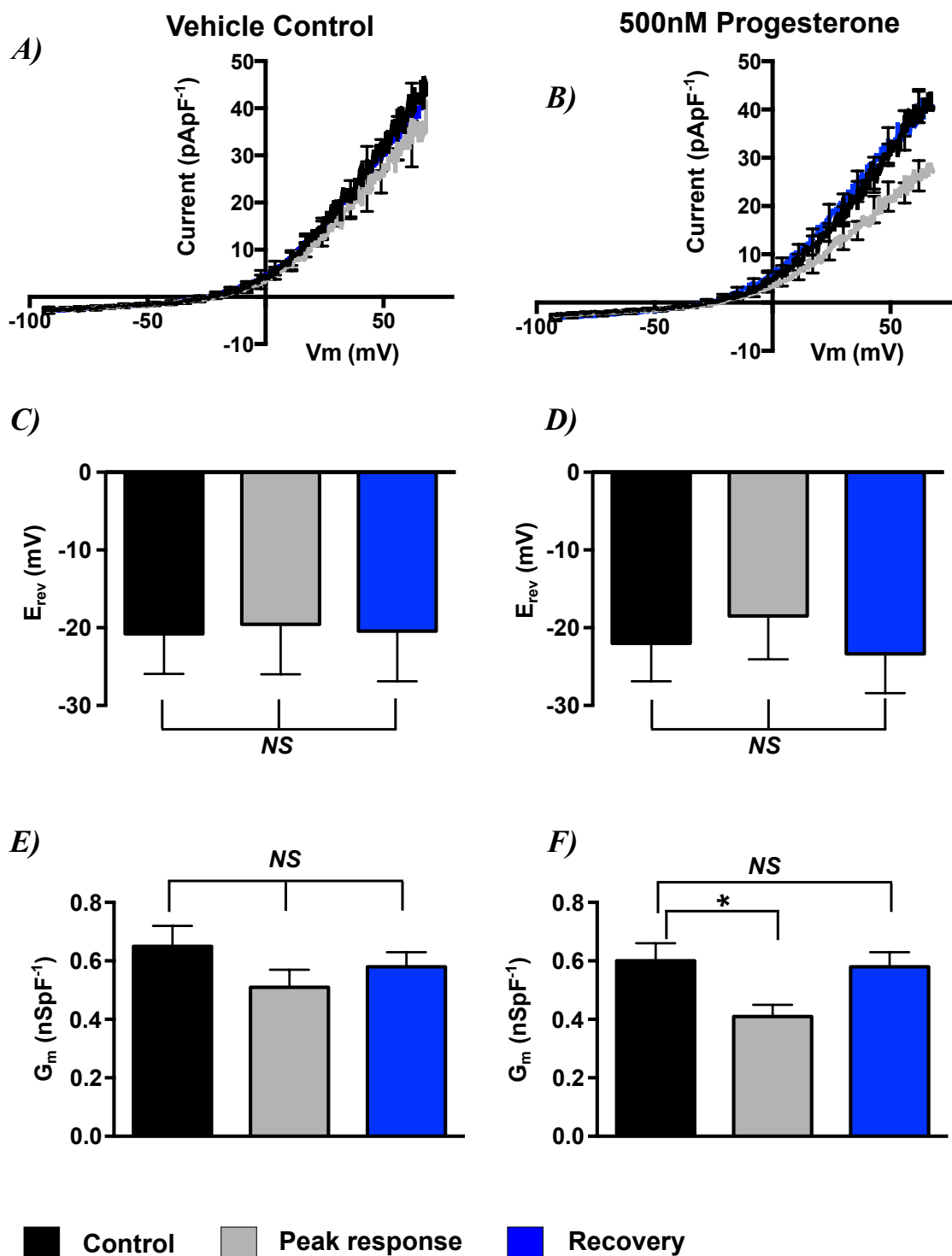


Figure 5.3: Further analysis of data from experiments that explored the effects on 500nM progesterone on $I_{T_{ran}}$. Data quantified prior to treatment with either vehicle control or 500nM progesterone (black), during transient inhibition (I_{tran}) of I_{out} (grey) and 40 seconds after treatment was removed from the bath (blue). I_m - V_m plots were quantified by analysis of data in Figure 5.1 in vehicle control (A) and progesterone (B) treated groups. Values for resting V_m quantified by analysis of data in A&B in both control (C) and progesterone treated groups (D). Membrane conductance (G_m) quantified for vehicle control (E) and progesterone treatment (F) group. All data presented as mean \pm s.e.m with asterisks denoting significance (* $p < 0.05$, $n_c = 8$, $N_D = 3$, One-way ANOVA).

5.3.4. Progesterone sensitive tail current

Figure 5.4 shows currents recorded using a leak subtracted single voltage pulse protocol to remove the influence of the passive current where V_m was depolarised to +68mV for 500ms before repolarisation to -92mV to elicit a tail current. Currents were recorded in control conditions and after 30 seconds of 500nM progesterone treatment. The data recorded confirmed progesterone had no effect on the outward current as previously shown in Figure 5.2B (control I_{Out} at 68mV: 48.51 ± 4.00 pApF⁻¹, 500nM progesterone I_{Out} at 68mV: 49.96 ± 4.36 pApF⁻¹, $n_c = 11$, $N_D = 3$, $p = 0.4$, Student's paired t-test). Analysis of I_{Tail} confirmed progesterone significantly augmented the tail current in the presence of 500nM progesterone (Control: -16.91 ± 1.81 pApF⁻¹, 500nM progesterone: -57.71 ± 5.61 pApF⁻¹, $n_c = 11$, $N_D = 3$, $p < 0.001$, Student's paired t-test). This data also indicated the absence of $I_{Steady State}$ at -92mV after leak subtraction. This indicates the progesterone has an affect on the background current however this was not further investigated.

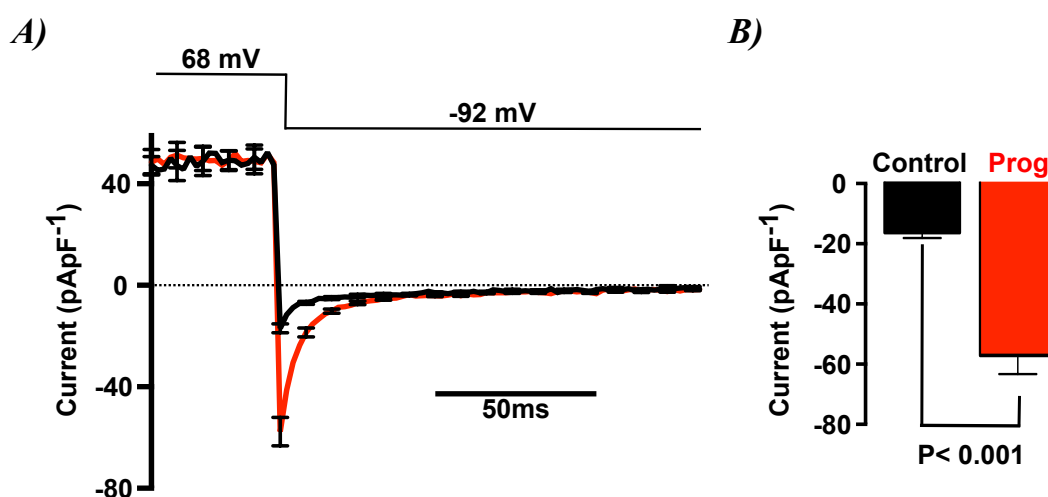


Figure 5.4: Confirmation of the progesterone induced tail current. A) I_m to time relationship of the tail current generated by repolarisation of V_m from 68mV to -92mV in control (black line) and after 30 seconds of 500nM progesterone treatment (red lines). B) Analysis of the peak tail current by further analysis of data in A under control (Black bar) and after 30 seconds progesterone treatment (red bar). All data represented at mean \pm s.e.m $n_c = 11$, $N_D = 3$.

5.3.5. I_{Tail} Ionic Conductance

Figure 5.5 shows a series of experiments that aimed to assess the ionic conductance of I_{Tail} . Tail currents were evoked by rapid repolarisation to -92mV from a depolarised potential of $+68\text{mV}$ using a leak-subtracted protocol. Control currents were recorded using a modified bath solution that contained low concentrations of Na^+ ($[\text{Na}^+]_o = 26\text{mM}$) and K^+ ($[\text{K}^+]_o = 3\text{mM}$). Osmolarity was maintained using NMDG^+ whilst Ca^{2+} ($[\text{Ca}^{2+}]_o = 2\text{mM}$) and Cl^- ($[\text{Cl}^-]_o = 144\text{mM}$) were maintained at their normal levels. The use of this solution allowed the external concentrations of Na^+ , K^+ or Ca^{2+} to be raised selectively by iso-osmotically substituting NMDG^+ (See Table 3 materials and methods). Figure 5.5A shows the results of an initial series of experiments that used this approach to explore the effects of raising K^+ . Under control conditions, repolarisation of V_m to -92mV demonstrated a tail current of $\sim -15 \text{ pApF}^{-1}$ and consistent in all control experiments. Increasing $[\text{K}^+]_o$ to 130mM caused an augmentation in I_{Tail} by $12.40 \pm 1.9 \text{ pApF}^{-1}$ (Figure 4.5A: $n_c = 16$, $N_D = 5$, $p < 0.001$) indicating the current is permeable to K^+ . Subsequent experiments using an identical protocol showed that increasing either external Na^+ to 156mM or Ca^{2+} to 10mM enhanced I_{Tail} by $4.95 \pm 1.4 \text{ pApF}^{-1}$ (Figure 5.5B: $n_c = 16$, $N_D = 5$, $p < 0.05$) and 12.06 ± 1.92 (Figure 4.5C: $n_c = 17$, $N_D = 6$, $p < 0.001$), respectively. This showed that I_{Tail} was also permeable to Na^+ and Ca^{2+} . The relative ionic conductance of the tail current was calculated using the equation $G_{ion} = \Delta I_{ion} / \Delta \Psi_{ion}$ where G_{ion} is the ionic conductance, ΔI_{ion} is the change in peak tail current magnitude when the ionic concentration is increased and $\Delta \Psi_{ion}$ is the change in driving force for that ion in high and low external concentrations. This showed that the tail current had relative $G_{\text{K}^+} / G_{\text{Na}^+}$ conductance of 1.4. However, analysis of the Ca^{2+} conductance of the tail current showed that the tail current had a high relative conductance compared to Na^+ or K^+ of 5.3 and 4, respectively (Figure 5.5D).

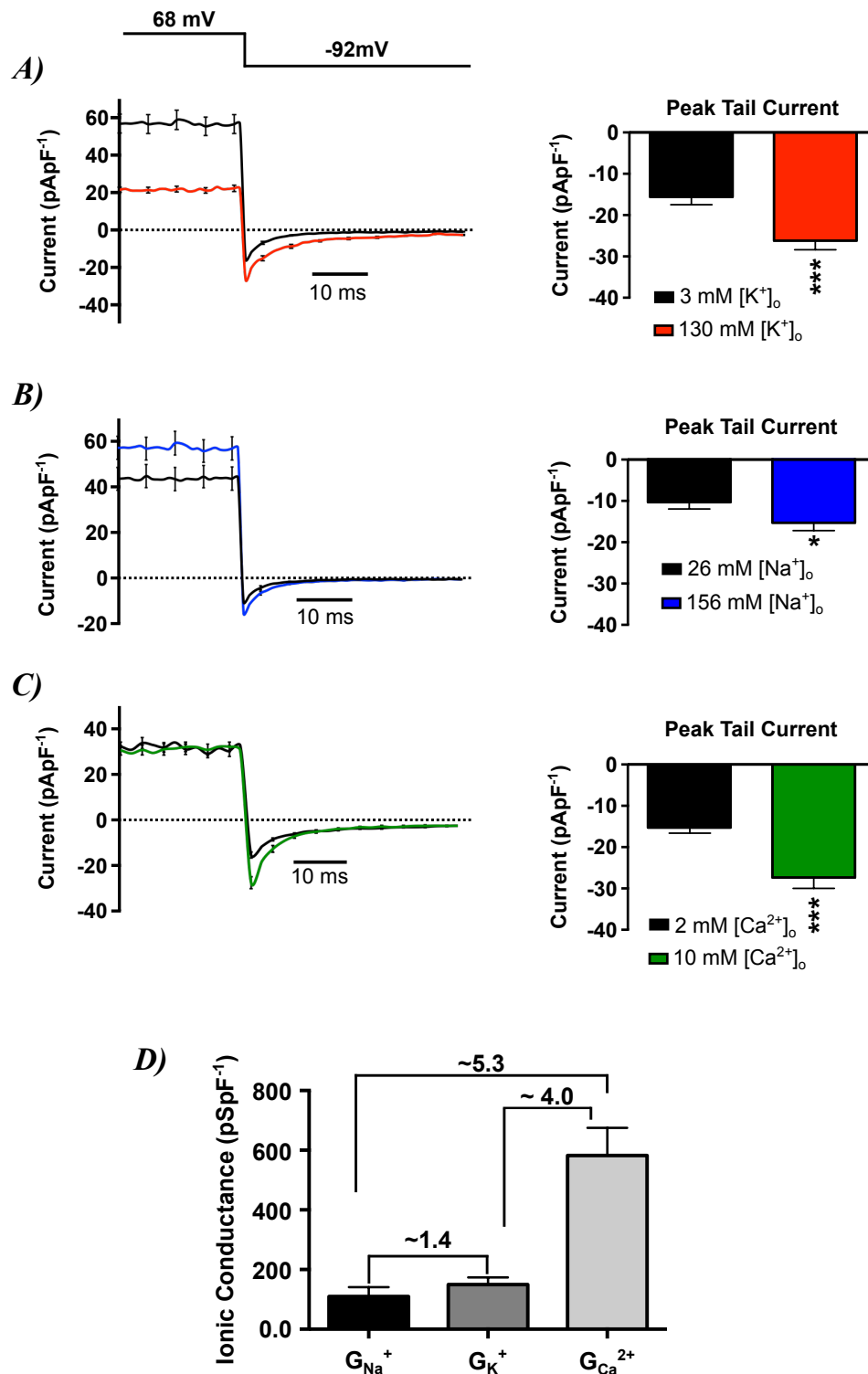


Figure 5.5: Ionic conductance of the tail current. Tail current generated by step repolarisation from 68mV to -92mV. Panels on the left show the I_m to time relationship under control bath conditions (black lines) and in 130mM [K⁺]_o (A, $n_c = 16$, $N_D = 5$ red line), 156 mM [Na⁺]_o (B, $n_c = 16$, $N_D = 5$ blue line) and 10mM [Ca²⁺]_o (C, $n_c = 17$, $N_D = 6$ green line) with corresponding mean peak tail currents on the left of each panel. D) Shows the ionic conductance of the tail current for K⁺, Na⁺ and Ca²⁺ quantified by assessment of the tail current in A, B and C. Values above each bar shows the relevant fold conductance. All data is presented as mean \pm s.e.m with asterisks denoting significance (* $p < 0.05$, **** $p < 0.001$).

5.3.6. Progesterone induced Ca^{2+} permeable tail current in human sperm

Progesterone has been shown to cause a rapid increase in intracellular Ca^{2+} which is thought to be through CatSper channels (Lishko et al., 2011; Strünker et al., 2011). Thus, the effects of progesterone on the Ca^{2+} conductance of the tail current were subsequently explored.

Experiments aimed to address this issue are presented in Figure 5.6. Cells were recorded using a step depolarisation protocol as described in Figure 5.5 in bath solution containing either 2mM or 10mM external Ca^{2+} ($[Na^+]_o = 26mM$, $[K^+]_o = 3mM$, See Table 2 materials and methods). Increasing extracellular Ca^{2+} caused an increase in the peak tail current from -15.30 ± 1.33 pApF⁻¹ to -26.04 ± 4.4 pApF⁻¹ ($n_c = 17$, $N_D = 6$, $p < 0.0001$, Student's paired t-test). The addition of 500nM progesterone caused an increase in the Ca^{2+} permeable tail current under 2mM external Ca^{2+} as indicated in figure 5.6A (2mM Ca^{2+} : Peak tail = -15.30 ± 1.33 pApF⁻¹, 2mM Ca^{2+} + 500nM progesterone = -40.66 ± 4.80 , $n_c = 6$, $N_D = 3$, $p < 0.001$). This effect was further enhanced when extracellular Ca^{2+} was increased to 10mM (10mM Ca^{2+} = -26.04 ± 4.4 pApF⁻¹, 10mM Ca^{2+} + 500nM progesterone = -67.04 ± 5.0 pApF⁻¹, $n_c = 6$, $N_D = 3$, $p < 0.001$). This indicated the magnitude of the progesterone response was governed by the concentration of external Ca^{2+} . The Ca^{2+} conductance of the tail current before and after the addition of 500nM progesterone was calculated by further analysis of data in Figure 5.6C. This was calculated using the equation $G_{Ca^{2+}} = \Delta I_{Ca^{2+}} / \Delta \Psi_{Ca^{2+}}$, where $G_{Ca^{2+}}$ is the Ca^{2+} conductance, $\Delta I_{Ca^{2+}}$ is the change in magnitude I_{Tail} induced by increasing $[Ca^{2+}]_o$ and $\Delta \Psi_{Ca^{2+}}$ is the change in driving force of Ca^{2+} in 2mM and 10mM $[Ca^{2+}]_o$. These calculations showed that progesterone caused a ~ 2 fold increase in the Ca^{2+} conductance of I_{Tail} from 0.59 ± 0.14 nSpF⁻¹ to 1.27 ± 0.17 nSpF⁻¹

(Figure 5.6D, $p < 0.001$ Student's paired t-test). This data shows the first evidence for the direct assessment of progesterone induced Ca^{2+} entry in human sperm.

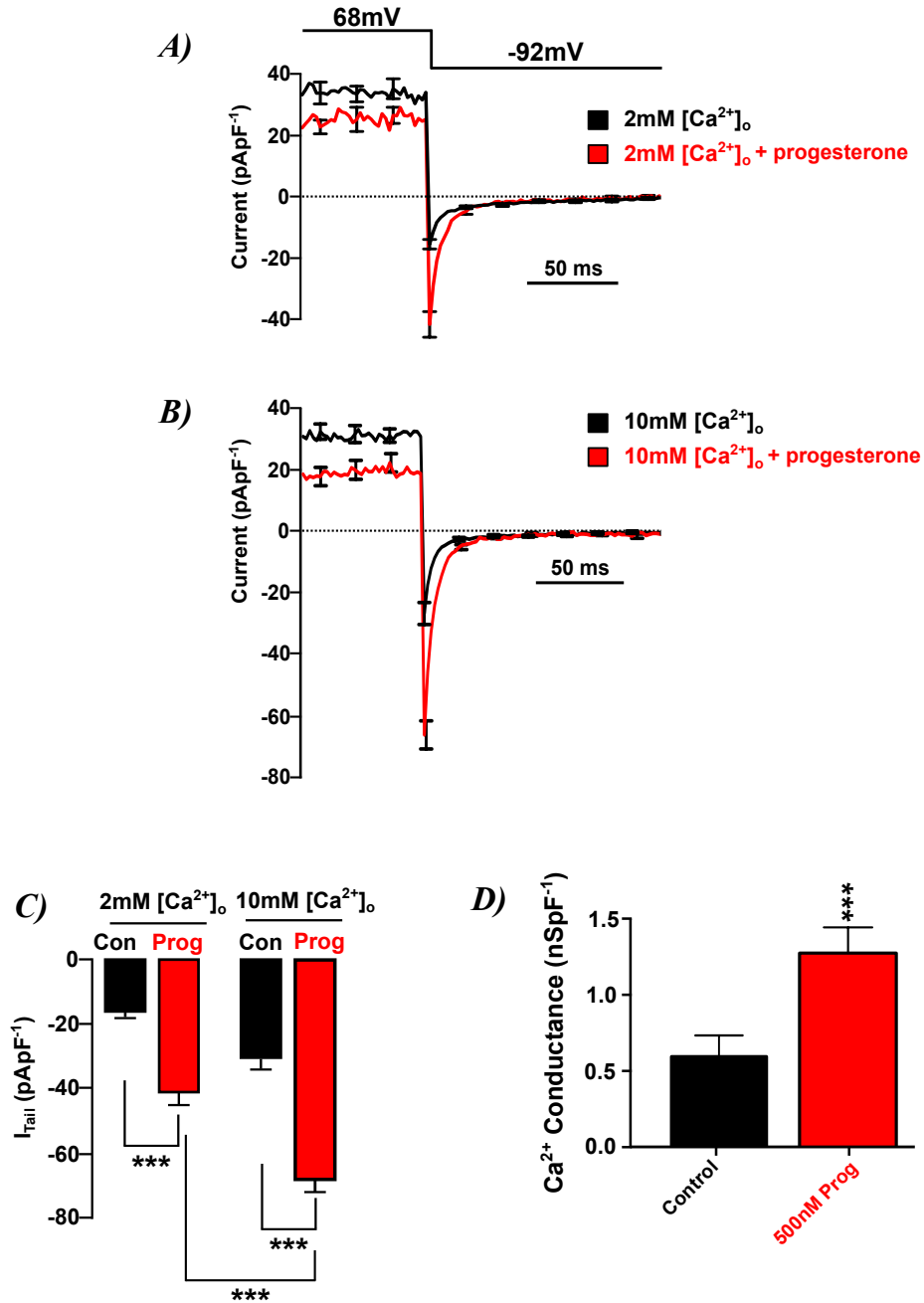


Figure 5.6: Progesterone enhances the Ca^{2+} permeable tail current. A) Tail currents evoked by step repolarisation to -92mV from 68mV under control (2mM [Ca²⁺]_o) and after 30 seconds exposure to 500nM progesterone ($n_c = 6$, $N_D = 3$). B) Currents evoked by identical protocol to A under control (10mM [Ca²⁺]_o) and after 30 seconds exposure to 500nM progesterone ($n_c = 6$, $N_D = 3$). C) Average peak tail currents quantified by analysis of data in A&B. D) Ca²⁺ conductance of the tail current under control and progesterone treated conditions calculated by $G_{\text{Ca}^{2+}} = \Delta I_{\text{Ca}^{2+}} / \Delta \Psi_{\text{Ca}^{2+}}$. All data presented as mean \pm s.e.m with asterisks denoting statistical significance (***) $p < 0.001$, Student's paired t-test).

5.3.7. Biophysical properties of the open channel

Figure 5.7 shows a set of experiments that aimed to assess the biophysical properties of the open channel. Currents were generated by leak subtracted step depolarisation from -92mV to 118mV over a 250ms period to cause maximal channel activation, after which the V_m was hyperpolarised to a series of test potentials to generate an instantaneous tail current in control (5mM K^+) and 130mM $[K^+]_o$ ($I_{Instant}$, Figure 5.7A). $I_{Instant}$ values were plotted against V_m in control and 130mM K^+ bath conditions shown in Figure 5.7B. Control data showed a linear I_m - V_m relationship with a maximal $I_{Instant}$ value of -16.89 ± 1.67 pApF⁻¹ at -82mV. Analysis of the reversal potential (E_{rev}) calculated by linear regression analysis showed that under control conditions E_{rev} was -41.45 ± 3.87 mV. Increasing extracellular K^+ from 5mM to 130mM caused a depolarising shift in E_{rev} of $\Delta 43.51 \pm 3.87$ mV confirming the open channel is permeable to K^+ ($n_c = 6$, $N_D = 3$, Figure 5.7B). The reversal potential under control conditions was used to calculate the proportion permeability of K^+ and Na^+ that contribute to the current flowing through the open channel using the Goldman, Hodgkin, Katz equation (GHK). This showed that the open channel had relative K^+ and Na^+ permeability of 0.7 and 0.2, respectively, indicating a 2.8 fold greater selectivity for K^+ over Na^+ (Figure 5.7C). This was similar to the calculated G_{K^+}/G_{Na^+} shown in Figure 5.5D. This was further confirmed by calculation of the theoretical E_{rev} value of a channel with a similar K^+ and Na^+ permeability. Figure 5.7D shows the recorded E_{rev} in 5 and 130mM $[K^+]_o$ with dotted lines indicating the predicted E_{rev} in 130mM $[K^+]_o$ calculated using the GHK equation. This showed that the E_{rev} recorded and predicted were virtually identical (130mM $[K^+]_o$: recorded = 2.06 ± 1.35 mV, $n_c = 6$, $N_D = 3$, predicted = 2.89 mV).

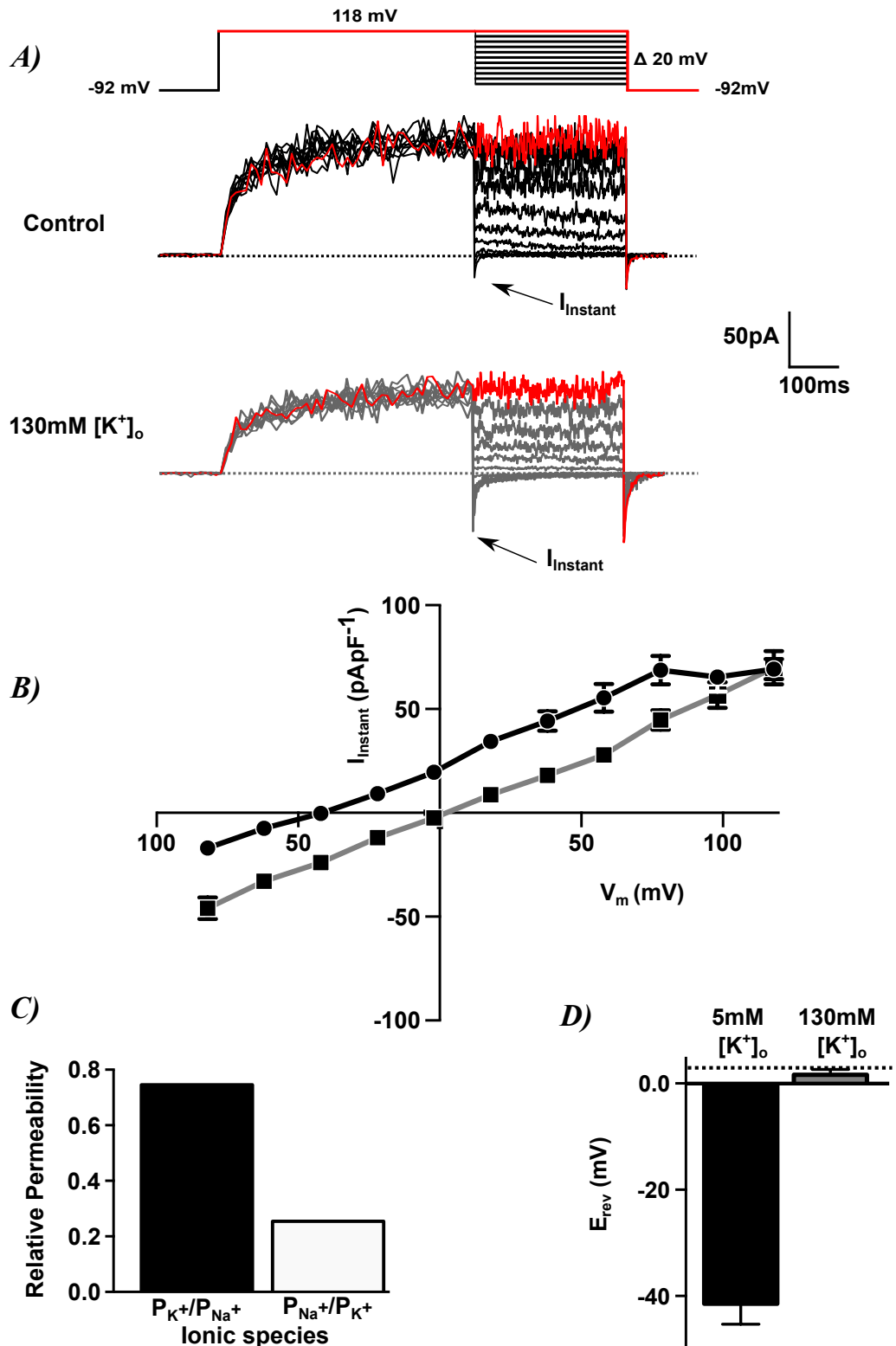


Figure 5.7: Biophysical properties of the open channel. A) Representative traces of a single spermatozoon under control (5mM $[K^+]_o$) and 130mM $[K^+]_o$ bath solutions. Instantaneous currents ($I_{Instant}$) were evoked by step repolarisation from an initial depolarised potential of 118mV to provide a read out of the current that flows through the open channel. B) I_m - V_m relationship of the instantaneous current plotted using data quantified in A in 5mM (Control) and 130mM external K^+ . C) Relative K^+ and Na^+ permeability of the open channel in 5mM external bath solution. D) Reversal potential of the open channel in 5mM and 130mM external K^+ with dotted line indicating the theoretical reversal potential as calculated using the derived K^+ and Na^+ permeability in B. Data in Figures B & D are expressed as mean \pm s.e.m $n_c = 6, N_D = 3$.

5.3.8. Time course of open channel inactivation

Figure 5.8 shows data from a set of experiments that assessed the time course of I_{Instant} inactivation. Instantaneous currents (I_{Instant}) were generated as described in section 5.3.7. Analysis of I_{Instant} evoked by stepping V_m to a series of test potentials between -82 and -22mV showed that the inactivation I_{Instant} could be modelled as a sum of two exponential processes (Figure 5.8A). This established that the time constants associated with τ_{Slow} and τ_{Fast} were voltage dependent as inactivation was slower at more depolarised potentials (Figure 5.8B). This data also indicated that the time of inactivation was fast and could potentially explain the lack of inward current at hyperpolarised potentials.

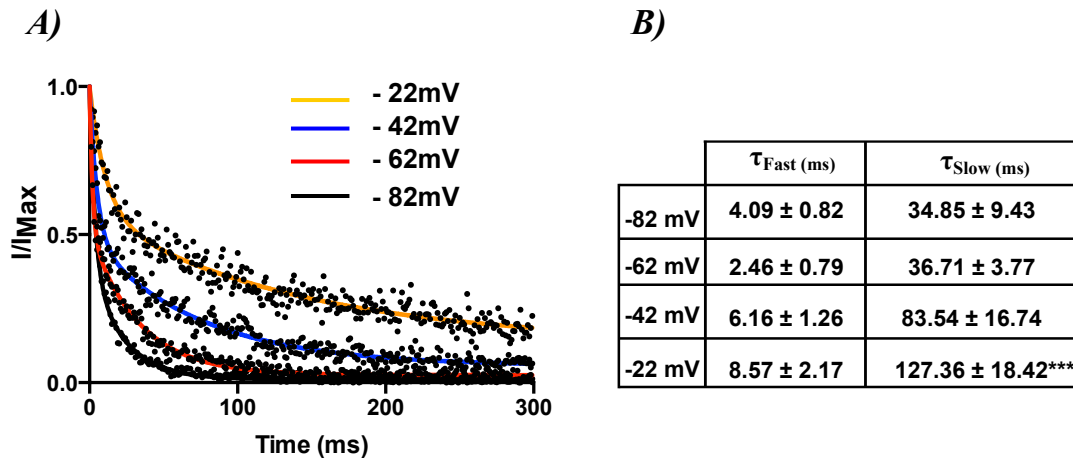


Figure 5.8: Voltage dependence of inactivation. A) Time course of inactivated of I_{Instant} over 300ms at different repolarised test potentials. Black dots indicate individual data points with solid colour lines indicating best-fit lines of the sum of two exponentials. B) Table of time constants of inactivation with asterisks denoting statistical significance (** $p < 0.001$). All data presented as mean \pm s.e.m, $n_c = 6$, $N_D = 3$.

5.3.9. Na^+ and NMDG^+ Permeability of the open channel

Figure 5.9 shows a set of experiments aimed to assess the Na^+ permeability of the open channel. Currents were recorded using a leak subtracted voltage pulse protocol as described in Figure 5.9. In order to remove the influence of K^+ , intracellular K^+ was iso-osmotically replaced with Na^+ (Final $[\text{Na}^+]_i = 115\text{mM}$, $[\text{K}^+]_i = 0\text{mM}$, Figure 5.9A top panel) or NMDG^+ (Final $[\text{NMDG}^+]_i = 115\text{mM}$, $[\text{K}^+]_i = 0\text{mM}$, Figure 5.9A bottom panel). Figure 5.9B shows the $I_m - V_m$ relationship of cells recorded under control bath solution ($5\text{mM } [\text{K}^+]_o$, $156\text{mM } [\text{Na}^+]_o$) with Na^+ (black line) or NMDG^+ based internal solution (grey line, See Table 2 materials and methods). Analysis of the $I_m - V_m$ relationship showed a linear relationship with a maximal I_{Instant} of $-9.50 \pm 1.24 \text{ pApF}^{-1}$ (Na^+ based pipette solution, $n_c = 3$, $N_D = 1$). Subsequent analysis of the $I_m - V_m$ relationship with NMDG^+ based pipette solution showed that no outward current was observed with a maximal I_{Instant} of $-26.56 \pm 4.60 \text{ pApF}^{-1}$ (NMDG^+ based pipette solution, $n_c = 3$, $N_D = 2$). Calculation of E_{rev} using the Nernst equation under Na^+ based pipette conditions showed that the recorded and predicted currents accorded well (Figure 5.9C: Recorded $E_{\text{rev}} = 8.99 \pm 7 \text{ mV}$, $n_c = 3$, $N_D = 1$, Predicted $E_{\text{rev}} = 7.97 \text{ mV}$).

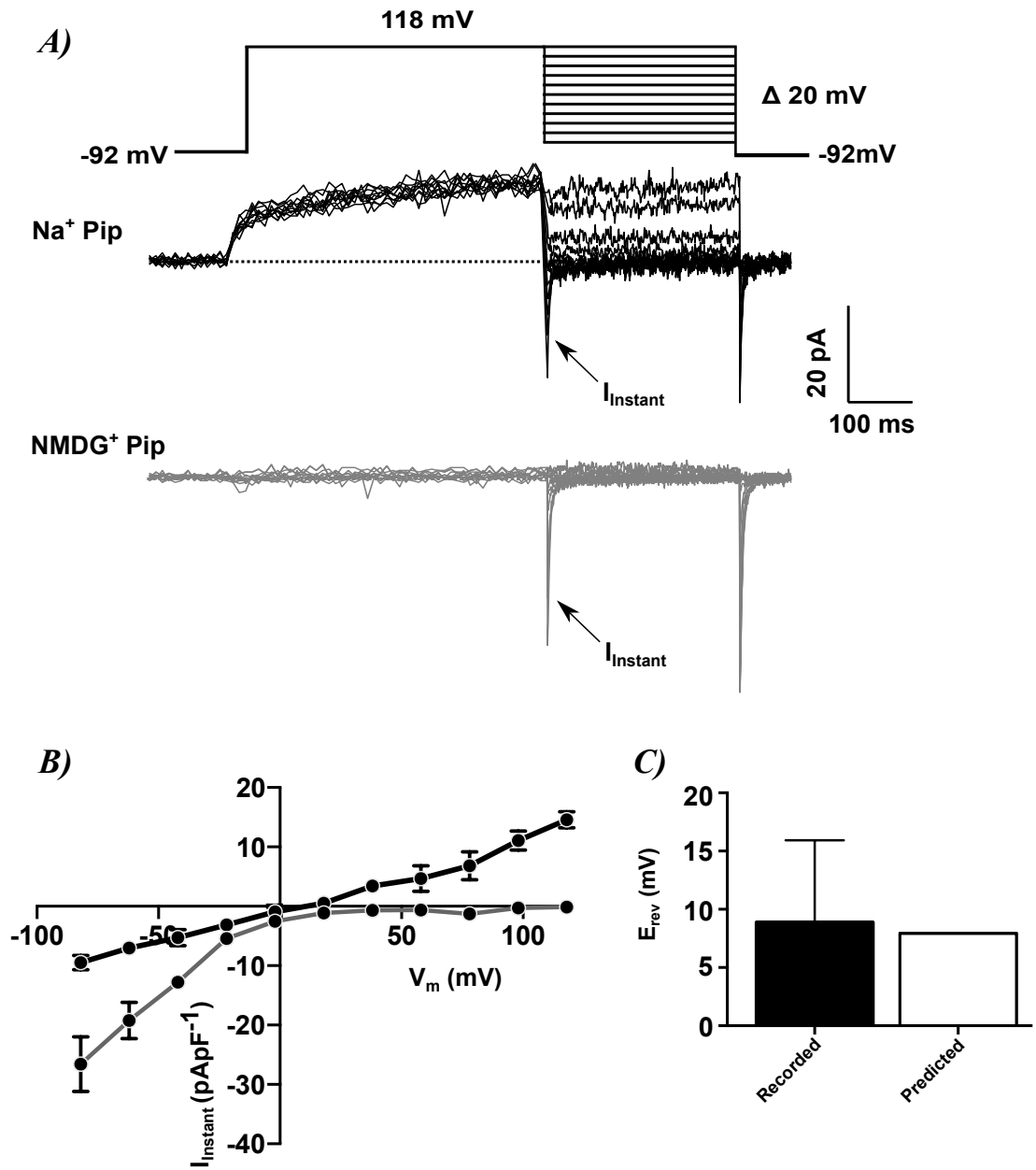


Figure 5.9: Na⁺ permeability of the open channel. Currents evoked by step hyperpolarisation from an initial depolarised potential of 118mV (top panel) were recorded using Na⁺-rich pipette solution. A) Representative trace of current generated using Na⁺ (top panel) and NMDG⁺ (bottom panel) rich pipette solution with instantaneous current indicated by I_{Instant} . B) I_m - V_m relationship of I_{Instant} generated by methods described in Figure 5.8A. C) The recorded and predicted reversal potential of the open channel using the GHK equation in Na⁺ rich pipette solution. All data is represented as mean \pm s.e.m. $n_c = 3$, $N_D = 1$.

5.3.10. Ionic permeability of the $I_{Steady\ State}$

Figure 5.10 shows the I_m - V_m steady state current relationship of the open channel quantified over the last 100ms of the test potential (Figure 5.10A), recorded under different internal and external conditions to assess the ionic permeability of the outward current. Analysis of the steady state current under conditions designed to maintain physiological K^+ , Na^+ and Cl^- gradients, showed a strongly outwardly rectifying hyperpolarising current that was activated at potentials $> -30mV$ with a maximal outward current of $73.83 \pm 6.12\ pApF^{-1}$ (Figure 5.10B). Under these conditions there was no observable inward current. Increasing external K^+ to 130mM caused a rightward shift in the potential at which the outward current was observed (potentials $>10mV$, Figure 5.10C). This indicated a contributing K^+ conductance. Under these conditions a small inward current was observed at $-22mV$ of $-2.28pApF^{-1}$. However, there was no difference in the maximal outward current compared to 5mM $[K^+]_o$ (Figure 5.10B: $73.92 \pm 7.62\ pApF^{-1}$). Analysis of $I_{Steady\ State}$ currents flowing at E_{Na^+} ($+68mV$) showed that the relative P_{K^+}/P_{Na^+} was ~ 6 . This accorded well with P_{K^+}/P_{Na^+} of the physiological current in Chapter 3. Figure 5.10C shows the steady state current recorded in the absence of intracellular K^+ (isotonic substitution with NaCl and Na-Gluconate, see Table 2 Materials and methods). This showed that the outward current was less permeable for Na^+ over K^+ , which accorded well with data collected in Chapter 3 (Figure 3.7A). Maximum outward current at 118mV was $14.59 \pm 1.37\ pApF^{-1}$ ($n_c = 3$, $N_D = 1$). Figure 5.10D shows steady state current when internal Na^+ and K^+ is iso-osmotically replaced with NMDG⁺ (See Table 2 materials and methods). This showed that the channel was completely impermeable to NMDG⁺ (current and $118mV = -0.57 \pm 0.87\ pApF^{-1}$, $n_c = 3$, $N_D = 2$). This data accords well with similar data

collected in Chapter 3 (Figure 3.7) indicating the outward steady state current is permeable to K^+ and Na^+ but impermeable to $NMDG^+$.

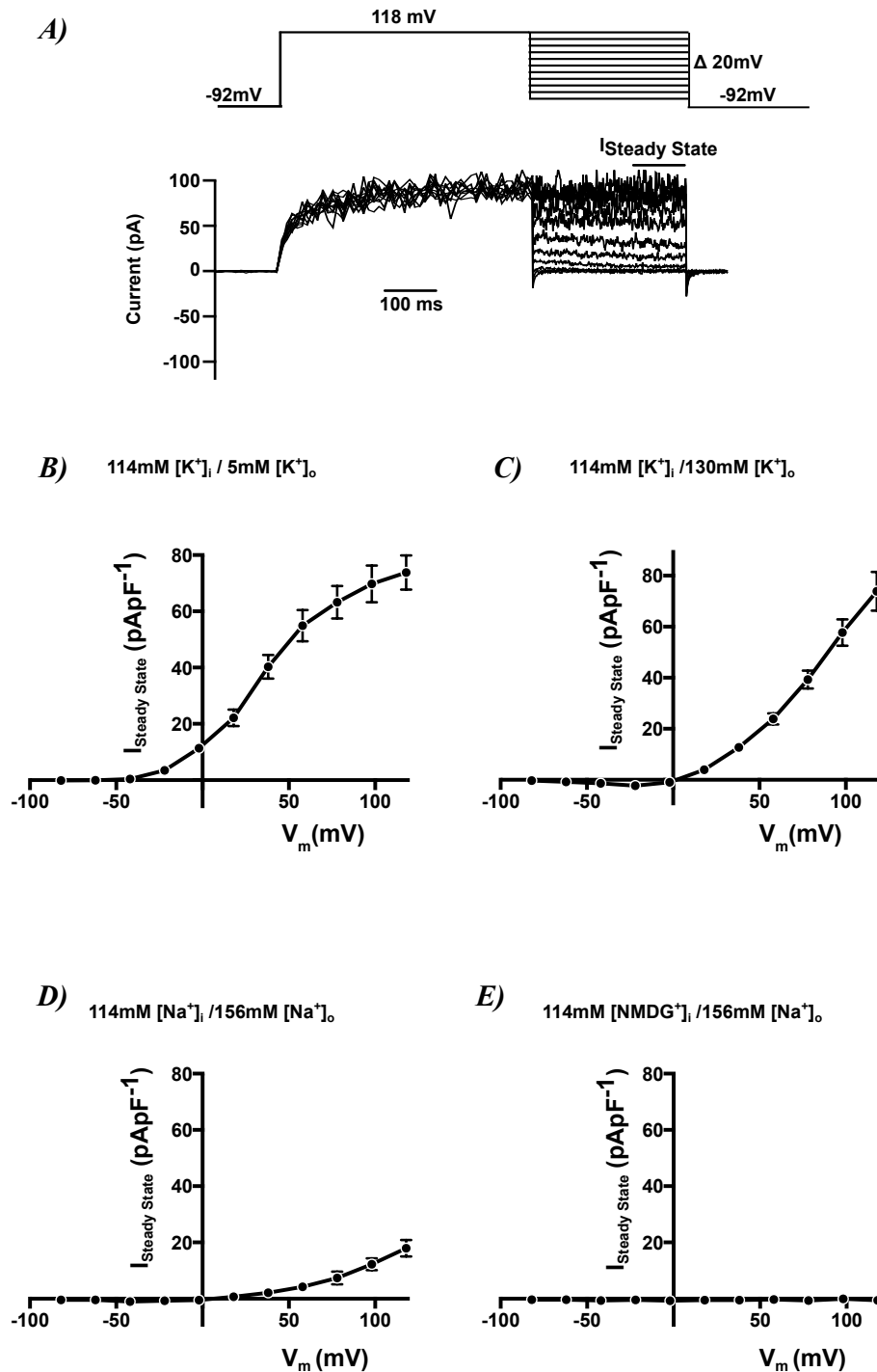


Figure 5.10: Ionic selectivity of I_{out} . Currents evoked by step hyperpolarisation from an initial depolarised potential of 118mV (top panel) were recorded under different internal and external ionic conditions. A) Representative trace from a single spermatozoon using protocol shown in top panel with steady state current indicated ($I_{\text{Steady State}}$). I_m - V_m relationship of the steady state current recorded control pipette and bath solutions (B), control pipette/ 130mM $[K^+]_o$ bath conditions (C), Na^+ rich pipette/control bath solutions (D) and $NMDG^+$ rich pipette /control bath solutions (E) All data presented as mean \pm s.e.m, $n_c = 3-6$, $N_D = 1-3$.

5.3.11. Biophysical properties of the tail current

Figure 5.11 shows the results from a series of experiments assessing the biophysical properties of the tail current generated by rapid repolarisation to -92mV from a series of depolarised test potentials. All currents were assessed under control pipette and bath conditions.

Figure 5.11A shows a representative leak subtracted outward current (I_{out}) from a single sperm evoked by step depolarisation to a series of test potentials (-42mV to 118mV) before rapid repolarisation to -92mV to elucidate a tail current (I_{Tail}). Figure 5.11B and C show the I_m - V_m relationship for I_{out} and I_{Tail} quantified over the last 100ms of the depolarising pulse (Figure 5.11B) and peak tail current upon repolarisation to -92mV (Figure 5.11C), respectively. This data showed that both I_{out} and I_{Tail} showed voltage dependent activation when V_m was depolarised past -42mV with a maximum I_{out} and I_{Tail} value of 65.80 ± 4.74 pApF⁻¹ and -15.38 ± 1.57 pApF⁻¹, respectively, at 118mV. Figure 5.12 shows the deactivation and activation kinetics of I_{Tail} . Deactivation kinetics of I_{Tail} were quantified by analysis of the peak tail current generated by repolarisation to -92mV from a series of depolarised test potentials. An initial voltage pulse to 118mV was performed to fully activate the channel (100% of channels active,) prior to the test potential (left hand panel, Figure 5.12A). Activation kinetics were quantified by further analysis of data in Figure 5.11C (Right hand panel, Figure 5.12B). The Boltzmann constant (κ) and half maximal activation (V_{50}) were calculated by solving the Boltzmann equation as previously describe in Chapter 3. This showed that the Boltzmann constant for both the activation and deactivation of I_{Tail} was ~ 21 mV⁻¹. Analysis of the half maximal deactivation and activation kinetics (V_{50}) were

32.9 ± 5.4 mV ($n_c = 6$, $N_D = 3$) and 45.6 ± 5.0 mV ($n_c = 31$, $N_D = 8$), respectively. The activation kinetics showed I_{Tail} became active at potentials > -40 mV, this is interesting as the resting membrane potential for capacitated human sperm was shown to be ~ -30 mV and would suggest I_{Tail} may allow small inward current under normal resting physiological conditions.

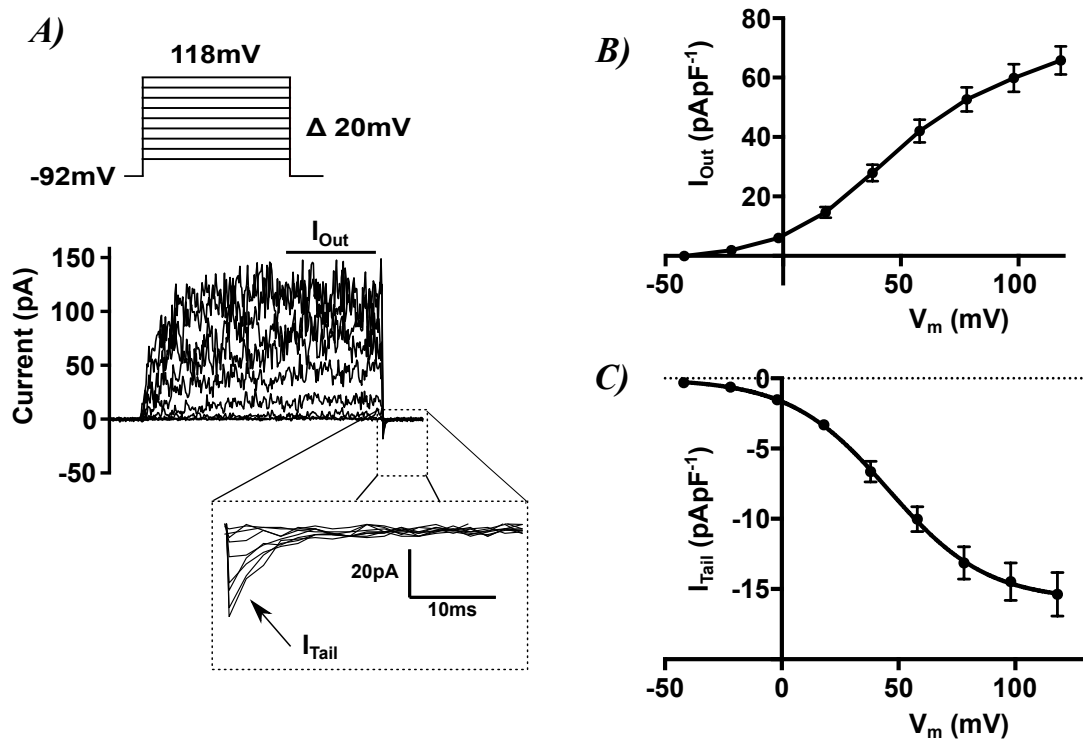


Figure 5.11: The biophysical properties of the tail current. A) Representative trace from a single spermatozoa where outward currents (I_{out}) were evoked by step depolarisation before repolarisation to -92 mV to elucidate a tail current (I_{Tail}) under control conditions B) I_m - V_m relationship of I_{out} by further analysis from data generated in A. C) I_m - V_m relationship of I_{Tail} by further analysis from data generated in A. Data represented as mean \pm s.e.m

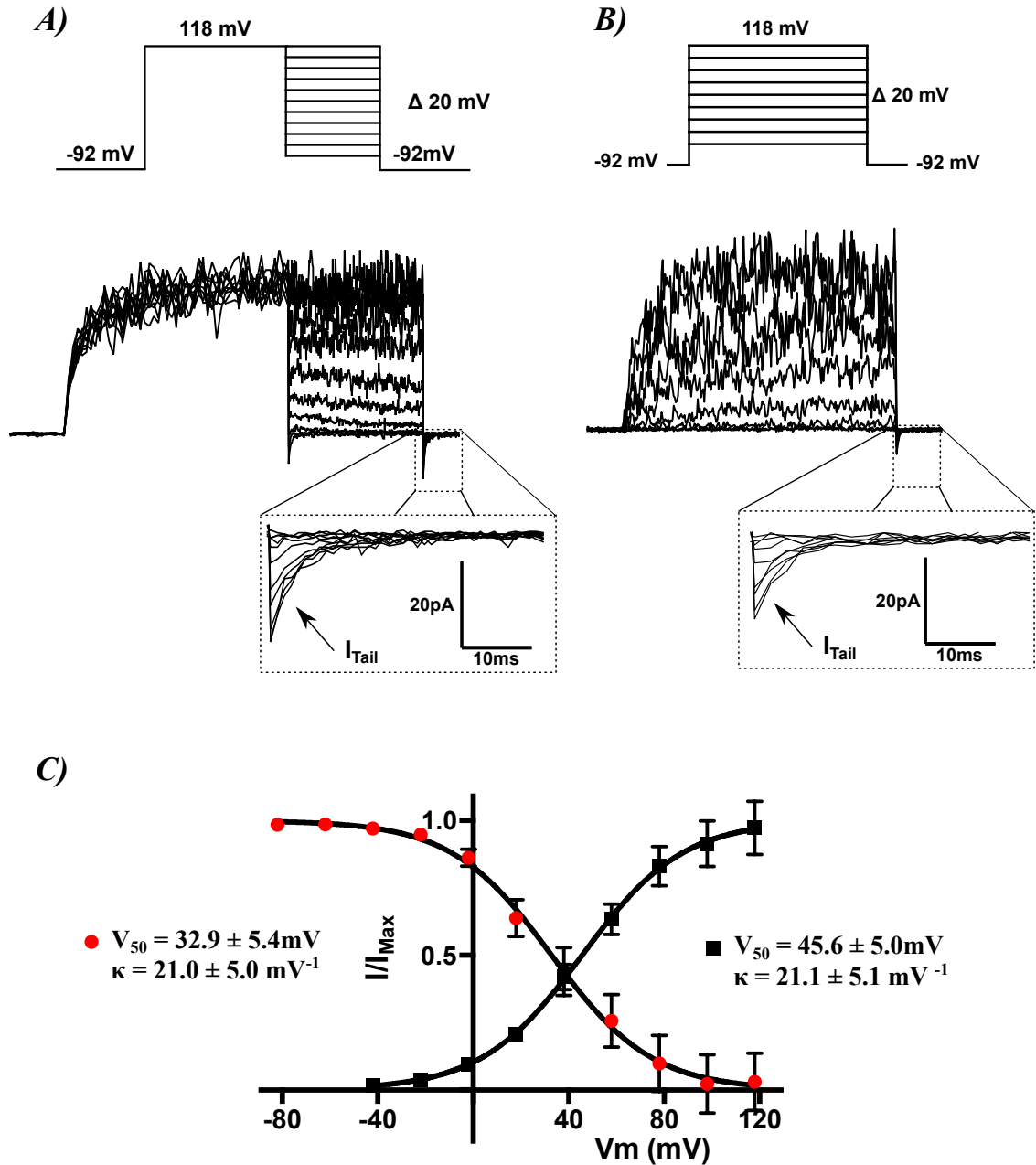


Figure 5.12: The biophysical properties of the tail current. A, B) Representative traces from 2 spermatozoa, outward currents (I_{out}) were evoked by step depolarisation before repolarisation to -92 mV to elucidate a tail current (I_{Tail}) under control conditions. Protocols designed to assess the deactivation (left) and activation (right) kinetics of I_{Tail} are shown above each trace. C) Activation (black dots) and deactivation (red dots) kinetics of I_{Tail} under control bath conditions. Data in B, C and D presented as mean \pm s.e.m ($n_c = 6 - 31$, $N_D = 3 - 8$).

5.4. Tail current pharmacology

The aim of this section is to assess the pharmacological profile of the tail current. Tail currents were generated as described in Figure 5.11A. All currents were recorded under control bath and pipette conditions before and after the addition of 50 μ M clofilium, 2mM 4-AP, 0.3mM quinidine or 500nM progesterone. These compounds were used because of their distinct and repeatable action on the outward current described in Chapters 3 and 4. From this data a comparison between the outward hyperpolarising current and the tail current can be used to assess if the currents flow through a single or two distinct channels.

5.4.1. Clofilium

Figure 5.13A and B show two representative traces of a single spermatozoon recorded under control conditions and after 1 minute of clofilium treatment. Panels on the right of each trace show amplified tail currents under control and clofilium treated conditions. Maximal tail current activation was observed when V_m was repolarised to -92mV from 118mV (red line Figure 5.13A) and was consistent with data collected in previous experiments. Perfusion of the chamber with 50 μ M clofilium for 1 minute completely abolished I_{out} as well as I_{Tail} (Control: $I_{out} = 58.57 \pm 6.45$ pApF $^{-1}$, $I_{Tail} = -18.66 \pm 4.26$ pApF $^{-1}$, 50 μ M clofilium: $I_{out} = 0.35 \pm 0.7045$ pApF $^{-1}$, $I_{Tail} = -6.03 \pm 0.83$ pApF $^{-1}$, $n_c = 5$, $N_D = 3$). Analysis of the I_m - V_m relationship, as indicated in Figure 5.13C, showed that clofilium caused a significant inhibition of the voltage dependent tail current. Further analysis of the peak tail current generated by repolarisation from 118mV, as indicated in Figure 5.13D, showed that clofilium significantly inhibited the maximal tail current (Control: -18.66 ± 4.26 pApF $^{-1}$, 50 μ M clofilium: -6.03 ± 0.83 pApF $^{-1}$, $n_c = 5$, $N_D = 3$, $p < 0.01$). This shows that the outward current and tail current show similar sensitivity to clofilium.

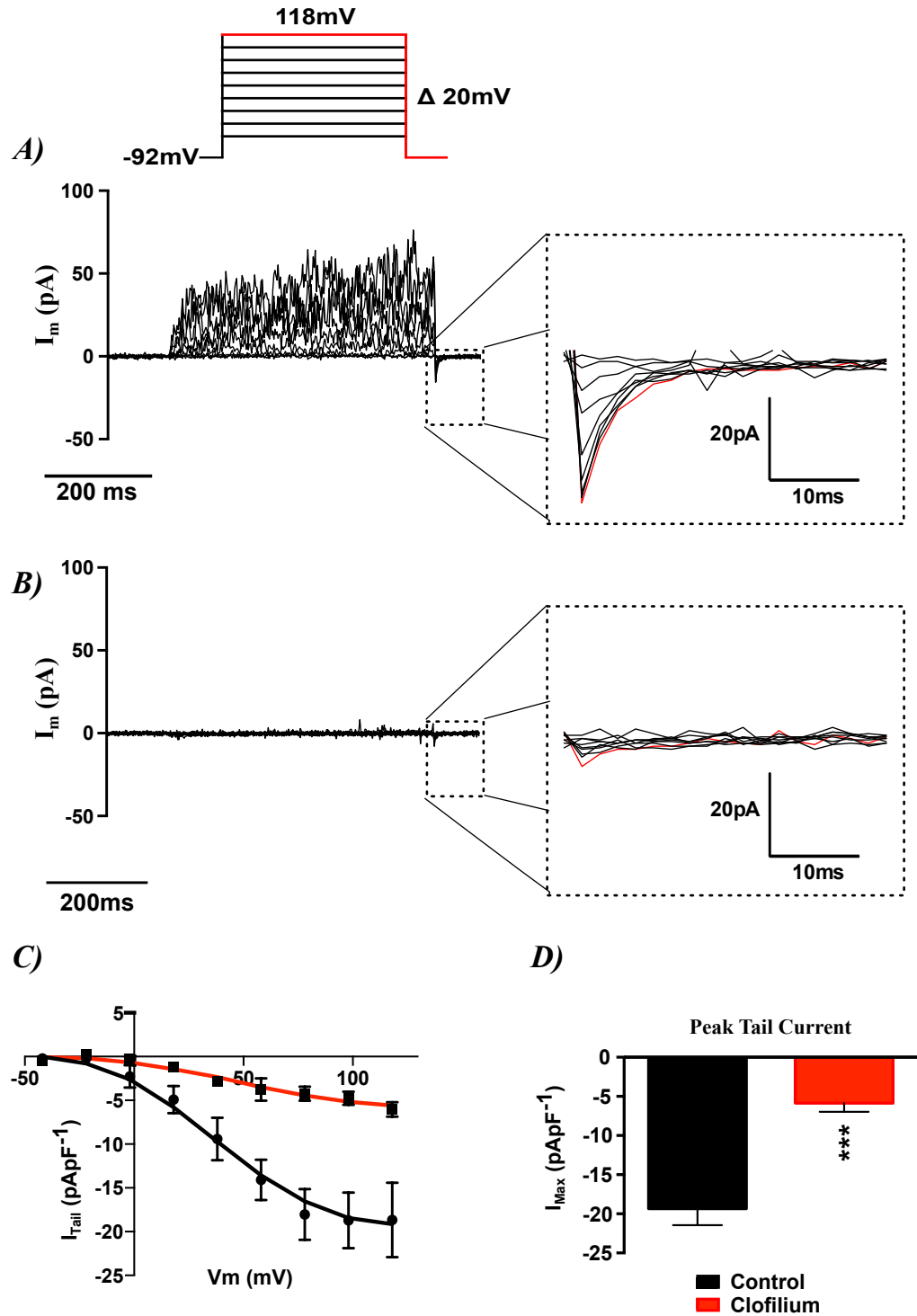


Figure 5.13: Effects of 50 μM clofilium on the tail current. A, B) Currents evoked by step repolarisation to -92mV from a series of depolarised test potentials. Representative currents recorded under standard bath and pipette solutions (A) and after 1 minute of 50 μM clofilium exposure (B) with enlarged tail currents represented on the right of each trace. C) Relationship between I_m and V_m quantified under control (black line) after 1 minute of clofilium exposure (red line). D) Mean peak tail current quantified by repolarisation from 118mV to -92mV in control and after 1 minute exposure to 50 μM clofilium. Error bars indicate s.e.m with asterisks denoting statistical significance (** $p < 0.001$).

5.4.2. 4-AP

Figure 5.14 A and B shows two representative traces from a single spermatozoon under control conditions and treatment with 2mM 4-AP. Amplified tail currents are shown on the right of each trace under control (Figure 5.14A) and 4-AP-treated (Figure 5.14B) conditions. This figure shows that 2mM 4-AP was ineffective at altering the hyperpolarising outward current (Control I_{out} at 118mV: 59.43 ± 6.7 pApF⁻¹, 2mM 4-AP: 60.76 ± 7.9 pApF⁻¹, $p > 0.5$, Student's paired t-test). This was consistent with data assessing the effect of 2mM 4-AP on the outward current in Chapter 3 (Figure 3.4). Perfusion of the chamber with 2mM 4-AP for 20-30 seconds increased in the magnitude of the voltage dependent tail current (Figure 5.14B). Analysis of the I_m-V_m relationship of the voltage dependent tail current confirmed that 2mM 4-AP effectively enhanced this current (Figure 5.14C). Further analysis of the peak tail current generated following repolarisation to -92mV from 118mV, as shown in Figure 5.14D, demonstrated that 2mM 4-AP caused a statistically significant increase in I_{Tail} from -15.9 ± 2.1 to -33.31 ± 3.8 pApF⁻¹ ($n_c = 8$, $N_D = 3$, $p < 0.001$, Student's paired t-test). This data provides evidence of two contrasting actions of 4-AP on the outward and tail currents, therefore suggesting the presence of two separate channels.

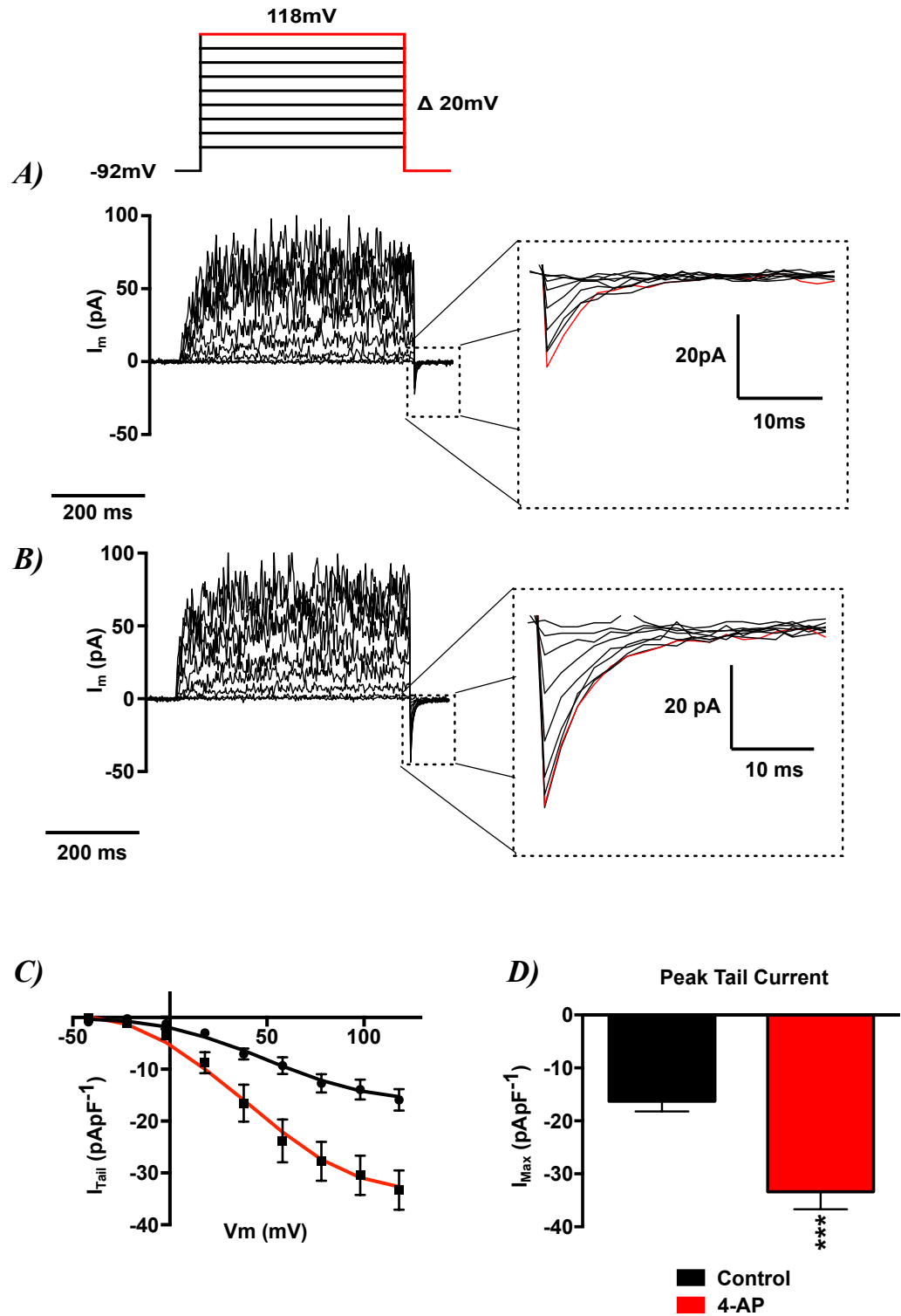


Figure 5.14: Effects of 2mM 4-AP on the tail current. Currents evoked by step repolarisation to -92mV from a series of depolarised test potentials. Currents were recorded under standard bath and pipette solutions in control (A, representative trace) and after 30 seconds of 2mM 4-AP (B, representative trace) exposure with enlarged tail currents represented on the right of each trace. C) Relationship between I_{m} and V_m quantified under control (black line) after 30 seconds of 4-AP exposure (red line). D) Mean peak tail current quantified by repolarisation from 118mV to -92mV in control and after 30 second exposure to 2mM 4-AP. Error bars indicate s.e.m with asterisks denoting statistical significance (***) $p < 0.001$.

5.4.3. Quinidine

Figure 5.15 A and B show two representative traces from a single spermatozoon under control and 0.3mM quinidine treated condition, respectively, as assessed by methods described in Figure 5.12. Amplified tail currents are shown on the right of each trace under control (Figure 5.15A) and quinidine treated (Figure 5.15B) conditions. This figure shows that 0.3mM quinidine caused a significant inhibition of the hyperpolarising outward current (control steady state at 118mV: 74.50 ± 8.6 pApF⁻¹, 0.3mM quinidine: 1.72 ± 0.9 pApF⁻¹, $p < 0.0001$, Student's paired t-test). This was also consistent with data collected in Chapter 3 indicating the sensitivity of the outward current to 0.3mM quinidine. Perfusion of the chamber with 0.3mM quinidine for 20-30 seconds caused an increase in the magnitude of the tail current (Figure 5.15B). The agonistic effect of 0.3mM quinidine was further confirmed by analysis of the I_m - V_m relationship of the tail current as indicated in Figure 5.15C. Analysis of the maximum peak tail current generated following repolarisation to -92mV from 118mV, as shown in Figure 5.15D, showed that 0.3mM quinidine caused a statistically significant increase in I_{Tail} from -12.6 ± 3.3 to -24.60 ± 3.8 pApF⁻¹ ($n_c = 10$, $N_D = 5$, $p < 0.001$, Student's paired t-test). The opposing action of quinidine on the outward and tail currents further suggests the presence of two distinct channels.

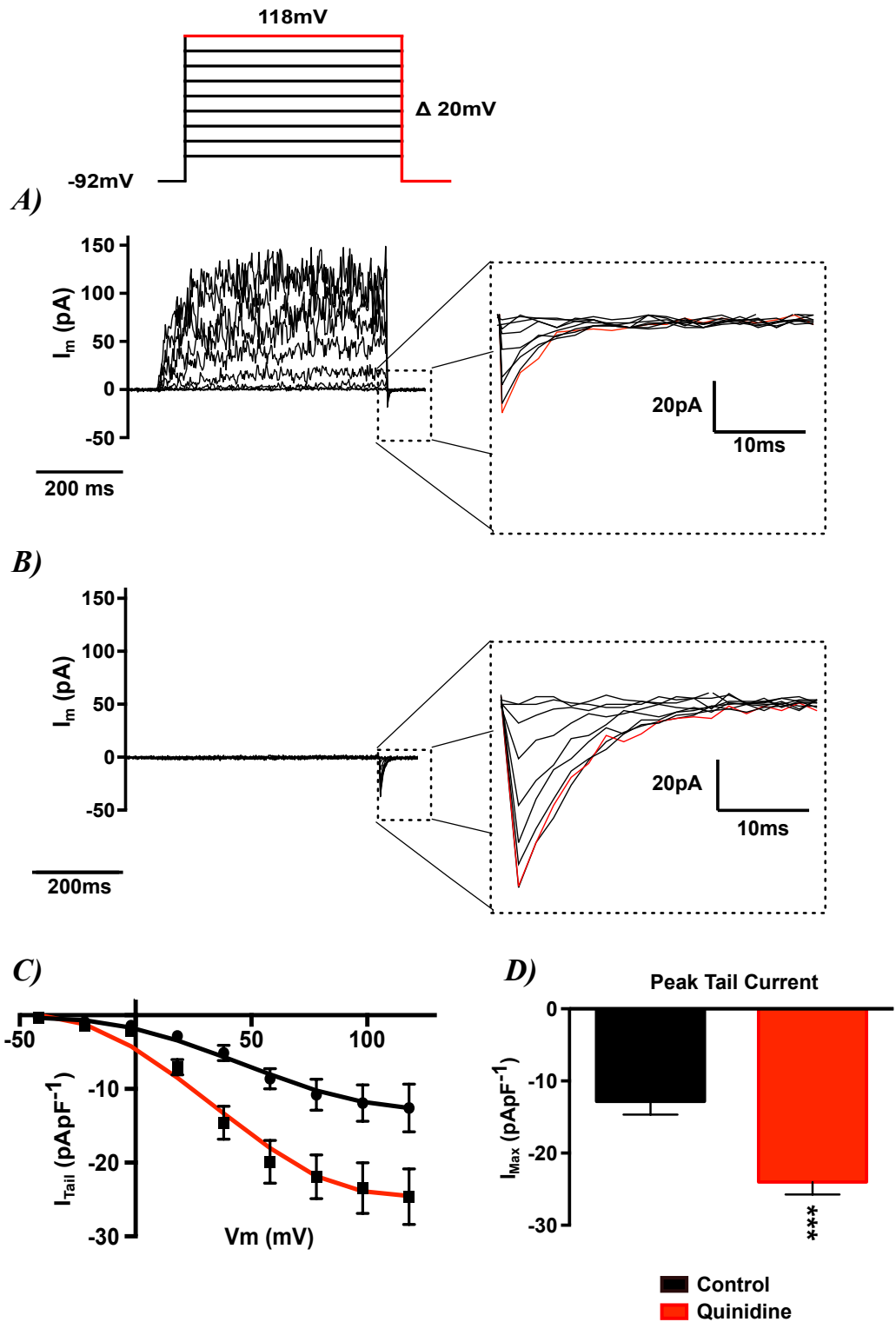


Figure 5.15: Effects of 0.3mM quinidine on the tail current. Currents evoked by step repolarisation to -92mV from a series of depolarised test potentials. Currents were recorded under standard bath and pipette solutions in control (A, representative trace) and after 30 seconds of 0.3mM quinidine (B, representative trace) exposure with enlarged tail currents represented on the right of each trace. C) Relationship between I_m and V_m quantified under control (black line) after 30 seconds of quinidine exposure (red line). D) Mean peak tail current quantified by repolarisation from 118mV to -92mV in control and after 30 seconds exposure to 0.3mM quinidine. Error bars indicate s.e.m. with asterisks denoting statistical significance (***) $p < 0.001$.

5.4.4. Progesterone

Figure 5.16A and B shows two representative traces of a single spermatozoon under control conditions and in the presence of 500nM progesterone, as assessed by methods described in figure 5.12. Amplified tail currents are shown on the right of each trace under control (Figure 5.16A) and progesterone treated (Figure 5.16B) conditions. This figure shows that 500nM progesterone did not significantly enhance the hyperpolarising outward current (Control steady state at 118mV: $42.90 \pm 5.24 \text{ pApF}^{-1}$, 500nM progesterone: $53.65 \pm 4.96 \text{ pApF}^{-1}$, $p > 0.05$, Student's paired t-test). This was consistent with data presented in Figures 5.1- 5.4. Perfusion of the chamber with 500nM progesterone for 20-30 seconds caused an increase in the magnitude of I_{Tail} (Figure 5.16B). The agonistic effect of progesterone was further confirmed by analysis of the I_m - V_m relationship of I_{Tail} (Figure 5.16C). Analysis of the maximum peak tail current generated following repolarisation to -92mV from 118mV, as shown in figure 5.16D, showed that progesterone significantly increased the tail current from -24.75 ± 2.76 to $-53.74 \pm 3.22 \text{ pApF}^{-1}$ ($n_c = 9$, $N_D = 9$, $p < 0.0001$, Student's paired t-test). This data confirms previous findings and further strengthens the possibility that the current flowing through I_{out} and I_{tail} are via two separate cation channels.

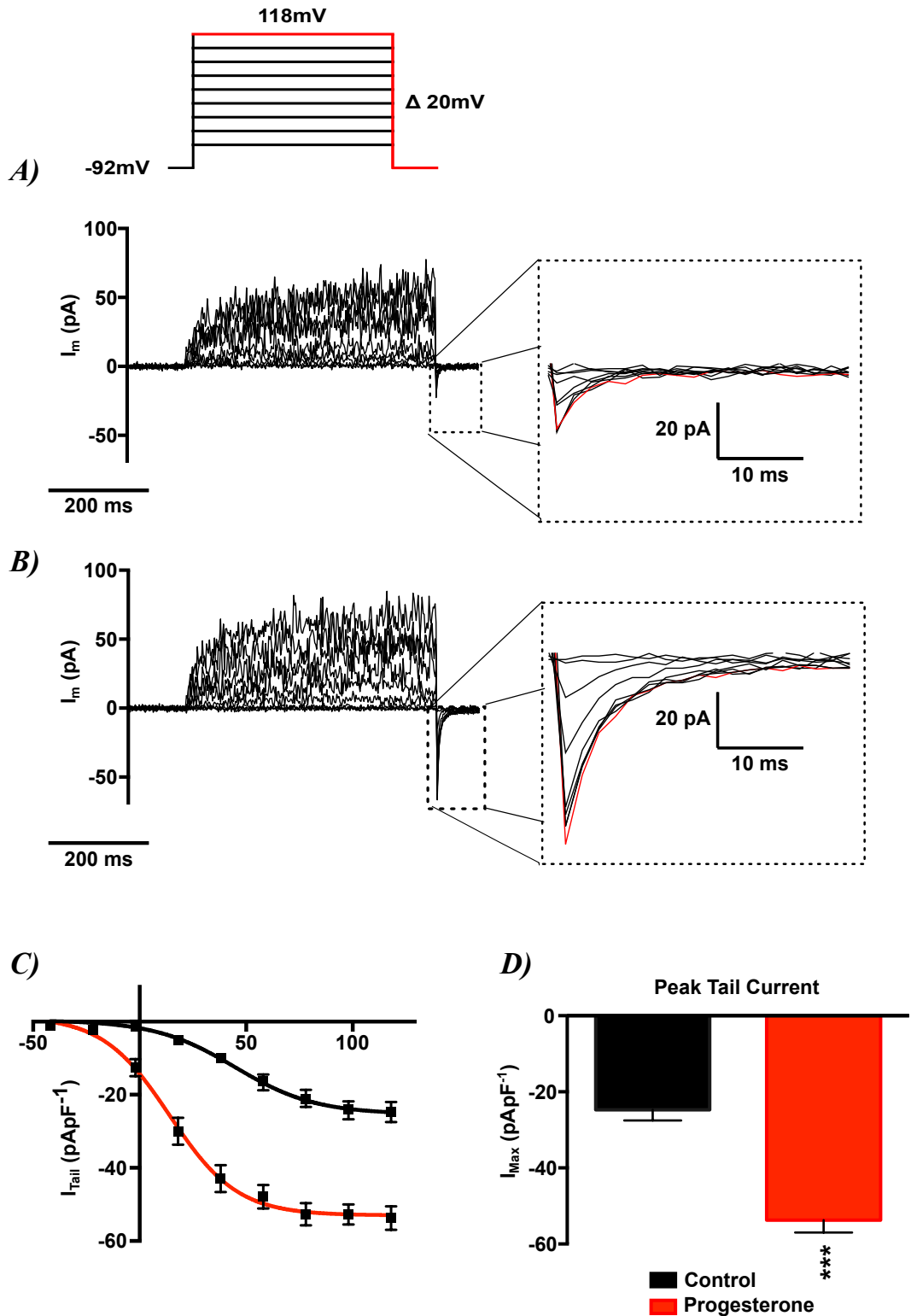
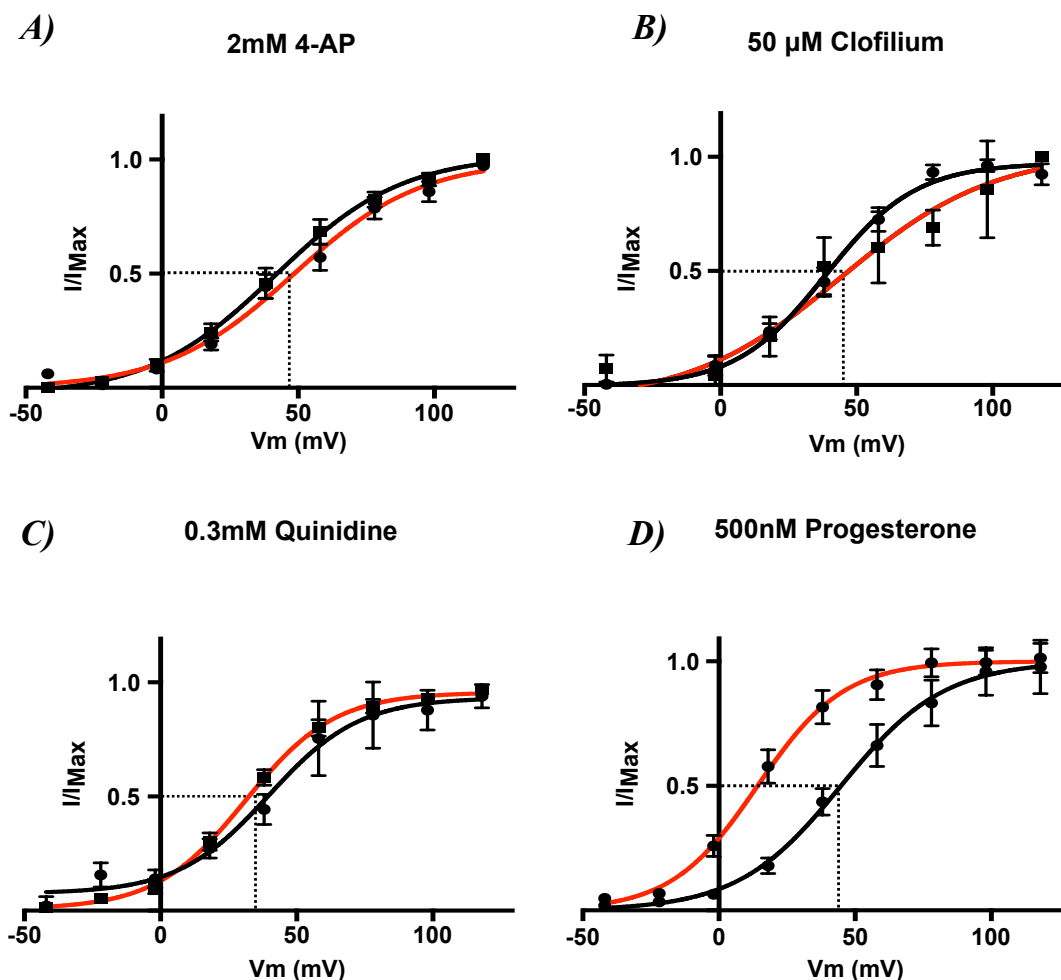


Figure 5.16: Effects of 500nM progesterone on the tail current. A, B) Currents evoked by step repolarisation to -92mV from a series of depolarised test potentials. Currents were recorded under standard bath and pipette solutions in control (A, representative trace) and after 30 seconds exposure to 500nM progesterone (B, representative trace) exposure with enlarged tail currents represented on the right of each trace. C) Relationship between I_m and V_m quantified under control (black line) after 30 seconds of progesterone exposure (red line). D) Mean peak tail current quantified by repolarisation from 118mV to -92mV in control and after 30 seconds exposure to 500nM progesterone. Error bars indicate s.e.m with asterisks denoting statistical significance (***) $p < 0.001$.

5.4.5. *Effect of clofilium, 4-AP, quinidine and progesterone on the biophysical properties of the channel.*

Figure 5.17 shows the Boltzmann sigmoidal relationship between $I_m/I_{m(\text{Max})}$ vs. V_m generated by further analysis of the tail current I_m - V_m relationships under control (black lines) and treated (red lines) conditions in Figures 5.13 - 5.16. Analysis of these data showed that under control conditions the half maximal activation (V_{50}) of the tail current occurred at roughly $\sim 40\text{mV}$, whilst the Boltzmann slope constant (κ), which described the channel's sensitivity to changes in voltage, was $\sim 20\text{mV}^{-1}$. This showed that the I_{Tail} is weakly voltage activated. Addition of 2mM 4-AP, 50 μM clofilium and 0.3mM quinidine did not significantly alter these parameters (Figures 5.17A, B, C and E). Conversely, addition of 500nM progesterone caused a highly significant leftward shift in V_{50} from $+44.8 \pm 5 \text{ mV}$ to $+14.8 \pm 4 \text{ mV}$ (Figures 5.17 D & E, $n_C = 9$, $N_D = 4$, $p < 0.001$, Student's paired t-test). Assessment of the Boltzmann constant showed that progesterone did not affect the channel's sensitivity to changes in voltage (Control: $\kappa = 19.0 \pm 5 \text{ mV}^{-1}$, 500nM progesterone: $\kappa = 16.0 \pm 3 \text{ mV}^{-1}$, $p > 0.5$ Student's paired t-test). From this it would appear 4-AP and quinidine act on the tail current *via* a different mechanism compared to progesterone. Analysis of the effect of quinidine (Figure 5.18B), progesterone (Figure 5.18C) and 4-AP (Figure 5.18D) on the time of tail inactivation could be modelled as the sum of two exponentials and are presented in Figure 5.18. Analysis of this data showed that besides from progesterone and 4-AP (Figure 5.18A), there was no effect on the time of tail current inactivation.



E)

	V_{50} (mV)	Boltzmann Constant (mV^{-1})
Control	38.0 ± 8	22.4 ± 8
2mM 4-AP	48.8 ± 8	23.5 ± 9
Control	38.1 ± 7	18.5 ± 8
50μM Clofilium	44.2 ± 13	25.4 ± 14
Control	46.2 ± 11	19.5 ± 10
0.3mM Quinidine	32.1 ± 6	16.3 ± 6
Control	44.8 ± 5	19.0 ± 5
500nM Progesterone	14.2 ± 4 ***	16.0 ± 3

Figure 5.17: Effects of clofilium, 4-AP, quinidine and progesterone on the biophysical properties of the tail current. Boltzmann sigmoids were generated by further analysis of the I_m - V_m relationship of the tail current in control (black lines) and after treatment (red lines) with 2mM 4-AP (A), 50 μ M clofilium (B), 0.3mM quinidine (C) and 500nM progesterone (D). Dotted lines indicated the half maximal activation of the channel (V_{50}). Data presented as current over maximal current (I/I_{max}) and plotted against V_m . E) Summary of V_{50} and the Boltzmann constant quantified by data in A-D fitted to the Boltzmann equation. All data presented as mean \pm s.e.m with asterisks denoting significance (***) $p < 0.001$.

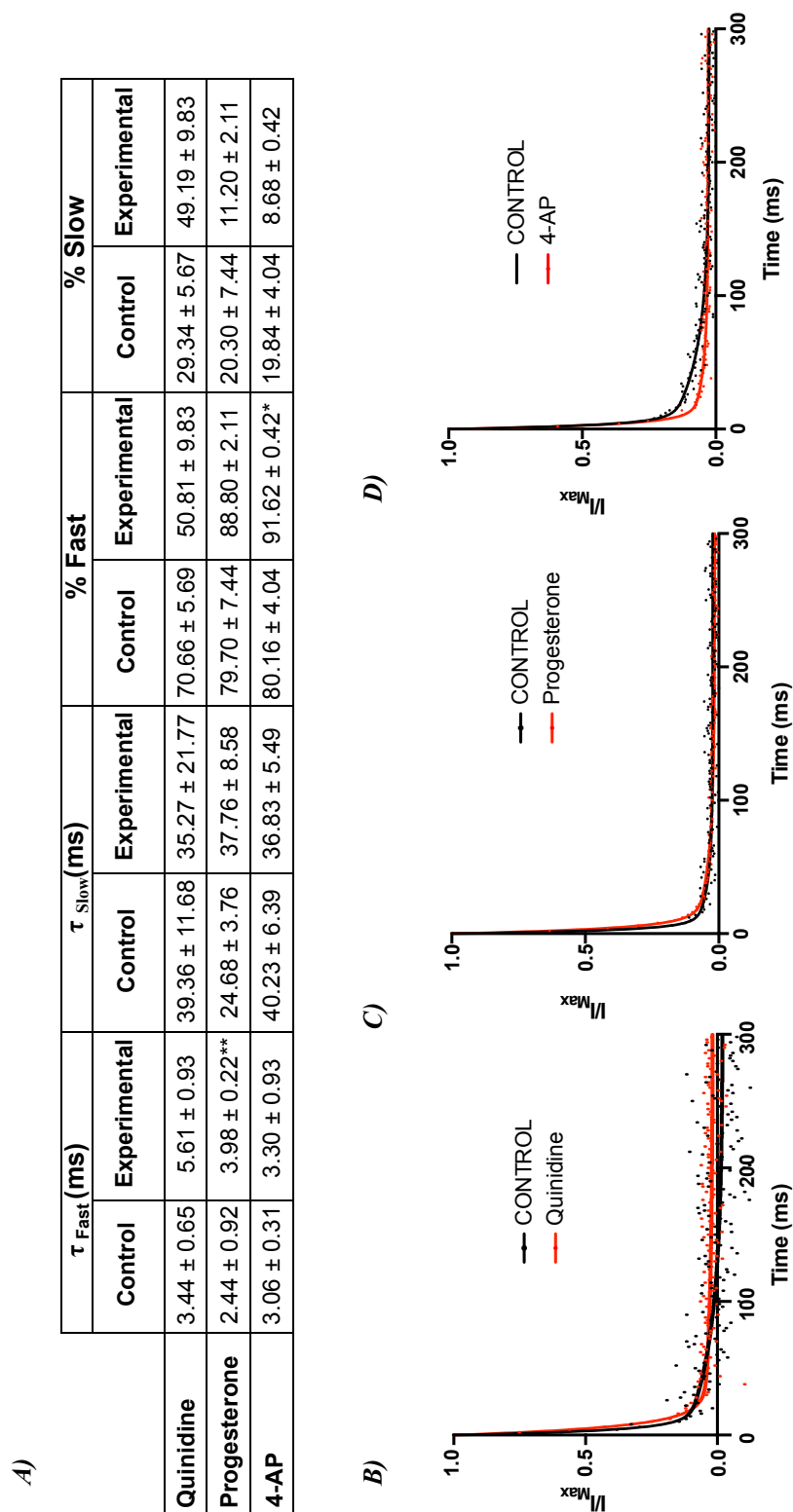


Figure 5.18 Pharmacological affect on the time course of tail current inactivation. A) Summary table assessing the affects of quinidine, progesterone and 4-AP on the parameters of tail current inactivation. Tail current time course of inactivation expressed as I/I_{max} fitted to the sum of two exponentials in control (black line) and in the presence of quinidine (B, red line), progesterone (C, red line) and 4-AP (D, red line). Data presented as mean \pm s.e.m with asterisks denoting statistical significance (* $p < 0.05$).

5.4.6. *Affects of clofilium, 4-AP, Quinidine and Progesterone on Sperm*

Motility and Hyperactivation.

Data in Figures 5.5 and 5.6 showed that the tail current had a high degree of Ca^{2+} permeability that was enhanced when cells were exposed to nanomolar concentrations of progesterone. Calcium has been implicated in the induction of hyperactivation, therefore the next set of experiments aimed to assess if compounds that increase I_{Tail} (4-AP, quinidine and progesterone) cause an increase in hyperactivated motility. In subsequent experiments motility parameters were assessed using computer assisted sperm analysis (CASA).

Figure 5.19 shows the results for percentage total motility, percentage progressive motility and percentage hyperactivated motility for human sperm recorded in capacitating media under control and after 2 minutes of treatment. Under control conditions percentage total motility was $87.39 \pm 1.8 \%$ ($n = 8$). Application of 0.3mM quinidine, 50 μM clofilium, 500nM progesterone or 2mM 4-AP did not significantly affect the percentage of total motile cells, therefore none of the compounds had a detrimental effect on the cells at this time point. Analysis of progressive motility classified as any cell moving $\geq 25\mu\text{m/s}$, a straightness of $\geq 80\%$ with a lateral head amplitude (ALH) between 2.5 and 7 μm , showed that 0.3mM quinidine and 2mM 4-AP caused a significant reduction in percentage progressive motility by $\sim 30\%$ (Figure 5.19B: $n = 7$, $p < 0.001$ unpaired Student's t-test). Conversely 50 μM clofilium and 500nM progesterone had no significant effect on percentage progressive motility. However, analysis of the percentage of hyperactivated cells (any cell with a curvilinear velocity (VCL) $\geq 150\mu\text{m/sec}$, linearity (LIN) $\leq 50\%$ and an ALH $\geq 7\mu\text{m}$) showed that compounds that enhance I_{Tail} e.g. quinidine, progesterone and 4-AP, increased percentage hyperactivation by 9% (quinidine: $n = 6$, $p < 0.05$, Mann-Whitney test), 9% (progesterone $n = 5$, $p < 0.05$, Mann-Whitney test) and 27% (4-AP: $n = 7$,

$p < 0.001$, Mann-Whitney test), respectively (Figure 5.19C). In comparison, addition of $50\mu\text{M}$ clofilium significantly reduced percentage hyperactivation by $\sim 8\%$ (Figure 5.19C; control: $9.72 \pm 1.69\%$, 2 minutes clofilium treatment: $1.43 \pm 0.65\%$, $n = 8$, $p < 0.001$, Mann-Whitney test on arcsine transformed % hyperactivation). This data hints to the possible role of I_{Tail} in the induction and maintenance of human sperm hyperactivation.

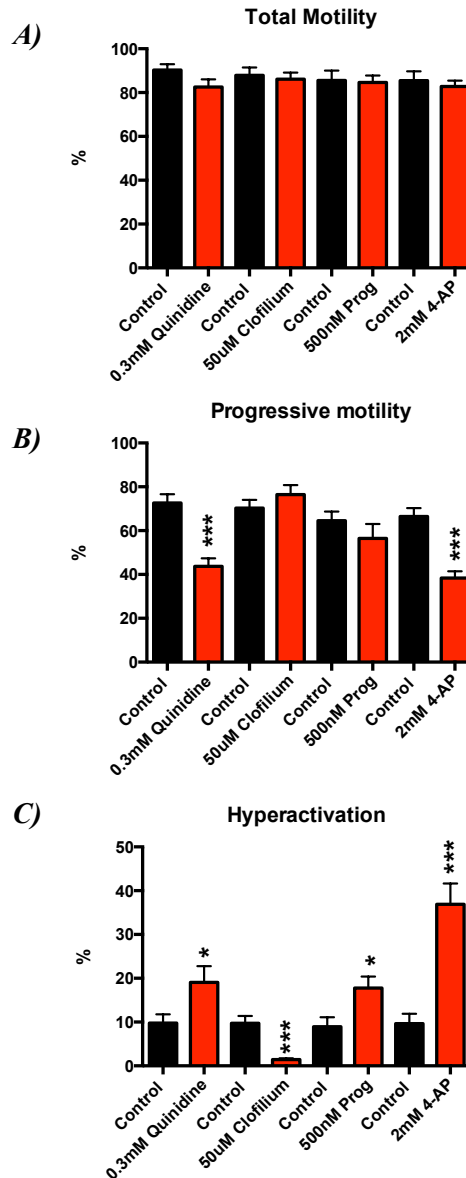


Figure 5.19: Motility assessment. CASA motility parameters for % total motility, % progressive motility and % hyperactivation of human sperm treated with 0.3mM quinidine ($n = 6$), $50\mu\text{M}$ clofilium ($n = 8$), 500nM progesterone ($n = 5$) or 2mM 4-AP ($n = 7$). Black bars show control values before the addition of the test compound; red bars show values for sperm treated with the test compound after 2 minutes of incubation. All data represented as mean \pm s.e.m. with asterisks denoting statistical significance (***) $p < 0.001$, Mann-Whitney test).

5.5. Discussion

Chapters 3 and 4 showed that the outward currents, under physiological conditions (K^+ current) and DVF conditions (CatSper current), shared the same pharmacology. This suggested that the currents might flow through the same channel. In order to further distinguish between the K^+ current and CatSper, the use of 500nM progesterone was employed, a potent activator of CatSper. The data presented in this chapter clearly demonstrates the presence of two channels; an outwardly rectifying current carried predominately by K^+ and a Ca^{2+} permeable progesterone sensitive tail current that may be implicated in the induction and maintenance of hyperactivation.

5.5.1. Progesterone response

The results presented in this chapter clearly show that progesterone has very little effect on the outward current with only a small transient inhibition observed. Conversely, progesterone caused a significant increase in the magnitude of the tail current over a 30 second period. As progesterone has not been shown to activate other channels besides from CatSper in human sperm, this therefore hinted that the tail current flowed *via* CatSper. In chapter 3, data showed that the outward current was important for the regulation of resting membrane potential. Therefore, we would expect that the small transient inhibition of I_{Out} should cause membrane depolarisation. However, the data presented here, demonstrates that this was not the case under these conditions. This is in contrast to fluorometric studies, which suggest progesterone exerts a depolarising effect on the resting membrane of human sperm cells (Foresta et al., 1993; Patrat et al., 2002). There are two possible explanations for this discrepancy. Firstly, the concentration of

progesterone was considerably higher in both these studies by as much as 20 times compared to the concentration used in this thesis (10 μ M vs 500nM). This concentration may cause a greater transient inhibition of the outward current that may result in depolarisation of V_m . However, it should be noted that human sperm would never be subjected to such an acute concentration of progesterone in the female reproductive tract; instead a concentration gradient is likely. Furthermore, data indicating pre-treatment with progesterone results in a desensitisation of the CatSper channel and reduces the progesterone induced Ca^{2+} influx upon subsequent addition of progesterone (Harper et al., 2003; Smith et al., 2013). This in turn brings into question the physiological authenticity of this effect. Notably this would require further experiments to validate this hypothesis. Secondly, Patrat ET AL also showed the progesterone induced depolarisation was only observed in a sub-population of cells ranging from 3 - 30% (Patrat et al., 2002), therefore it is plausible that the 8 cells recorded here were in a population that did not result in membrane depolarisation upon addition of progesterone.

The experiments presented in this chapter, show that progesterone exerts a reliable and potent effect on the tail current with no sustainable effect on the outward current at a working concentration of 500nM. Therefore, further experiments were carried out to characterise the current that contributes to the progesterone induced tail current.

5.5.2. Ionic permeability of the tail current

As progesterone increased the magnitude of the tail current, further experiments were carried out to characterise the ionic permeability of the tail current using ionic substitution methods. The data presented showed that the tail current showed some

permeability to both Na^+ and K^+ . This observation may explain why some studies have shown that addition of progesterone results in an increase in intracellular Na^+ (Foresta et al., 1993; Patrat et al., 2002) as an increase the magnitude of the tail current by progesterone should allow increased Na^+ entry. In contrast to the outwardly rectifying current present in Chapter 3 ($\text{K}^+/\text{Na}^+ = \sim 7$), the tail current showed poor permeability for K^+ over Na^+ with a relative conductance of ~ 1.4 . This poor selectivity was further investigated by the assessment of the open channel by step repolarisation from an initial depolarised potential to evoke an instantaneous current. Data collected using this protocol showed that the open channel was permeable to K^+ as increasing $[\text{K}^+]_o$ caused a rightward shift in E_{rev} . Replacement of intracellular K^+ with Na^+ further confirmed the open channel was permeable to Na^+ . Calculation of the relative permeability of the open channel using the GHK equation confirmed the open channel was poorly selective for K^+ and Na^+ with a relative permeability of 2.8, which accorded well with data in Figure 5.5. Furthermore, assessment of $I_{\text{Steady State}}$ at E_{Na^+} confirmed the outward current was more selective for K^+ with a relative permeability of ~ 6 which accorded well with a previous estimate of 7 (See Chapter 3, figure 3.7A). As well as this, substitution of intracellular Na^+ and K^+ with NMDG^+ caused a complete block of the outward that was previously observed in Chapter 3. Consequently this suggests the presence of two different channels, as relative permeability should be the roughly same in both directions if only a single channel was present.

One interesting observation is that the tail showed a high relative conductance for Ca^{2+} . This was ~ 4 fold higher compared to K^+ and ~ 5 fold higher compared Na^+ . Furthermore, 500nM progesterone sufficiently increased the ionic conductance of the

tail current in a Ca^{2+} -dependent manner. These results show, for the first time, direct evidence that progesterone can elicit a Ca^{2+} influx into human spermatozoa.

5.5.3. *Biophysical Properties of the Tail Current*

Assessment of the biophysical properties of the tail current showed that the tail current was weakly voltage dependent with a Boltzmann constant of $\sim 20\text{mV}^{-1}$, which was identical to the outward current and comparable to CatSper. However, assessment of V_{50} showed that tail current required more depolarised potentials for half the channels to become active. This observation was in contrast to the outward current where V_{50} was $\sim 25\text{mV}$. Substantial depolarised half maximum activations have been shown to be a characteristic property of CatSper channels in human sperm (Lishko et al., 2011). This property as well as the high degree of Ca^{2+} permeability and sensitivity to progesterone does suggest I_{Tail} is carried through CatSper. It should be noted the V_{50} value for CatSper recorded by Lishko was 70mV which was $\sim 25\text{mV}$ greater than the values recorded here. However, this discrepancy may be explained by the ionic composition of the solutions used to carry out these experiments. Assessment of I_{Tail} activation showed that under physiological conditions, the current became active at potentials $> -40\text{mV}$. Direct assessment of the resting membrane potential showed that capacitated human sperm had a resting V_m of $\sim 30\text{mV}$. This is important as it suggests that under physiological conditions there are a population of available CatSper channels that could allow Ca^{2+} to enter the cell. As Ca^{2+} has been shown to play an important role in the induction of hyperactivation (Suarez, 2008), it would be tempting to postulate that this small current may be important for the regulation of basal hyperactivation in human sperm. However, one major caveat to this hypothesis is that the channel shows very fast inactivation at hyperpolarised potentials. This property could explain why there was no observable current in previous ramp experiments at hyperpolarised potentials.

5.5.4. Pharmacology of the Tail current

Assessment of the pharmacological profile of the tail current using 0.3 mM quinidine, 2mM 4-AP, 50 μ M clofilium and 500nM progesterone showed that these compounds could be separated into 3 categories, these include: 1) inhibition of both outward and tail currents (50 μ M clofilium); 2) inhibition of outward current and enhancement of tail current (0.3mM quinidine) and; 3) no effect on outward current but enhancement of tail current (2mM 4-AP and 500nM progesterone). The pharmacological differences between of the outward and tail current further suggests the presence of two distinct channels. Interestingly assessment of the biophysical properties of the tail current after addition of quinidine, 4-AP and clofilium showed that there was no difference in the half maximal activation (~ 44 mV) or the Boltzmann constant (~ 20 mV⁻¹). This shows that these compounds have no effect on the channel's sensitivity to voltage. However, assessment of the biophysical properties of cells treated with 500nM progesterone showed that progesterone caused a negative shift in the activation kinetics of the channel. This observation has been documented before by Lishko *et al* who showed that progesterone caused a negative shift in the biophysical properties of CatSper that allowed that channel to become active at more physiological potentials (Lishko et al., 2011). The negative shift in the activation kinetics of I_{Tail} provides further evidence to the identification of CatSper as the channel underlying the tail current. To validate this, analysis of the DVF CatSper current presented in Chapter 4 (Figure 4.2) were carried out. This showed that the tail current generated by hyperpolarising of V_m to -87mV under DVF conditions (thought to provide a read out of CatSper activity) showed that the DVF tail current had an identical pharmacological profile to I_{Tail} (Data no shown). This therefore further adds validity to the identification of I_{Tail} as CatSper.

An unusual finding was that quinidine, a known antagonist of voltage gated K^+ and Na^+ channels, caused an augmentation of the tail current. The agonistic actions of quinidine have been documented before in isolated skate horizontal cells where it is proposed to act on hemi-gap-junction channels (Malchow et al, 1994). In this paper Malchow and colleagues showed that 200 μ M quinidine augmented the tail current upon repolarisation by the activation of these non-selective hemichannels. However, it is unlikely that quinidine is augmenting I_{Tail} *via* these channels in human sperm as Malchow showed that application of quinidine increased both the outward as well as inward currents. This is contrary to the data presented here as quinidine strongly inhibits the outward current but augmented I_{Tail} . Secondly, hemi-gap-junction channels are non-selective ion channels with an E_{rev} of 0mV. Whereas the data presented in chapter 5 shows I_{Tail} is only poorly selective with an E_{Rev} of ~ -42 mV. Another possible explanation for quinidine's agonistic effect may be a result of changes in intracellular pH. As both 4-AP and quinidine are alkaloids that are known for their alkalinising properties, it is possible that the mechanism for I_{Tail} activation by these compounds is through intracellular alkalinisation. However this is unlikely as the pipette solution contained 10mM HEPES which should be sufficient enough to maintain control of internal pH. Therefore the mechanism by which quinidine augments I_{Tail} remains to be elucidated. None-the-less this agonistic effect of quinidine on the tail current would explain the strong depolarising effect on V_m to values > 0 mV assessed by whole cell current clamp (Chapter 3).

5.5.5. Hyperactivation and the Tail Current

CatSper is thought to be the dominant ion channel responsible for the induction and regulation of hyperactivation in human and mouse sperm. This has been shown by

mouse knock-out studies, which highlighted that CatSper^{-/-} murine sperm were unable to undergo hyperactivation resulting in infertility (Chung et al., 2011; Ho et al., 2009; Jin et al., 2007; Qi et al., 2007; Ren et al., 2010). In humans there is no quantificational data regarding the level of hyperactivation in CatSper deficient sperm. However, diagnostic semen analysis of these men do report asthenozoospermia as a characteristic phenotype (Avenarius et al., 2009; Avidan et al., 2003; Smith et al., 2013). In section 5.4 data showed that compounds that activate the tail current (CatSper) also cause an increase in basal hyperactivation. Conversely clofilium, a compound that significantly reduced the tail current, significantly inhibited hyperactivation in human sperm. This data would fit with the idea that CatSper is important for the induction and regulation of hyperactivation in human sperm. Interestingly, inhibition of the tail current by clofilium had no effect on the percentage of motile cells at the time of analysis suggesting CatSper is not important for the maintenance of general motility. A previous PhD student has shown this where by inhibition of CatSper with NNC 55-0396 (putative CatSper-specific inhibitor) reduced basal hyperactivation without affecting motility (Alasmari, unpublished observation). Four-aminopyridine (4-AP) showed the greatest induction of hyperactivation compared to progesterone or quinidine, however it did not cause the largest increase in the tail current. This accords well with data in the literature that has shown 4-AP activates hyperactivation by mobilisation of intracellular Ca²⁺ stores either independently or in conjunction with CatSper (Alasmari et al., 2013).

5.6. Conclusion

The aim of this chapter was to use progesterone as a tool to investigate whether the K⁺ current and CatSper current flowed through the same population of ion channels. The data presented here clearly shows that this is not the case as the outward current and tail

current display different biophysical and pharmacological profiles. Furthermore, the high degree of Ca^{2+} conductance, progesterone sensitivity and distinct biophysical properties suggests the tail current is flowing through CatSper. Pharmacological modulation of this current has suggested a potentially novel link between this current and the regulation and induction of hyperactivation in human sperm. Therefore, the outward current and tail current must flow through two distinct ion channels.

Chapter 6 - General Discussion and Future Work

6.1. Aim of thesis

The aim of this thesis was to further the understanding of ion channels in human spermatozoa using whole cell electrophysiology and to assess how these channels contribute to normal sperm function.

6.2. Key findings

This work has identified the presence of two distinct ion channels using whole cell patch clamp electrophysiology. These include: 1) a poorly selective K^+ current involved in the regulation of V_m and 2) a progesterone sensitive and Ca^{2+} sensitive tail current potentially the regulation of basal hyperactivation.

The results presented in this thesis show the presence of an outwardly rectifying hyperpolarising K^+ current in human spermatozoa. In conjunction with the effects of K^+ channel antagonists; quinidine, clofilium and bupivacaine, on resting V_m as well as the depolarising effect of increased $[K^+]_o$, it can be concluded that the human KSper is the dominant hyperpolarising conductance and thus is important for the regulation of membrane potential. Data presented in Chapter 3 highlighted a possible species-specific difference between the human and mouse K^+ currents. In mouse sperm, Slo3 is activated by capacitation associated intracellular alkalinisation resulting in membrane hyperpolarisation (Santi et al. 2010). However, this data indicated that human KSper was only weakly sensitive to pH_i and that intracellular alkalinisation to pH 8 did not affect the resting V_m of the cell. A characteristic that has been suggested by other groups (Lishko et al. 2012). Work on mouse has shown that both KSper and CatSper are sensitive to pH. Under physiological conditions alkaline induced activation, as well as

increased K^+ permeability (Chávez et al. 2013) of Slo3, causes hyperpolarisation of the membrane during capacitation. Alkalisiation of intracellular environment also alters the activation kinetics of CatSper by shifting activation towards physiological potentials, thus increasing the number of available channels (Lishko et al. 2011). This shift in activation and increased driving force for Ca^{2+} entry is thought to be the mechanism for Ca^{2+} influx into the cell (Lishko et al. 2012).

In humans the mechanism for Ca^{2+} influx appears to be different. Data presented here (Chapter 5), as well as data by Lishko et al, shows that human CatSper requires very depolarised potentials for activation even after capacitation compared to mouse ($V_{50} = +70mV$ vs. $+11mV$ respectively) (Lishko et al. 2011). Therefore, hyperpolarisation past $-40mV$, as seen in murine sperm, would completely shut CatSper in human spermatozoa inhibiting the flow of Ca^{2+} into the cell, resulting in inhibition of hyperactivation and other Ca^{2+} dependent processes. This therefore suggests that human sperm do not undergo capacitated associated hyperpolarisation of V_m . Based on data assessing the activation kinetics of I_{Tail} , data presented in this thesis suggests that at resting V_m under physiological conditions ($\sim -30mV$) CatSper may allow a small influx of Ca^{2+} and this may set the level of basal hyperactivation in human sperm (Chapter 5). From current clamp data, results indicated a wide range of resting V_m from -20 to $-49mV$ from 31 cells indicating inherent intra- and inter-donor variation. Thus a potential hypothesis may be that, variations in resting V_m influence the level of basal hyperactivation. For example sperm from men with a more depolarised resting V_m of $\sim -20mV$ compared to $-30mV$ may have a higher level of basal hyperactivation, as this would increase the number of active CatSper channels. Conversely men with a more hyperpolarised resting V_m may have low basal hyperactivation as a result of

CatSper inactivation. This hypothesis can be tested by hyperpolarising the resting V_m using low Na^+ media. Preliminary experiments (data not shown) have indicated that lowering external Na^+ from 156mM to 11mM causes a small hyperpolarisation of the V_m . Using CASA, the level of basal hyperactivation of sperm bathed in low Na^+ can be evaluated. These experiments would form the basis of future work. It should be noted however, that hyperactivation is not solely induced by Ca^{2+} influx through CatSper. Previous work in by Alasmari et al has shown that the induction of hyperactivation is a complex process involving the release of intracellular Ca^{2+} from internal stores in the head and neck region of the sperm cell (Alasmari et al. 2013). Alasmari and colleagues showed that 4-AP is a potent agonist of hyperactivation by the mobilisation of Ca^{2+} stores independently of CatSper activation in human sperm. Our data is slightly conflicting, as 4-AP had no affect on the ‘classic’ outward CatSper current under DVF conditions. However, under physiological conditions 4-AP did show an agonistic affect on the tail current (CatSper). Secondly, data presented on the magnitude of the activated tail current would support the hypothesis that CatSper is not solely involved in hyperactivation (Chapter 5), as the magnitude of the activated tail current did not reflect the level of induced hyperactivation. One potentially consistent finding between the present study and the study by Alasmari et al was that CatSper might play a role in basal or spontaneous hyperactivation. This is based on observations that have shown that basal hyperactivation is inhibited with application of NNC 55-0396 (Alasmari et al. 2013). Indeed, inhibition of the tail current by clofilium under physiological conditions completely abolished hyperactivation in capacitated human sperm. Therefore, it is possible that basal hyperactivation could be regulated by CatSper whilst induced hyperactivation (increase in hyperactivation above basal) is regulated by Ca^{2+} induced Ca^{2+} release *via* internal stores.

Progesterone has been shown to have a clear agonistic affect on human sperm by facilitating Ca^{2+} influx *via* CatSper (Lishko et al. 2011; Strünker et al. 2011). The present data accords well with the literature as application of 500nM progesterone increases the Ca^{2+} conductance of the tail current (postulated to be CatSper) by ~2 fold. Furthermore, inhibition of the tail current with 50 μM clofilium (Chapter 5) causes an inhibition of progesterone induced Ca^{2+} influx as assessed by fluorometric studies (Chapter 4). These data also indicated that the mechanism for increased Ca^{2+} entry by progesterone appeared to be by shifting the activation kinetics of the channel toward resting V_m (Chapter 5). This negative shift in activation kinetics is another characteristic biophysical property of CatSper, as demonstrated by Lishko and colleagues (Lishko et al. 2011), that allows CatSper to become active at physiological potentials. In contrast to the work by Lishko et al, all our experiments were carried out under conditions designed to maintain physiological ionic gradients. As a result our data provides a more physiological representation of the role of progesterone.

In vivo, progesterone is produced by the cumulus cells that surround in the oocyte at the micromolar concentration. This is likely to form a concentration gradient down the reproductive tract until it reaches picomolar concentrations in cervical mucus (Adamopoulos et al. 2000). At this concentration CatSper does show activation in human sperm (Lishko et al. 2011). It is therefore tempting to speculate that progesterone acts as a ‘priming agent’ to kick start capacitation in cervical mucus by increasing Ca^{2+} influx through CatSper to improve penetration into cervical mucus directly after ejaculation. Furthermore, the ability to respond to progesterone at these concentrations may be a biochemical tool to ‘select’ sperm with the highest fertilising capacity (Gatica

et al. 2013). As the cell ascends the female reproductive tract, increasing concentrations of progesterone and activation of CatSper by intracellular alkalinisation of the cytoplasm, further shifts the activation kinetics of CatSper towards physiological potentials. This would increase the influx of Ca^{2+} influx into the cell and enhance hyperactivation and eventually acrosome reaction.

6.2.1. K^+ efflux through CatSper

A major source of investigation in the characterisation of the K^+ current was whether the poorly selective K^+ current recorded under physiological ionic gradients flowed *via* a human version of Slo3 or through CatSper. In Slo3^{-/-} murine sperm there is clear evidence of a residual K^+ current at depolarised potentials. Although it is believed to flow through endogenous CatSper channels there was no conclusive evidence to support this hypothesis (Zeng et al. 2011). The authors of this paper suggested that if CatSper were responsible for the residual K^+ current, it would have to be sensitive to both clofilium and quinidine. Secondly, a double Slo3^{-/-} / CatSper^{-/-} knockout mice would have to be generated to provide further evidence for this hypothesis. Very recently, such a mouse model has been generated with a double knockout for Slo3 and CatSper1. This study by Zeng and colleagues showed that in the absence of both channels there was a complete loss of residual K^+ current thereby confirming I_{Kres} was indeed flowing through endogenous CatSper channels in murine sperm (Zeng et al., 2013). The authors of this paper also suggested that CatSper could potentially contribute to the regulation of resting V_m under non-capacitating conditions. This discovery thereby indicated a potentially novel role for CatSper in murine spermatozoa. In the absence of a naturally occurring Slo3/CatSper deficient man, the presented studies focussed on the ability to distinguish the K^+ current from endogenous CatSper using pharmacological methods.

What the current data showed was that CatSper and the poorly selective K^+ current could not be distinguished based on their pharmacological profiles. One surprising result was that NNC 55-0396 (a putative CatSper channel antagonist) caused an inhibition of the physiological K^+ current. There are two possible explanations for this; firstly assuming NNC 55-0396 is a selective CatSper channel inhibitor then the K^+ current is flowing through CatSper. Thus, CatSper may be involved in the regulation of V_m in human sperm. Conversely the second explanation is that NNC 55 - 0396 has a previously undocumented antagonistic effect on Slo3. Indeed in order to investigate this hypothesis, the affects of NNC 55-0396 on native Slo3 in murine spermatozoa would have to be carried out. However, there is growing concern regarding the specificity of NNC 55-0396 as concentrations greater than $10\mu M$ do elicit a Ca^{2+} influx in human spermatozoa when assessed using fluorometric studies (Strünker et al. 2011). This suggests NNC 55-0396 is elucidating Ca^{2+} entry that could be potentially due to the depolarisation of V_m .

These observations lead to the possibility that the CatSper and K^+ currents were flowing through a single channel under physiological conditions. However, data presented in Chapter 5 indicated that there are potentially two separate channels. The data presented in Chapter 5 consistently shows the tail current but not the outward current was sensitive to progesterone. Furthermore, the tail current and outward current had different ionic conductances with the tail current having a lower G_{K^+}/G_{Na^+} compared to the outward current (2.8 vs. 7, respectively, Chapters 3 & 5). Finally pharmacological work clearly demonstrated that the tail and outward currents had completely different pharmacological profiles. One such example is quinidine, which had an antagonistic affect on the outward current but an agonistic affect on the tail current. This agonistic

affect on the tail current would explain why such strong depolarisation of V_m ($> 10\text{mV}$) were observed in cells recorded under whole cell current clamp (Chapter 3). Therefore based on the data collected here there is very little conclusive evidence to suggest that the poorly selective outward K^+ current flows *via* CatSper in human sperm under physiological conditions. What it does show is that current pharmacological compounds are not useful tools for the identification of native ion channels in human spermatozoa. As well as this, recording of CatSper using DVF conditions does not provide an accurate representation of CatSper channel activity for two reasons. Firstly such experiments only show that depolarisation activates a non-selective cation current in the absence of divalent cations, which does not represent channel activation *in vivo*. Secondly due to the large access resistances and large currents generated under these conditions the voltage drop is large ($\sim 30\%$ of the command potential), thus maintenance of voltage clamp is significantly compromised.

6.3. Conclusions and Future Work

The work presented in this thesis has demonstrated that human spermatozoa possess a poorly selective K^+ current that is important for the regulation of membrane potential. Recently electrophysiological studies on human sperm by Mannowetz et al have shown that the human form of K^+ conductance is pH insensitive. Furthermore, the channel that underlies this K^+ conductance in human sperm is Ca^{2+} sensitive, as raising $[\text{Ca}^{2+}]_i$ to $50\mu\text{M}$ causes activation of the channel. Based on these properties and the channel's sensitivity to nano molar concentrations of Slo1 specific toxins; Iberitoxin, charybdotoxin and paxilline, the authors of this paper proposed the dominant K^+ conductance of human sperm is via Slo1 and not Slo3 (Mannowetz et al 2013). Furthermore, the human K^+ conductance is inhibited by high concentrations of

progesterone ($>5\mu\text{M}$). Data presented in this thesis showed that progesterone had a negligible effect on I_{Out} as indicated in Chapter 5. This discrepancy is likely due to the concentration of progesterone used, as Mannonwetz et al showed that inhibition of the Slo1 only occurred at concentrations $> 5\mu\text{M}$ which is 10 times higher than that used in this thesis. The inhibition of Slo1 by micromolar concentrations of progesterone in human sperm is thought to cause depolarisation of the V_m , thereby further shifting the membrane potential into the activation window for CatSper. This in turn causes further increases in $[\text{Ca}^{2+}]_i$ resulting in hyperactivation allowing the cell to penetrate the outer vestments of the oocyte. Although the K^+ conductance described here does broadly match that of Mannonwetz et al, the ionic selectivity of the channel presented in Chapter 3 only shows poor ionic selectivity with a $P_{\text{K}^+}/P_{\text{Na}^+}$ of ~ 7 , a feature not consistent with Slo1 channels (Hoshi, 2012). As a result the K^+ current recorded here cannot be conclusively identified as either Slo1 or Slo3.

Due to pharmacological overlap between the outward K^+ current and CatSper, the importance of this channel for sperm function could not be accurately assessed. Therefore, future work would build on data collected assessing male patients attending the assisted conception unit for potential ion channel defects. The aim is to identify a number of patients with naturally occurring ion channel defects and assess how these defects manifest as sperm dysfunction. Towards the end of these studies, a patient with secondary infertility was identified to have a complete absence of the K^+ current on two separate assessments. Although this patient would have to be screened for other channel pathologies, his sperm may provide a naturally occurring K_{Sper} deletion for functional assessment.

References

- Adamopoulos DA, Kapolla N, Abrahamian A, Dessypris A, Nicopoulou S, Giannacodemos G. 2000. Sex steroids in cervical mucus of spontaneous or induced ovulatory cycles. *Steroids*, 65,1–7.
- Aitken, R J. 2010. Whither must spermatozoa wander? The future of laboratory seminology. *Asian J Androl*, 12, 99–103.
- Aitken R. J. 2006. Sperm function tests and fertility. *Int J Androl*, 29, 69–75.
- Alasmari W, Costello S, Correia J, Oxenham SK, Morris J, Fernandes L, Ramalho-Santos J, Kirkman-Brown J, Michelangeli F, Publicover S, Barratt CL. 2013. Ca^{2+} signals generated by CatSper and Ca^{2+} stores regulate different behaviors in human sperm. *J Biol Chem*, 288, 6248–58.
- Alasmari W, Barratt CL, Publicover SJ, Whalley KM, Foster E, Kay V, Martins da Silva S, Oxenham SK. 2013. The clinical significance of calcium-signalling pathways mediating human sperm hyperactivation. *Hum Reprod*, 28, 866–76.
- Alnawaiseh M, Albanna W, Chen CC, Campbell KP, Hescheler J, Lücke M, Schneider T. 2011. Two separate Ni^{2+} -sensitive voltage-gated Ca^{2+} channels modulate transretinal signalling in the isolated murine retina. *Acta Ophthalmol*, 89, 579–90.
- Andersen AG, Jensen TK, Carlsen E, Jørgensen N, Andersson AM, Krarup T, Keiding N, Skakkebaek NE. 2000. High frequency of sub-optimal semen quality in an unselected population of young men. *Hum Reprod*, 15, 366–72.
- Arnoult C, Cardullo RA, Lemos JR, Florman HM. 1996. Activation of mouse sperm T-type Ca^{2+} channels by adhesion to the egg zona pellucida. *Proc Natl Acad Sci U S A*, 93, 13004–9.
- Ashcroft F.M. 2006. From molecule to malady. *Nature*, 440, 440–7.
- Austin C.R. 1951. Observations on the penetration of the sperm in the mammalian egg. *Aust J Sci Res B*, 4, 581–96.
- Avenarius MR, Hildebrand MS, Zhang Y, Meyer NC, Smith LL, Kahrizi K, Najmabadi H, Smith RJ. 2009. Human male infertility caused by mutations in the CATSPER1 channel protein. *Am J Hum Genet*, 84, 505–10.
- Avidan N, Tamary H, Dgany O, Cattani D, Pariente A, Thulliez M, Borot N, Moati L, Barthelme A, Shalmon L, Krasnov T, Ben-Asher E, Olender T, Khen M, Yaniv I, Zaizov R, Shalev H, Delaunay J, Fellous M, Lancet D, Beckmann JS. 2003. CATSPER2, a human autosomal nonsyndromic male infertility gene. *Eur J Hum Genet*, 11, 497–502.

- Babcock DF, Bosma MM, Battaglia DE, Darszon A. 1992. Early persistent activation of sperm K^+ channels by the egg peptide speract. *Proc Natl Acad Sci U S A*, 89, 6001–5.
- Babcock DF, Rufo GA Jr, Lardy HA. 1983. Potassium-dependent increases in cytosolic pH stimulate metabolism and motility of mammalian sperm. *Proc Natl Acad Sci U S A*, 80, 1327–31.
- Barfield J.P, Yeung C.H. & Cooper T.G. 2006. Characterization of potassium channels involved in volume regulation of human spermatozoa. *Mol Hum Repro*, 11, 891–897.
- Barratt CL, Naeeni M, Clements S, Cooke ID. 1995. Clinical value of sperm morphology for in-vivo fertility: comparison between World Health Organization criteria of 1987 and 1992. *Hum Reprod*, 10, 587–93.
- Barratt CL, Mansell S, Beaton C, Tardif S, Oxenham SK. 2011. Diagnostic tools in male infertility-the question of sperm dysfunction. *Asian J Androl*, 13, 53–8.
- Barry PH. 1994. JPCalc, a software package for calculating liquid junction potential corrections in patch-clamp, intracellular, epithelial and bilayer measurements and for correcting junction potential measurements. *J Neurosci Methods*, 160,982–986.
- Barry P.H. & Lynch J.W. 1991. Liquid junction potentials and small cell effects in patch-clamp analysis. *J Membr Biol*, 121, 101–117.
- Bartoov B, Eltes F, Pansky M, Lederman H, Caspi E, Soffer Y. 1993. Estimating fertility potential via semen analysis data. *Hum Reprod*, 8, 65–70.
- Battistone MA, Da Ros VG, Salicioni AM, Navarrete FA, Krapf D, Visconti PE, Cuasnicú PS. 2013. Functional human sperm capacitation requires both bicarbonate-dependent PKA activation and down-regulation of Ser/Thr phosphatases by Src family kinases. *Mol Hum Reprod*, [Epub ahead of print]
- Bedu-Addo K, Costello S, Harper C, Machado-Oliveira G, Lefievre L, Ford C, Barratt C, Publicover S. 2008. Mobilisation of stored calcium in the neck region of human sperm-a mechanism for regulation of flagellar activity. *Dev Biol*, 52, 615–26.
- Beuckmann CT, Sinton CM, Miyamoto N, Ino M, Yanagisawa M. 2003. N-type calcium channel $\alpha 1B$ subunit Cav2.2 knock-out mice display hyperactivity and vigilance state differences. *J Neurosci*, 23, 6793–7.
- Biggers, J.D, 2012. IVF and embryo transfer: historical origin and development. *Reprod Biomed Online*,25, 118–27.
- Björling K, Morita H, Olsen MF, Prodan A, Hansen PB, Lory P, Holstein-Rathlou NH, Jensen LJ. 2013. Myogenic tone is impaired at low arterial pressure in mice deficient in the low-voltage-activated Cav 3.1 T-type Ca^{2+} channel. *Acta physiologica* , 207, 709–20.

- Blackmore PF, Beebe SJ, Danforth DR, Alexander N. 1990. Progesterone and 17-hydroxyprogesterone: Novel stimulators of calcium influx in human sperm. *J. Biol.Chem*, 265, 1376–1380.
- Boivin J, Bunting L, Collins JA, Nygren KG. 2007. International estimates of infertility prevalence and treatment-seeking: potential need and demand for infertility medical care. *Human Reprod*, 22, 1506–12.
- Brenker C, Goodwin N, Weyand I, Kashikar ND, Naruse M, Krähling M, Müller A, Kaupp UB, Strünker T. 2012. The CatSper channel: a polymodal chemosensor in human sperm. *EMBO J.*, 31,1654–65.
- Brewis IA, Morton IE, Mohammad SN, Browes CE, Moore HD. 2000. Measurement of intracellular calcium concentration and plasma membrane potential in human spermatozoa using flow cytometry. *J. Androl*, 21, 238–49.
- Caputo A, Caci E, Ferrera L, Pedemonte N, Barsanti C, Sondo E, Pfeffer U, Ravazzolo R, Zegarra-Moran O, Galiotta LJ. 2008. TMEM16A, a membrane protein associated with calcium-dependent chloride channel activity. *Science*, 322,590–4.
- Carlson AE, Westenbroek RE, Quill T, Ren D, Clapham DE, Hille B, Garbers DL, Babcock DF. 2003. CatSper1 required for evoked Ca^{2+} entry and control of flagellar function in sperm. *Proc Natl Acad Sci U S A.*, 100,14864–8.
- Carlson AE, Quill TA, Westenbroek RE, Schuh SM, Hille B, Babcock DF. 2005. Identical phenotypes of CatSper1 and CatSper2 null sperm. *J Biol Chem.*, 280, 32238–44.
- Carr D.W, Usselman M.C. & Acott T.S. 1985. Effects of pH, lactate, and viscoelastic drag on sperm motility: a species comparison. *Biol Reprod*, 33, 588–95.
- Castle A. 1991. Selective inhibition of potassium currents in rat ventricle by clofilium and its tertiary homolog. *J. Pharmacol. Exp. Ther*, 257,342–350.
- Chambers GM, Sullivan EA, Ishihara O, Chapman MG, Adamson GD. 2009. The economic impact of assisted reproductive technology: a review of selected developed countries. *Fertil Steril.*, 91,2281–94.
- Chang H. & Suarez SS. 2012. Unexpected flagellar movement patterns and epithelial binding behavior of mouse sperm in the oviduct. *Biol Reprod*, 86,140, 1–8.
- Chang M. 1951. Fertilizing Capacity of Spermatozoa Deposited into the Fallopian Tubes. *Nature*, 168, 697–698.
- Chen WY, Xu WM, Chen ZH, Ni Y, Yuan YY, Zhou SC, Zhou WW, Tsang LL, Chung YW, Höglund P, Chan HC, Shi QX. 2009. Cl^- is required for HCO_3^- entry necessary for sperm capacitation in guinea pig: involvement of a Cl^-/HCO_3^- exchanger (SLC26A3) and CFTR. *Biol Reprod*, 80,115–23.

- Chouabe C, Drici MD, Romey G, Barhanin J, Lazdunski M. 1998. HERG and KvLQT1/IsK, the cardiac K⁺ channels involved in long QT syndromes, are targets for calcium channel blockers. *Mol Pharmacol*, 54,695–703.
- Chung JJ, Navarro B, Krapivinsky G, Krapivinsky L, Clapham DE. 2011. A novel gene required for male fertility and functional CATSPER channel formation in spermatozoa. *Nat Commun*, 2, 153.
- Chávez JC, de la Vega-Beltrán JL, Escoffier J, Visconti PE, Treviño CL, Darszon A, Salkoff L, Santi CM. 2013. Ion permeabilities in mouse sperm reveal an external trigger for SLO3-dependent hyperpolarization. *PloS one*, 8, 60578.
- Connolly M.P, Hoorens S. & Chambers G.M. 2010. The costs and consequences of assisted reproductive technology: an economic perspective. *Hum Reprod update*, 16, 603–13.
- Cooper T. 2011. The epididymis, cytoplasmic droplets and male fertility. *Asian J Androl.*, 13, 130–8.
- Cooper T, Barfield J, Yeung CH. 2005. Changes in osmolality during liquefaction of human semen. *Int J Androl.*, 28, 58–60
- Costello S, Michelangeli F, Nash K, Lefievre L, Morris J, Machado-Oliveira G, Barratt C, Kirkman-Brown J, Publicover S. 2009. Ca²⁺ -stores in sperm : their identities and functions. *Reproduction*, 138, 425–437.
- Curi SM, Ariagno JI, Chenlo PH, Mendeluk GR, Pugliese MN, Sardi Segovia LM, Repetto HE, Blanco AM. 2003. Asthenozoospermia: Analysis of a Large Population. *Arch Androl.* 49, 343–349.
- Darszon A, Nishigaki T, Beltran C, Treviño CL. 2011. Calcium channels in the development, maturation, and function of spermatozoa. *Physiol Rev.*, 91,1305–55.
- Decoursey T.E. 2013. Voltage-Gated Proton Channels: Molecular Biology, Physiology, and Pathophysiology of the HV Family. *Physiological reviews*, 93, 599–652.
- Diabetes UK. 2011, Diabetes in the UK, key statistics on diabetes.
- El-Talatini MR, Taylor AH, Elson JC, Brown L, Davidson AC, Konje JC. 2009. Localisation and function of the endocannabinoid system in the human ovary. *PloS one*, 4, 4579.
- Espinosa F, de la Vega-Beltrán JL, López-González I, Delgado R, Labarca P, Darszon A. 1998. Mouse sperm patch-clamp recordings reveal single Cl⁻ channels sensitive to niflumic acid, a blocker of the sperm acrosome reaction. *FEBS Lett*, 426, 47–51.
- Espinosa F. & Darszon A. 1995. Mouse sperm membrane potential: changes induced by Ca²⁺. *FEBS Lett*, 372,119–25.

- Farley Ordozensky Staniec, J. & Webb, N.J., 2007. Utilization of infertility services: how much does money matter? *Health Serv Res.*, 42, 971–89.
- Ferraretti AP, Goossens V, de Mouzon J, Bhattacharya S, Castilla JA, Korsak V, Kupka M, Nygren KG, Nyboe Andersen A. 2012. Assisted reproductive technology in Europe, 2008: results generated from European registers by ESHRE. *Hum Reprod*, 27, 2571–84.
- Flesch FM, Brouwers JF, Nievelstein PF, Verkleij AJ, van Golde LM, Colenbrander B, Gadella BM. 2001. Bicarbonate stimulated phospholipid scrambling induces cholesterol redistribution and enables cholesterol depletion in the sperm plasma membrane. *J. Cell Sci*, 114, 3543–55.
- Foresta C, Rossato M. & Di Virgilio F. 1993. Ion fluxes through the progesterone-activated channel of the sperm plasma membrane. *J. Biochem*, 294, 279–83.
- Franken D R & Oehninger S. 2012. Semen analysis and sperm function testing. *Asian J Androl.*, 14, 6–13.
- Fürst J, Gschwentner M, Ritter M, Bottà G, Jakab M, Mayer M, Garavaglia L, Bazzini C, Rodighiero S, Meyer G, Eichmüller S, Wöll E, Paulmichl M. 2002. Molecular and functional aspects of anionic channels activated during regulatory volume decrease in mammalian cells. *Pflügers Archiv*, 444, 1–25.
- Garcia M. A & Meizel S. 1996. Importance of sodium ion to the progesterone-initiated acrosome reaction in human sperm. *Mol Reprod Dev.*, 45, 513–20.
- Garcia M. A, Meizel S. 1999. Regulation of intracellular pH in capacitated human spermatozoa by a Na⁺/H⁺ exchanger. *Mol Reprod Dev.*, 52, 189–95.
- Gatica LV, Guidobaldi HA, Montesinos MM, Teves ME, Moreno AI, Uñates DR, Molina RI, Giojalas LC. 2013. Picomolar gradients of progesterone select functional human sperm even in subfertile samples. *Mol Hum Reprod.*, [Epub ahead of print]
- Gibbons I. & Rowe, A.J. 1965. Dynein: A protein with adenosine triphosphatase activity from cilia. *Science*, 183, 139–141.
- Gomora J.C, Enyeart J.A. & Enyeart J.J. 1999. Mibefradil potently blocks ATP-Activated K⁺ channels in adrenal cells. *Mol Pharmacol*, 56, 1192–1197.
- Gorelik J, Gu Y, Spohr HA, Shevchuk AI, Lab MJ, Harding SE, Edwards CR, Whitaker M, Moss GW, Benton DC, Sánchez D, Darszon A, Vodyanoy I, Klenerman D, Korchev YE. 2002. Ion channels in small cells and subcellular structures can be studied with a smart patch-clamp system. *Biophys J.*, 83, 3296–303.
- Gu Y, Kirkman-Brown JC, Korchev Y, Barratt CL, Publicover SJ. 2004. Multi-state, 4-aminopyridine-sensitive ion channels in human spermatozoa. *Developmental biology*, 274, 308–17.

- Guerrero A, Sánchez J. A & Darszon A. 1987. Single-channel activity in sea urchin sperm revealed by the patch-clamp technique. *FEBS Lett*, 220, 295–8.
- Guzick DS, Overstreet JW, Factor-Litvak P, Brazil CK, Nakajima ST, Coutifaris C, Carson SA, Cisneros P, Steinkampf MP, Hill JA, Xu D, Vogel DL. 2001. Sperm morphology, motility, and concentration in fertile and infertile men. *N Engl J Med*, 345,1388–1393.
- HFEA, 2010a. *Fertility Facts and Figures 2008*,
- HFEA, 2010b. *Fertility treatment in 2010 trends and figures*,
- Hagiwara B.Y.S. & Kawa, K. 1984. calcium and potassium currents in spermatogenic cells dissociated from rat seminiferous tubules. *Journal of physiology*, 356, 135–149.
- Hargreave T. & Elton R.A. 1983. Is conventional sperm analysis of any use? *Br J Urol*, 55,774–9.
- Harper CV, Kirkman-Brown JC, Barratt CL, Publicover SJ. 2003. Encoding of progesterone stimulus intensity by intracellular $[Ca^{2+}]_i$ ($[Ca^{2+}]_i$) in human spermatozoa. *Biochem J.*, 372,407–17.
- Hartzell C, Putzier I. & Arreola J. 2005. Calcium-activated chloride channels. *Annual review of physiology*, 67,719–58.
- Ho H, Granish K.A. & Suarez SS. 2002. Hyperactivated Motility of bull sperm is triggered at the axoneme by Ca^{2+} and not cAMP *Dev Biol.*, 250,208–217.
- Ho H. & Suarez SS, 2001. Hyperactivation of mammalian spermatozoa : function and regulation. *Reproduction*, 122,519–526.
- Ho H.C. & Suarez S.S. 2001. An inositol 1,4,5-trisphosphate receptor-gated intracellular Ca^{2+} store is involved in regulating sperm hyperactivated motility. *Biol Reprod*, 65,1606–15.
- Ho K, Wolff C. A & Suarez, SS, 2009. CatSper-null mutant spermatozoa are unable to ascend beyond the oviductal reservoir. *Reprod Fertil Dev.*, 21,345–50.
- Hoshi T. 2012. Transduction of voltage and Ca^{2+} signals by Slo1 BK channels. *Physiology.*, 28, 172–189.
- Hull M. G, Glazener C. M, Kelly N. J, Conway D. I, Foster P. A, Hinton R. A, Coulson C, Lambert P. A, Watt E. M. & Desai K. M. 1985. Population study of causes, treatment, and outcome of infertility. *Br Med J (Clin Res Ed)*, 291, 1693-7.
- Inglis SK, Brown SG, Constable MJ, McTavish N, Olver RE, Wilson SM. 2007. A Ba^{2+} -resistant, acid-sensitive K^+ conductance in Na^+ -absorbing H441 human airway epithelial cells. *Am J Physiol Lung Cell Mol Physiol*, 292,1304–1312.

- Iovannisci D, Illek B. & Fischer H. 2010. Function of the HVCN1 proton channel in airway epithelia and a naturally occurring mutation, M91T. *J Gen Physiol.*, 136, 35–46.
- Jiménez-González MC, Gu Y, Kirkman-Brown J, Barratt CL, Publicover S. 2007. Patch-clamp “ mapping ” of ion channel activity in human sperm reveals regionalisation and co-localisation into mixed clusters. *J Cell Physiol.*, 213,801–808.
- Jin J, Jin N, Zheng H, Ro S, Tafolla D, Sanders KM, Yan W. 2007. Catsper3 and Catsper4 are essential for sperm hyperactivated motility and male fertility in the mouse. *Biol Reprod.*, 77, 37–44.
- De Jonge C. 2005. Biological basis for human capacitation. *Hum Reprod update*, 11, 205–14.
- De Jonge C. & Barratt C. eds. 2006. *The Sperm Cell*, Cambridge University Press.
- Katz D. & Yanagimachi R. 1980. Movement characteristics of hamster within the oviduct. *Biol Reprod*, 22,759–764.
- Kirichok Y. & Lishko P.V. 2011. Rediscovering sperm ion channels with the patch-clamp technique. *Molr Hum Reprod*, 17, 478–99.
- Kirichok Y, Navarro B. & Clapham DE, 2006. Whole-cell patch-clamp measurements of spermatozoa reveal an alkaline-activated Ca^{2+} channel. *Nature*, 439, 737–40.
- Kirkman-Brown JC, Bray C, Stewart PM, Barratt CL, Publicover SJ. 2000. Biphasic elevation of $[Ca^{2+}]_i$ in individual human spermatozoa exposed to progesterone. *Dev Biol.*, 222, 326–35.
- Koch HP, Kurokawa T, Okochi Y, Sasaki M, Okamura Y, Larsson HP. 2008. Multimeric nature of voltage-gated proton channels. *Proc Natl Acad Sci U S A*. 105, 9111–6.
- Krausz C, Bonaccorsi L, Maggio P, Luconi M, Criscuoli L, Fuzzi B, Pellegrini S, Forti G, Baldi E. 1996. Two functional assays of sperm responsiveness to progesterone and their predictive values in in-vitro fertilization. *Hum Reprod*, 11, 1661–7.
- Lee S.Y, Letts J. A & Mackinnon R. 2008. Dimeric subunit stoichiometry of the human voltage-dependent proton channel Hv1. *Proc Natl Acad Sci U S A*, 105, 7692–5.
- Lefièvre L, Bedu-Addo K, Conner SJ, Machado-Oliveira GS, Chen Y, Kirkman-Brown JC, Afnan MA, Publicover SJ, Ford WC, Barratt CL. 2007. Counting sperm does not add up any more: time for a new equation? *Reproduction*, 133, 675–684.
- Leonetti MD, Yuan P, Hsiung Y, Mackinnon R. 2012. Functional and structural analysis of the human SLO3 pH- and voltage-gated K^+ channel. *Proc Natl Acad Sci U S A*. 109, 19274–19279.

- Li K, Ni Y, He Y, Chen WY, Lu JX, Cheng CY, Ge RS, Shi QX. 2013. Inhibition of sperm capacitation and fertilizing capacity by adjudin is mediated by chloride and its channels in humans. *Hum Reprod.* 28, 47–59.
- Lishko PV, Botchkina IL, Fedorenko A, Kirichok Y. 2010. Acid extrusion from human spermatozoa is mediated by flagellar voltage-gated proton channel. *Cell*, 140, 327–37.
- Lishko PV, Clapham DE, Navarro B, Kirichok Y. 2013. Sperm Patch-Clamp. *Methods Enzymol.* 523, 59–83.
- Lishko PV, Kirichok Y, Ren D, Navarro B, Chung JJ, Clapham DE. 2012. The control of male fertility by spermatozoan ion channels *Annu Rev Physiol.*, 74, 453–75.
- Lishko PV, Botchkina I.L. & Kirichok, Y. 2011. Progesterone activates the principal Ca^{2+} channel of human sperm. *Nature*, 471, 387–91.
- Liu J, Xia J, Cho KH, Clapham DE, Ren D. 2007. CatSperbeta, a novel transmembrane protein in the CatSper channel complex. *J Biol Chem.*, 282, 18945–52.
- Lobley A, Pierron V, Reynolds L, Allen L, Michalovich D. 2003. Identification of human and mouse CatSper3 and CatSper4 genes: characterisation of a common interaction domain and evidence for expression in testis. *Reprod Biol Endocrinol.*, 1, 53.
- Lu J, Stewart AJ, Sadler PJ, Pinheiro TJ, Blindauer CA. 2008. Albumin as a zinc carrier: properties of its high-affinity zinc-binding site. *Biochem Soc Trans.*, 36, 1317–21.
- Luconi M, Francavilla F, Porazzi I, Macerola B, Forti G, Baldi E. 2004. Human spermatozoa as a model for studying membrane receptors mediating rapid nongenomic effects of progesterone and estrogens. *Steroids*, 69, 553–9.
- Lösel R. & Wehling M. 2003. Nongenomic actions of steroid hormones. *Nat Rev Mol Cell Biol.*, 4, 46–56.
- Macleod, J. & Gold, R.Z., 1951. The male factor in fertility and infertility. II. Spermatozoon counts in 1000 men of known fertility and in 1000 cases of infertile marriage. *J Urol*, 66, 436–49.
- Malchow RP, Qian H & Ripps H. 1994. A novel action of quinine and quinidine on the membrane conductance of neurons from vertebrate retina. *J. Gen Physiol.* 104, 1039-1055.
- Mannowetz N, Naidoo NM, Choo S-AS, Smith JF & Lishko PV. 2013. Slo1 is the principal potassium channel of human spermatozoa. *elife.* 2, e01009
- Marquez B & Suarez SS. 2007. Bovine sperm hyperactivation is promoted by alkaline-stimulated Ca^{2+} influx. *Biol Reprod*, 76, 660–5.

- Marquez B, Ignatz G. & Suarez SS. 2007. Contributions of extracellular and intracellular Ca^{2+} to regulation of sperm motility: Release of intracellular stores can hyperactivate CatSper1 and CatSper2 null sperm. *Dev Biol.*, 303, 214–21.
- Martínez-López P, Santi CM, Treviño CL, Ocampo-Gutiérrez AY, Acevedo JJ, Alisio A, Salkoff LB, Darszon A. 2009. Mouse sperm K^+ currents stimulated by pH and cAMP possibly coded by Slo3 channels. *Biochem Biophys Res Commun.*, 381, 204–9.
- Mitra A, Richardson R.T. & O’Rand M.G. 2010. Analysis of recombinant human semenogelin as an inhibitor of human sperm motility. *Biol Reprod*, 82, 489–96.
- Mortimer S T, Swan M. A & Mortimer D. 1998. Effect of seminal plasma on capacitation and hyperactivation in human spermatozoa. *Hum Reprod*, 13, 2139–46.
- Mortimer S T. 2000. CASA — Practical Aspects Andrology Lab Corner. *J Androl*, 21, 515–24.
- Munire M, Shimizu Y, Sakata Y, Minaguchi R, Aso T. 2004. Impaired hyperactivation of human sperm in patients with infertility. *J Med Dent Sci*, 51, 99–104.
- NICE, 2013. *Assessment and treatment for people with fertility problems*,
- NIG, 2013. *National infertility group report January 2013*,
- Nallella KP, Sharma RK, Aziz N, Agarwal A. 2006. Significance of sperm characteristics in the evaluation of male infertility. *Fertil Steril.* 85, 629–34.
- Lefièvre L, Nash K, Mansell S, Costello S, Punt E, Correia J, Morris J, Kirkman-Brown J, Wilson SM, Barratt CL, Publicover S. 2012. 2-APB-potentiated channels amplify CatSper-induced Ca^{2+} signals in human sperm. *Biochem J*, 1, 189–200.
- Navarro B, Kirichok Y, Chung JJ, Clapham DE. 2008. Ion channels that control fertility in mammalian spermatozoa. *Int J Dev Biol.*, 52, 607–13.
- Navarro B, Kirichok Y. & Clapham DE. 2007. KSper, a pH-sensitive K^+ current that controls sperm membrane potential. *Proc Natl Acad Sci U S A.*, 104, 7688–92.
- Navarro B, Miki K. & Clapham DE. 2011. ATP-activated P2X2 current in mouse spermatozoa. *Proc Natl Acad Sci U S A.* 108, 14342–14347.
- Grissmer S, Nguyen AN, Aiyar J, Hanson DC, Mather RJ, Gutman GA, Karmilowicz MJ, Auperin DD, Chandy KG. 1994. Pharmacological characterization of five cloned voltage-gated K^+ channels, types Kv1.1, 1.2, 1.3, 1.5, and 3.1, stably expressed in mammalian cell lines. *Mol Pharmacol*, 45, 1227–1234.
- Oehninger S, Franken DR, Sayed E, Barroso G, Kolm P. 2000. Sperm function assays and their predictive value for fertilization outcome in IVF therapy: a meta-analysis. *Human Reprod Update*, 6, 160–8.

- Orta G, Ferreira G, José O, Treviño CL, Beltrán C, Darszon A. 2012. Human spermatozoa possess a calcium-dependent chloride channel that may participate in the acrosomal reaction. *J Physiol.*, 590, 2659–75.
- Patrat C, Serres C & Jouannet P. 2002. Progesterone induces hyperpolarization after a transient depolarization phase in human spermatozoa. *Biol Reprod*, 66, 1775–80.
- Perchenet L & Clement-Chomienne O. 2000. Characterization of Mibefradil block of the human heart. *J. Pharmacol. Exp. Ther.*, 295, 771–778.
- Publicover S, Harper C.V, & Barratt C., 2007. $[Ca^{2+}]_i$ signalling in sperm-making the most of what you've got. *Nature Cell Biology*, 9, 235–42.
- Qi H, Moran MM, Navarro B, Chong JA, Krapivinsky G, Krapivinsky L, Kirichok Y, Ramsey IS, Quill TA, Clapham DE. 2007. All four CatSper ion channel proteins are required for male fertility and sperm cell hyperactivated motility. *Proc Natl Acad Sci U S A.*, 104, 1219–23.
- Quill TA, Ren D, Clapham DE, Garbers DL. 2001. A voltage-gated ion channel expressed specifically in spermatozoa. *Proc Natl Acad Sci U S A.*, 98, 12527–31.
- Quill TA, Sugden SA, Rossi KL, Doolittle LK, Hammer RE, Garbers DL. 2003. Hyperactivated sperm motility driven by CatSper2 is required for fertilization. *Proc Natl Acad Sci U S A.*, 100, 14869–74
- Ramsey IS, Moran MM, Chong JA, Clapham DE. 2006. A voltage-gated proton-selective channel lacking the pore domain. *Nature*, 440, 1213–6.
- Ren D, Navarro B, Perez G, Jackson AC, Hsu S, Shi Q, Tilly JL, Clapham DE. 2001. A sperm ion channel required for sperm motility and male fertility. *Nature*, 413, 603–9.
- Ren D & Xia, J., 2010. Calcium signaling through CatSper channels in mammalian fertilization. *Physiology (Bethesda, Md.)*, 25, 165–75.
- Saegusa H, Kurihara T, Zong S, Minowa O, Kazuno A, Han W, Matsuda Y, Yamanaka H, Osanai M, Noda T, Tanabe T. 2000. Altered pain responses in mice lacking alpha1E subunit of the voltage-dependent Ca^{2+} channel. *Proc Natl Acad Sci U S A.*, 97, 6132–37.
- Santi CM, Butler A, Kuhn J, Wei A, Salkoff L. 2009. Bovine and mouse SLO3 K^+ channels: evolutionary divergence points to an RCK1 region of critical function. *J Biol Chem.*, 284, 21589–98.
- Santi CM, Martínez-López P, de la Vega-Beltrán JL, Butler A, Alisio A, Darszon A, Salkoff L. 2010. The SLO3 sperm-specific potassium channel plays a vital role in male fertility. *FEBS Lett*, 584, 1041–1046.
- Sasaki M, Takagi M. & Okamura Y. 2006. A voltage sensor-domain protein is a voltage-gated proton channel. *Science*, 312, 589–92.

- Schreiber M, Wei A, Yuan A, Gaut J, Saito M, Salkoff L 1998. Slo3, a novel pH-sensitive K⁺ channel from mammalian spermatocytes. *J Biol Chem.*, 273, 3509–16.
- Schuel H, Burkman LJ, Lippes J, Crickard K, Mahony MC, Giuffrida A, Picone RP, Makriyannis A. 2002. Evidence that anandamide-signaling regulates human sperm functions required for fertilization. *Mol Reprod Dev.*, 63, 376–87.
- Shalgi R, & Phillips D.M. 1988. Motility of rat spermatozoa at the site of fertilization. *Biol Reprod*, 39, 1207–13.
- Shieh CC, Coghlan M, Sullivan JP, Gopalakrishnan M. 2000. Potassium channels: molecular defects, diseases, and therapeutic opportunities. *Pharmacol Rev.*, 52, 557–94.
- Smith JF, Syrityna O, Fellous M, Serres C, Mannowetz N, Kirichok Y, Lishko PV. 2013. Disruption of the principal, progesterone-activated sperm Ca²⁺ channel in a CatSper2-deficient infertile patient. *Proc Natl Acad Sci U S A.*, 110, 6823–6828.
- Smith, E. & Yang, P., 2004. The Radial spokes and central apparatus: mechano-chemical transducers that regulate flagellar motility. *Cell Motil Cytoskeleton*, 57, 8–17.
- Strünker T, Goodwin N, Brenker C, Kashikar ND, Weyand I, Seifert R, Kaupp UB. 2011. The CatSper channel mediates progesterone-induced Ca²⁺ influx in human sperm. *Nature*, 471, 382–6.
- Su T, Xue L. & Ozcan, A., 2012. High-throughput lensfree 3D tracking of human sperms reveals rare statistics of helical trajectories. *Proc Natl Acad Sci U S A*, 109, 16018–16022.
- Suárez, S S, Katz, D.F. & Overstreet, J.W., 1983. Movement characteristics and acrosomal status of rabbit spermatozoa recovered at the site and time of fertilization. *Biol Reprod*, 29, 1277–87.
- Suárez, S.S, 2008. Control of hyperactivation in sperm. *Hum Reprod update*, 14, 647–57.
- Suárez, S.S & Dai, X., 1992. Hyperactivation Enhances Mouse Sperm Capacity for Penetrating Viscoelastic Media. *Biol Reprod*, 46, 686–691.
- Sukcharoen N, Keith J, Irvine DS, Aitken RJ. 1995. Definition of the optimal criteria for identifying hyperactivated human spermatozoa at 25 Hz using in-vitro fertilization as a functional end-point. *Human reproduction*, 10, 2928–37.
- Suzuki, M., Morita, T. & Iwamoto, T, 2006. Diversity of Cl⁻ channels. *Cell Mol Life Sci.*, 63,12–24.
- Suárez, S.S. & Osman, R. A, 1987. Initiation of hyperactivated flagellar bending in mouse sperm within the female reproductive tract. *Biol Reprod*, 36, 1191–8.

- Sánchez, D, Labarca, P. & Darszon, A, 2001. Sea urchin sperm cation-selective channels directly modulated by cAMP. *FEBS lett*, 503, 111–5.
- Tang QY, Zhang Z, Xia J, Ren D, Logothetis DE. 2010. Phosphatidylinositol 4,5-bisphosphate activates Slo3 currents and its hydrolysis underlies the epidermal growth factor-induced current inhibition. *J Biol Chem.*, 285, 19259–66.
- Thomas, P. & Meizel, S., 1989. Phosphatidylinositol 4,5-bisphosphate hydrolysis in human sperm stimulated with follicular fluid or progesterone is dependent upon Ca^{2+} influx. *J. Biochem*, 264, 539–46.
- Tombola, F., Ulbrich, M.H. & Isacoff, E.Y., 2008. The voltage-gated proton channel H_v1 has two pores each controlled by one voltage sensor. *Neuron*, 58, 546–556.
- Tomlinson, J., Kessopoulou, E. & Barratt, CLR, 1999. The diagnostic and prognostic value of traditional semen parameters. *J. Androl*, 20, 588–93.
- Turner, R.M., 2003. Tales from the tail: what do we really know about sperm motility? *J. Androl*, 24, 790–803.
- Visconti PE, Westbrook VA, Chertihin O, Demarco I, Sleight S, Diekman AB. 2002. Novel signaling pathways involved in sperm acquisition of fertilizing capacity. *J Reprod Immunol.*, 53, 133–50.
- Visconti PE, Moore GD, Bailey JL, Leclerc P, Connors SA, Pan D, Olds-Clarke P, Kopf GS 1995. Capacitation of mouse spermatozoa pathway II. Protein tyrosine phosphorylation and capacitation are regulated by a cAMP- dependent pathway. *Development*, 1150, 1139–1150.
- Visconti PE, Ning X, Fornés MW, Alvarez JG, Stein P, Connors SA, Kopf GS. 1999. Cholesterol efflux-mediated signal transduction in mammalian sperm: cholesterol release signals an increase in protein tyrosine phosphorylation during mouse sperm capacitation. *Dev Biol.*, 274, 429–43.
- de Vries KJ, Wiedmer T, Sims PJ, Gadella BM. 2003. Caspase-Independent Exposure of Aminophospholipids and Tyrosine Phosphorylation in Bicarbonate Responsive Human Sperm Cells. *Biol Reprod.*, 68, 2122–2134.
- WHO, 2010. *Examination and processing of human semen* 5th ed.,
- Wang D, King SM, Quill TA, Doolittle LK, Garbers DL. 2003. A new sperm-specific Na^+/H^+ exchanger required for sperm motility and fertility. *Nat Cell Biol.*, 5, 1117–22.
- Wang D, Hu J, Bobulescu IA, Quill TA, McLeroy P, Moe OW, Garbers DL. 2007. A sperm-specific Na^+/H^+ exchanger (sNHE) is critical for expression and in vivo bicarbonate regulation of the soluble adenylyl cyclase (sAC). *Proc Natl Acad Sci U S A.*, 104, 9325–30.

- Wang H, Liu J, Cho KH, Ren D. 2009. A novel, single, transmembrane protein CATSPERG is associated with CATSPER1 channel protein. *Biol Reprod.*, 81, 539–44.
- Wennemuth G, Westenbroek RE, Xu T, Hille B, Babcock DF. 2000. $\text{Ca}_v2.2$ and $\text{Ca}_v2.3$ (N- and R-type) Ca^{2+} channels in depolarization-evoked entry of Ca^{2+} into mouse sperm. *J Biol Chem.*, 275, 21210–7.
- Wertheimer EV, Salicioni AM, Liu W, Trevino CL, Chavez J, Hernández-González EO, Darszon A, Visconti PE. 2008. Chloride is essential for capacitation and for the capacitation-associated increase in tyrosine phosphorylation. *J Biol Chem.*, 283, 35539–50.
- Wickenden, A, Priest, B. & Erdemli, G., 2012. Ion channel drug discovery: challenges and future directions. *Future Med Chem.*, 4, 661–79.
- Wild S, Roglic G, Green A, Sicree R, King H. 2004. Estimates for the year 2000 and projections for 2030. *Diabetes Care*, 27, 1047–1053.
- Wilton LJ, Teichtahl H, Temple-Smith PD, de Kretser DM. 1985. Structural heterogeneity of the axonemes of respiratory cilia and sperm flagella in normal men. *J Clin Invest.*, 75, 825–831.
- Woo, A.L., James, P.F. & Lingrel, J.B., 2002. Roles of the Na,K-ATPase alpha4 isoform and the Na^+/H^+ exchanger in sperm motility. *Mol Reprod Dev.*, 62, 348–56.
- Worrell RT, Butt AG, Cliff WH, Frizzell RA. 1989. A volume-sensitive chloride conductance in human colonic cell line T84. *Am J Physiol.*, 256, 1111–1119.
- Yang C, Zeng XH, Zhou Y, Xia XM, Lingle CJ. 2011. LRRC52 (leucine-rich-repeat-containing protein 52), a testis-specific auxiliary subunit of the alkalization-activated Slo3 channel. *Proc Natl Acad Sci U S A.*, 108, 19419–24.
- Yang J, Serres C, Philibert D, Robel P, Baulieu EE, Jouannet P. 1994. Progesterone and RU486: opposing effects on human sperm. *Proc Natl Acad Sci U S A.*, 91, 529–33.
- Yang YD, Cho H, Koo JY, Tak MH, Cho Y, Shim WS, Park SP, Lee J, Lee B, Kim BM, Raouf R, Shin YK, Oh U. 2008. TMEM16A confers receptor-activated calcium-dependent chloride conductance. *Nature*, 455, 1210–5.
- Yeung, C.H., Barfield, J.P. & Cooper, T.G., 2005. Chloride channels in physiological volume regulation of human spermatozoa. *Biol Reprod*, 73, 1057–63.
- Yoshida K, Yamasaki T, Yoshiike M, Takano S, Sato I, Iwamoto T. 2003. Quantification of seminal plasma motility inhibitor/semenogelin in human seminal plasma. *J Androl.*, 24, 878–84.

- Young HS, Skita V, Mason RP, Herbette LG. 1992. Molecular basis for the inhibition of 1,4-dihydropyridine calcium channel drugs binding to their receptors by a nonspecific site interaction mechanism. *Biophys J.*, 61,1244–55.
- Zeng XH, Yang C, Kim ST, Lingle CJ, Xia XM. 2011. Deletion of the Slo3 gene abolishes alkalization-activated K^+ current in mouse spermatozoa. *Proc Natl Acad Sci U S A.*, 108, 5879–84.
- Zeng XH, Navarro B, Xia XM, Clapham DE, Lingle CJ. 2013. Simultaneous knockout of Slo3 and Catsper1 abolishes all alkalization- and voltage-activated current in mouse spermatozoa. *J. Gen. Physiol.*, 142, 305–313.
- Zeng Y, Oberdorf JA, Florman HM. 1996. pH regulation in mouse sperm: identification of Na^+ -, Cl^- -, and HCO_3^- -dependent and arylaminobenzoate-dependent regulatory mechanisms and characterization of their roles in sperm capacitation. *Dev Biol.*, 173, 510–20.
- Zeng Y, Clark EN, Florman HM. 1995. Sperm membrane potential : Hyperpolarisation during capacitation regulates zona pellucida- dependent Acrosomal secretion. *Dev Biol.*, 171, 554–563
- Zhang, X., Zeng, X. & Lingle, C.J., 2006. Slo3 K^+ channels: Voltage and pH dependence of macroscopic currents. *J Gen Physiol.*, 128, 301–15.
- Zhang Y, Malekpour M, Al-Madani N, Kahrizi K, Zanganeh M, Lohr NJ, Mohseni M, Mojahedi F, Daneshi A, Najmabadi H, Smith RJ. 2007. Sensorineural deafness and male infertility: a contiguous gene deletion syndrome. *J Med Genet.*, 44, 233–40.

Appendix

RESEARCH SPERM DONORS - QUESTIONNAIRE

Full Name.....D.O.B.....

Address.....

.....

.....Current Occupation.....

E-mail address:.....@.....

Telephone (mobile number preferred):.....

- | | | | |
|-----|--|-----|----|
| 1. | Are you married or do you have a current girlfriend? | Yes | No |
| 2. | Have you had more than two sexual partners this year? | Yes | No |
| 3. | Have you ever contributed to a pregnancy? | Yes | No |
| 4. | Have you ever had a homosexual relationship? | Yes | No |
| 5. | Have you ever taken illegal drugs intravenously? | Yes | No |
| 6. | Have you ever been treated for a sexually transmitted disease? | Yes | No |
| 7. | Have you ever received a blood transfusion? | Yes | No |
| 8. | Do you smoke?
If YES: How much?..... | Yes | No |
| 9. | Do you consume alcohol beverages?
If YES: estimate weekly consumption..... | Yes | No |
| 10. | Have you ever taken prescribed drugs that may interfere with reproductive functions or "recreational drugs"? | Yes | No |
| 11. | Do you wish to be told if results of our analyses indicate potential problems with your general health or fertility? | Yes | No |

Consent

I consent for the semen samples that I provide to be used for research purposes, as detailed on the informed consent sheet.

I confirm I have read, understand and accept the above information.

Signed.....Date...../...../.....

Staff Member.....Signature.....Date..../..../.....

All data and information will be kept in accordance with the Data Protection Act 1998. The Data Controller for the purposes of this Act is The Assisted Conception Unit, Ninewells Hospital and any questions regarding the storage or access to this data should be addressed to the data controller.

2-APB-potentiated channels amplify CatSper-induced Ca^{2+} signals in human sperm

Linda LEFIÈVRE*†, Katherine NASH‡, Steven MANSELL§, Sarah COSTELLO‡, Emma PUNT‡, Joao CORREIA†‡, Jennifer MORRIS‡, Jackson KIRKMAN-BROWN*†, Stuart M. WILSON§, Christopher L. R. BARRATT§ and Stephen PUBLICOVER†‡¹

*Medical School, University of Birmingham, Birmingham B15 2TT, U.K., †Birmingham Women's Hospital, Birmingham B15 2TG, U.K., ‡School of Biosciences, University of Birmingham, Birmingham B15 2TT, U.K., and §Division of Cardiovascular Medicine, Medical Research Institute, Ninewells Hospital University of Dundee, Dundee DD1 9SY, Scotland, U.K.

Ca^{2+}_i signalling is pivotal to sperm function. Progesterone, the best-characterized agonist of human sperm Ca^{2+}_i signalling, stimulates a biphasic $[\text{Ca}^{2+}]_i$ rise, comprising a transient and subsequent sustained phase. In accordance with recent reports that progesterone directly activates CatSper, the $[\text{Ca}^{2+}]_i$ transient was detectable in the anterior flagellum (where CatSper is expressed) 1–2 s before responses in the head and neck. Pre-treatment with 5 μM 2-APB (2-aminoethoxydiphenyl borate), which enhances activity of store-operated channel proteins (Orai) by facilitating interaction with their activator [STIM (stromal interaction molecule)] 'amplified' progesterone-induced $[\text{Ca}^{2+}]_i$ transients at the sperm neck/midpiece without modifying kinetics. The flagellar $[\text{Ca}^{2+}]_i$ response was unchanged. 2-APB (5 μM) also enhanced the sustained response in the midpiece, possibly reflecting mitochondrial Ca^{2+} accumulation downstream of the potentiated $[\text{Ca}^{2+}]_i$ transient. Pre-treatment with 50–100 μM 2-APB failed to potentiate the transient and suppressed sustained $[\text{Ca}^{2+}]_i$ elevation. When applied during the $[\text{Ca}^{2+}]_i$

plateau, 50–100 μM 2-APB caused a transient fall in $[\text{Ca}^{2+}]_i$, which then recovered despite the continued presence of 2-APB. Loperamide (a chemically different store-operated channel agonist) enhanced the progesterone-induced $[\text{Ca}^{2+}]_i$ signal and potentiated progesterone-induced hyperactivated motility. Neither 2-APB nor loperamide raised pH_i (which would activate CatSper) and both compounds inhibited CatSper currents. STIM and Orai were detected and localized primarily to the neck/midpiece and acrosome where Ca^{2+} stores are present and the effects of 2-APB are focussed, but store-operated currents could not be detected in human sperm. We propose that 2-APB-sensitive channels amplify $[\text{Ca}^{2+}]_i$ elevation induced by progesterone (and other CatSper agonists), amplifying, propagating and providing spatio-temporal complexity in $[\text{Ca}^{2+}]_i$ signals of human sperm.

Key words: calcium, CatSper, hyperactivation, progesterone, sperm, store-operated channel.

INTRODUCTION

Within the female tract, mammalian sperm receive essential 'cues' from the tract itself and from the cumulus–oocyte complex. These cues regulate a variety of the sperm's activities through Ca^{2+} signalling [1]. Although $[\text{Ca}^{2+}]_i$ signals in sperm are diverse and often complex [1], patch-clamp studies have, so far, detected only a handful of channels, and only one Ca^{2+} -permeable channel, the pH_i -regulated channel CatSper, which is expressed only in the sperm flagellum [2,3]. CatSper is sensitive to pH_i , E_m (membrane potential) and a range of small organic molecules, such that it can be viewed as a 'polymodal chemosensor' [4]. Thus sperm Ca^{2+} signals, even those in the head, may be mediated primarily or completely through CatSper [4,5].

Progesterone, which is present at high micromolar levels in the cumulus and at low concentrations throughout the tract, is by far the best characterized natural agonist of human sperm activity, modulating the crucial functions of motility and acrosome reaction [6]. These effects are exerted through Ca^{2+} influx, which generates a $[\text{Ca}^{2+}]_i$ transient followed by a prolonged plateau [7,8]. This $[\text{Ca}^{2+}]_i$ signal is correlated with fertility [9,10], illustrating the importance of progesterone [and/or the signalling

process(es) that it activates] in sperm function. Consistent with a central role for CatSper channels in sperm $[\text{Ca}^{2+}]_i$ signalling, it has recently been shown that progesterone activates CatSper in human sperm [11,12]. A key question, therefore, is whether this CatSper-mediated Ca^{2+} entry is sufficient to explain fully progesterone-induced Ca^{2+} signalling in sperm and its crucial effects on sperm function.

Blackmore [13] and, more recently, Park et al. [14] proposed that CCE (capacitative Ca^{2+} entry), the process by which mobilization of stored Ca^{2+} induces Ca^{2+} -influx at the plasmalemma [15], may contribute to the action of progesterone. CCE requires both a membrane Ca^{2+} -permeable channel and a mechanism by which $[\text{Ca}^{2+}]_i$ in the store is monitored. In somatic cells, the protein STIM (stromal interaction molecule) situated in the endoplasmic reticulum membrane detects luminal $[\text{Ca}^{2+}]_i$. Upon store mobilization, STIM redistributes into 'puncta' adjacent to the plasma membrane, where it activates Ca^{2+} -permeable SOC (store-operated channels) [16]. SOC proteins include the Orai family (also named CRACM) and possibly members of the TRPC (transient receptor potential canonical) family, which may form heterologous tetramers with Orai subunits [17–19].

Abbreviations used: 2-APB, 2-aminoethoxydiphenyl borate; BCECF, 2',7'-bis-(2-carboxyethyl)-5(6)-carboxyfluorescein; CCD, charge-coupled-device; CCE, capacitative Ca^{2+} entry; DVF, divalent-free; GFP, green fluorescent protein; HEK, human embryonic kidney; IP_3R , inositol trisphosphate receptor; OGB, Oregon Green BAPTA; PHN, posterior head and neck; sEBSS, supplemented Earle's balanced salt solution; SERCA, sarcoplasmic/endoplasmic reticulum Ca^{2+} -ATPase; SOC, store-operated channel; STIM, stromal interaction molecule; TRPC, transient receptor potential canonical; TRPV3, transient receptor potential vanilloid 3.

¹ To whom correspondence should be addressed (email s.j.publicover@bham.ac.uk).

In cells transfected with STIM, low doses ($<10 \mu\text{M}$) of 2-APB (2-aminoethoxydiphenyl borate) [20] potentiate CCE by promoting the interaction of STIM with SOCs and also regulating gating of the channel [21–23]. 2-APB can also activate some STIM–Orai complexes without store mobilization [24–26]. At higher concentrations ($\geq 50 \mu\text{M}$), the drug inhibits CCE, although this effect is dependent on the isoform of Orai expressed [24,25,27,28]. 2-APB can affect other aspects of Ca^{2+} signalling [29,30] but these non-target effects occur at high doses ($\geq 100 \mu\text{M}$; IC_{50} for inhibition of microsomal IP_3Rs (inositol triphosphate receptors) = 220–1000 μM and IC_{50} for SERCA (sarcoplasmic/endoplasmic reticulum Ca^{2+} -ATPase) = 375–725 μM depending on isoform [31,32]). In the present study we report that Ca^{2+} signalling activated by progesterone is amplified by low concentrations of 2-APB and by loperamide, another modulator of these channels. These effects are not exerted through CatSper and are localized to the sperm neck and midpiece where Ca^{2+} stores are present and where we detect expression of STIM and Orai proteins.

EXPERIMENTAL

Saline solutions

sEBSS (supplemented Earle's balanced salt solution) contained 1.0167 mM NaH_2PO_4 , 5.4 mM KCl, 0.811 mM $\text{MgSO}_4 \cdot 7\text{H}_2\text{O}$, 5.5 mM $\text{C}_6\text{H}_{12}\text{O}_6$, 2.5 mM $\text{C}_3\text{H}_3\text{NaO}_3$, 19.0 mM $\text{CH}_3\text{CH}(\text{OH})\text{COONa}$, 1.8 mM $\text{CaCl}_2 \cdot 2\text{H}_2\text{O}$, 25.0 mM NaHCO_3 , 118.4 mM NaCl and 15 mM Hepes (pH 7.35, 285–295 mOsm), supplemented with 0.3 % fatty-acid-free BSA. In non-capacitating medium (bicarbonate-free sEBSS), NaHCO_3 was omitted and osmotic strength was maintained by adjusting NaCl. Low Ca^{2+} EGTA-buffered sEBSS ($\approx 3 \times 10^{-7}$ M Ca^{2+}) contained 5 mM Ca^{2+} and 6 mM EGTA.

Preparation and capacitation of spermatozoa

Donors were recruited in accordance with the Human and Embryology Authority Code of Practice (Version 7) and gave informed consent (University of Birmingham Life and Health Sciences ERC 07-009 and 08/S1402/6 from the Tayside Committee of Medical Research Ethics B). Cells were harvested by direct swim-up as described previously [33] and adjusted to 6×10^6 cells/ml. Aliquots of 200 μl were left to capacitate for 5–6 h.

For Western blotting analysis and immunoprecipitation, cells were separated from seminal plasma by densitometry using a two-layer Percoll gradient (40 and 80 %) as described previously [34] and were capacitated as described above.

Single-cell imaging of $[\text{Ca}^{2+}]_i$

Loading of cells with OGB {Oregon Green BAPTA [1,2-bis-(*o*-aminophenoxy)ethane-*N,N,N',N'*-tetra-acetic acid] 1} and time-lapse fluorescence imaging was as described previously [33]. All experiments were performed at $25 \pm 0.5^\circ\text{C}$ in a continuous flow of medium {sEBSS or EGTA-buffered saline ($[\text{Ca}^{2+}]_o \approx 3 \times 10^{-7}$ M)}. Images were captured at 0.1 Hz (except where stated otherwise) using a $40\times$ oil-immersion objective and a Q Imaging Rolera-XR cooled CCD (charge-coupled-device) camera or a Andor Ixon 897 EMCCD (electron-multiplying CCD) camera controlled by iQ software (Andor Technology).

Analysis of images, background correction and normalization of data was performed as described previously [33]. Unless stated otherwise, the region of interest was drawn around the PHN

(posterior head and neck) region of each cell. Raw intensity values were imported into Microsoft Excel and normalized using the equation:

$$\Delta F = [(F - F_{\text{rest}})/F_{\text{rest}}] \times 100 \%$$

where ΔF is the percentage change in fluorescence intensity at time t , F is fluorescence intensity at time t and F_{rest} is the mean of ≥ 10 determinations of F during the control period. To compare the responses between experiments, we calculated ΔF_{mean} , the mean ΔF of all the cells ($n = 50$ –200) in the experiment.

The amplitude of the progesterone-induced $[\text{Ca}^{2+}]_i$ transient was calculated from the three points spanning the peak of the ΔF_{mean} trace. Plateau amplitude was calculated from three consecutive points 4 min after application of progesterone. In experiments involving pre-treatment with 2-APB or loperamide transient peak and plateau values were corrected for ΔF (or ΔF_{mean}) immediately before progesterone application (Supplementary Figure S1 at <http://www.BiochemJ.org/bj/448/bj4480189add.htm>).

Population fluorimetry

$[\text{Ca}^{2+}]_i$ assessment was as described previously [35]. For assessment of pH_i , 2 ml aliquots were labelled with 1 μM BCECF-AM [2',7'-bis-(2-carboxyethyl)-5(6)-carboxyfluorescein acetoxymethyl ester; 30 min, 37°C , 5 % CO_2], centrifuged (300 g, 5 min) then resuspended in sEBSS. Sampling rate was 12.5 Hz using excitation 440/495 nm and emission 535 nm. pH_i was calibrated similarly to [36].

Patch-clamp

Whole-cell currents were evoked by 1 s voltage ramps from -80 mV to $+80$ mV from a holding potential of 0 mV (before correction for junction potential). DVF (divalent-free) medium for recording CatSper currents contained 140 mM caesium methanesulfonate, 40 mM Hepes and 1 mM EGTA, pH 7.4, as described by Lishko et al. [11]. The pipette saline contained 130 mM caesium methanesulfonate, 70 mM Hepes, 3 mM EGTA, 2 mM EDTA and 0.5 mM Tris/HCl, pH 7.4.

Detection of proteins by Western blotting

Sperm proteins were extracted using RIPA buffer [150 mM NaCl, 20 mM Tris/HCl, pH 7.4, 2 mM DTT (dithiothreitol) and 1 % Triton X-100] supplemented with 0.5 % SDS and Complete™ protease inhibitor cocktail (Roche). Following brief sonication (MSE Soniprep 150, 20 s at 20°C), samples were incubated for 30 min at 4°C then centrifuged at 18000 g for 15 min at 4°C to remove any insoluble material. Aliquots of supernatant (20 μl) were kept for SDS/PAGE.

Electrophoresis was performed as described previously [37]. Proteins were separated by SDS/PAGE using 10 % gels for STIM and 15 % gels for Orai. Membranes were incubated overnight (4°C) with the respective anti-Orai (1:250 dilution, ProSci; or 1:200 dilution, Sigma) or anti-STIM (1:1000 dilution, ProSci) antibodies. Where possible, pre-adsorption of antibodies with their corresponding antigenic peptides was carried out to assess the specificity of the detection. Antibody (1 μg) was pre-adsorbed with excess (1 μg) peptide for 1 h at room temperature (20°C). Incubations with peptide-pre-adsorbed and non-pre-adsorbed antibodies were performed in parallel.

Immunoprecipitation

Percoll-washed spermatozoa (at least 200×10^6 cells per condition) were solubilized using RIPA buffer supplemented with 0.5% SDS and Complete™ protease inhibitor cocktail. Following brief sonication, samples were incubated at 4°C for 1 h then diluted 10-fold with RIPA buffer to avoid SDS interference with immunoprecipitation procedures. Samples were centrifuged at 18000 g (15 min, 4°C) to remove insoluble material. A pre-clearing step involved incubation with 30 μl of a pre-washed Protein G plus/Protein A-agarose beads (33% slurry suspension; Calbiochem) for 30 min at 4°C followed by a centrifugation at 2500 g (5 min). Pre-cleared sperm lysate was further centrifuged (13000 g, 10 min) and the supernatant was transferred to a fresh microfuge tube and kept at 4°C.

Protein G plus/Protein A-agarose beads (20 μl) (33% slurry suspension) were incubated overnight with 1 μg of antibody in 750 μl of RIPA buffer then washed three times with RIPA buffer and the remaining supernatant was aspirated away. Pre-cleared sperm lysate was then added to the antibody-coated beads and incubated for 90 min (4°C). The immunocomplex was pelleted by centrifugation (2500 g, 5 min) and washed three times with 1 ml of immunoprecipitation buffer followed by twice with 1 ml of PBS. The immunoprecipitated proteins were resuspended in 20 μl of 1 \times SDS sample buffer, incubated at 70°C for 10 min and submitted to SDS/PAGE as described above.

Detection of Orai and STIM by immunofluorescence

Percoll-washed spermatozoa (2×10^5 cells) were prepared for immunocytochemistry as described in [35]. Slides were incubated overnight (4°C) with anti-Orai (1:10 dilution, ProSci and Sigma) and anti-STIM antibodies (1:25 dilution, ProSci). Where possible, pre-adsorption of Orai and STIM antibodies with their corresponding antigenic peptides was carried out (as described above) to assess specificity. Experiments using peptide-pre-adsorbed and non-pre-adsorbed antibodies were performed in parallel. Slides were then prepared as described in [35].

Assessment of distribution of STIM

After capacitation as described above or immediately after swim-up into non-capacitating sEBSS, 200 μl aliquots of spermatozoa were exposed to bis-phenol (15 μM). After 12 min, cells were centrifuged (2000 g, 5 min) then fixed in 4% formaldehyde (6 min). Cells were re-centrifuged, resuspended in PBS, smeared on poly-L-lysine-coated slides and air-dried. Permeabilization, antibody staining and processing for assessment of acrosome reaction were as described above.

Statistical analysis

Values given in the text are means \pm S.E.M. For most comparisons we used ΔF_{mean} values obtained from parallel control and pre-treatment experiments such that 'n' refers to the number of pairs of experiments. Each ΔF_{mean} value was the average of 50–200 normalized single-cell responses. Microsoft Excel was used to calculate correlation coefficients and perform paired or unpaired *t* tests and χ^2 tests as appropriate. Where *n* is the number of cells this is stated.

RESULTS AND DISCUSSION

Effect of 2-APB on resting $[\text{Ca}^{2+}]_i$ in human sperm

Treatment of sperm with 5 μM 2-APB increased $[\text{Ca}^{2+}]_i$ in $\sim 75\%$ of cells, inducing a plateau or a series of transients

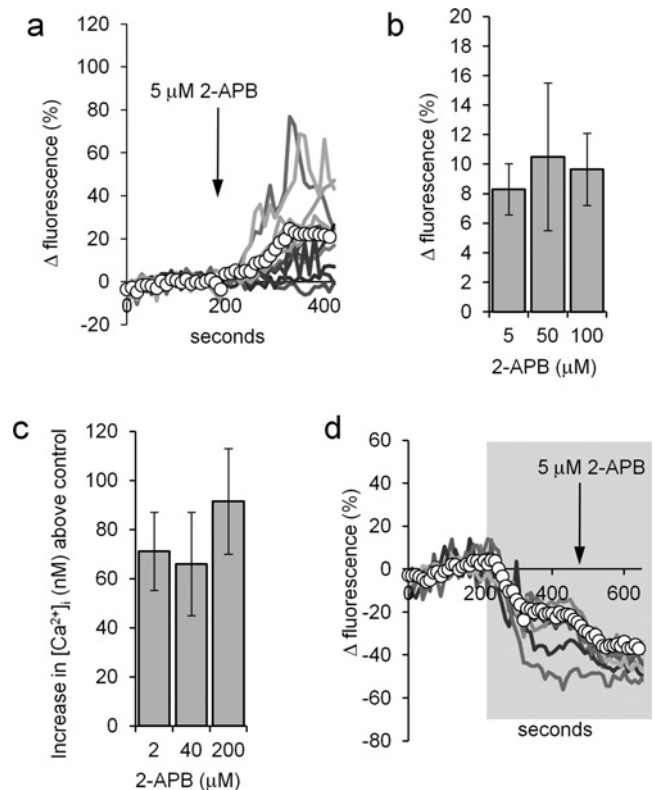


Figure 1 2-APB elevates resting $[\text{Ca}^{2+}]_i$

(a) 2-APB (5 μM ; arrow) causes a sustained increase in the PHN $[\text{Ca}^{2+}]_i$ of a subset of cells. The traces show ten individual cell responses and ΔF_{mean} (○-○) for all 87 cells in the experiment. (b and c) 2-APB-induced $[\text{Ca}^{2+}]_i$ elevation is dose-independent. (b) Increase in ΔF_{mean} 3 min after application of 2-APB. Results are means \pm S.E.M. for sets of four experiments in each of which aliquots from the sample were tested with each of the three concentrations of 2-APB. (c) Dose-dependence of 2-APB-induced $[\text{Ca}^{2+}]_i$ increase in fura-2-loaded cell populations (means \pm S.E.M. for 6–17 experiments). (d) 2-APB-induced rise in $[\text{Ca}^{2+}]_i$ is reversed in low- Ca^{2+} saline. Cells were superfused with EGTA-buffered saline (shown by shading) then exposed to 5 μM 2-APB (arrow). 2-APB-induced $[\text{Ca}^{2+}]_i$ increase was abolished and in many cells 2-APB induced a further fall in $[\text{Ca}^{2+}]_i$. Traces show six individual cell responses and ΔF_{mean} (○-○) for all 85 cells in the experiment.

(Figure 1a). Within ~ 100 s, ΔF_{mean} stabilized at an increased level and at 3 min was $15.6 \pm 3.7\%$ at the PHN and $8.5 \pm 2.9\%$ at the midpiece ($P = 0.008$; paired *t* test, $n = 11$ experiments). Higher doses of 2-APB (up to 100 μM) had similar effects to 5 μM (Figure 1b; $P > 0.5$; paired *t* test, $n = 4$) and the same dose-insensitivity was observed when $[\text{Ca}^{2+}]_i$ was measured in fura-2-loaded cell populations (Figure 1c). When cells were prepared under non-capacitating conditions (BSA and bicarbonate-free sEBSS but containing Ca^{2+}), the increase in resting $[\text{Ca}^{2+}]_i$ induced by 5 μM 2-APB was significantly smaller (PHN ΔF_{mean} at 3 min = $7.4 \pm 2.0\%$; $n = 7$; $P = 0.03$).

Superfusion of capacitated cells with EGTA-buffered medium ($\sim 3 \times 10^{-7}$ M Ca^{2+}) for 3 min prior to the application of 5 μM 2-APB caused a sustained fall in $[\text{Ca}^{2+}]_i$ and abolished the stimulatory effect of 2-APB, showing that the drug was not releasing stored Ca^{2+} . In addition, in more than 20% of cells ($22 \pm 3\%$; $n = 5$) application of 2-APB induced a further $[\text{Ca}^{2+}]_i$ decrease, which was visible as a fall in ΔF_{mean} (Figure 1d). Similar effects were seen with 50 and 100 μM 2-APB. This reversal of the effect of 2-APB upon buffering of $[\text{Ca}^{2+}]_o$ shows that it acts by increasing plasma membrane Ca^{2+} permeability.

2-APB might increase membrane Ca^{2+} flux by activating CatSper either directly [4] or by cytoplasmic alkalinization [11].

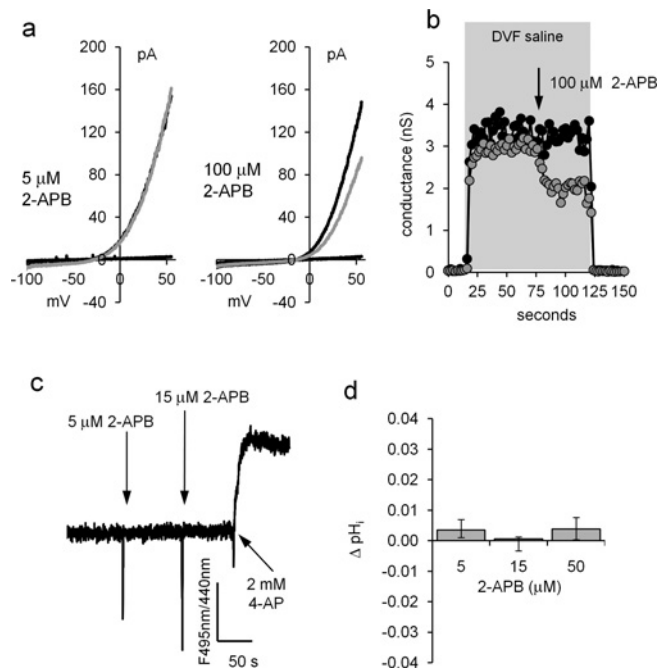


Figure 2 2-APB does not enhance CatSper currents

(a) Monovalent CatSper currents recorded before (black trace) and after (grey trace) application of 5 μM (left-hand panel) and 100 μM (right-hand panel) 2-APB. Horizontal (near zero) traces show currents in divalent cation-containing saline. (b) Time course of CatSper current block by 100 μM 2-APB. Cell conductance was calculated from the slope between +50 and +60 mV. Grey shading shows superfusion with DVF saline, arrow shows application of 2-APB. (c) 2-APB does not raise pH_i. 2-APB at 5 and 15 μM was added at the first and second arrows respectively. 4-Aminopyridine (2 mM; 4-AP; positive control) caused an immediate rise in pH_i. (d) Mean pH_i change (± S.E.M.) in response to 5 μM (*n* = 6), 15 μM (*n* = 3) and 50 μM (*n* = 3) 2-APB.

When human sperm monovalent CatSper currents were measured by whole-cell patch-clamping, the I–V curve showed a virtual absence of inward current, as described by Lishko et al. [11] using the same recording conditions. 2-APB (5 μM) had no effect on the large outward current (measured at +55 mV; *P* > 0.4, *n* = 6), but at 100 μM the current was inhibited by 43 ± 4% (*P* < 0.0002; *n* = 8; Figures 2a and 2b). We assessed the effect of 2-APB on pH_i using BCECF. Concentrations of 2-APB at 5, 15 and 50 μM increased pH_i by 0.003 ± 0.002, 0.001 ± 0.004 and 0.004 ± 0.003 respectively (not significant, *n* = 3; Figures 2c and 2d). In the absence of store mobilization, 2-APB dose-independently activates a plasma membrane Ca²⁺-permeable channel in human sperm that is not CatSper. 2-APB, at doses from 2 to 100 μM, has been shown to activate Ca²⁺ influx and SOC currents without mobilization of stored Ca²⁺ in cells expressing Orai 3 (where a change in pore characteristics occurred) [24,25] and also in cells co-expressing Orai with STIM2 [26].

2-APB enhances the progesterone-induced [Ca²⁺]_i transient

The non-genomic action of progesterone on [Ca²⁺]_i in human sperm has a biphasic dose–effect relationship, apparently reflecting effects at high- and low-affinity receptors [12,38]. Experiments were carried out using 3 μM progesterone because: (i) this dose reflects concentrations in follicular fluid and the cumulus oophorus [39]; and (ii) in our previous imaging and fluorimetric studies, this concentration fully saturated the high-affinity [Ca²⁺]_i response but did not recruit a low-affinity receptor response [40]. The latter is important, since exceeding the

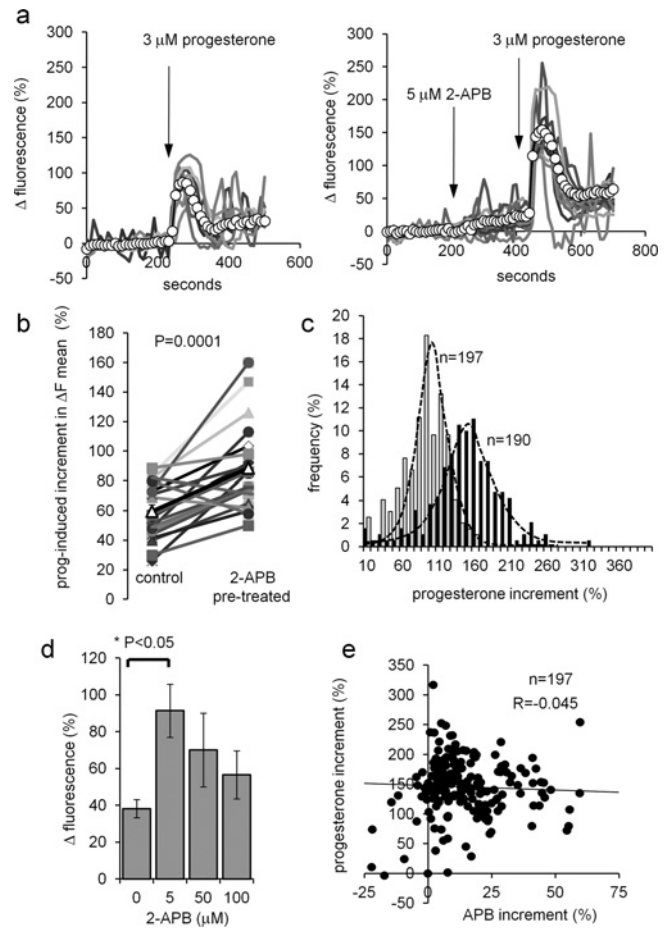


Figure 3 2-APB modulates the progesterone-induced [Ca²⁺]_i transient

(a) Elevation of [Ca²⁺]_i at the PHN in response to stimulation with 3 μM progesterone (arrow) under control conditions (left-hand panel) and after 200 s exposure to 5 μM 2-APB (right-hand panel). Both experiments used cells from the same preparation. Traces show 6–8 representative single-cell responses and ΔF_{mean} (○–○) for all 107 (left-hand panel) and 125 (right-hand panel) cells in the experiment. (b) Summary of results from 20 pairs of control and 5 μM 2-APB-pre-treated experiments. Each point shows the mean amplitude of the progesterone-induced transient (increment in ΔF_{mean}) for all of the cells in a single experiment (50–200 cells). Joined pairs of points show 5 μM 2-APB pre-treatment (right-hand point) and corresponding control (left-hand point) using cells from the same ejaculate – such as the pair shown in (a). Data from 20 pairs of experiments are shown and the overall mean for all 20 is shown by Δ–Δ. (c) Effect of 5 μM 2-APB on amplitude distribution of single-cell progesterone-induced transients. Grey bars show the control, black bars show the parallel 5 μM 2-APB-pre-treated experiment. (d) Dose-dependence of potentiation by 2-APB of the progesterone-induced [Ca²⁺]_i transient. Each bar shows the mean amplitude ± S.E.M. for four sets of experiments (50–200 cells each). In each set, four experiments were carried out with samples from the same ejaculate, using 0, 5, 50 or 100 μM 2-APB applied 200 s before progesterone. Only 5 μM 2-APB significantly enhanced the [Ca²⁺]_i transient. (e) Amplitude of 2-APB-induced resting [Ca²⁺]_i elevation (APB increment; x-axis) is not correlated with the amplitude of subsequent progesterone-induced [Ca²⁺]_i transient (progesterone increment; y-axis). Results are from 197 cells in one experiment.

saturation dose will both minimize effects of any variation in the concentration profile occurring during progesterone application and reduce any effects of 2-APB on the affinity of progesterone for its receptor. These effects could profoundly affect the responses to sub-saturating concentrations of progesterone.

[Ca²⁺]_i in PHN

In PHN, 3 μM progesterone induced a transient increase in [Ca²⁺]_i followed by a plateau in >90% of cells that was clearly visible in the ΔF_{mean} trace (Figure 3a, ○–○) [41]. To test the

effect of 2-APB on this response, experiments were carried out in pairs, where cells from the same semen sample were exposed to 3 μ M progesterone with and without 2-APB pre-treatment. In 17 out of 20 experiment pairs, pre-treatment with 5 μ M 2-APB (200 s) enhanced the amplitude of the progesterone-induced increment in ΔF_{mean} (pre-treated/control ratio = 1.58 ± 0.13 , $n = 20$; $P = 0.0001$, paired t test; Figures 3a and 3b). Population (fluorimetric) recordings from fura-2-loaded cells confirmed this observation, 2 μ M 2-APB increasing the amplitude of the [Ca²⁺]_i transient from 137 ± 28 nM to 289 ± 42 nM ($P = 0.0005$; $n = 14$). These effects occurred at doses $>50\times$ lower than the reported IC₅₀ values for inhibition of SERCAs or IP₃Rs [31,32]. That this potentiating action was not associated with the effects of 2-APB on Ca²⁺ clearance mechanisms was confirmed by analysis of the decay kinetics of progesterone-induced [Ca²⁺]_i transients. Inhibition of Ca²⁺ ATPases with bis-phenol (which does not increase the progesterone transient amplitude in human sperm) slows Ca²⁺ clearance, extending decay duration 2–3-fold [42,43]. In contrast, pre-treatment with 2-APB extended decay duration (from ΔF_{mean} peak to inflexion at the end of falling phase) by only 11% (from 107 ± 7 s to 119 ± 7 s; $P = 0.03$; paired t test, $n = 16$) and the absolute rate of decay was increased from 0.80 ± 0.09 to 1.16 ± 0.10 % per second ($P < 0.02$; paired t test, $n = 16$ experimental pairs), consistent with stimulation of Ca²⁺ clearance at increased [Ca²⁺]_i.

In eight experiment pairs where the effect of 5 μ M pre-treatment was large, we compared the amplitude distributions of single-cell [Ca²⁺]_i transients in control and 2-APB-pre-treated cells. The distribution was bell-shaped under control conditions, and in five out of the eight experiments, 5 μ M 2-APB simply shifted this distribution along the axis, only 5–10% of cells generating [Ca²⁺]_i transients of amplitude similar to the parallel control (Figure 3c). In the three other experiments the 2-APB pre-treatment resulted in a bi-modal or ‘smeared’ amplitude distribution (Supplementary Figure S2 at <http://www.BiochemJ.org/bj/448/bj4480189add.htm>).

Pre-treatment with 50 μ M or 100 μ M 2-APB enhanced [Ca²⁺]_i transient amplitude in some experiments (Supplementary Figure S3 at <http://www.BiochemJ.org/bj/448/bj4480189add.htm> and Figure 3d), but this effect was not significant ($P > 0.2$; paired t test, $n = 4$ sets of experiments). There was a clear difference in dose-dependence between the effects of 2-APB on resting [Ca²⁺]_i and on progesterone-induced signalling (compare Figures 1b and 1c with Figure 3d).

The amplitude of the progesterone-induced [Ca²⁺]_i signal in human sperm is capacitation-dependent [44]. We therefore investigated the effect of 5 μ M 2-APB pre-treatment on cells prepared in the absence of bicarbonate and BSA (non-capacitating conditions). The [Ca²⁺]_i transient in these experiments was reduced compared with ‘capacitated’ cells ($\Delta F_{\text{mean}} = 37.6 \pm 7.1$ %, $n = 7$ experiments and 59.6 ± 4.5 %, $n = 20$ experiments respectively; $P < 0.025$), but pre-treatment with 5 μ M 2-APB was still effective, enhancing transient amplitude (82 ± 30 %; $P = 0.017$; $n = 7$ experimental pairs; paired t test), an effect similar to that in cells prepared in capacitating medium ($P = 0.39$).

In experiments where 5 μ M 2-APB pre-treatment caused marked elevation of resting [Ca²⁺]_i, we analysed the relationship between this effect and the amplitude of the response (in the same cell) to subsequent application of progesterone (‘e’ and ‘c’ in Supplementary Figure S1). There was no correlation (Figure 3e; $R = 0.10 \pm 0.08$; $n = 10$ experiments). 2-APB has two discrete effects, potentiating progesterone-induced Ca²⁺ influx at low micromolar doses and also increasing resting Ca²⁺ influx.

[Ca²⁺]_i responses in the flagellum

In OGB-loaded human sperm, fluorescence is most intense at the PHN. This probably reflects the presence of the cytoplasmic droplet in this region and it is likely that the signal from this region also dominates fluorimetric population recordings. However, the initial site of action of progesterone on human sperm is likely to be CatSper channels in the principal piece of the flagellum [11,12]. We therefore compared the effects of 2-APB pre-treatment on progesterone-stimulated [Ca²⁺]_i responses in the PHN with those in the flagellum.

Midpiece. In control experiments, application of progesterone caused a transient rise in [Ca²⁺]_i in the midpiece resembling that occurring at the PHN. Kinetics of rise and decay of ΔF_{mean} were similar ($P > 0.05$; $n = 11$ pairs of experiments). Transient amplitudes in the two regions were correlated ($R = 0.74$; Supplementary Figure S4 at <http://www.BiochemJ.org/bj/448/bj4480189add.htm>), but ΔF_{mean} at the peak was ~ 25 % smaller in the midpiece ($P < 0.002$; $n = 11$ pairs of experiments). After pre-treatment with 5 μ M 2-APB, this relationship was maintained, but midpiece response amplitudes were supplemented by the recruitment of an extra ‘late’ component (Supplementary Figure S4; see below).

Principal piece. In five pairs of experiments (control and 5 μ M 2-APB pre-treatment) we measured the progesterone-induced [Ca²⁺]_i signal in the anterior flagellar principal piece, using only cells where this could be reliably assessed (visible and in focus throughout experiment). Duration of the [Ca²⁺]_i transient in the principal piece was short, 74 ± 8 s compared with 143 ± 8 s in the PHN of the same cells ($P < 0.0005$), but the amplitude (normalized to pre-stimulus fluorescence) was significantly larger ($P = 0.0004$; $n = 43$ cells; Figure 4a). 2-APB pre-treatment enhanced the [Ca²⁺]_i transient recorded at the PHN (compared with controls), but at the principal piece we detected no effect of 2-APB (Figure 4b), such that the ratio of transient amplitude at the PHN/transient amplitude at the principal piece (in the same cell) increased from 0.8 ± 0.1 in control cells to 1.5 ± 0.2 in cells pre-treated with 5 μ M 2-APB ($n = 43$ and $n = 57$ cells respectively; $P = 0.00011$; Figure 4c). We also assessed the effect of 2-APB on progesterone-potentiated CatSper currents. As reported previously [11,12], progesterone increased monovalent CatSper currents, particularly enhancing inward current (Figure 4d). 2-APB (5 μ M) reduced CatSper current amplitude in four out of four experiments, inhibiting inward and outward currents by 21 ± 2 % ($P < 0.02$) and 16 ± 6 % ($P = 0.12$) respectively. 2-APB (100 μ M) inhibited inward and outward currents by 68 ± 2 % ($P = 0.001$) and 72 ± 3 % ($P = 0.0003$) respectively ($n = 6$) (Figure 4d).

Thus 5 μ M 2-APB enhances the progesterone-induced [Ca²⁺]_i transient in the PHN and midpiece but does not enhance CatSper-mediated Ca²⁺-influx. Surprisingly, although 100 μ M 2-APB significantly inhibited monovalent CatSper currents (Figures 2a, 2b and 4d), it failed to reduce the [Ca²⁺]_i transient amplitude (Figure 3d). One possible explanation is that high-dose 2-APB potentiates Ca²⁺ influx similarly to 5 μ M 2-APB [24,25,27,28] and ‘compensates’ a smaller contribution from CatSper. In fact, since the kinetics of the 2-APB-enhanced response closely resemble those of the control response (mean time to peak being identical; $P = 0.5$; $n = 16$ pairs of experiments), 2-APB-sensitive channels may dominate the [Ca²⁺]_i signal recorded at the PHN.

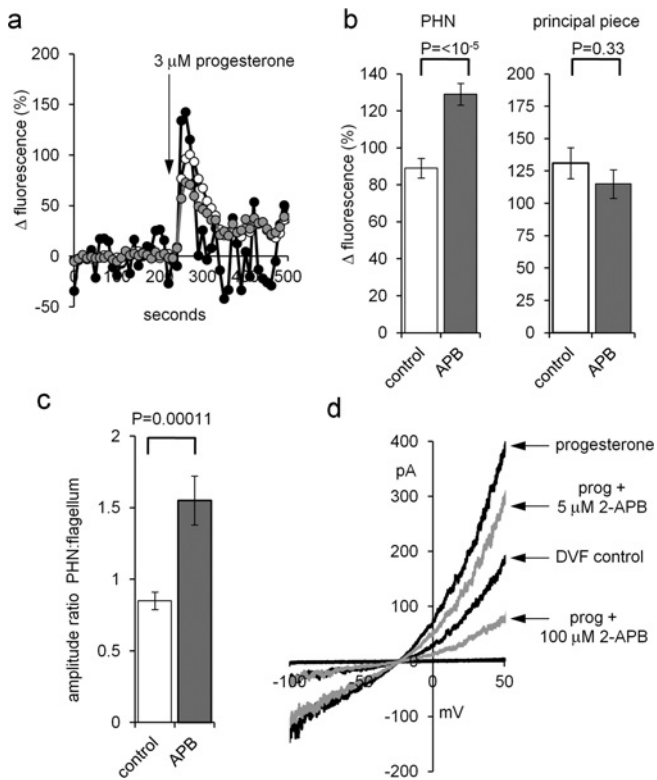


Figure 4 2-APB does not enhance the flagellar Ca^{2+} signal or potentiate activation of CatSper by progesterone

(a) $[\text{Ca}^{2+}]_i$ (OGB) signal from the PHN (white circles), midpiece (grey circles) and flagellum (black circles) in response to application of $3 \mu\text{M}$ progesterone (arrow). Each trace shows the mean response from the same nine cells. (b) Amplitude of progesterone-induced $[\text{Ca}^{2+}]_i$ transient at the PHN (left-hand panel) and midpiece (right-hand panel) under control conditions (white bars; $n = 43$ cells) and after pre-treatment with $5 \mu\text{M}$ 2-APB (grey bars; $n = 57$ cells). (c) Ratio of $[\text{Ca}^{2+}]_i$ transient amplitudes simultaneously recorded from the PHN and flagellum under control conditions (white bar; $n = 43$) and after pre-treatment with $5 \mu\text{M}$ 2-APB (grey bar; $n = 57$). (d) Monovalent currents (DVF control) were enhanced by 500 nM progesterone (upper black trace). Subsequent application of $5 \mu\text{M}$ 2-APB (upper grey trace) and 100 nM 2-APB (lower grey trace) reduced the amplitude of outward and inward currents.

Effects of 2-APB on the progesterone-induced sustained $[\text{Ca}^{2+}]_i$ elevation

Following the progesterone-induced $[\text{Ca}^{2+}]_i$ transient, there is a sustained elevation of $[\text{Ca}^{2+}]_i$ above resting levels. To assess the effect of 2-APB pretreatment on this $[\text{Ca}^{2+}]_i$ plateau, we used the value of ΔF_{mean} recorded 4 min after progesterone application ('b' and 'd' in Supplementary Figure S1). After 2-APB pretreatment, sustained $[\text{Ca}^{2+}]_i$ elevation at the PHN sometimes exceeded that in the parallel control (Figure 3a), but this effect was inconsistent and not significant (ΔF_{mean} at 240 s: control = $19 \pm 2\%$; 2-APB pre-treated = $20 \pm 3\%$; $P = 0.75$; paired t test; $n = 19$ pairs of experiments).

Recently, Park et al. [14] reported that progesterone-induced sustained $[\text{Ca}^{2+}]_i$ elevation was localized to the midpiece. In 11 of the experiment pairs (482 cells) we were able to analyse $[\text{Ca}^{2+}]_i$ at both the PHN and midpiece. As described above, the sustained $[\text{Ca}^{2+}]_i$ response (ΔF_{mean} 240 s after progesterone application) at the PHN showed no effect of pretreatment with $5 \mu\text{M}$ 2-APB (control = $18 \pm 5\%$; 2-APB = $20 \pm 6\%$; $P = 0.66$; $n = 11$ experiment pairs). However, in the same cells, the sustained increase in fluorescence at the midpiece was enhanced >3-fold, from $16 \pm 4\%$ (control) to $52 \pm 12\%$ (2-APB pre-treated; $P = 0.002$; $n = 11$ experiment pairs; Figures 5a–5c).

The amplitude distribution of these 2-APB-enhanced sustained midpiece responses was bimodal (Figures 5b and 5d). When cells were pre-treated with $100 \mu\text{M}$ 2-APB, ΔF_{mean} recorded at the midpiece 240 s after progesterone was significantly smaller than in parallel controls ($P < 0.05$, $n = 6$ experimental pairs; $P < 0.005$; Figure 5c).

Late activation of the midpiece sustained responses

The rising phase of the progesterone-induced $[\text{Ca}^{2+}]_i$ increase in the midpiece of 2-APB-pre-treated cells often showed an inflexion, apparently reflecting a second 'delayed' rise in fluorescence occurring 20–30 s after stimulation (Figure 5e, black trace; arrowhead). In six pairs of experiments where the midpieces were well-immobilized we assessed the occurrence of this 'late' response. Approximately one-third of $5 \mu\text{M}$ 2-APB pre-treated cells ($34 \pm 6\%$; 424 cells in six experiments) showed a clear inflexion, but this pattern of response was rare in parallel controls ($7.6 \pm 2.8\%$; $n = 443$ cells in six experiments; $P = 0.01$; paired t test). This 'late' rise in fluorescence at the midpiece was always followed by a large (>80% at 240 s; see Figure 5d) sustained increase in midpiece fluorescence. Association of these two events was highly non-random ($P = 10^{-10}$; χ^2 test). Thus it appears that the large type of sustained responses observed in the midpiece activates during the rising phase of the $[\text{Ca}^{2+}]_i$ transient, adding a 'step' to the signal. In three experiments we followed the kinetics of the response to progesterone in more detail by using an increased camera frame rate (10 Hz). Consistent with recent reports that progesterone directly activates CatSper channels [11,12], the $[\text{Ca}^{2+}]_i$ response in the anterior principal piece preceded that in the PHN region by 1.6 ± 0.2 s ($n = 29$ cells; $P < 10^{-8}$) (Figure 5f). A similar spatio-temporal pattern has recently been reported upon photolysis of caged progesterone [45]. When a sustained $[\text{Ca}^{2+}]_i$ increase occurred in the midpiece there was often a clear inflexion in the rising phase after 10–30 s (Figures 5f and 5g; Supplementary Movies S1 and S2 at <http://www.BiochemJ.org/bj/448/bj4480189add.htm>).

The sperm midpiece contains the sperm's mitochondria. Since the large 2-APB-potentiated sustained response is localized here and occurs 20–30 s after initiation of the $[\text{Ca}^{2+}]_i$ transient, it is likely that it includes a contribution from OGB within the mitochondrial matrix compartment, which will fluoresce upon mitochondrial Ca^{2+} accumulation. Imaging data do not allow us to distinguish confidently between mitochondrial Ca^{2+} accumulation and a discrete 'late' Ca^{2+} influx at the midpiece, but it may be significant that $5 \mu\text{M}$ 2-APB is reported to slow the export of Ca^{2+} from mitochondria [46]. Since Ca^{2+} uptake by mitochondria is by a low-affinity transporter [47], if this late response reflects mitochondrial Ca^{2+} accumulation it reveals a large increase in $[\text{Ca}^{2+}]_i$ in the midpiece of these sperm.

Application of 2-APB during the sustained component of the progesterone-induced $[\text{Ca}^{2+}]_i$ increase

To investigate further the effects of 2-APB on the sustained $[\text{Ca}^{2+}]_i$ increase, we applied the drug 6–7 min after progesterone stimulation, following completion of the $[\text{Ca}^{2+}]_i$ transient. 2-APB at $5 \mu\text{M}$ caused a reversible tonic increase in fluorescence at the PHN ($21 \pm 6\%$ increase in ΔF_{mean} at 4 min after application, four experiments; Figure 6a). The midpiece did not show the large sustained response that occurred when 2-APB was applied prior to progesterone. When $50 \mu\text{M}$ 2-APB was applied in this way there was an immediate but transient fall in $[\text{Ca}^{2+}]_i$. The $[\text{Ca}^{2+}]_i$ plateau ('b' in Supplementary Figure S1) was reduced by $62 \pm 13\%$

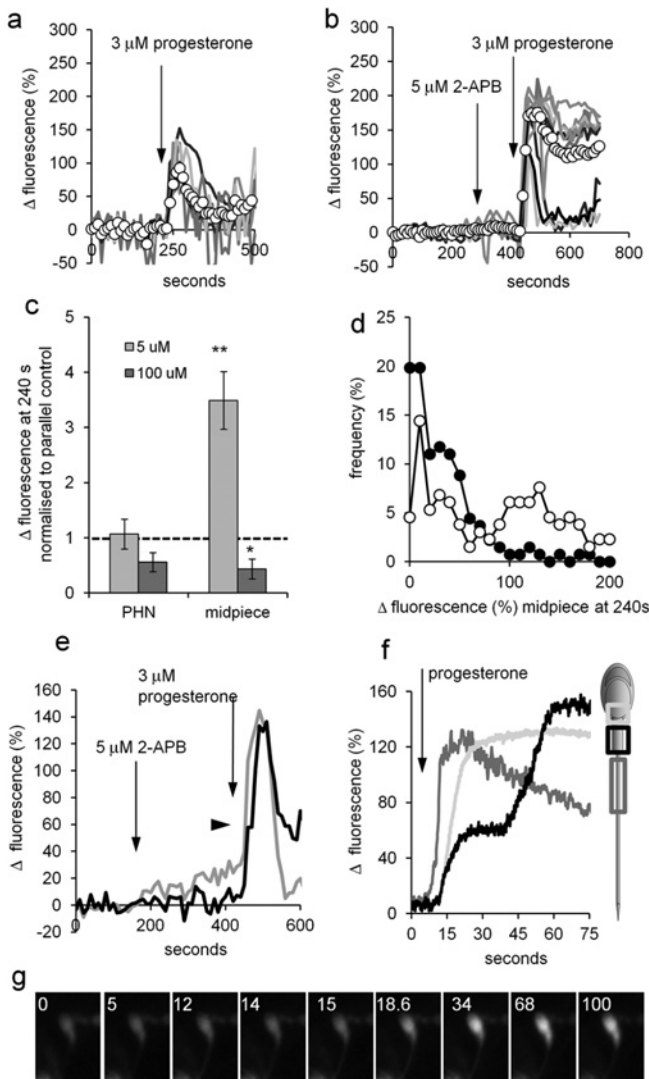


Figure 5 2-APB ($5 \mu\text{M}$) enhances sustained elevation of $[Ca^{2+}]_i$ in the midpiece

(a and b) Progesterone-induced responses at the midpiece under control conditions (a) and after application of $5 \mu\text{M}$ 2-APB (first arrow; b). Each plot shows six to nine representative single-cell traces and ΔF_{mean} (○—○) for all 25 (a) and 31 (b) cells in the experiment. (c) Dose-dependence of the effect of 2-APB pre-treatment on the sustained $[Ca^{2+}]_i$ signal. The amplitude of the sustained response (240 s after progesterone addition) in PHN (left-hand bars) and midpiece (right-hand bars) after exposure to $5 \mu\text{M}$ 2-APB (light grey bars) and $100 \mu\text{M}$ 2-APB (dark grey bars) was normalized to the amplitude of the parallel control (shown by a broken line). Each bar shows the means \pm S.E.M. of 11 ($5 \mu\text{M}$ 2-APB) and six ($100 \mu\text{M}$ 2-APB) experiments. * $P < 0.05$; ** $P < 0.005$ compared with control. (d) Amplitude distribution of single-cell sustained $[Ca^{2+}]_i$ increases (240 s after progesterone addition). Open circles (○—○) show responses of 2-APB pre-treated cells (136 cells from five experiments), closed circles (●—●) show responses from 135 cells in the five parallel control experiments. (e) Progesterone-stimulated $[Ca^{2+}]_i$ elevation in the PHN (grey trace) and midpiece (black trace) of a $5 \mu\text{M}$ 2-APB pre-treated cell. 2-APB was added at the first arrow, $3 \mu\text{M}$ progesterone at the second arrow. An inflection in the rising phase of the midpiece trace occurs ~ 20 s after application of progesterone (arrowhead). (f) Progesterone-stimulated $[Ca^{2+}]_i$ elevation in the anterior flagellum (dark grey), PHN (light grey) and midpiece (black) of a $5 \mu\text{M}$ 2-APB pre-treated cell imaged at 10 Hz. Progesterone was applied at 7 s (arrow). The anterior flagellar response precedes responses in the other two compartments and the rising phase of the midpiece response shows an inflexion ~ 25 s after onset. (g) Image series of the same cell as (f), showing the delayed $[Ca^{2+}]_i$ rise in the midpiece. Numbers show time in seconds. Progesterone was applied at 7 s.

($P < 0.02$; nine experiments). $[Ca^{2+}]_i$ oscillations (when present) slowed or stopped for 2–3 min (Figure 6b). $[Ca^{2+}]_i$ then recovered to levels slightly above those seen before application of the

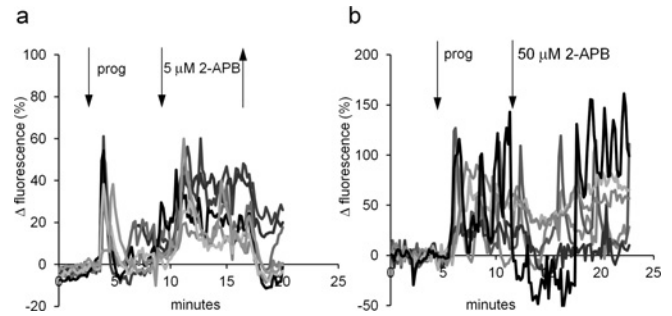


Figure 6 2-APB modifies the sustained $[Ca^{2+}]_i$ elevation

(a) 2-APB ($5 \mu\text{M}$) was applied to cells already stimulated with $3 \mu\text{M}$ progesterone (prog). 2-APB caused a tonic increase in $[Ca^{2+}]_i$ that reversed upon washout (↑) of the drug. Traces show PHN responses from seven individual representative cells. (b) 2-APB ($50 \mu\text{M}$) was applied to cells already stimulated with $3 \mu\text{M}$ progesterone. Upon application of the drug, $[Ca^{2+}]_i$ fell and oscillations were suppressed, but $[Ca^{2+}]_i$ then recovered despite the continued presence of the drug. Traces show PHN responses from six individual representative cells.

drug (increment in ΔF_{mean} 4 min after 2-APB = $5 \pm 2\%$; nine experiments, $P < 0.05$; Figure 6b). 2-APB at $100 \mu\text{M}$ had a similar effect.

In summary, although the progesterone-induced $[Ca^{2+}]_i$ signal was detectable first in the flagellum, where CatSper is present, pretreatment with 2–5 μM 2-APB ‘amplified’ the progesterone-induced $[Ca^{2+}]_i$ transient of human sperm at the PHN and midpiece by enhancing activation of a Ca^{2+} -permeable channel that is not CatSper. Pretreatment with high doses of 2-APB (50–100 μM) failed to potentiate the transient and had an inhibitory effect on the sustained $[Ca^{2+}]_i$ increase. Intriguingly, when applied during the $[Ca^{2+}]_i$ plateau, high doses of 2-APB exerted a strong but transient inhibitory action, which was not evident when applied prior to stimulation with progesterone. If 2-APB-sensitive channels contribute to sustained Ca^{2+} influx, inhibition of CatSper by 2-APB (Figure 4d) might release the 2-APB-sensitive channels from inhibitory regulation by $[Ca^{2+}]_i$, leading to recovery of the Ca^{2+} influx.

Orai and STIM proteins are expressed in human sperm

2-APB modulates interaction of STIM with store-operated channel subunits (Orai and possibly TRPC) in the plasma membrane. To investigate STIM and Orai expression in human sperm, we used anti-Orai and anti-STIM antibodies to probe Western blots and to perform immunofluorescent staining.

STIM1

In Western blots, the anti-STIM1 (ProSci catalogue number 4119 and BD Biosciences catalogue number 610954) antibody gave very weak bands. However, after immunoprecipitation with the BD Biosciences antibody, we obtained a strong band at ~ 95 kDa (Figure 7a), consistent with reports that glycosylation causes the protein to migrate with an apparent mass ≥ 90 kDa rather than the predicted 77 kDa [48]. Immunoprecipitation with the Sigma antibody gave a less intense band (results not shown). The positive control [STIM1–GFP (green fluorescent protein) transfected HEK (human embryonic kidney)-293 cells] gave a clear band at ~ 110 kDa, reflecting the presence of the 25 kDa GFP tag (Figure 7a).

Immunofluorescent staining with the ProSci antibody gave a bright spot at the sperm neck region and also stained the midpiece, which often appeared as two parallel streaks. Antibody

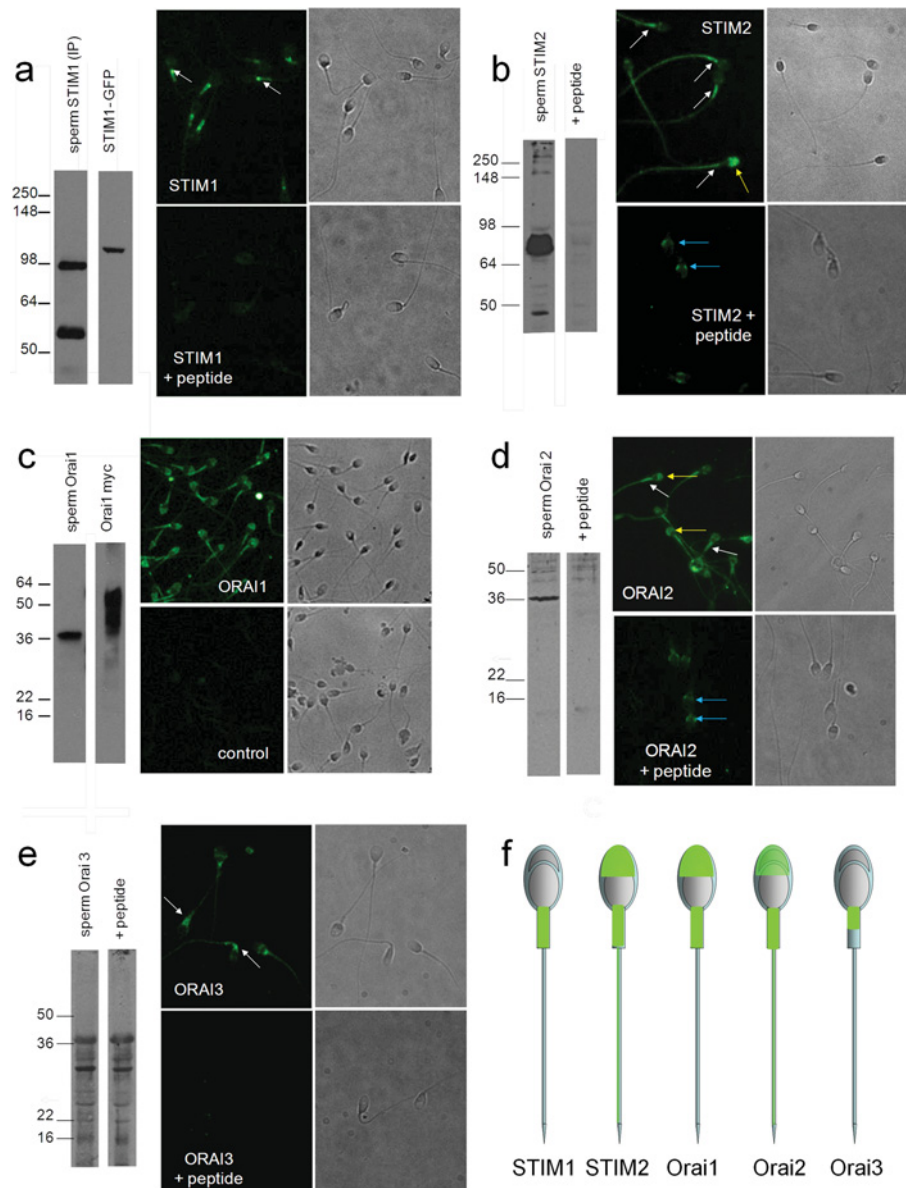


Figure 7 Expression of Orai and STIM in human sperm

(a) STIM1. Left-hand panels: Western blot for STIM1 (ProSci 4119); lane 1: human sperm proteins purified by immunoprecipitation with an anti-STIM1 antibody. A band is seen at ~95 kDa and also at 55–60 kDa due to the presence of anti-STIM1 antibody from the immunoprecipitation procedure. Lane 2 is protein from STIM1–GFP-transfected HEK-293 cells. STIM1 appears at ~110 kDa due to the presence of the 25 kDa GFP tag. Separation of images in this and other gels indicates that lanes were not originally directly adjacent. Right-hand panels: immunofluorescent staining with anti-STIM1 antibody (ProSci). Upper panels show STIM1 staining and the corresponding phase image. Fluorescence occurs over the midpiece with a bright spot at the sperm neck (arrows). Lower panels show cells incubated with antibody pre-adsorbed with the antigenic peptide, which abolished staining. **(b)** STIM2. Left-hand panels: Western blot for STIM2 (ProSci antibody 4123); lane 1: human sperm proteins. An intense doublet is present at 85–90 kDa. Lane 2: as lane 1, but antibody was pre-adsorbed with the antigenic peptide. Right-hand panels: immunofluorescent staining with anti-STIM2 antibody. The upper panels show STIM2 staining and corresponding phase image. Staining occurs over the flagellum, being heaviest at the midpiece (white arrows). In a minority of cells (< 10%), we observed staining over the acrosome (yellow arrow). The lower panels show cells incubated with antibody pre-adsorbed with the antigenic peptide, which abolished flagellar and acrosomal staining but resulted in fluorescence just behind the equatorial segment (blue arrows). **(c)** Orai 1. Left-hand panels: Orai 1 immunoblot (Sigma antibody O8264); lane 1: human sperm proteins. Lane 2: proteins extracted from Myc-tagged Orai 1-transfected HEK-293 cells. Deduced molecular mass of non-glycosylated Orai 1 is ~35 kDa. Right-hand panel: immunofluorescent staining with anti-Orai 1 antibody. Upper panels show Orai 1 staining (Sigma antibody O8264) and corresponding phase image. Staining occurs primarily over the acrosome and midpiece and weakly on the principal piece. Lower panels show cells stained similarly but omitting the primary antibody. **(d)** Orai 2. Left-hand panels: Western blot for Orai 2 (ProSci antibody 4111); lane 1: human sperm proteins. Lane 2: as lane 1, but antibody pre-adsorbed with the antigenic peptide. Right-hand panel: immunofluorescent staining with anti-Orai 2 antibody. Upper panels show Orai 2 staining and corresponding phase image. Staining occurs over the midpiece (white arrows) and acrosome (yellow arrows), with weaker staining over the principal piece. Lower panels show cells incubated with antibody pre-adsorbed with the antigenic peptide, which reduces/abolishes staining of the acrosome, midpiece and flagellum, but resulted in fluorescence just behind the equatorial segment (blue arrows). **(e)** Orai 3. Left-hand panels: Western blot for Orai 3 (ProSci antibody 4215). Lane 1: human sperm proteins. Lane 2: as lane 1, but antibody was pre-adsorbed with the antigenic peptide, which did not block band detection. Right-hand panels: immunofluorescent staining with anti-Orai 3 antibody. Upper panels show Orai 3-staining and corresponding phase image. Staining occurs primarily over the anterior midpiece and sperm neck (arrows). Lower panels show cells incubated with antibody pre-adsorbed with the antigenic peptide, which abolished staining. **(f)** Diagrammatic representation of 'typical' localization (immunofluorescence pattern) for each of the proteins investigated.

pre-adsorption with the blocking peptide abolished this staining (Figure 7a). Similar localization of STIM1 in human sperm was observed using a different antibody [14].

STIM2

The anti-STIM2 (ProSci catalogue number 4123) antibody gave an intense doublet at 85–90 kDa and a weak band at ~45 kDa. Pre-adsorption with the blocking peptide abolished this staining (Figure 7b). Immunofluorescent staining occurred on the flagellum, particularly the midpiece. In <10 % of cells we also saw staining over the acrosome (Figure 7b). Antibody pre-adsorption with the blocking peptide completely blocked this staining, but we observed some fluorescence at the equatorial segment that was not seen with unblocked antibody (Figure 7b). The strong STIM2 doublet in the Western blot is consistent with expression of both STIM2 and pre-STIM2 which is cytoplasmic [49], which may explain the surprising finding of staining by anti-STIM2 in the principal piece, where there are no intracellular membranous organelles reported.

Orai 1

In Western blots, anti-Orai 1 (Sigma catalogue number O8264 or ProSci catalogue number 4041) antibody gave a clear band at ~35 kDa, the predicted mass for the unglycosylated form of the protein. Protein from HEK-293 cells expressing recombinant Myc-tagged Orai 1 (positive control) gave heavy staining between 35 and 50 kDa (Figure 7c), probably reflecting glycosylation [50]. Immunofluorescent staining (Sigma antibody) showed fluorescence over the acrosome and midpiece and weak signal from the principal piece of the flagellum (Figure 7c). Controls without primary antibody gave no significant fluorescence.

Orai 2

Anti-Orai 2 (ProSci catalogue number 4111) gave a strong band of ~36 kDa in Western blots. The predicted mass is ~29 kDa, but glycosylation is known to cause Orai migration at higher than predicted molecular mass on SDS/PAGE. Pre-adsorption with the blocking peptide specifically abolished staining of this band (Figure 7d). Immunostaining gave fluorescence over the midpiece and principal piece that was inhibited by pre-adsorption with blocking peptide but, as with STIM2, some staining of the equatorial segment occurred which was not apparent with unblocked antibody (Figure 7d). Controls with no primary antibody gave no fluorescent signal (results not shown).

Orai 3

Western blotting of sperm lysate with anti-Orai 3 (ProSci catalogue number 4215) gave several bands, including one at the predicted mass of ~36 kDa. Pre-adsorption with the blocking peptide had no effect. Immunofluorescence with the same antibody showed staining primarily over the anterior midpiece and neck that was abolished by pre-adsorption with the blocking peptide (Figure 7e). Owing to the ambiguous nature of these data, we attempted to detect Orai3 by MS but were not able to do so. Proteins of low abundance that are known to be present in sperm can be difficult to detect by this approach, only ~1000 proteins have been identified so far out of an estimated 2500–3000 in human sperm [51].

TRPV3 (transient receptor potential vanilloid 3)

2-APB at concentrations <10 μM enhances activity of STIM–Orai. The only non-Orai channel type known to be activated by such doses of 2-APB is TRPV3 [52]. Western blotting of human keratinocyte proteins (positive control) for TRPV3 gave a band of the appropriate molecular mass. TRPV3 could not be detected in human sperm (Supplementary Figure S5 at <http://www.BiochemJ.org/bj/448/bj4480189add.htm>).

Ca²⁺ store mobilization and distribution of STIM proteins

In somatic cells, Ca²⁺ store mobilization causes redistribution of STIM1 to regions of the endoplasmic reticulum close to the plasmalemma, forming distinct puncta [53]. We used 15 μM bis-phenol, which inhibits both SERCA and the secretory pathway Ca²⁺-ATPase [42] to activate sperm CCE and investigated the effect on distribution of STIM1. Bis-phenol caused sustained [Ca²⁺]_i elevation within 4 min ($\Delta F_{\text{mean}} = 48.7 \pm 3.4\%$; $n = 17$; Supplementary Figure S6a at <http://www.BiochemJ.org/bj/448/bj4480189add.htm>), an effect that was abolished in EGTA-buffered saline ([Ca²⁺]_i ≈ 3 × 10⁻⁷ M). Application of Ca²⁺ (1.8 mM) to cells treated with bis-phenol in Ca²⁺-free conditions caused a large sustained [Ca²⁺]_i elevation, consistent with activation of CCE (Supplementary Figure S6b). We exposed sperm to 15 μM bis-phenol (12 min) in sEBSS, stained for STIM1 and assessed fluorescence in the midpiece as a percentage of the total. In control cells, 60–70 % of total fluorescence was present in the neck/midpiece (Supplementary Figure S6c). Exposure to bis-phenol caused no change ($P > 0.05$; three experiments, 170 cells).

The localization of STIM and Orai primarily to the neck, midpiece and acrosomal regions (Figure 7f) coincides with the locations of Ca²⁺ stores in mammalian sperm [54,55]. TRPC proteins in sperm are also present in these regions [56] and may combine with Orai to form store-regulated or receptor-operated channels [18]. Low concentrations of 2-APB facilitate STIM–Orai interaction [21–23] and the 2-APB-enhanced [Ca²⁺]_i signalling described above is localized to the PHN. We propose that 2–5 μM 2-APB enhances progesterone-induced Ca²⁺ influx by modulating the activation by STIM of channels incorporating Orai. The presence of STIM2, pre-STIM2 and (potentially) Orai 3 may explain the ability of 2-APB to induce Ca²⁺ influx in the absence of progesterone stimulation and even at doses ≥50 μM. The mechanism by which progesterone activates these 2-APB-sensitive channels is not yet established. Although activation of Ca²⁺ influx by treatments that mobilize stored Ca²⁺ has been reported on numerous occasions [54] (Supplementary Figure S6b), we were not able to detect conventional CCE currents in human sperm held under conventional whole-cell clamp (results not shown).

Effects of loperamide on progesterone-induced [Ca²⁺]_i and sperm motility

Loperamide (3–30 μM) is an agonist of SOCs, increasing the Ca²⁺ influx upon store depletion [57]. Loperamide at 10 μM increased resting [Ca²⁺]_i in 66 ± 7 % of cells ($n = 8$ experiments; Figure 8a). The ΔF_{mean} 90 s after application of loperamide was 24 ± 4 %, increasing to 31 ± 7 % after 3 min ($n = 8$). Superfusion with EGTA-buffered saline (~3 × 10⁻⁷ M) for 3 min prior to loperamide application abolished this effect (results not shown). The cytoplasmic alkalinizing effect of 10 μM loperamide was negligible (0.013 ± 0.005 units; $n = 3$). Inward monovalent

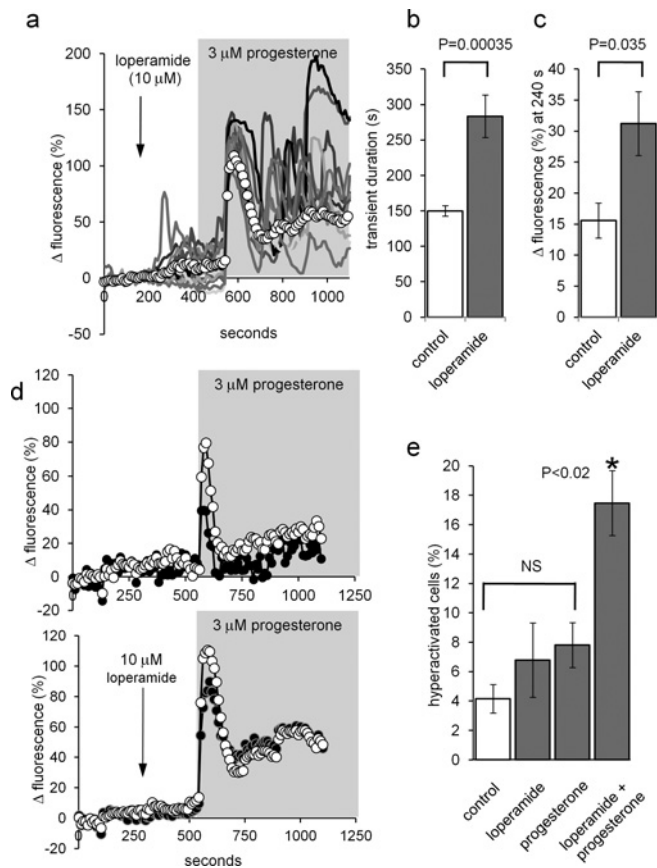


Figure 8 Loperamide potentiates the response of human sperm to progesterone

(a) Pre-treatment with 10 μM loperamide (arrow) followed by application of 3 μM progesterone (shading). Traces show nine representative single-cell PHN responses and ΔF_{mean} (O–O) for all 81 cells in the experiment. Loperamide elevates resting $[\text{Ca}^{2+}]_i$ and subsequent exposure to progesterone induced an initial $[\text{Ca}^{2+}]_i$ transient followed by large $[\text{Ca}^{2+}]_i$ oscillations. (b) Duration of the progesterone-induced $[\text{Ca}^{2+}]_i$ transient in the PHN was increased by loperamide pre-treatment. Bars show means \pm S.E.M. for 11 paired experiments. (c) Progesterone-induced sustained $[\text{Ca}^{2+}]_i$ increase (ΔF_{mean} at 240 s after progesterone) was enhanced by loperamide pre-treatment. Bars show means \pm S.E.M. for nine paired experiments. (d) Mean normalized fluorescence (ΔF_{mean}) in the PHN (O–O) and in the midpiece (●–●) under control conditions (upper panel; mean of 19 cells) and after pre-treatment with 10 μM loperamide (lower panel; mean of 33 cells). Potentiation by loperamide of $[\text{Ca}^{2+}]_i$ transient duration and sustained $[\text{Ca}^{2+}]_i$ elevation are similar in the two compartments. (e) Loperamide enhances progesterone-induced hyperactivation. Each bar shows the percentage of hyperactivated cells (means \pm S.E.M.; $n = 7$). Progesterone (3 μM) and loperamide (10 μM), applied individually, failed significantly to increase hyperactivation (not significant; NS). When cells were pre-treated with loperamide (3 min), progesterone significantly increased the proportion of hyperactivated cells over all the other conditions ($*P < 0.02$).

CatSper currents were insensitive to loperamide and outward currents were semi-reversibly inhibited (Supplementary Figure S7 at <http://www.BiochemJ.org/bj/448/bj4480189add.htm>).

Effects of 10 μM loperamide on the amplitude of the progesterone-induced $[\text{Ca}^{2+}]_i$ transient were inconsistent ($P = 0.38$, paired t test). However, duration of the progesterone-induced $[\text{Ca}^{2+}]_i$ transient (ΔF_{mean} initiation to end of falling phase) was significantly increased, from 150 ± 8 to 284 ± 30 s ($P = 0.00035$; paired t test; $n = 11$; Figure 8b). In 10–20% of cells, the transient peak persisted for 50–100 s and the $[\text{Ca}^{2+}]_i$ transient was often followed by a second large plateau or a series of $[\text{Ca}^{2+}]_i$ oscillations (Figure 8a). Similarly to pre-treatment with 5 μM 2-APB, an inflexion occurred in the rising phase of the midpiece response in >20% of cells, indicating activation

of the late sustained component of the response. Sustained $[\text{Ca}^{2+}]_i$ elevation (ΔF_{mean} 240 s after progesterone) was enhanced ($P < 0.05$; paired t test; $n = 9$) at both the PHN and midpiece (Figures 8c and 8d).

Application of progesterone to free swimming sperm, by mixing or uncaging, induces a burst of transitional or hyperactivated motility, probably associated with the consequent Ca^{2+} transient [58,59], but this rapidly decays, such that effects recorded by CASA are small. Since loperamide pre-treatment both prolongs the $[\text{Ca}^{2+}]_i$ transient and enhances the sustained phase, we investigated the effects of loperamide on progesterone-induced hyperactivation. Progesterone (3 μM) alone increased the proportion of cells classified as hyperactivated from 4.2 ± 1.0 to just 7.8 ± 1.5 ($P < 0.01$) and 10 μM loperamide had no significant effect ($P > 0.05$; paired t test, $n = 7$ experiments; Figure 8e). However, when cells were exposed to loperamide for 200 s, then progesterone was applied before introduction into the chamber, the proportion of hyperactivated cells increased to $17.5 \pm 2.2\%$, significantly greater than progesterone or loperamide exposure alone (Figure 8e; $P = 0.02$; paired t test, $n = 7$ experiments). The loperamide-enhanced sustained $[\text{Ca}^{2+}]_i$ signal powerfully modifies motility in human sperm.

Effective progesterone-induced $[\text{Ca}^{2+}]_i$ signalling is characteristic of fertile human sperm [9,10]. Our understanding of this non-genomic action of progesterone has recently been transformed by the discovery that CatSper channels in the flagellum of patch-clamped human sperm are activated by this steroid. We have shown in the present study that Ca^{2+} -permeable channels at the sperm neck region, sensitive to 2-APB and loperamide, amplify and prolong progesterone-induced Ca^{2+} signals initiated in the anterior flagellum. Subcellular localization of the Ca^{2+} signal, patch-clamp measurements of CatSper currents and assessment of pH_i confirm that these effects are not by direct or indirect activation of CatSper channels and occur under conditions where CatSper may be partially inhibited. STIM and Orai proteins, which are sensitive to and can be directly activated by low doses of 2-APB, are localized primarily at the sperm neck. We propose that 2-APB-sensitive channels at the sperm neck (probably STIM-regulated Orai or TRPCs) are essential for human sperm Ca^{2+} signalling activated through CatSper, providing amplification, spatio-temporal complexity and flexibility to the sperm Ca^{2+} -signalling toolkit. Release of stored Ca^{2+} and CCE may underlie this propagation from the flagellum into the sperm neck region, but we were unable to detect conventional CCE currents in human sperm, so the mechanism of activation of these channels remains an open question.

AUTHOR CONTRIBUTION

Linda Lefièvre, Katherine Nash, Steven Mansell, Sarah Costello, Emma Punt, Joao Correia and Jennifer Morris performed the experimental work. Linda Lefièvre, Katherine Nash, Steven Mansell, Joao Correia, Jackson Kirkman-Brown, Jennifer Morris, Stuart Wilson, Christopher Barratt and Stephen Publicover designed experiments and analysed the data. Stephen Publicover and Christopher Barratt wrote the paper.

ACKNOWLEDGEMENTS

We thank Yuriy Kirichok and Polina Lishko for sharing their sperm-patching expertise, Mike Tomlinson (School of Biosciences, University of Birmingham, Birmingham, U.K.) for Orai1- and STIM1-GFP-expressing cells and Neil Hotchin (School of Biosciences, University of Birmingham, Birmingham, U.K.) for keratinocyte protein extracts.

FUNDING

This work was supported by the Wellcome Trust [grant number 086470] and studentships from the Biotechnology and Biological Sciences Research Council (to K.N. and E.P.) and the Infertility Research Trust (to S.M.).

REFERENCES

- 1 Publicover, S., Harper, C. V. and Barratt, C. (2007) [Ca²⁺] signalling in sperm—making the most of what you've got. *Nat. Cell Biol.* **9**, 235–242
- 2 Kirichok, Y. and Lishko, P. V. (2011) Rediscovering sperm ion channels with the patch-clamp technique. *Mol. Hum. Reprod.* **17**, 478–499
- 3 Lishko, P. V., Kirichok, Y., Ren, D., Navarro, B., Chung, J. J. and Clapham, D. E. (2012) The control of male fertility by spermatozoan ion channels. *Annu. Rev. Physiol.* **74**, 453–475
- 4 Brenker, C., Goodwin, N., Weyand, I., Kashikar, N. D., Naruse, M., Krahling, M., Muller, A., Kaupp, U. B. and Strunker, T. (2012) The CatSper channel: a polymodal chemosensor in human sperm. *EMBO J.* **31**, 1654–1665
- 5 Ren, D. and Xia, J. (2010) Calcium signaling through CatSper channels in mammalian fertilization. *Physiology (Bethesda)* **25**, 165–175
- 6 Baldi, E., Luconi, M., Muratori, M., Marchiani, S., Tamburrino, L. and Forti, G. (2009) Nongenomic activation of spermatozoa by steroid hormones: facts and fictions. *Mol. Cell. Endocrinol.* **308**, 39–46
- 7 Thomas, P. and Meizel, S. (1988) An influx of extracellular calcium is required for initiation of the human sperm acrosome reaction induced by human follicular fluid. *Gamete Res.* **20**, 397–411
- 8 Blackmore, P. F., Beebe, S. J., Danforth, D. R. and Alexander, N. (1990) Progesterone and 17 α -hydroxyprogesterone. Novel stimulators of calcium influx in human sperm. *J. Biol. Chem.* **265**, 1376–1380
- 9 Krausz, C., Bonaccorsi, L., Maggi, P., Luconi, M., Crisculi, L., Fuzzi, B., Pellegrini, S., Forti, G. and Baldi, E. (1996) Two functional assays of sperm responsiveness to progesterone and their predictive values in *in-vitro* fertilization. *Hum. Reprod.* **11**, 1661–1667
- 10 Forti, G., Baldi, E., Krausz, C., Luconi, M., Bonaccorsi, L., Maggi, M., Bassi, F. and Scarselli, G. (1999) Effects of progesterone on human spermatozoa: clinical implications. *Ann. Endocrinol. (Paris)* **60**, 107–110
- 11 Lishko, P. V., Botchkina, I. L. and Kirichok, Y. (2011) Progesterone activates the principal Ca²⁺ channel of human sperm. *Nature* **471**, 387–391
- 12 Strunker, T., Goodwin, N., Brenker, C., Kashikar, N. D., Weyand, I., Seifert, R. and Kaupp, U. B. (2011) The CatSper channel mediates progesterone-induced Ca²⁺ influx in human sperm. *Nature* **471**, 382–386
- 13 Blackmore, P. F. (1993) Thapsigargin elevates and potentiates the ability of progesterone to increase intracellular free calcium in human sperm: possible role of perinuclear calcium. *Cell Calcium* **14**, 53–60
- 14 Park, K. H., Kim, B. J., Kang, J., Nam, T. S., Lim, J. M., Kim, H. T., Park, J. K., Kim, Y. G., Chae, S. W. and Kim, U. H. (2011) Ca²⁺ signaling tools acquired from prostasomes are required for progesterone-induced sperm motility. *Sci. Signaling* **4**, ra31
- 15 Putney, J. W. (2009) Capacitative calcium entry: from concept to molecules. *Immunol. Rev.* **231**, 10–22
- 16 Cahalan, M. D. (2009) STIMulating store-operated Ca²⁺ entry. *Nat. Cell Biol.* **11**, 669–677
- 17 Yuan, J. P., Zeng, W., Huang, G. N., Worley, P. F. and Muallem, S. (2007) STIM1 heteromultimerizes TRPC channels to determine their function as store-operated channels. *Nat. Cell Biol.* **9**, 636–645
- 18 Liao, Y., Plummer, N. W., George, M. D., Abramowitz, J., Zhu, M. X. and Birnbaumer, L. (2009) A role for Orai in TRPC-mediated Ca²⁺ entry suggests that a TRPC:Orai complex may mediate store and receptor operated Ca²⁺ entry. *Proc. Natl. Acad. Sci. U.S.A.* **106**, 3202–3206
- 19 Cheng, K. T., Liu, X., Ong, H. L. and Ambudkar, I. S. (2008) Functional requirement for Orai1 in store-operated TRPC1-STIM1 channels. *J. Biol. Chem.* **283**, 12935–12940
- 20 Maruyama, T., Kanaji, T., Nakade, S., Kanno, T. and Mikoshiba, K. (1997) 2APB, 2-aminoethoxydiphenyl borate, a membrane-penetrable modulator of Ins(1,4,5)P₃-induced Ca²⁺ release. *J. Biochem.* **122**, 498–505
- 21 Wang, Y., Deng, X., Zhou, Y., Hendron, E., Mancarella, S., Ritchie, M. F., Tang, X. D., Baba, Y., Kurosaki, T., Mori, Y. et al. (2009) STIM protein coupling in the activation of Orai channels. *Proc. Natl. Acad. Sci. U.S.A.* **106**, 7391–7396
- 22 Navarro-Borely, L., Somasundaram, A., Yamashita, M., Ren, D., Miller, R. J. and Prakriya, M. (2008) STIM1-Orai1 interactions and Orai1 conformational changes revealed by live-cell FRET microscopy. *J. Physiol.* **586**, 5383–5401
- 23 Yamashita, M., Somasundaram, A. and Prakriya, M. (2011) Competitive modulation of Ca²⁺ release-activated Ca²⁺ channel gating by STIM1 and 2-aminoethoxydiphenyl borate. *J. Biol. Chem.* **286**, 9429–9442
- 24 DeHaven, W. I., Smyth, J. T., Boyles, R. R., Bird, G. S. and Putney, Jr, J. W. (2008) Complex actions of 2-aminoethoxydiphenyl borate on store-operated calcium entry. *J. Biol. Chem.* **283**, 19265–19273
- 25 Zhang, S. L., Kozak, J. A., Jiang, W., Yeromin, A. V., Chen, J., Yu, Y., Penna, A., Shen, W., Chi, V. and Cahalan, M. D. (2008) Store-dependent and -independent modes regulating Ca²⁺ release-activated Ca²⁺ channel activity of human Orai1 and Orai3. *J. Biol. Chem.* **283**, 17662–17671
- 26 Parvez, S., Beck, A., Peinelt, C., Soboloff, J., Lis, A., Monteilh-Zoller, M., Gill, D. L., Fleig, A. and Penner, R. (2008) STIM2 protein mediates distinct store-dependent and store-independent modes of CRAC channel activation. *FASEB J.* **22**, 752–761
- 27 Lis, A., Peinelt, C., Beck, A., Parvez, S., Monteilh-Zoller, M., Fleig, A. and Penner, R. (2007) CRACM1, CRACM2, and CRACM3 are store-operated Ca²⁺ channels with distinct functional properties. *Curr. Biol.* **17**, 794–800
- 28 Schindl, R., Bergsmann, J., Frischauf, I., Derler, I., Fahrner, M., Muik, M., Fritsch, R., Groschner, K. and Romanin, C. (2008) 2-Aminoethoxydiphenyl borate alters selectivity of Orai3 channels by increasing their pore size. *J. Biol. Chem.* **283**, 20261–20267
- 29 Bootman, M. D., Collins, T. J., Mackenzie, L., Roderick, H. L., Berridge, M. J. and Peppiatt, C. M. (2002) 2-Aminoethoxydiphenyl borate (2-APB) is a reliable blocker of store-operated Ca²⁺ entry but an inconsistent inhibitor of InsP₃-induced Ca²⁺ release. *FASEB J.* **16**, 1145–1150
- 30 Peppiatt, C. M., Collins, T. J., Mackenzie, L., Conway, S. J., Holmes, A. B., Bootman, M. D., Berridge, M. J., Seo, J. T. and Roderick, H. L. (2003) 2-Aminoethoxydiphenyl borate (2-APB) antagonises inositol 1,4,5-trisphosphate-induced calcium release, inhibits calcium pumps and has a use-dependent and slowly reversible action on store-operated calcium entry channels. *Cell Calcium* **34**, 97–108
- 31 Bilmen, J. G. and Michelangeli, F. (2002) Inhibition of the type 1 inositol 1,4,5-trisphosphate receptor by 2-aminoethoxydiphenylborate. *Cell. Signalling* **14**, 955–960
- 32 Bilmen, J. G., Wootton, L. L., Godfrey, R. E., Smart, O. S. and Michelangeli, F. (2002) Inhibition of SERCA Ca²⁺ pumps by 2-aminoethoxydiphenyl borate (2-APB). 2-APB reduces both Ca²⁺ binding and phosphoryl transfer from ATP, by interfering with the pathway leading to the Ca²⁺-binding sites. *Eur. J. Biochem.* **269**, 3678–3687
- 33 Harper, C. V., Barratt, C. L. and Publicover, S. J. (2004) Stimulation of human spermatozoa with progesterone gradients in simulated approach to the oocyte. Induction of [Ca²⁺]_i oscillations and cyclical transitions in flagellar beating. *J. Biol. Chem.* **279**, 46315–46325
- 34 Lefievre, L., Chen, Y., Conner, S. J., Scott, J. L., Publicover, S. J., Ford, W. C. and Barratt, C. L. (2007) Human spermatozoa contain multiple targets for protein S-nitrosylation: an alternative mechanism of the modulation of sperm function by nitric oxide? *Proteomics* **7**, 3066–3084
- 35 Harper, C., Wootton, L., Michelangeli, F., Lefievre, L., Barratt, C. and Publicover, S. (2005) Secretory pathway Ca²⁺-ATPase (SPCA1) Ca²⁺ pumps, not SERCAs, regulate complex [Ca²⁺]_i signals in human spermatozoa. *J. Cell Sci.* **118**, 1673–1685
- 36 Fraire-Zamora, J. J. and Gonzalez-Martinez, M. T. (2004) Effect of intracellular pH on depolarization-evoked calcium influx in human sperm. *Am. J. Physiol. Cell Physiol.* **287**, C1688–C1696
- 37 Moseley, F. L., Jha, K. N., Bjorndahl, L., Brewis, I. A., Publicover, S. J., Barratt, C. L. and Lefievre, L. (2005) Protein tyrosine phosphorylation, hyperactivation and progesterone-induced acrosome reaction are enhanced in IVF media: an effect that is not associated with an increase in protein kinase A activation. *Mol. Hum. Reprod.* **11**, 523–529
- 38 Luconi, M., Bonaccorsi, L., Maggi, M., Pecchioli, P., Krausz, C., Forti, G. and Baldi, E. (1998) Identification and characterization of functional nongenomic progesterone receptors on human sperm membrane. *J. Clin. Endocrinol. Metab.* **83**, 877–885
- 39 Osman, R. A., Andria, M. L., Jones, A. D. and Meizel, S. (1989) Steroid induced exocytosis: the human sperm acrosome reaction. *Biochem. Biophys. Res. Commun.* **160**, 828–833
- 40 Harper, C. V., Kirkman-Brown, J. C., Barratt, C. L. and Publicover, S. J. (2003) Encoding of progesterone stimulus intensity by intracellular [Ca²⁺] ([Ca²⁺]_i) in human spermatozoa. *Biochem. J.* **372**, 407–417
- 41 Kirkman-Brown, J. C., Bray, C., Stewart, P. M., Barratt, C. L. and Publicover, S. J. (2000) Biphasic elevation of [Ca²⁺]_i in individual human spermatozoa exposed to progesterone. *Dev. Biol.* **222**, 326–335
- 42 Brown, G. R., Benyon, S. L., Kirk, C. J., Wictome, M., East, J. M., Lee, A. G. and Michelangeli, F. (1994) Characterisation of a novel Ca²⁺ pump inhibitor (bis-phenol) and its effects on intracellular Ca²⁺ mobilization. *Biochim. Biophys. Acta* **1195**, 252–258
- 43 Bedu-Addo, K., Barratt, C. L., Kirkman-Brown, J. C. and Publicover, S. J. (2007) Patterns of [Ca²⁺]_i mobilization and cell response in human spermatozoa exposed to progesterone. *Dev. Biol.* **302**, 324–332
- 44 Garcia, M. A. and Meizel, S. (1999) Progesterone-mediated calcium influx and acrosome reaction of human spermatozoa: pharmacological investigation of T-type calcium channels. *Biol. Reprod.* **60**, 102–109
- 45 Servin-Vences, M. R., Tatsu, Y., Ando, H., Guerrero, A., Yumoto, N., Darszon, A. and Nishigaki, T. (2012) A caged progesterone analog alters intracellular Ca²⁺ and flagellar bending in human sperm. *Reproduction* **144**, 101–109
- 46 Prakriya, M. and Lewis, R. S. (2001) Potentiation and inhibition of Ca²⁺ release-activated Ca²⁺ channels by 2-aminoethoxydiphenyl borate (2-APB) occurs independently of IP₃ receptors. *J. Physiol.* **536**, 3–19

- 47 Raffaello, A., De Stefani, D. and Rizzuto, R. (2012) The mitochondrial Ca^{2+} uniporter. *Cell Calcium* **52**, 16–21
- 48 Manji, S. S., Parker, N. J., Williams, R. T., van Stekelenburg, L., Pearson, R. B., Dziadek, M. and Smith, P. J. (2000) STIM1: a novel phosphoprotein located at the cell surface. *Biochim. Biophys. Acta* **1481**, 147–155
- 49 Graham, S. J., Dziadek, M. A. and Johnstone, L. S. (2011) A cytosolic STIM2 preprotein created by signal peptide inefficiency activates ORAI1 in a store-independent manner. *J. Biol. Chem.* **286**, 16174–16185
- 50 Gwack, Y., Srikanth, S., Feske, S., Cruz-Guilloty, F., Oh-hora, M., Neems, D. S., Hogan, P. G. and Rao, A. (2007) Biochemical and functional characterization of Orai proteins. *J. Biol. Chem.* **282**, 16232–16243
- 51 Baker, M. A. (2011) The 'omics revolution and our understanding of sperm cell biology. *Asian J. Androl.* **13**, 6–10
- 52 Chung, M. K., Lee, H., Mizuno, A., Suzuki, M. and Caterina, M. J. (2004) 2-aminoethoxydiphenyl borate activates and sensitizes the heat-gated ion channel TRPV3. *J. Neurosci.* **24**, 5177–5182
- 53 Stathopoulos, P. B., Zheng, L., Li, G. Y., Plevin, M. J. and Ikura, M. (2008) Structural and mechanistic insights into STIM1-mediated initiation of store-operated calcium entry. *Cell* **135**, 110–122
- 54 Costello, S., Michelangeli, F., Nash, K., Lefievre, L., Morris, J., Machado-Oliveira, G., Barratt, C., Kirkman-Brown, J. and Publicover, S. (2009) Ca^{2+} stores in sperm: their identities and functions. *Reproduction* **138**, 425–437
- 55 Ho, H. C. and Suarez, S. S. (2001) An inositol 1,4,5-trisphosphate receptor-gated intracellular Ca^{2+} store is involved in regulating sperm hyperactivated motility. *Biol. Reprod.* **65**, 1606–1615
- 56 Darszon, A., Sanchez-Cardenas, C., Orta, G., Sanchez-Tusie, A. A., Beltran, C., Lopez-Gonzalez, I., Granados-Gonzalez, G. and Trevino, C. L. (2012) Are TRP channels involved in sperm development and function? *Cell Tissue Res.* **349**, 749–764
- 57 Harper, J. L., Shin, Y. and Daly, J. W. (1997) Loperamide: a positive modulator for store-operated calcium channels? *Proc. Natl. Acad. Sci. U.S.A.* **94**, 14912–14917
- 58 Gakamsky, A., Armon, L. and Eisenbach, M. (2009) Behavioral response of human spermatozoa to a concentration jump of chemoattractants or intracellular cyclic nucleotides. *Hum. Reprod.* **24**, 1152–1163
- 59 Kilic, F., Kashikar, N. D., Schmidt, R., Alvarez, L., Dai, L., Weyand, I., Wiesner, B., Goodwin, N., Hagen, V. and Kaupp, U. B. (2009) Caged progesterone: a new tool for studying rapid nongenomic actions of progesterone. *J. Am. Chem. Soc.* **131**, 4027–4030

Received 24 February 2012/22 August 2012; accepted 3 September 2012

Published as BJ Immediate Publication 3 September 2012, doi:10.1042/BJ20120339

SUPPLEMENTARY ONLINE DATA

2-APB-potentiated channels amplify CatSper-induced Ca^{2+} signals in human sperm

Linda LEFIÈVRE*†, Katherine NASH‡, Steven MANSELL§, Sarah COSTELLO‡, Emma PUNT‡, Joao CORREIA†‡, Jennifer MORRIS‡, Jackson KIRKMAN-BROWN*†, Stuart M. WILSON§, Christopher L. R. BARRATT§ and Stephen PUBLICOVER†¹

*Medical School, University of Birmingham, Birmingham, B15 2TT, U.K., †Birmingham Women's Hospital, Birmingham, B15 2TG, U.K., ‡School of Biosciences, University of Birmingham, Birmingham, B15 2TT, U.K., and §Division of Cardiovascular Medicine, Medical Research Institute, Ninewells Hospital University of Dundee, Dundee DD1 9SY, Scotland, U.K.

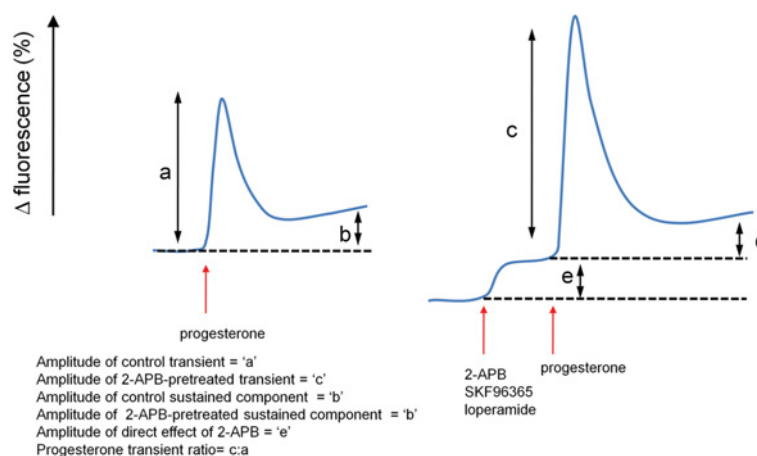


Figure S1 Diagrammatic illustration showing quantified components of $[\text{Ca}^{2+}]_i$ traces in control experiments (left) and after pre-treatment with 2-APB (right)

'a' and 'b' show transient and sustained response amplitudes under control conditions. 'c' and 'd' show transient and sustained response amplitudes in 2-APB and loperamide experiments. 'e' shows the amplitude of response to 2-APB or loperamide.

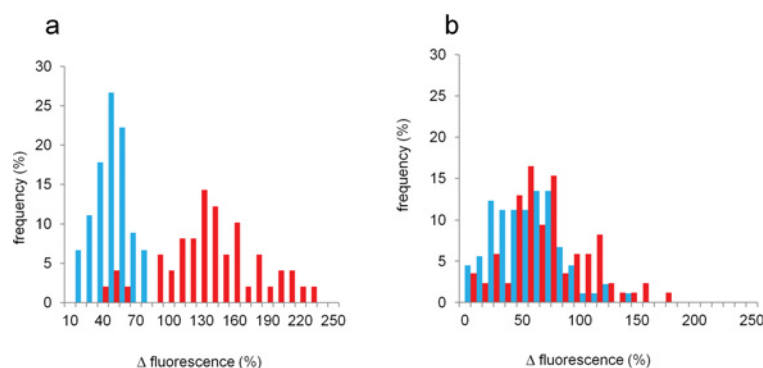


Figure S2 Amplitude distribution for single-cell progesterone transients recorded at the PHN from two pairs of experiments

In each graph, blue bars show the amplitude distribution for the control experiment and red bars show the distribution for a parallel experiment where cells were pre-treated with $5 \mu\text{M}$ 2-APB. In experiment (a), most cells show a large shift to the right after 2-APB pre-treatment but approximately 10% are clustered at amplitudes similar to the control mean. In experiment (b), 2-APB increases the transient amplitude in only a subset of cells, the distribution peak remaining at a ΔF of $\sim 70\%$.

¹ To whom correspondence should be addressed (email s.j.publicover@bham.ac.uk)

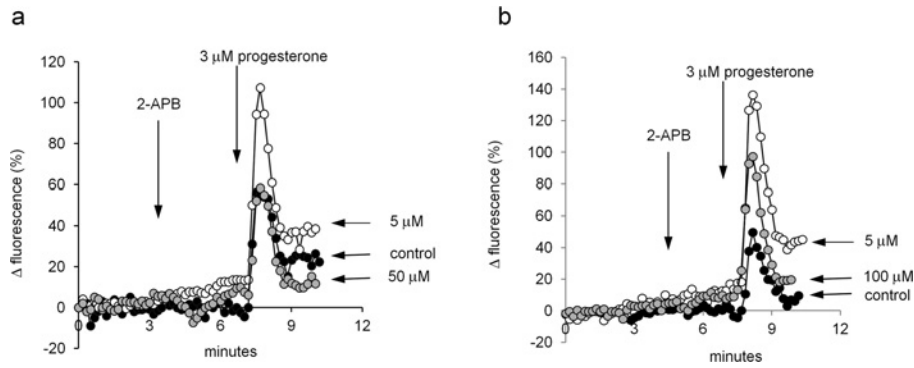


Figure S3 Dose-dependence of effect of pre-treatment with 2-APB on the $[Ca^{2+}]_i$ transient induced by $3 \mu M$ progesterone

2-APB (except controls) was added at the first arrow, progesterone ($3 \mu M$) was added at the second arrow. (a) Black circles, vehicle control; white circles, $5 \mu M$ 2-APB; grey circles, $50 \mu M$ 2-APB. (b) Black circles, vehicle control; white circles, $5 \mu M$ 2-APB; grey circles, $100 \mu M$ 2-APB.

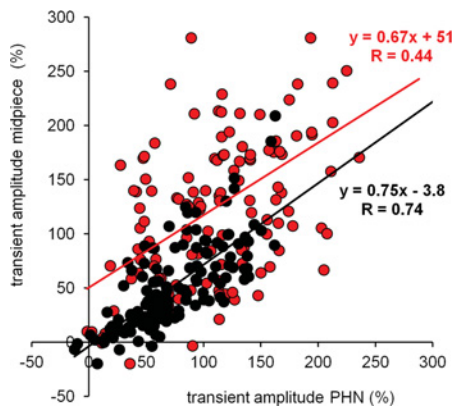


Figure S4 Relationship between the amplitude of the progesterone-induced $[Ca^{2+}]_i$ transient recorded at the PHN (x axis) and midpiece (y axis)

Under control conditions (black circles), midpiece amplitude is typically $\sim 75\%$ of amplitude at PHN ($y = 0.75x - 3.8$). In $5 \mu M$ 2-APB-pretreated cells (red circles), both PHN and midpiece transients are larger but also the line of best fit is 'shifted' upward due to recruitment of an extra midpiece component in a sub-population of cells ($y = 0.67 \times 51$). The results are from five pairs of experiments; each data set shows > 130 cells.

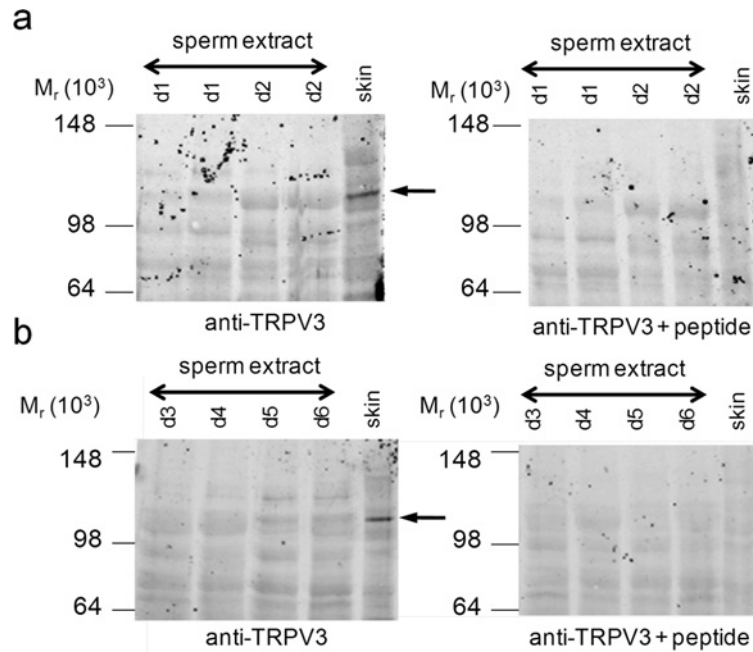


Figure S5 TRPV3 is not detectable in human sperm

(a) The left-hand panel shows the immunoblot for TRPV3 with sperm preparations from two different donors (d1 and d2). The final lane shows the positive control (human keratinocyte proteins; skin). The arrow on lane 5 shows the strong band corresponding to the predicted mass for TRPV3. The right-hand panel shows an identical blot, carried out in parallel, after pre-adsorbing the TRPV3 antibody with the antigenic peptide. The band detected in the positive control has been lost. (b) As for (a), but using four further donors (d3–d6).

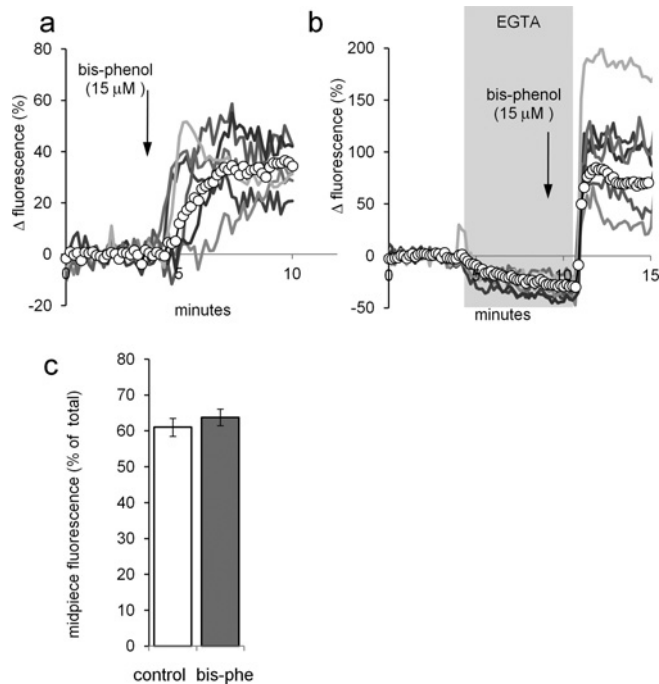


Figure S6 Activation of SOCs does not cause redistribution of STIM1

(a) Bis-phenol (15 μM), an inhibitor of Ca²⁺-store ATPases, causes a sustained increase in [Ca²⁺]_i. Six representative single-cell responses and the means for all cells in the experiment (circles) are shown. (b) In EGTA-buffered saline, bis-phenol fails to significantly increase [Ca²⁺]_i, but upon reintroduction of 1.8 mM Ca²⁺, a large prolonged [Ca²⁺]_i elevation was seen, indicating the activation of SOCs by store depletion. (c) Intensity of immunofluorescent staining of STIM1 in the sperm midpiece (as a proportion of total fluorescence of the sperm) under control conditions (white bar) and after incubation for 12 min in the presence of 15 μM bis-phenol (grey bar). Each bar shows the mean ± S.E.M. of fluorescence in 170 cells from three experiments.

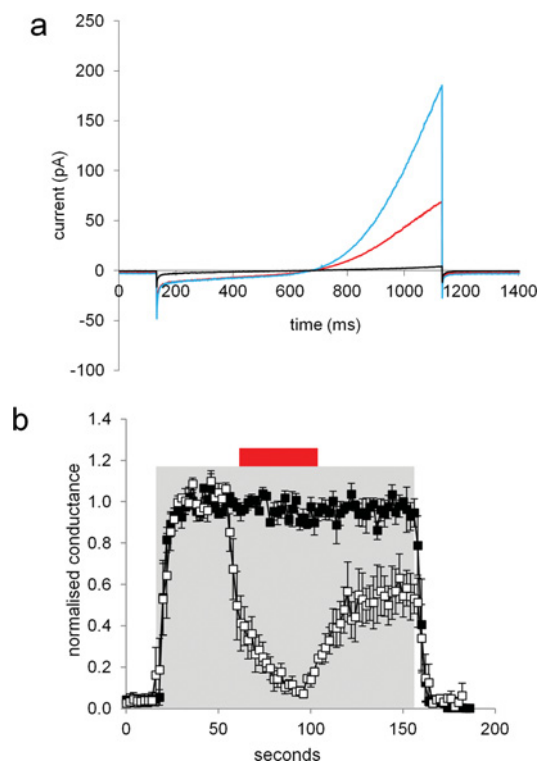


Figure S7 Loperamide does not enhance currents through CatSper channels

(a) Currents in a whole-cell clamped sperm induced by a 1 s voltage ramp from -80 mV to $+80$ mV. Black trace shows current in HS medium with 2 mM Ca^{2+} [1]. Blue trace shows current in DVF (divalent cation-free) medium. Red trace shows current in the presence of 10 μM loperamide. (b) Time-course of inhibition by 10 μM loperamide of outward conductance (normalized to maximum). Filled squares show control experiments where conductance is reversibly enhanced in DVF medium (shading). Open squares show the effect of 10 μM loperamide (red bar). Each line shows the mean of four experiments \pm S.E.M. Conductance was calculated using $\delta I/\delta V$ at 70 – 80 mV.

REFERENCE

- 1 Lishko, P. V., Botchkina, I. L. and Kirichok, Y. (2011) Progesterone activates the principal Ca^{2+} channel of human sperm. *Nature* **471**, 387–391

Received 24 February 2012/22 August 2012; accepted 3 September 2012
Published as BJ Immediate Publication 3 September 2012, doi:10.1042/BJ20120339

REVIEW

Diagnostic tools in male infertility—the question of sperm dysfunction

Christopher LR Barratt^{1,2}, Steven Mansell¹, Catherine Beaton¹, Steve Tardif¹ and Senga K Oxenham¹

Sperm dysfunction is the single most common cause of infertility, yet what is remarkable is that, there is no drug a man can take or add to his spermatozoa *in vitro* to improve fertility. One reason for the lack of progress in this area is that our understanding of the cellular and molecular workings of the mature spermatozoon is limited. However, over the last few years there has been considerable progress in our knowledge base and in addressing new methods to diagnose sperm dysfunction. We review the current state of the field and provide insights for further development. We conclude that: (i) there is little to be gained from more studies identifying/categorizing various populations of men using a basic semen assessment, where an effort is required in making sure the analysis is performed in an appropriate high quality way; (ii) technological development is likely to bring the reality of sperm function testing closer to implementation into the clinical pathways. In doing this, these assays must be robust, cheap (or more appropriately termed cost effective), easy to use and clinically useful; and (iii) clinical necessity, e.g., the need to identify the highest quality spermatozoon for injection is driving basic research forward. This is an exciting time to be an andrologist and, likely, a fruitful one.

Asian Journal of Andrology (2011) 13, 53–58; doi:10.1038/aja.2010.63; published online 22 November 2010

Keywords: gamete biomarker; male fertility; sperm biomarker; sperm dysfunction

INTRODUCTION

Infertility is a significant global problem affecting approximately 80 million (1:7) couples worldwide.¹ In a landmark study by Mike Hull and colleagues, in which a representative British population was studied, sperm dysfunction (lacking ‘normal’ function) was identified as the single most common cause of infertility.² Subsequent studies have confirmed these observations³ and highlighted dysfunctional cells in men with ‘normal’ semen parameters and conversely normal sperm function in oligozoospermic men.⁴ What is remarkable is that, for this group, there is no drug a man can take or add to his spermatozoa *in vitro* to improve fertility. The only option is assisted reproductive technology (ART) which usually consists of a graduation of treatment depending on severity, i.e., intrauterine insemination for mild, *in vitro* fertilisation (IVF) for moderate and intracytoplasmic sperm injection (ICSI) for men with severe sperm dysfunction. One reason for the lack of progress in this area is that our understanding of the cellular and molecular workings of the mature spermatozoon is limited. However, over the last few years there has been considerable progress in our knowledge base and in addressing new methods to diagnose sperm dysfunction. The purpose of this paper is to review the current state of the field and provide insights for further development. The initial focus is on the value of semen analysis as a clinical tool with the discussion progressing to examining sperm dysfunction in detail.

WHERE IS SEMEN ANALYSIS NOW AND WHERE IS IT GOING?

The recent fifth edition of the WHO semen analysis manual⁵ addresses many of the criticisms levelled at previous versions⁶ and now includes

step by step methods, constructive discussion of quality control and quality assurance, detailed descriptions of the assessment of sperm morphology and, for the very first time, biologically based reference ranges. The WHO manual has always been the bedrock of andrology and the fifth version is likely to assist the development of the field still further. However, based on previous experiences, major challenges remain to be addressed.⁷ These have continually been present yet, the evidence to date suggests that although the problems can be easily identified there is often minimal or no resolution. Three particular aspects merit further attention.

Firstly, technicians are not using the detailed laboratory methods even when provided in comprehensive manuals.⁸ An example of this is the review of practice in the UK.⁹ Remarkably, in a country that has had semen training course for many years, only 5% of laboratories carried out the WHO standard method for morphology assessments. Equally surprising was that 69% of laboratories counted ≤ 100 sperm for morphology assessments making the assay effectively redundant. This poor practice is of course not limited to the UK and has been highlighted by a number of authors.^{10,11}

Secondly, training methods exist—but are they used/useful? A plethora of data shows that there are robust training methods available for assessment of basic semen analysis.¹² A series of programs have been developed and proven to reduce variability.¹³ What these programs show is: (i) technicians currently performing semen assessments often produce great variability; (ii) proven techniques and intensive instruction can improve education and reduce variability dramatically; and (iii) with ongoing training, even when the technicians return back to

¹Reproductive and Developmental Biology, Maternal and Child Health Science Laboratories, Centre for Oncology and Molecular Medicine, Ninewells Hospital, University of Dundee, Dundee, DD1 9SY, Scotland, UK and ²Assisted Conception Unit, NHS Tayside, Ninewells Hospital, Dundee, DD1 9SY, Scotland, UK
Correspondence: Dr C L R Barratt (c.barratt@dundee.ac.uk)

Received: 18 October 2010; Revised: 24 October 2010; Accepted: 25 October 2010; Published online: 22 November 2010

their home laboratory environment, standards can be maintained. However, what is observed from, for example, external quality control programs is that the majority of laboratories have a great deal of error in their analysis.¹⁴ Clearly there is a discourse here—training works, but the clinical assessments are often poor. The reasons behind this discourse are unclear. One possibility is that although methods to train technicians exist, there are not enough courses available for the vast number of people doing semen assessments and/or technicians are not attending these courses. The alternative hypothesis is that traditional teaching methods are not the way to address the problem. It is very likely that demand for intensive courses is not being met for a variety of economical and practical reasons and clearly this needs to be urgently addressed. However, newer methods and/or structures of training laboratory andrologists, e.g., via the Internet must be developed. Complementary training can be instigated by using a sophisticated laboratory book system which allows comprehensive detailed supervised training on site. An example is the structure adopted by the Association of Biomedical Andrologists (www.aba.uk.net). The hypothesis (and hope) is that the improvements in the training of staff will be translated into higher standards of semen assessments.

Thirdly, consistently both scientists and clinicians in our discipline denigrate the value of semen assessments with arguments based on a series of false assumptions.^{11,14,15} An example is the assumption that semen assessments are currently performed in an adequate manner. This is wrong. The evidence from external quality control schemes demonstrates that some patients will be referred for inappropriate treatment, e.g., ICSI when they may not even need ART. In simplistic terms, we are exposing a large number of couples to inappropriate financial and psychological stress. Additionally, we are potentially exposing the female to harmful procedures, e.g., IVF. Perhaps this third lesson will not be executed until legal action ensues.

WHY DOES MALE INFERTILITY REQUIRE MORE ROBUST DIAGNOSTIC TOOLS THAN A BASIC SEMEN ANALYSIS?

Although the diagnostic and predictive value of traditional semen parameters has been debated for over 80 years, the inescapable conclusion remains that its clinical value is limited. The remits of this limitation are contentious but two facts are clear: (i) at the lower ends of the spectrum, e.g., low concentrations of motile spermatozoa, there are significantly higher chances of subfertility;^{16,17} and (ii) except in rare cases, e.g., globozoospermia,¹⁸ values above these limits provide minimal diagnostic clarity.^{19,20} This information is not new and was highlighted by MacLeod and colleagues who concluded that ‘The greatest difference between the two groups (infertile and fertile) is seen at the count levels under 20 million/cc. Only 5% of fertile men compared with 16% of the ‘infertile’ group fall into this category’.²¹ Importantly, for the robustness of the conclusions, a plethora of subsequent studies have repeated these experiments in various guises and, not surprisingly, come to the similar conclusions. The most recent of these, undertaken by the WHO,²² provide new reference values for semen assessment which not surprisingly are remarkably similar (with exception of morphology) to that proposed by MacLeod and Gould in 1951.²¹

Therefore, the conclusions regarding the clinical relevance of semen assessment are unlikely to change. New studies are not required. What are urgently needed are new assessments of male reproductive potential. This is the focus of the following discussion.

SPERM DYSFUNCTION—OLD TESTS LYING DORMANT?

To date, the assessment of sperm function has failed to make a significant impact on the clinical management of couples. The reasons for

this, e.g., lack of standardized protocols have been rehearsed elsewhere.²⁰ In summary, the logarithmic progress that has been made in understanding the basic science around how a spermatozoon develops, prepares for fertilisation and contributes to a healthy birth has not (yet) been translated into routine clinical practice.²³

It is disappointing to arrive at this conclusion, but it is heartening to realize that this is very likely to change in the near future. One example will suffice. A primary functional assay is the human zona-binding test. Whilst the paradigm of sperm binding and subsequent acrosome reaction may be questioned in mice,²⁴ consistently, robust clinical data demonstrates its usefulness for ART success. A large range of patients have been identified with poor or adequate binding but minimal induction of the acrosome reaction in response to the zona.²⁵ However, a key problem with the widespread use of human zona-binding assays, in fact its universal restriction, is the availability of material. The initial promise of using recombinant zona pellucida protein 3 (ZP3) as a surrogate for the human zona was not fulfilled primarily because: (i) techniques to produce the recombinant proteins were not optimized; and (ii) our knowledge base of what proteins were present in the zona and their structures was unavailable. These points have and are being addressed (respectively). Exciting data from a series of experiments using what appears to be robust preparations of recombinant human zona proteins has been published.²⁶ An *in vitro* sperm function assay using recombinant products is now much more of a reality.

Whilst the objective of robust assays of sperm function must inevitably be to simplify the tools for routine use, we are dealing with complex systems; thus, the challenges in developing these assays are considerable. An example of this is the regulation of calcium by the cell which is clearly critical for key physiological processes, e.g., motility and acrosome reaction. Whilst our knowledge of how calcium is regulated in the cell has increased substantially,^{27,28} there are still fundamental gaps, e.g., the role of the putative calcium stores in the sperm neck/midpiece region. However, decades of clinical research suggest that calcium regulation can potentially be used as a tool for identifying dysfunctional cells.²⁹ What are missing are robust assays. In our laboratory, we have been using an FLUOstar assay (BMG labtech, Offenburg, Germany) for the rapid screening of calcium mobilisation in prepared semen samples and although the assays are accurate and rapid, there are practical problems with their routine use. For example, currently it requires a minimum of 0.5 million cells post preparation to obtain robust data points. This excludes a number of men referred for ART where we have no information and arguably (see above); these are the men who have the most to gain from detailed sperm function testing. Additionally, currently progesterone is used as an agonist to induce a response and although there is considerable clinical data to support its use,³⁰ we have minimal knowledge of what progesterone actually does in the cell, e.g., mobilisation of stores, interacting with the receptors. Maybe other agonists would provide better tools, but they have yet to be identified. Abnormalities in signalling do exist, but presently we do not have a reliable method to assess these problems and although progress in basic research is very impressive, we need to complement this with a translational focus.

SPERM FUNCTION TESTING AND ICSI

There has been a plethora of studies suggesting that, in the overwhelming majority of cases, the quality of the semen has little or no influence on the success rates of ICSI.³¹ Not surprisingly, there is a lack of data on sperm function testing and the focus of activity has been in attempting to improve the selection process of spermatozoa, e.g.,

hyaluronic acid binding (Table 1). However, it is increasingly apparent that studies are hampered by the lack of knowledge of what defines a functional spermatozoon and the destructive nature of the investigations. This results in extensive data on surrogate quality indicators of entire populations but fails to address the individual quality of a single spermatozoon. As a result, a wide variety of techniques have been tried based on current knowledge in the hope of improving pregnancy outcomes. These include externalisation of phosphatidylserine (magnetic-activated cell sorting),³² cell charge (zeta charge),³³ maturity markers (hyaluronic acid binding)^{34–36} and detailed morphological analysis (intracytoplasmic morphologically selection sperm injection).^{37–40} Although some studies have recorded significant improvements in clinical pregnancy rates, these studies generally fail to present useful statistical data that will indicate the effectiveness of this method over conventional ICSI. Such data include, number needed to treat (number of oocytes injected before pregnancy is achieved compared to the control), relative risk (the risk of falling pregnant using this method compared to the control) and odds ratio (the odds of falling pregnant compared to the control). As well as this, the lack of studies reporting live birth rates is noticeable, preventing the assessment of the take home baby rate and the overall effectiveness of the method. Another question is what levels of improvement is truly significant, 2% or 20% and are these new methods applicable to a busy IVF laboratory both financially and logistically.

Another way to look at this problem is to address if, and how, sperm are capable of confessing their errors/flaws externally,⁴¹ which may allow non-invasive sperm selection, e.g., in response to DNA damage⁴². However, it remains to be seen whether such biomarkers do exist or if the heterogeneity of spermatozoa is too great for such selection methods to be applicable to every patient. Instead, case-by-case assessments may have to be used, adding time and additional effort. What is certain is that a clear clinical requirement (identification of the ‘best’ spermatozoon) is acting as a welcome catalyst and focus on the detection of high quality cells in ART will continue to have a direct effect on the proliferation of basic research in the area.

THE USEFULNESS OF ANIMAL STUDIES: ZONADHESIN AS AN EXAMPLE

With relatively few exceptions the data from mouse knockout studies has not been successfully translated into the clinical arena. There are a number of reasons for this with differences in the reproduction process being one;⁴³ however, with respect to sperm dysfunction, there are sufficient key similarities between mice and men to provide a more in depth understanding and the potential to identify candidate proteins to be used as a biomarker of dysfunction. An example is the intra-acrosomal protein zonadhesin.

Zonadhesin was first discovered in pigs based on the ability to bind the ZP and subsequent studies identified it in mouse, hamster, horse, donkey, zebra, rat, guinea pig, chinchilla, dog and human (Tardif *et al.*, unpubl. data).^{44–47} Importantly, sperm–ZP adhesion activity confers species specificity and to date, zonadhesin is the only sperm protein among sperm–ZP adhesion candidates showing species specificity during fertilisation. This was established by the high affinity of zonadhesin for native ZP between homologous gametes and, more recently, using zonadhesin-null mice.⁴⁸ Interestingly, mouse zonadhesin was only detectable at the sperm surface of live spermatozoa after incubation in conditions supporting sperm capacitation. Preliminary data suggest that the same is true for human cells and the question is—can this intra-acrosomal protein be used as a potential biomarker for human sperm function/dysfunction?

Table 1 Selection of sperm for ICSI using HA binding^a

Reference	Method(s) and P value	Study type	Putative selection against	Patient no.	Cycles	Women's mean ages (years)	No. of oocytes injected	No. of embryos transferred	Fertilisation rate (%)	Good-quality embryos (%)	Implantation rate (%)	Clinical pregnancy rate (%)
Parmegiani <i>et al.</i> (2010) ³⁵	HA-ICSI	Retrospective	DNA damage, chromosomal aneuploidy and poor nuclear morphology	293	331	34.8±3.4	2.8±0.8	326	93.4	35.2	17.1	32.8
	Conventional ICSI			86	97	35.0±3.6	2.6±0.6	96	87.1	22.3	10.3	21.6
Parmegiani <i>et al.</i> (2010) ³⁶	P value			—	—	NS	NS	—	—	0.011	0.047	NS
	HA-ICSI	Prospective	DNA fragmentation and abnormal spermatozoon	112	125	37.5±0.4	2.1±0.1	125	91.6	35.8	12.4	24.8
Nasr-Esfahani <i>et al.</i> (2008) ³⁴	Conventional ICSI			94	107	37.1±0.4	2.1±0.1	105	85.8	24.1	24.1	20.9
	P value			—	—	NS	NS	—	NS	0.046	NS	NS
(2008) ³⁴	HA-ICSI	Prospective	Immature spermatozoa	50	—	—	4.98±2.57	1.44±0.89	79.4±26.0	96.4±14.1	20	46
	Conventional ICSI			50	—	—	5.34±2.42	1.70±1.31	67.7±23.5	97.6±8.7	16	40
	P value			—	—	—	NS	NS	0.02	NS	NS	NS

Abbreviations: HA, hyaluronic acid; ICSI, intracytoplasmic sperm injection; NS, not significant.

^a Results compared to control (conventional ICSI). Selection of three studies based on clinical trials using HA binding in comparison to traditional ICSI. Studies for inclusion were selected from articles published on PubMed over the last 4 years. Studies were excluded based on use of animal models, cryopreserved samples, lack of clinical pregnancy rate and/or experimental methods. Significance $P \leq 0.05$. Note no significant improvement was observed in clinical pregnancy rates using HA binding.

Based on the zonadhesin exposure during capacitation in the mouse, we proposed a putative model (Figure 1), where human zonadhesin could be exposed after capacitation (or latter stages of) differently between fertile and subfertile men. Zonadhesin exposure could be reduced in spermatozoa unable to undergo capacitation due possibly to problems in protein trafficking. Conversely, under non-capacitating conditions zonadhesin exposure would not be expected or only present in a very small percentage of cells, but in some subfertile men there may be premature exposure due to a misregulation of transduction events.

Currently there is a paucity of markers of human sperm function at a molecular level. One variation between fertile and subfertile men could reside in how the proteins are post-translationally modified as opposed to their mere presence or absence. In this context we have observed, in two different subfertile patients who experienced failed fertilisation at IVF, significantly different polypeptide distribution and processing of zonadhesin compared to controls (Tardif *et al*, unpubl.

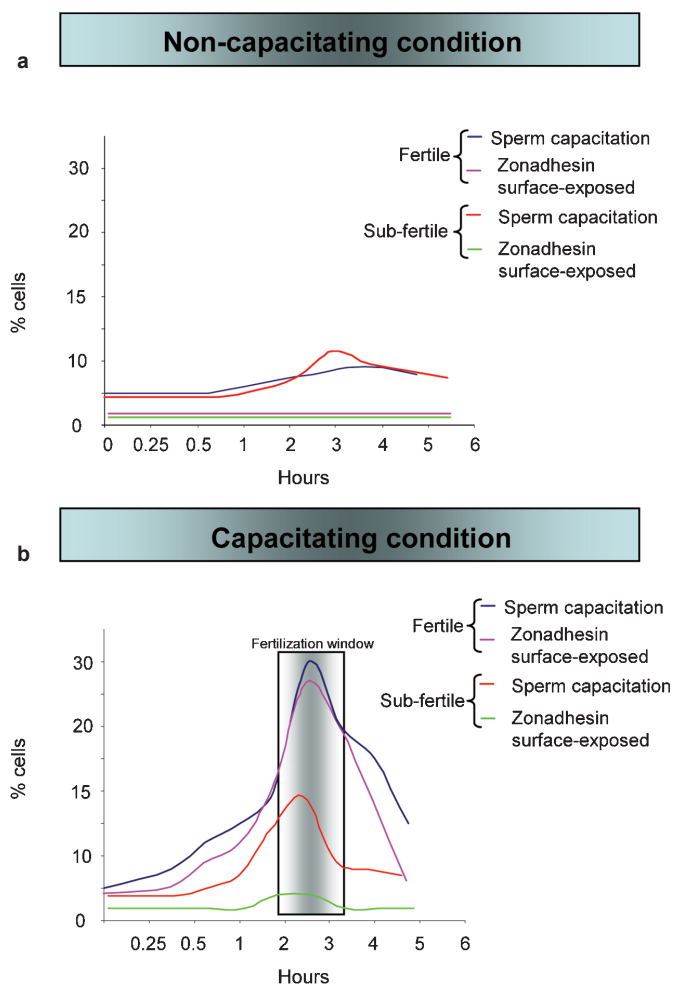


Figure 1 Putative model of human zonadhesin exposure during sperm incubation under (a) non-capacitating or (b) capacitating conditions in fertile and subfertile men. Diagram indicates time course of sperm capacitation (red and blue) and zonadhesin exposure (pink and green) in fertile and subfertile men respectively. This model suggests that sperm capacitation is closely related to zonadhesin exposure in fertile men; however, a decrease of zonadhesin exposure could be associated with subfertile men related to compromised capacitation. Shaded area in (b) represents the fertilisation window.

data). Whilst preliminary, our data suggest that zonadhesin has the potential to be a biomarker for evaluating a fertile sperm population.

POTENTIAL NEW PARADIGMS—HOME TESTING FOR MALE INFERTILITY

An area which has seen considerable progress is the development of a number of putative home sperm tests.^{49–51} The details of these and arguments for and against their use are presented elsewhere,^{20,51} but for widespread acceptance these assays need to be: (i) testing some functional capacity of the cell rather than numbers; (ii) robust; (iii) cheap; and (iv) widely available. Whilst currently no test fulfils all of these criteria, with the rapid developments in new technologies, it is likely that new and more robust versions of home test will become available in the very near future. Interestingly, these tests may also be taken a step further—from diagnosis to treatment. For example, they may indicate that the man has sperm present but that these cells are functionally defective, e.g., produce high levels of lipid peroxidation end products. If antioxidant therapy is, in the future, a proven treatment for oxidative stress, then it is feasible that a man could have a diagnosis and order (self-) treatment (for example vitamin E) all within one hour! Although exciting, this is at present a fantasy. Critically, what has to be established is where in the patient's pathway these assays will be of most benefit? The original hypothesis was that they would be the first stage for a couple who were enquiring about their fertility.^{20,51} Following the test, the couple could make a choice (depending on the result) to continue trying or seek earlier referral. The logic was that seeking earlier referral would increase the chances of conception particularly in couples where female age was a pressing problem. However, whilst attractive, this concept remains untested and although patients may find home testing very appealing, there is as yet no direct evidence that over the counter tests would improve the chances of conception.

FUTURE MARKERS OF SPERM DYSFUNCTION—NEW TECHNOLOGIES

This is a particular exciting time in andrology. For example, following the somewhat controversial discovery of mRNA in mature human sperm,⁵² there have been a number of studies suggesting that these mRNAs could be used as a diagnostic tool—equivalent to a transcriptome.⁵³ Whilst the data to support this is in its infancy, this is likely to be an area of rapid development which holds great promise.

The power of proteomics is now increasingly being applied to mature spermatozoa.⁵⁴ Although technical difficulties are preventing the complete sperm proteome from being available,⁵⁵ the cataloguing to date is impressive and consistently brings new thoughts to the field on how the cell works.⁵⁶ Comparison to the proteome of other species could answer fundamental questions such as: what is the basic machinery necessary to make a functionally mature male gamete?⁵⁷ Complementary to completing the tool kit of the sperm proteome, another area where proteomics is having an impact is the identification of putative candidate biomarkers of high- and poor-quality cells. Impressive data are rapidly appearing, for example comparing potential differences in men with specific pathologies, e.g., asthenozoospermia.⁵⁸

Driven by the overwhelming clinical need to identify subfertile men without the requirement for a semen assessment, we may soon be able to obtain metabolomic profiling on blood samples which act as a surrogate for fertility. This is a very difficult area as comparable experiments in other disciplines, e.g., cancer highlights the herculean challenges in the identification of robust candidates of dysfunction which can be readily translated into clinical practice.⁵⁹ However, this is

potentially very exciting. Additionally, other techniques such as Raman spectroscopy are beginning to be used to identify (non-invasively) genetically compromised cells driven by the imperative to inject the most genetically functional cell at ICSI.⁶⁰

Whatever new tests of sperm function, or reworking of old ones are proposed, we need to heed the lessons of the past. A classic example is the sperm chromatin/DNA damage assays. The primary data supporting these was presented in 1980 and although they are consistently suggested as important tools in the armamentarium, they face considerable challenges before they can become part of routine clinical management.⁶¹

SUMMARY—WHERE TO GO NOW?

The arguments presented suggest that for semen analysis, there is little to be gained from more studies identifying/categorizing various populations of men. Where an effort is required is making sure the analysis is performed in an appropriate high-quality way.

Technological development is likely to bring the reality of sperm function testing closer to implementation into the clinical pathways. In doing this, these assays must be: (i) robust; (ii) cheap (or more appropriately termed cost effective); (iii) easy to use; and (iv) clinically useful. To achieve the last tenet is a major challenge that requires special consideration. If these assays are to be routinely used, there must be a rigorous examination of their application using standardized procedures.⁶² Additionally, there needs to be a critical determination of where these assays fit within the patient pathway.⁶³ To date, assays of the functional competence of sperm have not yet been evaluated in this critical manner. Real progress depends on enforcing these tenets.

There is a palpable excitement in andrology. Importantly, clinical requirements are acting as a catalysts and focus on the detection of high-quality cells in ART which is having a direct effect on the proliferation of basic research. Additionally, there are very clear advances in our understanding of the mature cell in no small part being brought about by application of proven technology from other areas. This is an exciting time to be an andrologist and, likely, a fruitful one.

AUTHOR CONTRIBUTIONS

CLRB designed the concept and framework of the paper and wrote the first draft. All authors contributed to the drafting and final editing of the manuscript.

COMPETING FINANCIAL INTERESTS

The authors declare no relevant commercial interest.

ACKNOWLEDGMENTS

Work in the author's laboratories is funded by The Wellcome Trust, TENOVUS (Scotland), University of Dundee, MRC (Developmental Pathway Funding Scheme), NHS Tayside and Scottish Enterprise.

The authors are very grateful to all members of the Assisted Conception Unit at Ninewells Hospital for assistance with obtaining donors and patient's samples for research and training purposes. The senior author (CLRB) is very grateful to W. Christopher L. Ford for many interesting discussions regarding the concept of sperm function testing.

- 3 Irvine DS. Epidemiology and aetiology of male infertility. *Hum Reprod* 1998; **13** Suppl 1: 33–44.
- 4 Aitken RJ. Sperm function tests and fertility. *Int J Androl* 2006; **29**: 69–75.
- 5 World Health Organization. WHO Laboratory Manual for the Examination and Processing of Human Semen. 5th edn. Geneva: WHO Health Organization, 2010. <http://www.who.int/reproductivehealth/publications/infertility/9789241547789/en/>.
- 6 Barratt CL. On the accuracy and clinical value of semen laboratory tests. *Hum Reprod* 1995; **10**: 250–2.
- 7 de Jonge CJ, Barratt CL. WHO manual...who should care? *Hum Reprod* 1999; **14**: 2431–3.
- 8 Mortimer D. Practical Laboratory Andrology. Oxford: Oxford University Press; 1994.
- 9 Riddell D, Pacey A, Whittington K. Lack of compliance by UK andrology laboratories with World Health Organization recommendations for sperm morphology assessment. *Hum Reprod* 2005; **20**: 3441–5.
- 10 Ombelet W, Pollet H, Bosmans E, Vereecken A. Results of a questionnaire on sperm morphology assessment. *Hum Reprod* 1997; **12**: 1015–20.
- 11 Pacey AA. Quality assurance and quality control in the laboratory andrology. *Asian J Androl* 2010; **12**: 21–5.
- 12 Björndahl L, Barratt CL, Fraser LR, Kvist U, Mortimer D. ESHRE basic semen analysis courses 1995–1999: immediate beneficial effects of standardized training. *Hum Reprod* 2002; **17**: 1299–305.
- 13 Franken DR, Aneck-Hahn N, Lombaard C, Kruger TF. Semenology training programs: 8 years' experience. *Fertil Steril* e-pub ahead of print 28 May 2010; PMID: 20553675.
- 14 Pacey AA. Is quality assurance in semen analysis still really necessary? A view from the andrology laboratory. *Hum Reprod* 2006; **21**: 1105–9.
- 15 Holt WV. Is quality assurance in semen analysis still really necessary? A spermatologist's viewpoint. *Hum Reprod* 2005; **20**: 2983–6.
- 16 Hargreave TB, Elton RA. Fecundability rates from an infertile male population. *Br J Urol* 1986; **58**: 194–7.
- 17 Guzik DS, Overstreet JW, Factor-Litvak P, Brazil CK, Nakajima ST *et al*. Sperm morphology, motility, and concentration in fertile and infertile men. *N Engl J Med* 2001; **345**: 1388–93.
- 18 Kilani Z, Ismail R, Ghunaim S, Mohamed H, Hughes D *et al*. Evaluation and treatment of familial globozoospermia in five brothers. *Fertil Steril* 2004; **82**: 1436–9.
- 19 Tomlinson MJ, Kessopoulou E, Barratt CL. The diagnostic and prognostic value of traditional semen parameters. *J Androl* 1999; **20**: 588–93.
- 20 Lefèvre L, Bedu-Addo K, Conner SJ, Machado-Oliveira GS, Chen Y *et al*. Counting sperm does not add up any more: time for a new equation? *Reproduction* 2007; **133**: 675–84.
- 21 MacLeod J, Gold RZ. The male factor in fertility and infertility. II. Spermatozoon counts in 1000 men of known fertility and in 1000 cases of infertile marriage. *J Urol* 1951; **66**: 436–49.
- 22 Cooper TG, Noonan E, von Eckardstein S, Auger J, Baker HW *et al*. World Health Organization reference values for human semen characteristics. *Hum Reprod Update* 2010; **16**: 231–45.
- 23 Ford WC. Comments on the release of the 5th edition of the WHO Laboratory Manual for the Examination and Processing of Human Semen. *Asian J Androl* 2010; **12**: 59–63.
- 24 Baibakov B, Gauthier L, Talbot P, Rankin TL, Dean J. Sperm binding to the zona pellucida is not sufficient to induce acrosome exocytosis. *Development* 2007; **134**: 933–43.
- 25 Liu DY, Liu ML, Baker HW. Enhancement of sperm–zona pellucida (ZP) binding capacity by activation of protein kinase A and C pathways in certain infertile men with defective sperm–ZP binding. *Hum Reprod* 2009; **24**: 20–7.
- 26 Gupta SK, Bansal P, Ganguly A, Bhandari B, Chakrabarti K. Human zona pellucida glycoproteins: functional relevance during fertilization. *J Reprod Immunol* 2009; **83**: 50–5.
- 27 Costello S, Michelangeli F, Nash K, Lefevre L, Morris J *et al*. Ca²⁺-stores in sperm: their identities and functions. *Reproduction* 2009; **138**: 425–37.
- 28 Publicover S, Harper CV, Barratt C. Ca²⁺ signalling in sperm—making the most of what you've got. *Nat Cell Biol* 2007; **9**: 235–242.
- 29 Krausz C, Bonaccorsi L, Maggio P, Luconi M, Criscuolo L *et al*. Two functional assays of sperm responsiveness to progesterone and their predictive values in *in-vitro* fertilization. *Hum Reprod* 1996; **11**: 1661–7.
- 30 Luconi M, Francavilla F, Porazzi I, Macerola B, Forti G *et al*. Human spermatozoa as a model for studying membrane receptors mediating rapid nongenomic effects of progesterone and estrogens. *Steroids* 2004; **69**: 553–9.
- 31 Lewis SE. Is sperm evaluation useful in predicting human fertility? Review. *Reproduction* 2007; **134**: 31–40.
- 32 Dirican EK, Ozgün OD, Akarsu S, Akin KO, Ercan O *et al*. Clinical outcome of magnetic activated cell sorting of non-apoptotic spermatozoa before density gradient centrifugation for assisted reproduction. *J Assist Reprod Genet* 2008; **25**: 375–81.
- 33 Kheirollahi-Kouhestani M, Razavi S, Tavalaei M, Deemeh MR, Mardani M *et al*. Selection of sperm based on combined density gradient and Zeta method may improve ICSI outcome. *Hum Reprod* 2009; **24**: 2409–16.
- 34 Nasr-Esfahani MH, Razavi S, Vahdati AA, Fathi F, Tavalaei M. Evaluation of sperm selection procedure based on hyaluronic acid binding ability on ICSI outcome. *J Assist Reprod Genet* 2008; **25**: 197–203.
- 35 Parmegiani L, Cognigni GE, Ciampaglia W, Pocognoli P, Marchi F *et al*. Efficiency of hyaluronic acid (HA) sperm selection. *J Assist Reprod Genet* 2010; **27**: 13–6.
- 36 Parmegiani L, Cognigni GE, Bernardi S, Troilo E, Ciampaglia W *et al*. 'Physiologic ICSI': hyaluronic acid (HA) favours selection of spermatozoa without DNA

1 Boivin J, Bunting L, Collins JA, Nygren KG. International estimates of infertility prevalence and treatment-seeking: potential need and demand for infertility medical care. *Hum Reprod* 2007; **22**: 1506–12.

2 Hull MG, Glazener CM, Kelly NJ, Conway DI, Foster PA *et al*. Population study of causes, treatment, and outcome of infertility. *Br Med J (Clin Res Ed)* 1985; **291**: 1693–7.

- fragmentation and with normal nucleus, resulting in improvement of embryo quality. *Fertil Steril* 2010; **93**: 598–604.
- 37 Bartoov B, Berkovitz A, Eltes F, Kogosovsky A, Yagoda A *et al*. Pregnancy rates are higher with intracytoplasmic morphologically selection sperm injection than with conventional intracytoplasmic injection. *Fertil Steril* 2003; **80**(6): 1413–9.
- 38 Berkovitz A, Eltes F, Yaari S, Katz N, Barr I *et al*. The morphological normalcy of the sperm nucleus and pregnancy rate of intracytoplasmic injection with morphologically selected sperm. *Hum Reprod* 2005; **20**: 185–90.
- 39 Hazout A, Dumont-Hassan M, Junca AM, Cohen Bacrie P, Tesarik J. High-magnification ICSI overcomes paternal effect resistant to conventional ICSI. *Reprod Biomed Online* 2006; **12**: 19–25.
- 40 Antinori M, Licata E, Dani G, Cerusico F, Versaci C *et al*. Intracytoplasmic morphologically selected sperm injection: prospective randomized trial. *Reprod Biomed Online* 2008; **16**: 835–41.
- 41 Cohen J. Cross-overs, sperm redundancy and their close association. *Heredity* 1973; **31**: 408–13.
- 42 Aitken RJ, Koppers AJ. Apoptosis and DNA damage in human spermatozoa. *Asian J Androl*; e-pub ahead of print 30 August 2010; PMID: 20802502.
- 43 Conner SJ, Lefièvre L, Kirkman-Brown JC, Michelangeli F, Jimenez-Gonzalez C *et al*. Understanding the physiology of pre-fertilisation events in the human spermatozoa—a necessary prerequisite to developing rational therapy. *Soc Reprod Suppl* 2007; **63**: 237–256.
- 44 Hardy DM, Garbers DL. Species-specific binding of sperm proteins to the extracellular matrix (zona pellucida) of the egg. *J Biol Chem* 1994; **269**: 19000–400.
- 45 Gao Z, Garbers DL. Species diversity in the structure of zonadhesin, a sperm-specific membrane protein containing multiple cell adhesion molecule-like domains. *J Biol Chem* 1998; **273**: 4315–21.
- 46 Olson GE, Winfrey VP, Nagdas SK. Acrosome biogenesis in the hamster: ultrastructurally distinct matrix regions are assembled from common precursor polypeptide. *Biol Reprod* 1998; **58**: 361–70.
- 47 Tardif S, Brady HA, Breazeale KR, Bi M, Thompson LD *et al*. Zonadhesin D3-polypeptides vary among species but are similar in *Equus* species capable of interbreeding. *Biol Reprod* 2010; **82**: 413–21.
- 48 Tardif S, Wilson MD, Wagner R, Hunt P, Gertsenstein M *et al*. Zonadhesin is essential for species specificity of sperm adhesion to the egg zona pellucida. *J Biol Chem* 2010; **285**: 24863–70.
- 49 Coppola MA, Klotz KL, Kim KA, Cho HY, Kang J, Shetty J, Howards SS, Flickinger CJ, Herr JC. SpermCheck Fertility, an immunodiagnostic home test that detects normozoospermia and severe oligozoospermia. *Hum Reprod* 2010; **25**: 853–61.
- 50 Segerink LI, Sprenkels AJ, ter Braak PM, Vermes I, van den Berg A. On-chip determination of spermatozoa concentration using electrical impedance measurements. *Lab Chip* 2010; **10**: 1018–24.
- 51 Björndahl L, Kirkman-Brown J, Hart G, Rattle S, Barratt CL. Development of a novel home sperm test. *Hum Reprod* 2006; **21**: 145–9.
- 52 Miller D, Tang PZ, Skinner C, Lilford R. Differential RNA fingerprinting as a tool in the analysis of spermatozoal gene expression. *Hum Reprod* 1994; **9**: 864–9.
- 53 Lalancette C, Miller D, Li Y, Krawetz SA. Paternal contributions: new functional insights for spermatozoal RNA. *J Cell Biochem* 2008; **104**: 1570–9.
- 54 Baker MA, Reeves G, Hetherington L, Muller J, Baur I *et al*. Identification of gene products present in the Triton X soluble and insoluble fractions of human spermatozoa lysates using LC-MS/MS analysis. *Proteomics Clin Appl* 2007; **1**: 524–32.
- 55 Oxenham SK. Sperm proteomics: thinking outside the collision cell. *J Androl* 2010; **31**: 431–3.
- 56 Oliva R, de Mateo S, Estanyol JM. Sperm cell proteomics. *Proteomics* 2009; **9**: 1004–17.
- 57 Findlay GD, Swanson WJ. Proteomics enhances evolutionary and functional analysis of reproductive proteins. *Bioessays* 2010; **32**: 26–36.
- 58 Zhao C, Huo R, Wang FQ, Lin M, Zhou ZM *et al*. Identification of several proteins involved in regulation of sperm motility by proteomic analysis. *Fertil Steril* 2007; **87**: 436–8.
- 59 Goodsaid FM, Mendrick DL. Translational medicine and the value of biomarker qualification. *Sci Transl Med* 2010; **2**: 47ps44.
- 60 Huser T, Orme CA, Hollars CW, Corzett MH, Balhorn R. Raman spectroscopy of DNA packaging in individual human sperm cells distinguishes normal from abnormal cells. *J Biophotonics* 2009; **2**: 322–32.
- 61 Barratt CL, Aitken RJ, Björndahl L, Carrell DT, de Boer P *et al*. Sperm DNA: organization, protection and vulnerability: from basic science to clinical applications—a position report. *Hum Reprod* 2010; **25**: 824–38.
- 62 Gluud C, Gluud LL. Evidence based diagnostics. *BMJ* 2005; **330**: 724–6.
- 63 Bossuyt PM, Irwig L, Craig J, Glasziou P. Comparative accuracy: assessing new tests against existing diagnostic pathways. *BMJ* 2006; **332**: 1089–92.

p,p'-DDE activates CatSper and compromises human sperm function at environmentally relevant concentrations

Renata S. Tavares^{1,2}, Steven Mansell³, Christopher L.R. Barratt³,
Stuart M. Wilson³, Stephen J. Publicover⁴, and João Ramalho-Santos^{1,2,*}

¹Biology of Reproduction and Stem Cell Group, CNC—Center for Neuroscience and Cell Biology, University of Coimbra, Coimbra 3001-401, Portugal ²Department of Life Sciences, University of Coimbra, Coimbra 3001-401, Portugal ³Medical Research Institute, Ninewells Hospital and Medical School, Dundee DD1 9SY, UK and ⁴School of Biosciences, University of Birmingham, Birmingham B15 2TT, UK

*Correspondence address. Department of Life Sciences, University of Coimbra, PO Box 3046, Coimbra 3001-401, Portugal.
Tel: +351-239-855-760; Fax: +351-239-855-789; E-mail: jramalho@ci.uc.pt

Submitted on May 30, 2013; resubmitted on August 21, 2013; accepted on September 4, 2013

STUDY QUESTION: Is the environmental endocrine disruptor *p,p'*-dichlorodiphenyldichloroethylene (*p,p'*-DDE) able to induce non-genomic changes in human sperm and consequently affect functional sperm parameters?

SUMMARY ANSWER: *p,p'*-DDE promoted Ca^{2+} flux into human sperm by activating CatSper channels even at doses found in human reproductive fluids, ultimately compromising sperm parameters important for fertilization.

WHAT IS KNOWN ALREADY: *p,p'*-DDE may promote non-genomic actions and interact directly with pre-existing signaling pathways, as already observed in other cell types. However, although often found in both male and female reproductive fluids, its effects on human spermatozoa function are not known.

STUDY DESIGN, SIZE, DURATION: Normozoospermic sperm samples from healthy individuals were included in this study. Samples were exposed to several *p,p'*-DDE concentrations for 3 days at 37°C and 5% CO_2 *in vitro* to mimic the putative continuous exposure to this toxicant in the female reproductive tract *in vivo*. Shorter *p,p'*-DDE incubation periods were also performed in order to monitor sperm rapid Ca^{2+} responses. All experiments were repeated on a minimum of five sperm samples from different individuals.

PARTICIPANTS/MATERIALS, SETTING, METHODS: All healthy individuals were recruited at the Biosciences School, University of Birmingham, the Medical Research Institute, University of Dundee and in the Human Reproduction Service at University Hospitals of Coimbra. Intracellular Ca^{2+} concentration ($[\text{Ca}^{2+}]_i$) was monitored by imaging single spermatozoa loaded with Oregon Green BAPTA-1AM and further whole-cell patch-clamp recordings were performed to validate our results. Sperm viability and acrosomal integrity were assessed using the LIVE/DEAD sperm vitality kit and the acrosomal content marker PSA-FITC, respectively.

MAIN RESULTS AND THE ROLE OF CHANCE: *p,p'*-DDE rapidly increased $[\text{Ca}^{2+}]_i$ ($P < 0.05$) even at extremely low doses (1 pM and 1 nM), with magnitudes of response up to 200%, without affecting sperm viability, except after 3 days of continuous exposure to the highest concentration tested ($P < 0.05$). Furthermore, experiments performed in a low Ca^{2+} medium demonstrated that extracellular Ca^{2+} influx was responsible for this Ca^{2+} increase ($P < 0.01$). Mibefradil and NNC 55-0396, both inhibitors of the sperm-specific CatSper channel, reversed the *p,p'*-DDE-induced $[\text{Ca}^{2+}]_i$ rise, suggesting the participation of CatSper in this process ($P < 0.05$). In fact, whole-cell patch-clamp recordings confirmed CatSper as a target of *p,p'*-DDE action by monitoring an increase in CatSper currents of $> 100\%$ ($P < 0.01$). Finally, acrosomal integrity was adversely affected after 2 days of exposure to *p,p'*-DDE concentrations, suggesting that $[\text{Ca}^{2+}]_i$ rise may cause premature acrosome reaction ($P < 0.05$).

LIMITATIONS, REASONS FOR CAUTION: This is an *in vitro* study, and caution must be taken when extrapolating the results.

WIDER IMPLICATIONS OF THE FINDINGS: A novel non-genomic *p,p'*-DDE mechanism specific to sperm is shown in this study. *p,p'*-DDE was able to induce $[\text{Ca}^{2+}]_i$ rise in human sperm through the opening of CatSper consequently compromising male fertility. The promiscuous nature of CatSper activation may predispose human sperm to the action of some persistent endocrine disruptors.

STUDY FUNDING/COMPETING INTEREST(S): The study was supported by both the Portuguese National Science Foundation (FCT; PEst-C/SAU/LA0001/2011) and the UK Wellcome Trust (Grant #86470). SM was supported by the Infertility Research Trust. RST is a recipient of a PhD fellowship from FCT (SFRH/BD/46002/2008). None of the authors has any conflict of interest to declare.

Key words: *p,p'*-DDE / intracellular Ca^{2+} concentration / Ca^{2+} influx / CatSper / acrosome reaction

Introduction

Exposure to numerous environmental toxicants may have contributed to a decline in human semen quality, particularly in terms of sperm counts, reported worldwide (Carlsen et al., 1992). In particular, the so-called endocrine disruptors may influence male reproductive function by interfering with hormonal activity (Sharpe, 1995). *p,p'*-Dichlorodiphenyldichloroethylene (*p,p'*-DDE), a well-known environmental endocrine disruptor, is a persistent dichlorodiphenyl trichloroethane (DDT) metabolite often found in human reproductive fluids (Kumar et al., 2000; Dallinga et al., 2002; Younglai et al., 2002; Pant et al., 2004) that has been associated with failed fertilization (Younglai et al., 2002). Moreover, high levels of *p,p'*-DDE correlate with diminished standard semen parameters (Ayotte et al., 2001; De Jager et al., 2006; Toft et al., 2006; Aneck-Hahn et al., 2007), sperm viability (De Jager et al., 2006; Aneck-Hahn et al., 2007), enhanced sperm chromatin/DNA damage (De Jager et al., 2006) and altered accessory sex gland secretions (Ayotte et al., 2001; Pant et al., 2004). It should be noted, however, that current data includes contradictory results (Hauser et al., 2002, 2003; Rignell-Hydbom et al., 2005a, 2005b; Stronati et al., 2006). In rats, exposure to *p,p'*-DDE *in utero* and through lactation significantly decreased cauda epididymal sperm counts (Loeffler and Peterson, 1999) and affected anogenital distance and nipple retention, both accurate indicators of endocrine disruption (You et al., 1998; Loeffler and Peterson, 1999).

While most studies have focused on the long-term effects of *p,p'*-DDE, it has become clear that this compound may also promote rapid non-genomic actions, and interact directly with pre-existing signaling pathways. However, there is no data on such non-genomic effects in human spermatozoa. Calcium (Ca^{2+}) is an intracellular messenger involved in several cellular events, and the amplitude, spatial and temporal features of Ca^{2+} signaling establish specific responses (Younglai et al., 2006). *p,p'*-DDE, related DDT metabolites and/or other pesticides have been shown to adversely affect function by interfering with Ca^{2+} signals in many cell types, including human placenta (Treinen and Kulkarni, 1986), granulosa-lutein cells (Younglai et al., 2004; Wu et al., 2006) and umbilical vein endothelial cells (HUVE; Younglai et al., 2006). Moreover, similar effects were reported not only in bovine oviductal (Tiemann et al., 1998) and rat myometrial and vascular smooth muscle cells (Juberg et al., 1995; Ruehlmann et al., 1998) but also in mice pancreatic β cells (Nadal et al., 2000) and in a pituitary tumor cell line (Wozniak et al., 2005).

Despite their small size and low cytoplasm content, sperm cells are equipped with extraordinary mechanisms capable of regulating intracellular Ca^{2+} concentration ($[\text{Ca}^{2+}]_i$) and production of complex Ca^{2+} signals (reviewed in Jimenez-Gonzalez et al. (2006)). In ejaculated spermatozoa, $[\text{Ca}^{2+}]_i$ was shown to control several key events (Eisenbach, 1999; Carlson et al., 2003; Spehr et al., 2003; Suarez and Ho, 2003; Alasmari et al., 2013) such as the acrosome reaction (AR; Kirkman-Brown et al.,

2002), an exocytic process without which spermatozoa would be unable to successfully fertilize an oocyte (Ramalho-Santos et al., 2007). *In vitro* experiments conducted in a porcine model have shown that exposure to an organochlorine mixture containing *p,p'*-DDE increased cytosolic Ca^{2+} levels, possibly leading to an enhanced AR (Campagna et al., 2009).

The present work was carried out to determine whether *p,p'*-DDE at environmentally relevant concentrations modulates intracellular Ca^{2+} levels, and alters AR, thus potentially affecting human male fertility. Here, we report not only that *p,p'*-DDE raises $[\text{Ca}^{2+}]_i$ and stimulates AR but also that CatSper, a sperm-specific ion channel, is a target of *p,p'*-DDE.

Materials and Methods

All reagents were provided by Sigma-Aldrich (St. Louis, MO, USA) unless stated otherwise. A 99.1% chemically pure *p,p'*-DDE was dissolved in dimethyl sulphoxide (DMSO) to a stock concentration of 62.88 mM.

Human biological samples

Fresh normozoospermic sperm samples from both human healthy donors recruited at the Biosciences School, University of Birmingham, and Medical Research Institute, University of Dundee (Ethics number 08/S1402); as well as healthy patients undergoing routine semen analysis or fertility treatments in the Human Reproduction Service at University Hospitals of Coimbra were used accordingly to the proper ethical and Internal Review Board of the participating Institutions. All individuals signed informed consent forms. Samples were obtained by masturbation after 3–5 days of sexual abstinence and seminal analysis was performed according to the World Health Organization guidelines (WHO, 2010). All samples used in this study had no detectable leukocytes (or any other round cells) and presented >80% viable sperm after processing.

Single-cell Ca^{2+} imaging experiments

After liquefaction, spermatozoa were prepared by direct swim-up and allowed to capacitate in a supplemented Earle's balanced salt solution (sEBSS) containing 1.8 mM CaCl_2 , 5.4 mM KCl, 0.81 mM MgSO_4 , 25.0 mM NaHCO_3 , 1.0 mM NaH_2PO_4 , 116.4 mM NaCl, 5.5 mM D-glucose , 2.5 mM Na-pyruvate, 41.8 mM Na-lactate and 0.3% (w/v) BSA, for at least 3 h at 37°C under 5% $\text{CO}_2/95\%$ air before starting imaging. $[\text{Ca}^{2+}]_i$ measurements were performed after loading 4 million/ml sperm with the Ca^{2+} fluorescent marker Oregon Green BAPTA-1AM (10 μM ; Molecular Probes, Eugene, OR, USA) for 1 h at 37°C under 5% $\text{CO}_2/95\%$ air, as described elsewhere (Mota et al., 2012). All experiments were carried out in a dark room at 25°C with a constant perfusion rate of 0.4 ml/min. Real-time recordings were performed at intervals of 2.5 s using an IQ acquisition software platform (Andor Technology, Belfast, UK). Analysis of images, background correction and normalization of data was performed as described previously (Kirkman-Brown et al., 2000). The region of interest was drawn around the posterior head and neck region of each cell and raw intensity values were imported into Microsoft Excel and normalized using the equation $\Delta F = [(F - F_{\text{basal}}) / F_{\text{basal}}] \times 100\%$, where ΔF is % change in intensity at time t , F is fluorescence

intensity at time t and F_{basal} is the mean basal F established in the beginning of each experiment before application of any stimulus. Each cell was considered to respond when the mean of 10 determinations of normalized F during the exposure period differed significantly from the mean of 10 determinations of normalized F during control (or inhibitor) treatment ($P < 0.05$). Mean amplitudes and percent responsive cells were calculated for each concentration in each sperm sample analyzed.

Measurements of intracellular Ca²⁺ levels

To evaluate the effect of p,p'-DDE on [Ca²⁺]_i, spermatozoa were exposed to a wide range of concentrations (1 pM–50 μM) diluted in standard sEBSS. To further assess the contribution of the internal Ca²⁺ stores, similar experiments were performed in a low-Ca²⁺ sEBSS medium (Ca²⁺ was adjusted to 5 and 6 mM EGTA was added; final [Ca²⁺] < 500 nM). Finally, inhibition studies were performed using 30 μM mibefradil and 10 μM NNC 55-0396 (Brenker *et al.*, 2012). These drugs have been shown to effectively block CatSper currents at these concentrations. When a plateau in the p,p'-DDE-induced [Ca²⁺]_i rise was reached, either mibefradil or NNC 55-0396 was added, allowing the amplitudes of agonist and antagonist effects to be compared in each cell. Before finishing each experiment, spermatozoa were washed with standard sEBSS and exposed to 3.2 μM progesterone to determine if they were responding properly to the physiological stimuli (positive control). Solvent controls were carried out with 0.3% (v/v) DMSO.

Whole-cell patch-clamp experiments

Cells were prepared by swim-up and capacitated as described by Lishko *et al.* (2011). Whole-cell currents were evoked by 1 s voltage ramps from –80 to +80 mV from a holding potential of 0 mV (before correction for junction potential). As previously described, seals were formed either at the human sperm cytoplasmic droplet located in the neck region in HS solution (Lishko *et al.*, 2011). Pipettes were filled with a Cs⁺-based medium (Lishko *et al.*, 2011) containing 130 mM Cs-methane sulphonate, 40 mM HEPES, 1 mM Tris–HCl, 3 mM EGTA, 2 mM EDTA, pH adjusted to 7.4 with CsOH. A divalent-free bath solution comprising 140 mM CsMeSO₃, 40 mM HEPES and 3 mM EGTA (pH 7.4) was used, thus allowing proper recordings of CatSper monovalent currents. 5 μM p,p'-DDE was added at specific time points. All experiments were performed at 25°C.

Extended sperm incubations with p,p'-DDE

After liquefaction, spermatozoa were isolated by density gradient centrifugation (Isolate[®] Sperm Separation Medium, Irvine Scientific, CA, USA) and allowed to capacitate for at least 3 h at 37°C under 5% CO₂/95% air. Spermatozoa (10 million/ml) were then exposed to several p,p'-DDE concentrations (1, 10, 25 and 50 μM) for 3 days at 37°C under 5% CO₂/95% air in order to mimic the putative continuous exposure to toxicants in the female reproductive tract *in vivo*. Cells were maintained in a phosphate buffered saline (PBS; Invitrogen, Paisley, UK) containing 0.9 mM CaCl₂, 0.5 mM MgCl₂, 5 mM D-glucose, 1.0 mM Na-pyruvate, 10.0 mM Na-lactate, 0.3% (w/v) BSA and 1% (v/v) penicillin/streptomycin, pH 7.2–7.4, according to our formerly described long-standing culture system (Amaral *et al.*, 2011). All sperm parameters were assessed daily and medium was changed every day after a 10-min centrifugation at 528g. Solvent controls were performed by adding 0.3% (v/v) DMSO.

Sperm viability

In order to evaluate membrane integrity, spermatozoa were incubated with the LIVE/DEAD Sperm Vitality kit (Molecular Probes) as previously described (Amaral and Ramalho-Santos, 2010). Two hundred spermatozoa

were observed in each slide using a Zeiss Axioplan 2 Imaging fluorescence microscope (Carl Zeiss, Göttingen, Germany). Results were displayed as percentage of live spermatozoa relative to the control.

Acrosomal integrity

Acrosomal integrity was evaluated using the acrosomal content marker *Pisum Sativum* agglutinin coupled to fluorescein isothiocyanate (PSA-FITC), as described elsewhere (Mota *et al.*, 2012). The proportion of spermatozoa with intact acrosome was observed under a Zeiss Axioplan 2 Imaging fluorescence microscope and two hundred spermatozoa were scored in each slide. Results are presented as percentage of intact acrosomes relative to the control.

Statistical analysis

Statistical analysis was carried out using the SPSS version 19.0 software for Windows (SPSS Inc., Chicago, IL, USA). All variables were checked for normal distribution and multiple comparisons were performed by paired t-test or one-way analysis of variance (ANOVA). Correlations were performed by the Spearman non-parametric test. Results are expressed as mean% ± SEM. $P < 0.05$ was considered significant.

Results

p,p'-DDE promotes an intracellular Ca²⁺ rise

Using a continuous exposure system to better mimic *in vivo* conditions we determined that p,p'-DDE did not affect sperm viability, except after 3 days of continuous exposure to the highest p,p'-DDE concentration tested (50 μM; $P < 0.05$, Fig. 1). However, single-cell assessment of [Ca²⁺]_i showed that a wide range of p,p'-DDE concentrations (1 pM–50 μM) caused a clear increase in Ca²⁺ levels within seconds of exposure (when compared with the control), reversible upon sEBSS media washout (Fig. 2A). At 25 and 50 μM of p,p'-DDE, >91% of spermatozoa

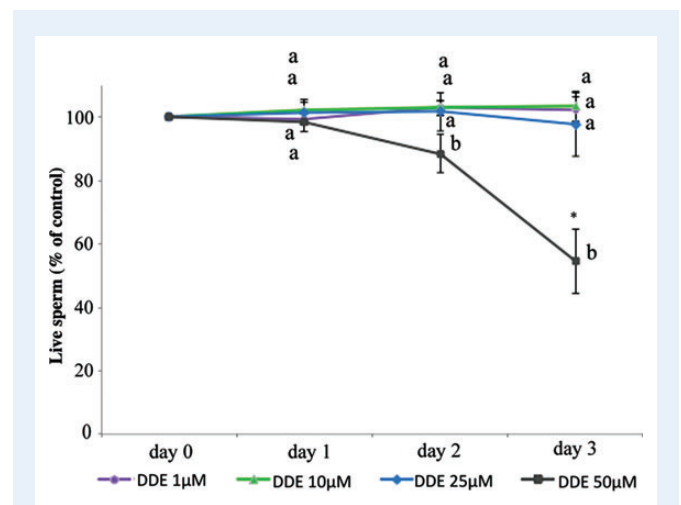


Figure 1 Daily assessment of sperm survival during continuous exposure to p,p'-DDE concentrations at 37°C and 5% CO₂. Results represent mean percentage ± SEM relative to control (100 × %live/% live in control), $n = 5$. Asterisk and different letters represent significant differences compared with control and between concentrations, respectively ($P < 0.05$).

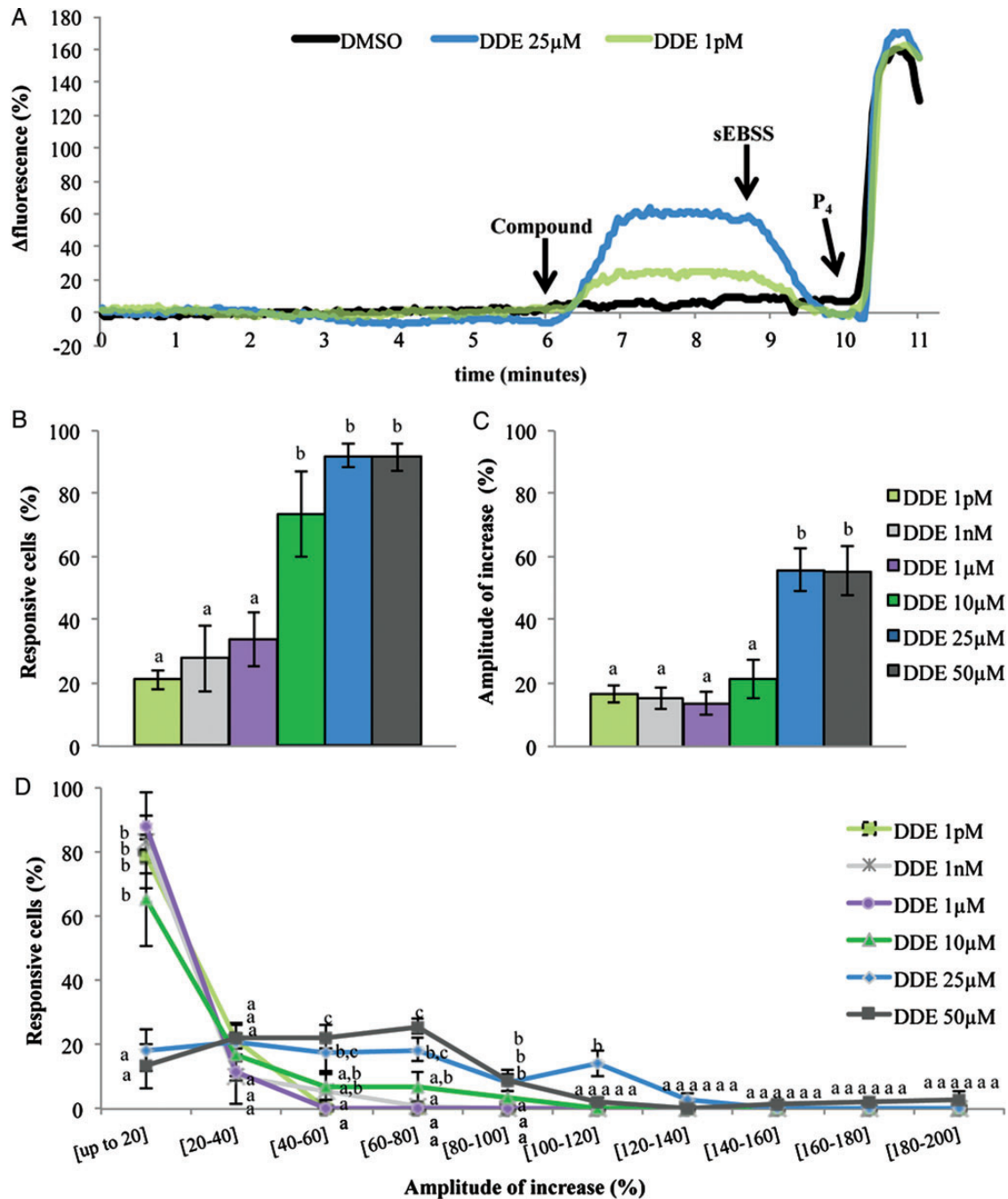


Figure 2 Intracellular Ca^{2+} levels during p,p' -DDE exposure in human sperm. **(A)** Fluorescence-time traces representing intracellular Ca^{2+} changes in three individual cells exposed to different conditions. DMSO (black trace), 1 pM (green trace) or 25 μM p,p' -DDE (blue trace) were added after 6 min of perfusion with standard sEBSS. After a further 3 min p,p' -DDE was washed out by perfusion with fresh sEBSS. Arrows indicate the exact time points in which spermatozoa were bathed with different solutions. P_4 —3.2 μM progesterone. **(B)** Proportion of cells responsive to p,p' -DDE. **(C)** Magnitude of Ca^{2+} response in responsive cells. **(D)** Amplitude distribution of $[\text{Ca}^{2+}]_i$ increase (significant increase in fluorescence) at each dose tested. Results represent mean percentage \pm SEM from 500 cells analyzed individually in a total of five independent experiments for each p,p' -DDE concentration. Different letters denote statistical differences between concentrations ($P < 0.05$). (EBSS, Earle's balanced salt solution.)

showed a significant increase in $[\text{Ca}^{2+}]_i$ ($P < 0.05$, Fig. 2B) and similar mean Ca^{2+} response amplitudes (55.6 ± 6.7 and $55.5 \pm 8.1\%$, respectively; Fig. 2C). p,p' -DDE was found to be so effective that even at concentrations as low as 1 pM and 1 nM, we observed elevated Ca^{2+} levels in

21.1 \pm 3.0 and 28.0 \pm 10.65% of cells ($P < 0.05$, Fig. 2B), with mean amplitudes of response of 16.7 \pm 2.8 and 15.4 \pm 3.6%, respectively (Fig. 2C). Whereas the dose–effect curve for the proportion of responsive cells was roughly sigmoidal, the curve for $[\text{Ca}^{2+}]_i$ response amplitudes

appeared biphasic, with markedly greater responses at 25 and 50 μM p,p'-DDE (Fig. 2B and C). When we analyzed the amplitude distribution of the single-cell responses we observed that from 1 pM to 10 μM p,p'-DDE most responsive cells showed an increase in fluorescence intensity of up to 20%, but at higher doses the shape of the distribution was completely different, with 'enhanced' response amplitudes ranging between 20 and 100% and occasional responses of up to 200% (Fig. 2D). A positive control was included by adding the physiological stimulus progesterone, which causes increased Ca²⁺ levels and triggers AR, to ensure that all samples were responding normally.

The effect of p,p'-DDE on [Ca²⁺]_i is abolished in low-Ca²⁺ medium

We next evaluated whether p,p'-DDE effect on human sperm was due to a Ca²⁺ influx from the medium or to the mobilization of intracellular Ca²⁺ stores present in sperm (reviewed in Jimenez-Gonzalez *et al.*, 2006; Costello *et al.*, 2009). These and subsequent Ca²⁺ imaging experiments were performed with 1 pM and 1 nM p,p'-DDE, concentrations within the range often found in human reproductive fluids (mean values ranging from 47 pM to 111 nM according to Kumar *et al.*, 2000; Dallinga *et al.* 2002; Younglai *et al.*, 2002; Pant *et al.*, 2004) and also at 25 μM , the minimal saturating concentration for the observed effects on [Ca²⁺]_i.

Perfusion of the recording chamber with low-Ca²⁺ medium (<500 nM) caused an immediate decrease in sperm [Ca²⁺]_i that stabilized at a new level within 3 min of exposure and remained unaltered when p,p'-DDE was added (Fig. 3A). At 1 pM and 1 nM no cells showed [Ca²⁺]_i responses ($P < 0.01$ compared with experiments in standard sEBSS, Fig. 3B) and at 25 μM p,p'-DDE only $2.0 \pm 1.2\%$ of cells responded with an increase in Ca²⁺ levels ($P < 0.01$ when compared with the $91.9 \pm 3.7\%$ of cells in standard sEBSS; Fig. 3B). Furthermore, the magnitude of response provoked by 25 μM p,p'-DDE was only of $22.8 \pm 10.7\%$ compared with the $55.6 \pm 6.7\%$ observed in standard sEBSS ($P < 0.05$). When we analyzed the distribution of the

single-cell response we found that $72.2 \pm 14.7\%$ of cells responded with an increase in fluorescence intensity of up to 20%, resembling the response observed in spermatozoa exposed from 1 pM to 10 μM p,p'-DDE in standard sEBSS medium. In all these experiments performed in a low-Ca²⁺ medium, when standard sEBSS was returned to the chamber [Ca²⁺]_i levels increased as expected, and responded normally to the progesterone stimulus (Fig. 3A).

p,p'-DDE effect on [Ca²⁺]_i is reversed by CatSper blockers

CatSper, the only Ca²⁺ conductance channel that has been detected in patch-clamped human sperm (Kirichok and Lishko, 2011), is highly promiscuous, activating in response to a wide range of small organic molecules (Brenker *et al.*, 2012). In order to investigate whether activation of CatSper might mediate p,p'-DDE-induced Ca²⁺ influx, we used 30 μM mibefradil and 10 μM NNC 55-0396, both of which inhibit CatSper currents in human sperm (Lishko *et al.*, 2011; Strünker *et al.*, 2011). Cells were first exposed to p,p'-DDE (1 pM, 1 nM and 25 μM) to establish Ca²⁺-influx and after a delay of 2.5 min the inhibitors were added in separate experiments (Fig. 4A). Both the drugs caused a transient increase in fluorescence, as previously described (Strünker *et al.*, 2011; Brenker *et al.*, 2012) which also occurred in control experiments in the absence of p,p'-DDE (Fig. 4A DMSO trace). However, within few minutes [Ca²⁺]_i significantly decreased and stabilized at a new, lower level (Fig. 4A and B). 30 μM mibefradil strongly reversed the effect of p,p'-DDE in >90% of cells (Fig. 4A–C). This effect was observed at all doses and when mibefradil was applied during 1 pM or 1 nM p,p'-DDE exposure [Ca²⁺]_i decreased below control conditions ($P > 0.05$, Fig. 4A), therefore showing a reversal effect >100% (Fig. 4C). Examination of individual cell responses showed that the magnitudes of the rise in fluorescence caused by p,p'-DDE and the subsequent decrease upon application of mibefradil were clearly correlated ($P < 0.05$, Fig. 4D), confirming that mibefradil was acting by blocking the effect of p,p'-DDE.

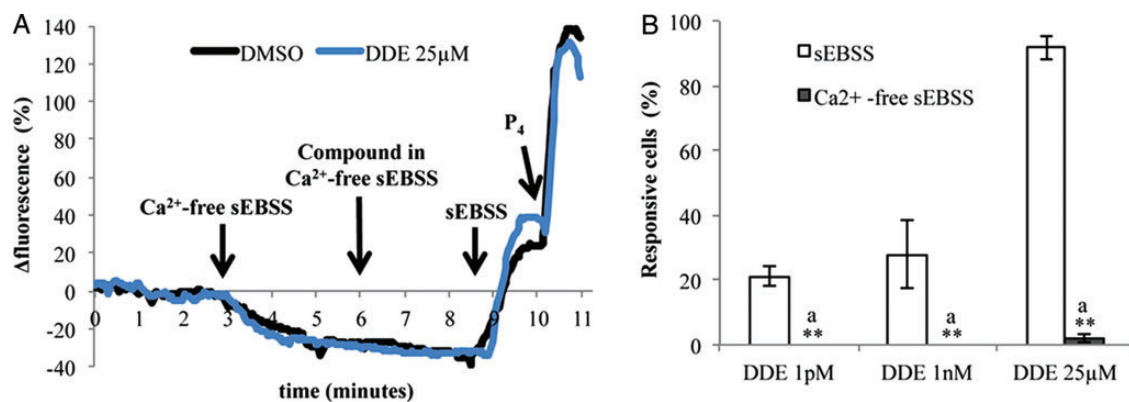


Figure 3 Effect of p,p'-DDE in a low-Ca²⁺ sEBSS medium (<500 nM). **(A)** Fluorescence-time traces representing intracellular Ca²⁺ changes in two individual cells exposed to different conditions. DMSO (black trace) or 25 μM p,p'-DDE (blue trace), both diluted in low-Ca²⁺-sEBSS medium, were added after 6 min of perfusion. Arrows represent the exact time points in which spermatozoa were bathed with different solutions. P₄—3.2 μM progesterone. **(B)** Percentage of p,p'-DDE responsive cells. Results represent mean percentage \pm SEM from 500 cells evaluated individually in a total of eight independent experiments for each p,p'-DDE dose. Double asterisks correspond to statistical differences between concentrations subjected to different conditions ($P < 0.01$). Similar letters represent lack of statistical significance. (EBSS, Earle's balanced salt solution.)

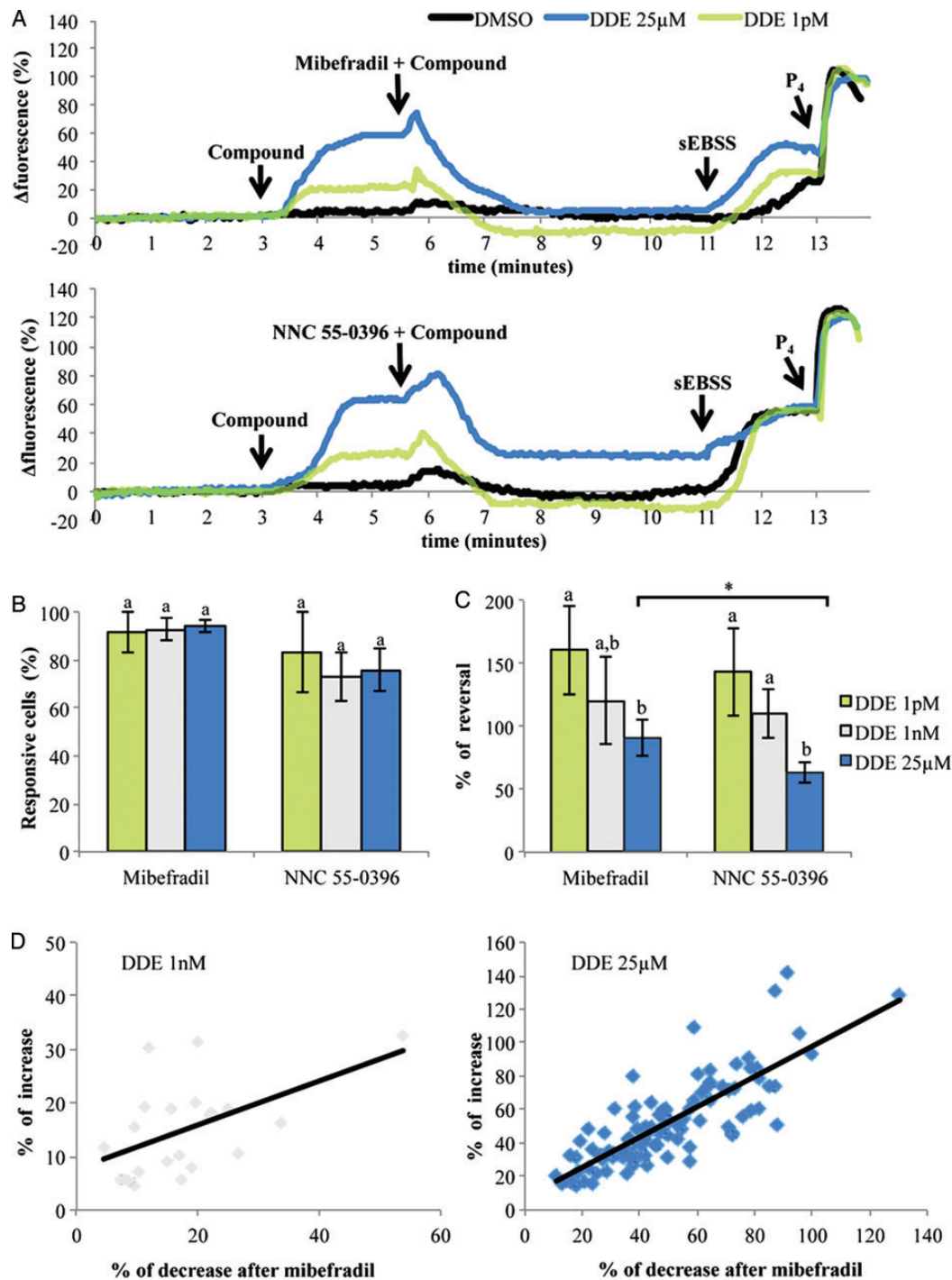


Figure 4 Mibefradil and NNC 55-0396 effects following p,p' -DDE-induced $[Ca^{2+}]_i$ rise. **(A)** Fluorescence-time traces representing intracellular Ca^{2+} changes in six individual cells exposed to different conditions. DMSO (black traces), 1 pM (green traces) or 25 μ M p,p' -DDE (blue traces) were added after 3 min of perfusion with standard sEBSS. Thirty micromolars of mibefradil or 10 μ M NNC 55-0396 were applied after a further 2.5 min when effects on $[Ca^{2+}]_i$ had stabilized. Arrows represent the exact time points in which spermatozoa were bathed with different solutions. P_4 —3.2 μ M progesterone. **(B)** Proportion of responsive cells. **(C)** Percentage reversal by mibefradil and NNC 55-0396 of the preceding increase induced by p,p' -DDE. Mibefradil and NNC 55-0396 alone had no effect (not shown). Results represent mean percentage \pm SEM from 500 cells analyzed individually in a total of five independent experiments for each p,p' -DDE concentration. Different letters denote statistical significance between concentrations within each inhibitor experiments ($P < 0.05$) and asterisk represents statistical differences between the same concentrations exposed to both inhibitors ($P < 0.05$). **(D)** Correlation between amplitudes of the p,p' -DDE-induced $[Ca^{2+}]_i$ rise and the subsequent fall in $[Ca^{2+}]_i$ upon mibefradil application in individual sperm exposed to 1 nM (left panel) or 25 μ M p,p' -DDE (right panel). Significant correlations were found for both 1 nM ($\rho = 0.492$, $P < 0.05$) and 25 μ M p,p' -DDE ($\rho = 0.804$, $P < 0.001$). Each panel shows all cells from a single experiment. (EBSS, Earle's balanced salt solution.)

10 μM NNC 55-0396 also reversed the p,p'-DDE-induced $[\text{Ca}^{2+}]_i$ rise in most cells ($P < 0.05$; Fig. 4A–C). However, NNC 55-0396 reversal of the $[\text{Ca}^{2+}]_i$ rise caused by 25 μM p,p'-DDE was only partial when compared with mibefradil ($P < 0.05$; Fig. 4C). Analysis of individual spermatozoa responses showed that, similarly to the effect of mibefradil, the amplitude of the effect of NNC 55-0396 was correlated with the amplitude of the preceding rise induced by p,p'-DDE ($P < 0.05$, Supplementary data, Fig S1).

p,p'-DDE enhances CatSper currents in human sperm

The action of p,p'-DDE on $[\text{Ca}^{2+}]_i$ is mediated by Ca²⁺ influx and can be reversed by CatSper antagonistic drugs, suggesting that this DDT metabolite activates CatSper. To confirm this, we investigated the effect of 5 μM p,p'-DDE (a concentration that gave detectable $[\text{Ca}^{2+}]_i$ responses in 50.0% of cells but where response amplitude was not 'enhanced' as suggested by Fig. 2D) on CatSper in human sperm held under whole-cell clamp. Using divalent-free conditions and Cs methanesulphonate-based bath and pipette media, large CatSper currents, carried by Cs⁺, were induced by 1 s voltage ramps from -80 to $+80$ mV (Lishko *et al.*,

2011). Five micromolars of p,p'-DDE, increased CatSper current by $116.0 \pm 10.0\%$ ($n = 5$; $P < 0.01$) without changing reversal potential or the characteristic outward rectification of the current (Fig. 5A), similarly to the agonistic effect of 3.2 μM progesterone (Fig. 5B). Examination of the time-course of the action of p,p'-DDE showed that currents increased slowly over a period of 10–20 s and then stabilized (Fig. 5C). In most cells, seals became unstable after 1–2 min and recordings were lost abruptly or after a second rapid rise in current.

p,p'-DDE induces spontaneous acrosomal loss

To evaluate if changes in $[\text{Ca}^{2+}]_i$ could affect sperm function, acrosomal integrity was assessed (Fig. 6). Although p,p'-DDE did not affect the percentage of intact acrosomes at day 1 ($P > 0.05$), 25 and 50 μM p,p'-DDE significantly reduced acrosomal integrity after 2 days of exposure ($P < 0.01$ and 0.05 , respectively). This effect was further observed at Day 3 for both 25 and 10 μM p,p'-DDE ($P < 0.05$). No differences were observed at 1 μM p,p'-DDE in this 3-day long approach. Differences between concentrations were only found at day 3 for 1 and 25 μM p,p'-DDE ($P < 0.05$, Fig. 6). Due to the strong decrease observed in sperm viability (Fig. 1), acrosomal integrity was not evaluated following

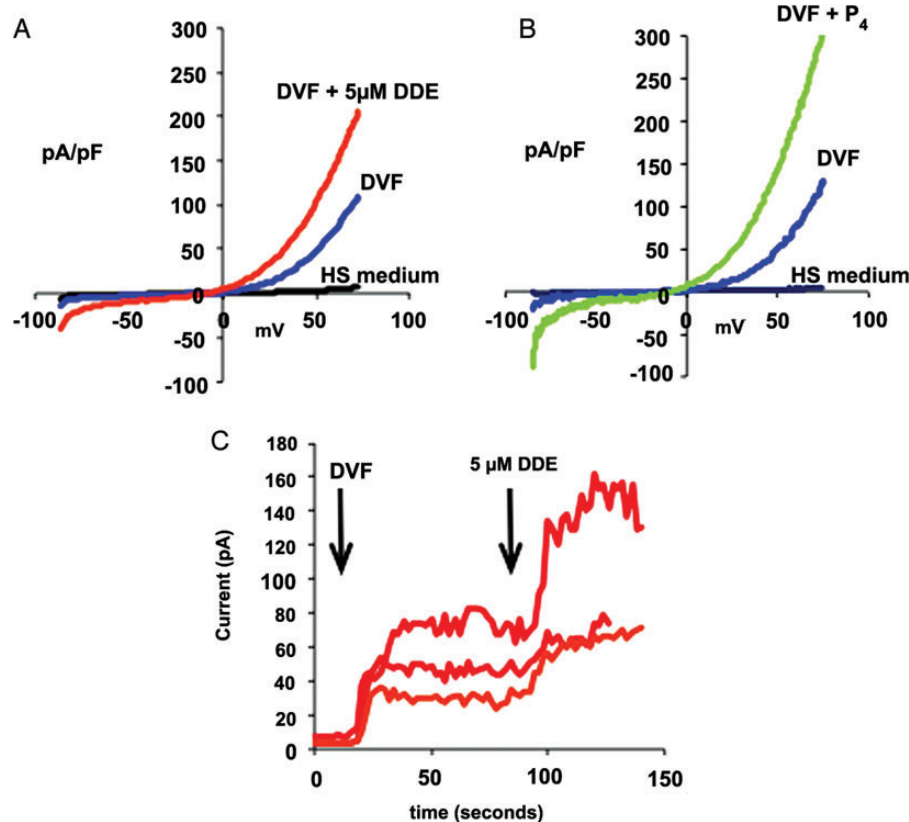


Figure 5 Effect of 5 μM p,p'-DDE on monovalent CatSper currents in human sperm. (A) Example of currents induced by applying a 1 s voltage ramp from -80 to 80 mV to a cell bathed in divalent cation-containing medium (black trace), after superfusion with divalent-free Cs⁺-based medium (DVF; blue trace) and then after application of 5 μM p,p'-DDE (red trace). (B) An example of a similar experiment in which the current was recorded first in divalent cation-containing medium (black trace), then after superfusion with DVF (blue trace) and finally in the presence of 3.2 μM progesterone (P₄; green trace). (C) Time-course of changes in current induced by 5 μM p,p'-DDE. Current amplitude was quantified using the average current over the last 3 mV of the voltage ramp (77–80 mV). Traces show responses of three different cells. The first arrow shows superfusion with DVF and the second shows application of 5 μM p,p'-DDE.

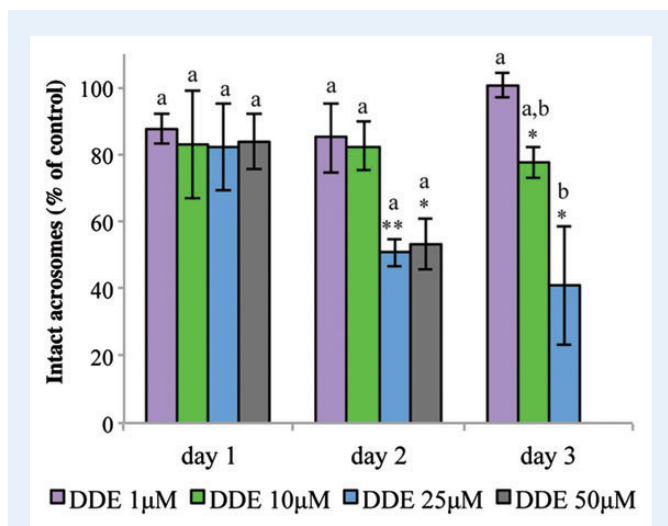


Figure 6 Daily evaluation of acrosomal integrity during continuous exposure to *p,p'*-DDE concentrations at 37°C and 5% CO₂. Results represent mean percentage ± SEM relative to the control (100 × % acrosome intact/% acrosome intact in control), *n* = 6. **P* < 0.05 and ** < 0.01 denote differences towards DMSO and different letters between concentrations (*P* < 0.05).

3 days of continuous exposure to 50 μM *p,p'*-DDE (Fig. 6), given that this data could be misleading, reflecting the loss of viability. It should also be noted that, while subtle changes in Ca²⁺ levels were detected in previous experiments, acrosomal integrity monitored here reflects an all-or-nothing measurement, and relevant changes in the sperm secretory vesicle may occur much earlier. Further experiments, also using longer incubation periods with CatSper inhibitors, are warranted to further clarify this issue.

Discussion

Several studies have focused on the likely genomic effects of *p,p'*-DDE on male fertility (You et al., 1998; Loeffler and Peterson, 1999; Ayotte et al., 2001; Hauser et al., 2002, 2003; Rignell-Hydbom et al., 2005a, 2005b; De Jager et al., 2006; Toft et al., 2006; Stronati et al., 2006; Aneck-Hahn et al., 2007), without exploring possible rapid non-genomic actions on human sperm. This is especially important as sperm can be exposed to *p,p'*-DDE through seminal fluid and/or in secretions in the female reproductive tract (Kumar et al., 2000; Younglai et al., 2002; Pant et al., 2004), where male gametes can survive for several days (Amaral et al., 2011). Additionally, spermatozoa are excellent models for the analysis of non-genomic effects of environmental pollutants/endocrine disruptors since they are transcriptionally inactive, and thus genomic effects will not confound the analysis. We found that *p,p'*-DDE consistently promoted a [Ca²⁺]_i rise in human sperm, as observed by single-cell imaging. High concentrations of *p,p'*-DDE caused a large and rapid rise in [Ca²⁺]_i fluorescence which increased by up to 200%, but even concentrations as low as 1 pM and 1 nM induced significant responses.

Effects on cytosolic Ca²⁺ levels after exposure to several toxicants, including *p,p'*-DDE, have been reported in many cell types, apparently mimicking the action of steroids (Ruehlmann et al., 1998; Nadal et al., 2000; Younglai et al., 2004, 2006; Wu et al., 2006), but dose dependence and

magnitude of the effect vary greatly. *p,p'*-DDE and other pesticides such as kepone, methoxychlor and the isomer *o,p'*-DDE were found to increase cytosolic Ca²⁺ levels in granulosa-lutein and HUVE cells (Younglai et al., 2004; Wu et al., 2006), although in granulosa-lutein cells the Ca²⁺ changes induced by methoxychlor and *o,p'*-DDE were not as clear or consistent as those induced by kepone (Wu et al., 2006). Furthermore, methoxychlor at high concentrations (2.8–280 μM) failed to induce changes in Ca²⁺ levels (Wu et al., 2006). In fact, contrary to the sigmoid curve of dose–response found in this study, the effect of methoxychlor is another example of a non-classical response, showing an inverse U-shaped curve (Wu et al., 2006). The traditional dose–response effect observed in many toxicological studies is not always applicable, especially when environmental toxicants acting as endocrine disruptors are involved (Krimsky, 2001). In mouse β pancreatic cells bisphenol A (BPA), diethylstilbestrol and *o,p'*-DDT increased the frequency of glucose-provoked [Ca²⁺]_i fluctuations (Ruehlmann et al., 1998). A similar response was observed at pico- and nanomolar concentrations in a GH3/B6 pituitary cell line exposed to *o,p'*-DDE (Wozniak et al., 2005), showing the concerning extensive range of action of these endocrine disruptors in the environment. Accordingly, although 10 μM *p,p'*-DDE failed to affect [Ca²⁺]_i in rat myometrial smooth muscle cells, 50 and 100 μM *p,p'*-DDE-induced [Ca²⁺]_i rise by 586% and 921%, respectively (Juberg et al., 1995), effects far greater than those reported here.

To further assess *p,p'*-DDE mechanisms of action in human sperm we exposed cells to the compound in a low-Ca²⁺ medium. Under these conditions the effect was largely abolished, showing that *p,p'*-DDE mainly promotes Ca²⁺ influx at the plasma membrane. Intriguingly, although higher concentrations of *p,p'*-DDE resulted in larger [Ca²⁺]_i signals (Fig. 2C), this effect apparently occurred by ‘recruitment’ of a larger ‘type’ of Ca²⁺ signal (Fig. 2D). This may possibly reflect a secondary release of stored Ca²⁺ downstream of Ca²⁺ influx (Harper et al., 2004). To further explore which plasma membrane Ca²⁺ channel(s) were involved, a pharmacological approach was used. In mouse and human sperm, CatSper is believed to be the principal plasma membrane Ca²⁺ channel (Kirichok et al., 2006; Qi et al., 2007; Smith et al., 2013). Using the Catsper blockers mibefradil and NNC 55-0396 (Lishko et al., 2011; Strünker et al., 2011), we observed a strong suppression of the *p,p'*-DDE-induced Ca²⁺ increase in the large majority of cells. NNC 55-0396, the putatively more potent Catsper inhibitor (Lishko et al., 2011) induced a lower decrease of Ca²⁺ levels at 25 μM *p,p'*-DDE when compared with mibefradil, but this may reflect the significant rise in [Ca²⁺]_i caused by NNC 55-0396 itself (Strünker et al., 2011). We further confirmed *p,p'*-DDE action on CatSper using whole-cell patch-clamp recordings with divalent cation-free bath and pipette solutions where Cs⁺ was the only permeable cation, conditions under which the large monovalent currents show CatSper activity (Kirichok et al., 2006; Lishko et al., 2011; Strünker et al., 2011). Treatment with *p,p'*-DDE caused instability and ultimately loss of the seal within 1–2 min, an effect that is apparently related to patch formation and/or the recording conditions used, since cell viability was not affected (Fig. 1). It has been shown by patch clamp that human sperm CatSper currents are powerfully potentiated by progesterone (Kirichok and Lishko, 2011; Strünker et al., 2011), whereas the steroid had no effect on currents in sperm from an infertile CatSper-deficient patient (Smith et al., 2013), suggesting that CatSper is central to the non-genomic action of the steroid. The high potency of *p,p'*-DDE in elevating [Ca²⁺]_i in human sperm may therefore reflect a steroid-like effect and

p,p'-DDE might even bind the same activating site as progesterone and thus promote Ca²⁺ influx, although the sustained nature of the p,p'-DDE-induced signal does not resemble the biphasic [Ca²⁺]_i elevation induced by progesterone. Alternatively, this action of p,p'-DDE may reflect a more general feature of CatSper. In addition to progesterone the channel is activated by membrane potential, pH_i, prostaglandins, odorants and other small organic molecules (Lishko *et al.*, 2011; Strünker *et al.*, 2011; Brenker *et al.*, 2012), apparently acting as a polymodal sensor upon which diverse stimuli converge to generate [Ca²⁺]_i signals in sperm. The promiscuous nature of the channel, though apparently important for detection of cues in the female tract (Brenker *et al.*, 2012), may render sperm sensitive to organochlorine pollutants such as p,p'-DDE.

After observing these intracellular Ca²⁺ changes, we suspected that AR, a strongly Ca²⁺-dependent event, would be affected. In fact, by mimicking the female reproductive tract conditions, where sperm can be maintained for days, potentially with constant p,p'-DDE exposure, we found decreased acrosomal integrity suggesting the induction of spontaneous AR following 2 and 3 days of exposure. Although other pathways may certainly be involved, and further studies are warranted, we hypothesize that this effect was possibly achieved by sustained Ca²⁺ overload promoted by p,p'-DDE. Elevated p,p'-DDE concentrations not only promoted [Ca²⁺]_i rise in a higher percentage of cells with higher magnitudes of response but also induced acrosomal loss earlier in time. In contrast, since 10 μM p,p'-DDE induced smaller magnitudes of response a decrease in acrosomal integrity was only detected after 3 days of exposure (Figs 2 and 6). In accordance, an environmentally relevant mixture containing p,p'-DDE was found to induce increased [Ca²⁺]_i and potentiated spontaneous AR rates in boar sperm (Campagna *et al.*, 2009). Although the authors did not explore which was the source responsible for the observed higher Ca²⁺ levels, they suggested that this mixture could modify the sperm plasma membrane, allowing non-regulated Ca²⁺ entry that would finally lead to AR, thus lowering sperm survival, among other effects (Campagna *et al.*, 2009). In contrast, the organochlorine pesticide lindane was found to inhibit spontaneous AR in human sperm (Silvestroni and Pallesch, 1999). This compound was able to quickly and transiently depolarize the sperm plasma membrane, opening channels and causing an increase in intracellular Ca²⁺ levels, but probably by inducing biophysical changes on the sperm surface (Silvestroni *et al.*, 1997) and AR was reduced (Silvestroni and Pallesch, 1999). On the contrary, both BPA and octylphenol failed at inducing AR and modifying [Ca²⁺]_i in human sperm (Luconi *et al.*, 2001). Recently, we observed the same complete lack of effects on AR and [Ca²⁺]_i among other functional parameters, in human sperm directly exposed to the classical dioxin 2,3,7,8-tetrachlorodibenzo-p-dioxin (TCDD; Mota *et al.*, 2012), using the same approach and compound solvent, serving, in essence, as a negative control for the data presented here. In general, these data clearly support the involvement of different mechanisms of action through which endocrine disruptors exert their effects, but the highly promiscuous nature of CatSper may cause sperm sensitivity to several compounds that interact with key site(s) on the channel.

In this study, prolonged p,p'-DDE exposure was shown to decrease sperm survival, although only at the highest concentration tested, at day 3. Overall, these findings suggest that the p,p'-DDE-induced [Ca²⁺]_i rise may prematurely trigger acrosomal loss (either via spontaneous AR or damage to sperm membranes) and affect sperm viability long before they reach the oocyte, thus adversely affecting male fertility. p,p'-DDE concentrations in follicular fluid have already been correlated

with failed fertilization (Younglai *et al.*, 2002) and described as being higher in semen from infertile patients (Pant *et al.*, 2004), suggesting an important role of p,p'-DDE in human (in)fertility.

Conclusion

Even at concentrations found in reproductive fluids, p,p'-DDE was able to induce a rise in [Ca²⁺]_i in human sperm through a novel non-genomic mechanism involving the opening of the sperm-specific cation channel CatSper and consequently affected acrosome status and sperm survival, ultimately compromising male fertility.

Supplementary data

Supplementary data are available at <http://humrep.oxfordjournals.org/>.

Acknowledgements

R.S.T. and J.R.S. thank Prof. Teresa Almeida-Santos and Ana Paula Sousa (Human Reproduction Service, University Hospitals of Coimbra) for all the support in sperm collections, and Paula Mota, Sandra Amaral, Marta Baptista and Carla Paiva for many useful discussions. Jennifer Morris and João Correia are especially thanked for all the help with the Ca²⁺ imaging experiments.

Authors' roles

J.R.S., R.S.T., S.J.P., S.M.W. and C.L.B. established the concept and design. R.S.T. and S.M. acquired data. R.S.T., S.J.P. and J.R.S. wrote the paper and all authors contributed to the analysis and interpretation of the results, drafting, revising and approving the article.

Funding

This work was supported by the Portuguese National Science Foundation (FCT) through a grant attributed to the CNC Institution (PEst-C/SAU/LA0001/2011) and a Wellcome Trust Grant #86470 provided to S.J.P. and C.L.R.B. S.M. was supported by the Infertility Research Trust. R.S.T. is the recipient of a PhD fellowship from FCT (SFRH/BD/46002/2008). Funding to pay the Open Access publication charges for this article was provided by The Wellcome Trust.

Conflict of interest

None declared.

References

- Alasmari W, Costello S, Correia J, Oxenham SK, Morris J, Fernandes L, Ramalho-Santos J, Kirkman-Brown J, Michelangeli F, Publicover S, Barratt CL. Ca²⁺ signals generated by CatSper and Ca²⁺ stores regulate different behaviors in human sperm. *J Biol Chem* 2013;**288**:6248–6258.
- Amaral A, Ramalho-Santos J. Assessment of mitochondrial potential: implications for the correct monitoring of human sperm function. *Int J Androl* 2010;**33**:e180–186.
- Amaral A, Paiva C, Baptista M, Sousa AP, Ramalho-Santos J. Exogenous glucose improves long-standing human sperm motility, viability, and mitochondrial function. *Fertil Steril* 2011;**96**:848–850.

- Aneck-Hahn NH, Schulenburg GW, Bornman MS, Farias P, De Jager C. Impaired semen quality associated with environmental DDT exposure in young men living in a malaria area in the Limpopo Province, South Africa. *J Androl* 2007;**28**:423–434.
- Ayotte P, Giroux S, Dewailly E, Hernández Avila M, Farias P, Danis R, Villanueva Díaz C. DDT spraying for malaria control and reproductive function in Mexican men. *Epidemiology* 2001;**12**:366–367.
- Brenker C, Goodwin N, Weyand I, Kashikar ND, Naruse M, Krähling M, Müller A, Kaupp UB, Strünker T. The CatSper channel: a polymodal chemosensor in human sperm. *EMBO J* 2012;**31**:1654–1665.
- Campagna C, Guillemette C, Ayotte P, Bailey JL. Effects of an environmentally-relevant organochlorine mixture and a metabolized extract of this mixture on porcine sperm parameters in vitro. *J Androl* 2009;**30**:317–324.
- Carlsen E, Giwercman A, Keiding N, Skakkeblek NE. Evidence for decreasing quality of semen during past 50 years. *BMJ* 1992;**305**:609–613.
- Carlson AE, Westenbroek RE, Quill T, Ren D, Clapham DE, Hille B, Garbers DL, Babcock DF. CatSper1 required for evoked Ca^{2+} entry and control of flagellar function in sperm. *Proc Natl Acad Sci USA* 2003;**100**:14864–14868.
- Costello S, Michelangeli F, Nash K, Lefievre L, Morris J, Machado-Oliveira G, Barratt C, Kirkman-Brown J, Publicover S. Ca^{2+} -stores in sperm: their identities and functions. *Reproduction* 2009;**138**:425–437.
- Dallinga JW, Moonen EJ, Dumoulin JC, Evers JL, Geraedts JP, Kleinjans JC. Decreased human semen quality and organochlorine compounds in blood. *Hum Reprod* 2002;**17**:1973–1979.
- De Jager C, Farias P, Barraza-Villarreal A, Avila MH, Ayotte P, Dewailly E, Dombrowski C, Rousseau F, Sanchez VD, Bailey JL. Reduced seminal parameters associated with environmental DDT exposure and p,p'-DDE concentrations in men in Chiapas, Mexico: A cross-sectional study. *J Androl* 2006;**27**:16–27.
- Eisenbach M. Sperm chemotaxis. *Rev Reprod* 1999;**4**:56–66.
- Harper CV, Barratt CL, Publicover SJ. Stimulation of human spermatozoa with progesterone gradients to simulate approach to the oocyte. Induction of $[\text{Ca}^{2+}]_i$ oscillations and cyclical transitions in flagellar beating. *J Biol Chem* 2004;**279**:46315–46325.
- Hauser R, Altshul L, Chen Z, Ryan L, Overstreet J, Schiff I, Christiani DC. Environmental organochlorines and semen quality: results of a pilot study. *Environ Health Perspect* 2002;**110**:229–233.
- Hauser R, Singh NP, Chen Z, Pothier L, Altshul L. Lack of an association between environmental exposure to polychlorinated biphenyls and p,p'-DDE and DNA damage in human sperm measured using the neutral comet assay. *Hum Reprod* 2003;**18**:2525–2533.
- Jimenez-Gonzalez C, Michelangeli F, Harper CV, Barratt CLR, Publicover SJ. Calcium signalling in human spermatozoa: a specialized 'toolkit' of channels, transporters and stores. *Hum Reprod Update* 2006;**12**:253–267.
- Juberg DR, Stuenkel EL, Loch-Carusio R. The chlorinated insecticide 1,1-dichloro-2,2-bis(4-chlorophenyl)ethane (p,p'-DDD) increases intracellular calcium in rat myometrial smooth muscle cells. *Toxicol Appl Pharmacol* 1995;**135**:147–155.
- Kirichok Y, Lishko PV. Rediscovering sperm ion channels with the patch-clamp technique. *Mol Human Reprod* 2011;**17**:478–499.
- Kirichok Y, Navarro B, Clapham DE. Whole-cell patch-clamp measurements of spermatozoa reveal an alkaline-activated Ca^{2+} channel. *Nature* 2006;**439**:737–740.
- Kirkman-Brown JC, Bray C, Stewart PM, Barratt CL, Publicover SJ. Biphasic elevation of $[\text{Ca}^{2+}]_i$ in individual human spermatozoa exposed to progesterone. *Dev Biol* 2000;**222**:326–335.
- Kirkman-Brown JC, Punt EL, Barratt CL, Publicover SJ. Zona pellucida and progesterone-induced Ca^{2+} signalling and acrosome reaction in human spermatozoa. *J Androl* 2002;**23**:306–315.
- Krinsky S. An epistemological inquiry into the endocrine disruptor thesis. *Ann N Y Acad Sci* 2001;**948**:130–142.
- Kumar R, Pant N, Srivastava SP. Chlorinated pesticides and heavy metals in human semen. *Int J Androl* 2000;**23**:145–149.
- Lishko PV, Botchkina IL, Kirichok Y. Progesterone activates the principal Ca^{2+} channel of human sperm. *Nature* 2011;**471**:387–391.
- Loeffler IK, Peterson RE. Interactive effects of TCDD and p,p'-DDE on male reproductive tract development in *in utero* and lactationally exposed rats. *Toxicol Appl Pharmacol* 1999;**154**:28–39.
- Luconi M, Bonaccorsi L, Forti G, Baldi E. Effects of estrogenic compounds on human spermatozoa: evidence for interaction with a nongenomic receptor for estrogen on human sperm membrane. *Mol Cell Endocrinol* 2001;**178**:39–45.
- Mota PC, Tavares RS, Cordeiro M, Pereira SP, Publicover SJ, Oliveira PJ, Ramalho-Santos J. Acute effects of TCDD administration: special emphasis on testicular and sperm mitochondrial function. *APJR* 2012;**1**:269–276.
- Nadal A, Roperio AB, Laribi O, Maillet M, Fuentes E, Soria B. Nongenomic actions of estrogens and xenoestrogens by binding to a plasma membrane receptor unrelated to estrogen receptor α and estrogen receptor β . *Proc Natl Acad Sci USA* 2000;**97**:11603–11608.
- Pant N, Mathur N, Banerjee AK, Srivastava SP, Saxena DK. Correlation of chlorinated pesticides concentration in semen with seminal vesicle and prostatic markers. *Reprod Toxicol* 2004;**19**:209–214.
- Qi H, Moran MM, Navarro B, Chong JA, Krapivinsky G, Krapivinsky L, Kirichok Y, Ramsey IS, Quill TA, Clapham DE. All four CatSper ion channel proteins are required for male fertility and sperm cell hyperactivated motility. *Proc Natl Acad Sci USA* 2007;**104**:1219–1223.
- Ramalho-Santos J, Amaral A, Sousa AP, Rodrigues AS, Martins L, Baptista M, Mota PC, Tavares R, Amaral S, Gamboa S. Probing the structure and function of Mammalian sperm using optical and fluorescence microscopy. In: Mendez-Villas A, Diaz J (eds). *Modern Research and Educational Topics in Microscopy*. Badajoz, Spain: FORMATEX, 2007, 394–402.
- Rignell-Hydbom A, Rylander L, Elzanaty S, Giwercman A, Lindh CH, Hagmar L. Exposure to persistent organochlorine pollutants and seminal levels of markers of epididymal and accessory sex gland functions in Swedish men. *Hum Reprod* 2005a;**20**:1910–1914.
- Rignell-Hydbom A, Rylander L, Giwercman A, Jönsson BAG, Lindh C, Eleuteri P, Rescia M, Leter G, Cordelli E, Spano M et al. Exposure to PCBs and p,p'-DDE and human sperm chromatin integrity. *Environ Health Perspect* 2005b;**113**:175–179.
- Ruehlmann DO, Steinert JR, Valverde MA, Jacob R, Mann GE. Environmental estrogenic pollutants induce acute vascular relaxation by inhibiting L-type Ca^{2+} channels in smooth muscle cells. *FASEB J* 1998;**12**:613–619.
- Sharpe RM. Another DDT connection. *Nature* 1995;**375**:538–539.
- Silvestroni L, Pallesch S. Effects of organochlorine xenobiotics on human spermatozoa. *Chemosphere* 1999;**39**:1249–1252.
- Silvestroni L, Fiorini R, Palleschi S. Partition of the organochlorine insecticide lindane into the human sperm surface induces membrane depolarization and Ca^{2+} influx. *Biochem J* 1997;**321**:691–698.
- Smith JF, Syrystyna O, Fellous M, Serres C, Mannowetz N, Kirichok Y, Lishko PV. Disruption of the principal, progesterone-activated sperm Ca^{2+} channel in a CatSper2-deficient infertile patient. *Proc Natl Acad Sci USA* 2013;**110**:6823–6828.
- Spehr M, Gisselmann G, Poplawski A, Riffell JA, Wetzell CH, Zimmer RK, Hatt H. Identification of a testicular odorant receptor mediating human sperm chemotaxis. *Science* 2003;**299**:2054–2058.
- Stronati A, Manicardi GC, Cecati M, Bordicchia M, Ferrante L, Spano M, Toft G, Bonde JP, Jönsson BAG, Rignell-Hydbom A et al. Relationships between sperm DNA fragmentation, sperm apoptotic markers and serum levels of CB-153 and p,p'-DDE in European and Inuit populations. *Reproduction* 2006;**132**:949–958.

- Strünker T, Goodwin N, Brenker C, Kashikar ND, Weyand I, Seifert R, Kaupp UB. The CatSper channel mediates progesterone-induced Ca²⁺ influx in human sperm. *Nature* 2011;**471**:382–386.
- Suarez SS, Ho HC. Hyperactivated motility in sperm. *Reprod Domest Anim* 2003;**38**:119–124.
- Tiemann U, Pöhland R, Küchenmeister U, Viergutz T. Influence of organochlorine pesticides on transmembrane potential, oxidative activity, and ATP-induced calcium release in cultured bovine oviductal cells. *Reprod Toxicol* 1998;**12**:551–557.
- Toft G, Rignell-Hydbom A, Tyrkiel E, Shvets M, Giwercman A, Lindh CH, Pedersen HS, Ludwicki JK, Lesovoy V, Hagmar L et al. Semen quality and exposure to persistent organochlorine pollutants. *Epidemiology* 2006;**17**:450–458.
- Treinen KA, Kulkarni AP. Human placental Ca²⁺-ATPase: in vitro inhibition by DDT homologs. *Toxicol Lett* 1986;**30**:223–229.
- World Health Organization. *WHO Laboratory Manual for the Examination and Processing of Human Semen*. 5th edn. Geneva, Switzerland: WHO Press, 2010.
- Wozniak AL, Bulayeva NN, Watson CS. Xenoestrogens at picomolar to nanomolar concentrations trigger membrane estrogen receptor- α -mediated Ca⁺⁺ fluxes and prolactin release in GH3/B6 pituitary tumor cells. *Environ Health Perspect* 2005;**113**:431–439.
- Wu Y, Foster WG, Younglai EV. Rapid effects of pesticides on human granulosa-lutein cells. *Reproduction* 2006;**131**:299–310.
- You L, Casanova M, Archibeque-Engle S, Sar M, Fan LQ, Heck HA. Impaired male sexual development in perinatal Sprague-Dawley and Long-Evans hooded rats exposed in utero and lactationally to p,p'-DDE. *Toxicol Sci* 1998;**45**:162–173.
- Younglai EV, Foster WG, Hughes EG, Trim K, Jarrell JF. Levels of environmental contaminants in human follicular fluid, serum, and seminal plasma of couples undergoing in vitro fertilization. *Arch Environ Contam Toxicol* 2002;**43**:121–126.
- Younglai EV, Kwan TK, Kwan C-Y, Lobb DK, Foster WG. Dichlorodiphenyl chloroethylene elevates cytosolic calcium concentrations and oscillations in primary cultures of human granulosa-lutein cells. *Biol Reprod* 2004;**70**:1693–1700.
- Younglai EV, Wu Y, Foster WG. Rapid action of pesticides on cytosolic calcium concentrations in cultures of human umbilical vein endothelial cells. *Reprod Toxicol* 2006;**21**:271–279.

- (15) Simon LI, Proutski M, Stevenson D, Jennings J, McManus D, Lutton SEM. Lewis Sperm DNA damage has negative association with live birth rates after IVF. *Reprod Biomed Online* 2013;26:68–78.
- (16) Robinson L, Gallos ID, Conner SJ, Rajkhowa M, Miller D, Lewis S, Kirkman-Brown J, Coomarasamy A. The effect of sperm DNA fragmentation on miscarriage rates: a systematic review and meta-analysis. *Hum Reprod* 2012;27(10):2908–17.
- (17) Van Rumste MME, Evers JLH, Farquhar CM. Intra-cytoplasmic sperm injection versus conventional techniques for oocyte insemination during in vitro fertilisation in patients with non-male subfertility. *Cochrane database Syst Rev (Online)* 2003;2:CD001301.
- (18) World Health Organization. WHO laboratory manual for the examination and processing of human semen. 5th ed. Department of Reproductive Health and Research, WHO; 2010
- (19) Zini A, Sigman M. Are tests of sperm DNA damage clinically useful? *Prosand cons. J Androl* 2009;30:219–29.

Sheena E.M. Lewis

*Reproductive Medicine, Centre for Public Health,
Queen's University Belfast,*

*Room 0017, Ground Floor, Institute of Pathology, Grosvenor
Road, Belfast, BT12 6BJ, Northern Ireland, UK
Tel.: +442890633987.*

E-mail address se.lewis@qub.ac.uk

Andrology is desperate for a new assay – Let us make sure we get it right this time . . .

**Comment by: Christopher L.R. Barratt,
Steven A. Mansell**

Although the diagnostic and predictive value of traditional semen parameters is limited, two facts are clear: (1) at the lower ends of the spectrum, e.g. low concentrations of motile spermatozoa, there are significantly higher chances of sub fertility (9,11) (2) except in rare cases values above these limits of semen analysis provide minimal diagnostic clarity (14). Consequently, semen analysis is very helpful, but andrology requires more robust sophisticated functional assays to be placed in the patient's pathway to assist/change management decisions. Unfortunately, the search for this Holy Grail has been littered with false dawns (2,13) continually blighted by two key problems (1) poor technical and methodological control of purported assays (2) low quality clinical trial information exemplified by poor design often accompanied by low numbers. Not surprisingly, the resultant data often produce conflicting results.

Two key questions arise: will the testing of DNA and its packaging in the human spermatozoon be an important tool in the armamentarium? Is it not already (3)? **We suggest the answers here are yes and no, respectively.**

The assessment of DNA integrity in the spermatozoon is not new. In 1980, a landmark publication by Don Evenson suggested that DNA integrity may be a useful and potentially independent marker of fertility for both animals and men (8). Significant data are now available to suggest that higher levels

of DNA damage is present in men with severe sperm defects and is an indication of a potentially negative impact on both natural and assisted conception outcomes (4). So why do we answer no to the second question? Simply, aside from a relatively low (but significant negative) influence of high levels of DNA on miscarriage (15), three comprehensive reviews of the clinical data concluded that the significance of sperm DNA integrity assessment for natural and ART remains unclear (7,4,16). Routine testing is not supported. This has been reinforced recently by the clinical practice guidelines produced by the British Fertility Society (19). The BFS concludes that 'there is evidence of a relationship between sperm DNA damage and either semen parameters and/or outcome of assisted conception. However, reports conflict and depend largely on the laboratory test utilized. Results are unlikely to alter patient management'. The draft document presented by the American Society for Reproductive Medicine (1) on 'The clinical utility of sperm DNA integrity testing: a guideline' concurs with these conclusions. Its final recommendation is: 'there is insufficient evidence to recommend the routine use of sperm DNA integrity tests in the evaluation and treatment of the infertile couple (Evidence Level B)'.

These are powerful, consistent and persuasive conclusions. But why is this so? Unfortunately assessment of DNA is affected by the three key problems identified for sperm function testing. Firstly clear technical difficulties of performing the three key assays used to test DNA integrity in sperm – SCSA, TUNEL and Comet have affected their clinical usefulness. However, rigorous attention to detail and defined methods now exists for all these methods, e.g. see (12) for TUNEL. Application of robust protocols will, hopefully, minimize future methodological challenges. Secondly, to date the clinical evidence is based on relatively low numbers and poorly designed trials. Surprisingly, in this area there are a large percentage of uncritical reviews compared to primary data which distort the field (3). In 2012 for example there was only one high quality clinical study examining outcomes for IVF/ICSI using relatively large numbers (18). This is very disappointing and unacceptable. No progress will be made if this is not urgently addressed. Thirdly, it has been unclear where the assays (when validated) fit within the patient pathway. For example, diagnostic tests can be used as replacement, triage or add-on with their usefulness being dependent on a large number of factors (6). A critical factor will be cost effectiveness. Two examples suffice here. Mitchell and colleagues showed that the TUNEL assay was highly correlated to sperm viability (12) demonstrating that a simple viability assay could effectively replace an expensive estimate of DNA damage. Improved methodology in the TUNEL assay now allows assessment of DNA damage in live cells – a substantial improvement. A second example is provided by a study comparing progressive motility and DNA assessment for IVF success where it was concluded that DNA assessment was more significant. However, close examination of the data shows this to be a relatively small difference and it is questionable if this is actually cost effective (17). Future studies in cost effectiveness clearly need to establish the additional role of DNA integrity assessment alongside a high quality semen assessment (See (19)).

For the field to progress we must address the above points. These are not new (10) or specific to reproductive medicine (5). However, to date, DNA damage assays have not been evaluated in a critical manner and, quite simply, they need to be. We are very hopeful that this will occur and DNA assessment

will become a valuable clinical tool. Andrology, desperately needs this to be the case but being desperate is no excuse to compromise on intellectual rigor.

References

- (1) ASRM. The clinical utility of sperm DNA integrity Testing: a guideline. The Practice Committee of the American Society of Reproductive Medicine. Circulated for comment November 2012.
- (2) Barratt CL, Mansell S, Beaton C, Tardif S, Oxenham SK. Diagnostic tools in male infertility-the question of sperm dysfunction. *Asian J Androl* 2011;13:53–8.
- (3) Barratt CL, De Jonge CJ. Clinical relevance of sperm DNA assessment: an update. *Fertil Steril* 2010;94:1958–9.
- (4) Barratt CL, Aitken RJ, Björndahl L, Carrell DT, de Boer P, Kvist U, et al. Sperm DNA: organization, protection and vulnerability: from basic science to clinical applications – a position report. *Hum Reprod* 2010;25:824–38.
- (5) Begley CG, Ellis LM. Drug development: raise standards for preclinical cancer research. *Nature* 2012;483:531–3.
- (6) Bossuyt PM, Irwig L, Craig J, Glasziou P. Comparative accuracy: assessing new tests against existing diagnostic pathways. *BMJ* 2006;332:1089–92.
- (7) Collins JA, Barnhart KT, Schlegel PN. Do sperm DNA integrity tests predict pregnancy with in vitro fertilization? *Fertil Steril* 2008;89:823–31.
- (8) Evenson DP, Darzynkiewicz Z, Melamed MR relation of mammalian sperm chromatin heterogeneity to fertility. *Science* 1980;210:1131–3.
- (9) Hargreave TB, Elton RA. Is conventional sperm analysis of any use? *Br J Urol* 1983;55:774–9.
- (10) Lefèvre L, Bedu-Addo K, Conner SJ, Machado-Oliveira GS, Chen Y, Kirkman-Brown JC, et al. Counting sperm does not add up any more: time for a new equation? *Reproduction* 2007;133:675–84.
- (11) MacLeod J, Gold RZ. The male factor in fertility and infertility. III. An analysis of motile activity in the spermatozoa of 1000 Fertile men and 1000 men in infertile marriage. *Fertil Steril* 1951;2:187–204.
- (12) Mitchell LA, De Iuliis GN, Aitken RJ. The TUNEL assay consistently underestimates DNA damage in human spermatozoa and is influenced by DNA compaction and cell vitality: development of an improved methodology. *Int J Androl* 2011;34:2–13.
- (13) Pacey AA. Quality assurance and quality control in the laboratory andrology. *Asian J Androl* 2010;12:21–5.
- (14) Publicover SJ, Barratt CL. Sperm motility: things are moving in the lab! *Mol Hum Reprod* 2011;17:453–6.
- (15) Robinson L, Gallos ID, Conner SJ, Rajkhowa M, Miller D, Lewis S. The effect of sperm DNA fragmentation on miscarriage rates: a systematic review and meta-analysis. *Hum Reprod* 2012;27:2908–17.
- (16) Sakkas D, Alvarez JG. Sperm DNA fragmentation: mechanisms of origin, impact on reproductive outcome, and analysis. *Fertil Steril* 2010;93:1027–36.
- (17) Simon L, Lewis SE. Sperm DNA damage or progressive motility: which one is the better predictor of fertilization in vitro? *Syst Biol Reprod Med* 2011;57:133–8.
- (18) Simon L, Proutski I, Stevenson M, Jennings D, McManus J, Lutton D, et al. Sperm DNA damage has a negative association with live-birth rates after IVF. *Reprod Biomed Online* 2012 [Epub ahead of print].
- (19) Tomlinson MJ, Morroll D. Semen quality and its relationship to natural and assisted conception. *British Fertility Society Guidelines for Practice. Human Fertility*, in Press.

Christopher L.R. Barratt

*Reproductive and Developmental Biology,
University of Dundee Medical School,
Ninewells Hospital, Dundee,
DD1 9SY Scotland, United Kingdom*

*Assisted Conception Unit, NHS Tayside, Ninewells Hospital,
Dundee, DD1 9SY Scotland,
United Kingdom
Tel.: +44 1382383398
E-mail address: c.barratt@dundee.ac.uk*

Steven A. Mansell

*Assisted Conception Unit, NHS Tayside,
Ninewells Hospital, Dundee, DD1 9SY Scotland,
United Kingdom*